Author note: This document contains the following 4 sections (each with page numbering starting with page 1):
1) all responses to both referees as also posted on the ACPD site for acp-2020-811 (pages 1-17)
2) a marked-up version of our revised manuscript (pages 1-66)
3) the revised manuscript without markups (pages 1-66)
4) a marked-up version of the revised supplement (pages 1-22)

Formatted: Font: +Body (Calibri), Not Italic, Font color: Text 1

Section 1:

We thank the two referees for their comments, which have led to considerable improvements in our manuscript.

Response to Anonymous Referee #1

The authors thank Anonymous Referee #1 for this detailed review, which has resulted in revisions that have strengthened the manuscript. Below are our point-by-point responses, showing how we have addressed each of the referee's concerns. All referee comments are in black bold text, preceded by RC. Author comments are in blue italics and preceded by AC. All line numbers quoted below refer to the manuscript version without markups.

RC: The manuscript provides an overview of particle number and composition measurements over remote marine locations and aims at explaining sources of these particles by deploying the GEOS-Chem-TOMAS model. While it is a really unique set of measurements that is very difficult to obtain over remote locations, especially extending over various seasons, I feel that the model results are often over-interpreted. Particularly, for the cases where model simulations do not quite agree with the measurements, but important claims are made from these anyway. The manuscript has a potential, owing to the measurements, to bring valuable insights and provide new knowledge, however, several key issues must be resolved before publication.

AC: In response to the reviewer's comments, we have carefully revised the manuscript to avoid over-interpretation of the model results. We agree that these are a really unique set of measurements over various seasons that can provide valuable insights. Details of the revisions conducted in response to this review are provided below.

RC1: My main concern is that the paper seems to be biased to discussing and evaluating sources that were selected based on the literature, but not on the current measurements. To name a few: new particle formation near the surface was not accounted for, nor primary marine sources were seriously considered. E.g. sea salt and sea spray, including organic matter, can be as small as 10 nm in diameter (de Leeuw et al., 2011), however, their effects to DRE and AIE were not evaluated, nor their contribution to vertical distributions analysed.

AC1: Thank you for this constructive comment. We agree that the manuscript would be improved by discussion and evaluation of the role of both new particle formation (NPF) near the surface, and primary marine sources (sea salt and sea spray).

To address these concerns, we added a section on sea spray to the main text (lines 719-740, Sect. 3.6), and we added a new simulation with no sea spray emissions (noSS, Table 1). As well, in the supplement, we now include a simulation with 3-fold scaling up of sea spray emissions. The revised Sect. 3.6 discusses the revised Figs. 2-5, which now include the noSS simulation. These revised figures enable evaluation of sea-spray-related contributions to both the vertical profiles and the MBL ship-track size distributions. Figures 7 and 8 in the radiative effects section (new Sect. 3.7) were also revised to present an evaluation of sea spray contributions to the DRE and AIE.

The abstract was revised to include the following as related to sea spray during the May/June phytoplankton bloom maxima, "and (5) primary sea spray emissions (AIE: +0.04 W m^{-2}, DRE: -0.79 W m^{-2})" (lines 43-44).

The conclusion was also revised to state "The maximum regional-mean (40-60 ^{o}N, 20-50 ^{o}W) DRE for our simulations was -1.37 W m^{-2}, attributed to sea spray during the March/April accumulating phase, which is a time of strong synoptic-scale storms in the Northwest Atlantic, enhancing wind-generated sea spray" (lines 906-909).

Although sea spray contributes to particles as small as 10 nm in diameter in our simulations, we caution that, "A coupled parameterization for primary organic aerosol from sea spray was not available for our aerosol size-resolved GEOS-Chem-TOMAS simulations, such that some sea spray organics could be misrepresented as sea salt" (lines 288-291).

To address the role of new particle formation near the surface, we revised the text to clarify that our simulations do account for NFP near the surface. The revised text states that, "All simulations include particle nucleation in the boundary layer that is parameterized with the ternary (H_2SO_4-NH_3-H_2O) scheme of Napari et al. (2002), which was scaled by 10^{-5} to better match continental boundary-layer measurements (Westervelt, 2013) (lines 315-317).

As well, we added Supplementary Figs. S5-S8 and Supplementary Table S3, which show the effect of extending our surrogate nucleation parameterization through the entire MBL. The following related text was also added to the main manuscript, "Extending the surrogate activation-style parameterization to the surface (Supplementary Figs. S5-S8 and Supplementary Table 3), leads to overprediction of the number of particles with diameters less than 50 nm in the MBL and yields higher MFEs (ranging from 0.20 to 0.56) than for simulation BASE, although the errors were not as large as those for noABLNUC. For the vertical profiles, this extra NPF extended into the MBL yields overprediction of N3, N10, and N3-N10 below 1 km in all seasons. Aerosol surface area and volume (in the SMPS particle-diameter size range of 10 nm - 282 nm) were over predicted during the August/September declining phase, when the simulated temperature-dependent MSOA source was strongest, growing these extra new particles to larger sizes. These challenges highlight the relevance of ongoing research to better understand NPF in the marine environment" (lines 544-553).

RC2: Near surface or MBL NPF was completely omitted, while authors admit that MSOA NPF, which supposedly happens near the surface, can potentially have an impact (lines 275-277). The question is then why they were not included or

evaluated? Without the proper evaluation, their role cannot be dismissed and conclusions stating that only cloud base or MBL top NPF are important are based on wrong assumptions.

AC2: We agree that the manuscript would benefit from improved clarity regarding MBL NPF in our simulations. To address this concern, we have revised the text to more clearly indicate that all simulations do include MBL NPF using a standard ternary scheme (quoted in AC1, lines 315-317).

To evaluate the impact of including the surrogate nucleation scheme throughout the MBL, we added Supplementary Figs. S5-S8 and Supplementary Table S3 and related discussion in the main text (lines 544-553, quoted in AC1).

As well, we revised the text to include the following evaluation of the ternary NPF scheme in the MBL, "Without the surrogate NPF scheme employed near and above the MBL top, the ternary NPF scheme in the MBL in simulation noABLNUC fails to simulate sufficient particle number, although vertical-profile campaign-median ammonium concentrations below 4 km altitude had acceptable agreement with observations (MFE ranges from 0.12 to 0.48, not shown). Figure 4 shows about a one-order-of-magnitude underprediction of N3 below about 2 km for noABLNUC. NoABLNUC has an unacceptable seasonal-mean model-measurement agreement across the measurement set (MFE ranges from 0.66 to 0.78, Supplementary Table S2)" (lines 503-510).

RC3: Moreover, the conclusion on the dominant near MBL top NPF effect was based on very uncertain measurements near the ground. As the reliability of near ground measurements poses some questions, e.g. how the aircraft data were extrapolated to the ground level as, I assume, the airplane did not go down to 0m altitude?

AC3: To address this concern, we revised the manuscript to provide greater clarity about the near-ground measurements. During NAAMES, the lowest aircraft flight level altitude was around 150-200 m GPS altitude. We revised the text as follows to offer support for the reliability of the near-ground measurement.

We revised the methods section to explicitly indicate the approach that was used for binning the measurements into various altitude ranges, "For consideration of vertical profiles, we binned the measurement and simulation values using a 500 m height resolution, starting from the surface to 500 m as the first bin. Campaign-median values are calculated within each bin and plotted at the mid-point of the bin, starting at 250 m. During NAAMES, the lowest aircraft flight level altitude was around 150-200 m GPS altitude. We use a plane-flight diagnostic in the model to sample the simulation interpolated between grid-cell centers to the aircraft flight track position during the times when measurement data was available for each respective instrument. We find consistent results with bin resolutions of 250, 500 and 1000 m, giving support for our selected binning resolution. The vertical profiles show measurements and model output along the aircraft flight tracks only and do not include any measurements or model output for the ship track" (lines 376-386).

RC4: And, to my understanding from the methods section, the ship measurements were for particles >20nm in diameter? Therefore, Figure 4 showing N3 and N10 down to 0m as well as
lines 406-408 are misleading as they do not represent the real N measurements.

AC4: Thank you for noting the need for greater clarity in regard to the particle size ranges for Fig. 2 (ship measurements) relative to Fig. 4 (aircraft measurements). To address this concern, we revised lines 414-415 to state "Figure 2 shows the campaign-median marine-influenced aerosol size distributions from SEMS (particle diameters 20-500 nm) for the four R/V Atlantis cruises".

We also revised the text in the methods section to clarify the sizes ranges for the two CPCs and to better explain the terminology used, "As well, we give attention to measurements of total particle number concentration from the Condensation Particle Counters (CPCs) with differing nominal lower detection diameters: 3 nm for the CPC 3025 (yielding N3 measurements) and 10 nm for the CPC 3772 (TSI Inc., St. Paul, MN) (yielding N10 measurements) aboard the C130 aircraft" (lines 227-231).

As well, lines 439-441 related to Fig. 4 were revised to clarify that, "Figure 4 shows the vertical-profile campaign-median total particle number concentrations from CPCs, for aerosols with diameters larger than 3 nm (N3), larger than 10 nm (N10), and the difference between the two (N3-N10)".

To improve clarity, we also revised the Fig. 4 caption (and all other vertical profile captions) to state the range of the altitude bins, "All measurement and model output is binned at 500 m resolution and campaign-median values are plotted at the mid-point of each bin starting at 250 m above the surface". As well, captions for all vertical-profile figures were revised to state that the presented measurements were taken aboard aircraft.

As quoted in AC3, the revised text also indicates that these vertical profiles do not include ship-board measurements (lines 384-386).

RC5: Moreover, in high biological activity May/June period, the N3-N10 maximum extends over the broad amplitude range (~2km wide), as opposed to only the top of the MBL as stated by authors (408-412), therefore, the question is whether the drop in concentration that occurs at the very surface is due to measurement uncertainty?

AC5: We agree that rewording related to the altitude range would improve the clarity and accuracy of the discussion. To address this concern, we revised the text to indicate May/June N3-N10 maximum extends over a broad range, "For the May/June 2016 climax transition (phytoplankton bloom maximum), there are enhancements in observed number concentration (N3, N10 and N3-N10) below about 2 km in the free troposphere, indicating NPF at these altitudes (Fig, 4)" (lines 441-443).

To support that the drop in N3-N10 concentration towards the surface was not due to measurement uncertainty, we revised the text to provide additional details (as quoted in AC3 and AC4) about the method used for preparing the vertical profiles.

RC6: In which case, the NPF might have occurred over the whole boundary layer and not only at the MBL top, but was not detected due to these measurement limitations?

AC6: We agree that NPF can occur over the whole boundary layer. For clarity, the revised text acknowledges that, "NPF does occur in the MBL. However, those levels above the MBL clouds favor oxidative chemistry that yields particle precursors, particularly from the wide-spread and persistent DMS sources in the marine environment (Kazil et al., 2011)" (lines 537-539).

RC7: While, if indeed real, such strong gradient in number concentration would imply a constant source that occurs over larger geographical areas as these new particles are not mixed down into boundary layer within normal 15-20 min mixing, which would diminish the gradient if the source is not constant. The existence of such strong constant and wide source does not seem likely.

AC7: Thank you for this discussion. We have revised the main text as noted in AC3-AC6 to provide support and discussion related to the number gradient, while being careful to indicate that NPF can occur at all levels. The revised text indicates that our study supports DMS as a relatively constant source of particle precursors, which extends over a large geographic area as quoted in AC6 (lines 537-539).

As well, the revised text states that, "The lower free tropospheric region near and above the MBL top is an important region for marine NPF. These altitudes above the MBL clouds are generally very clean, which favors NPF, and strongly sunlit, which favors the photochemical oxidative production of particle precursors for NPF" (lines 444-448) and with regard to our simulations that "Although our simulations do include NPF within the MBL, simulated NPF occurs more strongly near and above the MBL top and the resultant particles grow by condensation of available vapors and cloud processing while descending into the MBL. This role for NPF is in agreement with previous studies including those of Clarke et al. (2013), Quinn et al. (2017), and Williamson et al. (2019)" (lines 531-535).

RC8: The statement on the number concentration maxima observed at 1 km (lines 30-32) is also not robust. The total number concentration, in Figure 3, shows 2 peaks, one at _1km and other just below 2 km, with the latter being even stronger, so why 1 km maxima is highlighted and how the second maxima is explained? Is that the measurement uncertainty or just noise rather than the real maxima?

AC8: We agree that these statements brought too much focus to the 1 km level. To address this concern, we have revised the abstract text to state, "Observations from the NAAMES campaigns show enhancements in the campaign-median number of aerosols with diameters larger than 3 nm in the lower troposphere (below 6 km), most pronounced during the phytoplankton bloom maxima (May/June) below 2 km in the free troposphere" (lines 30-33).

The text regarding Fig.3 was also revised to state, "These profiles exhibit several particle number maxima in the lower free troposphere below 6 km, including below 2 km during the May/June climax transition period" (lines 428-430).

The revised text also provides additional details about the binning method used for the vertical profiles, which offers support that the maxima in the presented campaign-median profiles are not noise.

RC9: Similarly, lines 396-397 point to one maximum in figure 3, which is quite subjective as there are many 'maximas' in that figure, but no explanation is provided.

AC9: We agree that the discussion would be improved by indicating that there can be several maxima in the lower free troposphere. The text is revised as quoted in AC8 (lines 30-33 and lines 428-430). The text was also revised to explain that, "As shown in Fig. 3, aerosol surface area and volume are less at altitudes below about 3 km, relative to altitudes above 3 km. This lower particle surface area at these altitudes favors NPF over growth of pre-existing particles as available vapors condense in these relatively cleaner atmospheric layers (Kazil et al., 2011). Transport of aerosols (in part associated with continental emissions) contributes to particles in all seasons. Fast et al. (2016) characterized summertime North Atlantic transport layers in the free troposphere associated with synoptic-scale lifting" (lines 430-436).

The revised text also discusses evidence for levels where NPF contributes relatively more strongly to the number maxima and states, "For the May/June 2016 climax transition (phytoplankton bloom maximum), there are enhancements in observed number concentration (N3, N10 and N3-N10) below about 2 km in the free troposphere, indicating NPF at these altitudes (Fig. 4)" (lines 441-443).

RC10: Therefore, the statement 'that NPF near/above the MBL has a strong control on the development of the total particle number maxima near 1 km altitude...' (lines 464-467) is not exactly based on the measurements.

AC10: We agree that the original text was overly focused on the 1 km altitude and that the total particle number maxima could have a variety of contributors. To address this concern, we have revised the text as quoted in AC9 to acknowledge that there are a variety of contributors to the particle maxima, and that measurements suggest the strongest role for NPF in the lowest 2 km in May/June phytoplankton bloom period.

RC11: Moreover, neither Base nor noABLNUC simulations agree with the measurements, actually, for this season, all N3-N10 simulations are very far from the measurements, so the claims on the processes influencing the number concentrations in the high biological activity season are not substantiated by the measurements or data in this paper.

AC11: In response to this comment, we have revised the text to acknowledge that the N3-N10 is very challenging to the model, "The simulated N3-N10 (Fig. 4) illustrates that representation of NPF is a challenge for models, because there are difficulties capturing the magnitude and altitudes of the N3-N10 maxima. These discrepancies reflect key knowledge gaps related to the

species that can form new particles in the marine environment (e.g., Veres et al. 2020). As well, the coefficient that we used for the surrogate activation-style nucleation parameterization was derived for a continental environment. The empirical ('A') value used by the parameterization appears to yield excessive NPF for the NAAMES marine environment. Activation-style nucleation was added in our simulations as a proxy for missing nucleation when the condensation sink is low, and conditions favor high oxidation rates. We acknowledge that this approach will miss variability in the timing and rates because it is a surrogate and not exactly the correct mechanism. As well in the summertime, the simulations underpredict N3-N10 concentrations above 2km, suggesting the need for future work to better understand the NPF processes at these levels, where the binary scheme of Vehkamaki et al. (2002) does not generate sufficient NPF" (lines 516-528).

However, we consider that simulation BASE has acceptable performance such that it can be used for interpreting these measurements. For more complete evaluation of simulation BASE relative to noABLNUC, we extended our calculation of MFEs to all panels presented in the main text. These MFEs are summarized in the new Supplementary Table S2 and indicate that BASE offers an overall seasonal-mean acceptable simulation (mean MFE ranges from 0.43-0.50) and represents an improvement over noABLNUC (mean MFE ranges from 0.66-0.78). The text was revised to state, "For each season the mean MFE across the parameters considered in Figs. 2 to 5 (BASE versus measurements, Supplementary Table S2) is satisfactory (MFE ranges 0.43 to 0.50)" (lines 492-494). Also, the revised text states," NoABLNUC has an unacceptable seasonal-mean model-measurement agreement across the measurement set (MFE ranges from 0.66 to 0.78) (Supplementary Table S2)" (lines 508-510).

We consider that our study can help to direct future research efforts by identifying key challenges in marine aerosol simulation. At the same time, simulation BASE shows satisfactory model-measurement agreement, which supports conclusions made by comparing the simulation set with measurements, such as the following revised statement, "Without the surrogate NPF scheme employed near and above the MBL top, the ternary NPF scheme in the MBL in simulation noABLNUC fails to simulate sufficient particle number, although vertical-profile campaign-median ammonium concentrations below 4 km altitude had acceptable agreement with observations (MFE ranges from 0.12 to 0.48, not shown). Figure 4 shows about a one-order-of-magnitude underprediction of N3 below about 2 km for noABLNUC" (lines 503-508).

AC12: Similarly, the following statement on MBLtop NPF influencing the concentrations of near surface particles (lines 476-748) is not based on the findings as, without model simulations agreeing with the measurements, these are only speculations.

AC12: To address this concern, we added additional quantitative analysis as noted in AC11 and presented in Supplementary Table S2. This analysis indicates that across the measurement set, simulation BASE provides acceptable agreement with the measurements (MFE ranges from 0.43 to 0.50 for seasonal mean across the measurement set), unlike noABLNUC (MFE ranges from 0.66 to 0.78 for seasonal mean across the measurement set). This analysis is supportive of the role of NPF near and above the MBL top as a key contributor to the MBL size distributions.

We also revised the text to clarify how we defined acceptable model-measurement agreement. Lines 373-374 state, "We adopt the convention of Boylan and Russell (2006) to consider a MFE of 0.5 or less as acceptable."

AC13: There are other features in the simulations that were not properly discussed or explained, like high DMS contribution in winter (Figure 2 and Figure 7, lines 562-565). Provide quantitative (%) estimates when talking about differences between Base and noDMS. It is not so trivial to judge by just looking at the graphs. Also, high DMS effects (as well as MSOA) over continents are not discussed (figure 7).

AC13: Thank you for pointing out the need for greater clarity in the discussion related to DMS. To address these concerns, we revised the original lines 562-565 to quantify the difference between BASE and noDMS and to clarify that there is not a high contribution of DMS in the winter. The revised text states, "Figure 2 shows that DMS also has a control on the simulated MBL aerosol size distributions (BASE versus noDMS) for the four seasons of the NAAMES campaigns. The total simulated number of particles attributed to DMS is lowest during the phytoplankton bloom minima (winter, November 2015) and greater in other seasons. For example, for particle diameters at 40 nm, the DMS-related contribution to the size distribution (Fig. 2) is about 200-300 cm^{-3} in all seasons, except less than 50 cm^{-3} during the bloom minima" (lines 654-659)".

We revised the caption of Fig. 6 to caution, "Note the horizontal scale change between panels".

As well, we revised the text related to DMS and Fig. 7 to clarify/quantify that "The DRE is -0.10 Wm^{-2} over the region between 40-60 ^{o}N and 20-50 ^{o}W during the bloom maxima and diminishes to -0.005 Wm^{-2} during the bloom minima" (lines 773-775).

We also revised the text to include discussion about the DMS-related radiative effects over the continents. The revised text states, "DMS (similar to MSOA) also contributes to the DRE over the continents as these vapors have a lifetime of about a day in our simulations and can be transported before their oxidation products are available for condensation. Once available for condensation, DMS products and MSOA contribute to growing particles (of both marine and continental origin) to sizes that can interact more strongly with radiation (diameters near 100 -200 nm. Particles arising from DMS grow during transport, and some particles may only reach sizes large enough to interact with radiation when they are over the continents" (lines 777-783).

RC14: Finally, the ship emission control does not look so modest to me (lines 593-594 and Figure 2), so, please provide a quantitative estimate of the difference. Also, it seems, that noSHIPS agrees better with the measurements than the BASE in figure 2? Discuss that in more details.

AC14: We agree with this comment and have removed the word 'modest' from the discussion and added a quantitative statement about the differences between noSHIPS and BASE. The revised text states that "Our simulations suggest that ship emissions are also a control on the NAAMES-region MBL marine-influenced aerosol size distributions (Fig. 2, noSHIPS versus

BASE). For example, for the simulated summertime MBL size distribution at particle diameters at 40 nm, about 100-200 cm^{-3} are attributed to ship emissions (Fig. 2)" (lines 689-693).

We also added the following discussion about the model-measurement agreement for noSHIPS versus BASE, "Table 2 shows that during the phytoplankton bloom and March/April accumulating phase, the noSHIPS simulation agrees more closely with the measurements than the BASE simulation, although both are within acceptable agreement (MFE < 0.5). These simulation challenges highlight the importance of future work to better understand the role of oxidants from ship emissions on particle production in the marine environment and to understand the size distribution of primary marine emissions" (lines 693-698).

RC15: Also, why the ship emission effect (Figure 7 and 8) is the highest for the high biological
period, discuss the observed seasonality in detail.

AC15: We revised the text to comment more clearly on the seasonality of the ship effects. The text states, "Ships enhance oxidant levels, which promote formation of biogenic aerosol precursors such as sulfuric acid and MSA that arise from oxidation of DMS. Condensing vapors of marine origin (such as DMS products and MSOA precursors) can also help to grow particles arising from ship emissions to sizes large enough to interact directly with radiation. As a result, the largest DRE attributed to ship emissions is during the phytoplankton bloom maxima" (lines 795-800).

The text related to the AIE was also revised to include the following discussion, "Ship emissions enhance the oxidation rate of DMS, such that the largest AIE attributed to ships occurs during the phytoplankton bloom due to increased particle formation/growth during this season" (lines 839-841).

RC16: How do you explain ship effects over continents?

AC16: We added the following discussion related to effects over the continents. "Figure 7 also suggests that ship emissions could contribute to the DRE over the continents. This effect occurs because ship emissions include both particle precursors, oxidants, and primary particles that are transported and interact with continental pollution to form and grow particles to sizes that can interact with radiation over the continents as well as over the oceans" (lines 800-804).

RC17: High AIE effect (lines 693-695) might as well point to over-prediction of ship influence rather than location-dependence? This would explain better agreement with measurements in Figure 2 when Ship emissions were not included?

AC17: We revised the text to indicate that noSHIPS agrees more closely with the measurements than BASE in some seasons as related to Fig 2, "Table 2 shows that during the phytoplankton bloom and March/April accumulating phase, the noSHIPS simulation agrees more closely with the measurements than the BASE simulation, although both are within acceptable agreement (MFE < 0.5) (lines 693-695)".

As a result, Fig. 2 does not provide conclusive support that the ship emissions are over predicted. As noted in AC15, this stronger regional AIE compared to the global mean could be related to the interaction of the ship emissions with the products of the phytoplankton bloom maxima in this region. However, as acknowledged in AC14, there were simulation challenges related to ship emissions, which require future study.

RC18: Specific comments: Figure 4: noABLNUC is not visible in some panels, e.g. bottom and middle panels in the right column, please adjust colours or patterns.

AC18: In response to this comment, we have revised Fig. 4 to more clearly identify simulation noABLNUC by adding square symbols to the plot for ABLNUC. Other figures were also revised for consistency. Thank you for noting this problem with visibility.

RC19: Ship measurements do not cover particles smaller than 20nm, how can Figure 4 show the concentrations down to the ground level? Surely the aircraft could not have measured at these low altitudes. Were the measurements extrapolated then? How reliable are these extrapolations?

AC19: To address this concern we revised the caption of Fig. 4 to clarify that these profiles do show aircraft measurements, not ship measurements. We also added details about the aircraft flight altitudes and the method used for binning of the measurements by altitude as quoted in AC3. The reliability of the measurements is supported by this additional discussion regarding our methodology.

AC20: Similarly, for Figure 5, how do composition measurements extend to the ground? Provide details on the extrapolation in the method section

AC20: Thank you for noting the need for greater clarity in the discussion about the methodology for production of the vertical profile figures. These details are added to the revised text as noted in AC3-AC5. Also, the caption for Fig. 5 was revised to clarify the binning resolution used.

RC21: How the total number in figure 3 over August/September can be reconciled with Figure 4 data for the same phase for N10. N20 from fig 3 shows higher concentrations near the ground with reducing trend towards boundary layer top, which would resemble what is expected for a winter boundary layer with sea salt contributions, but N10 shows the opposite trend. Explain this in more details.

AC21: The SMPS (Fig. 3) and CPC (Fig. 4) were operated during similar times, but there were some differences in the times of data availability from the SMPS and CPC that could contribute to the differences between these 2 figures. However, for all model-measurement comparisons, the model was only sampled at times when a measurement from the respective instrument was available. This is now clarified in the method with the following revised text, "We use a plane-flight diagnostic in the model to sample the simulation interpolated between grid-cell centers to

the aircraft-flight-track position during the times when measurement data was available for each respective instrument" (lines 379-382).

Response to Anonymous Referee #2

The authors thank Anonymous Referee #2 for this constructive review. The following point-by-point responses indicate how we have addressed each of the referee's concerns. All referee comments are in black bold text, preceded by RC. Author comments are in blue italics and preceded by AC. All line numbers quoted below refer to the manuscript version without markups.

RC: The paper by Croft et al. provides an assessment of size distributions and it's controls over the Northwest Atlantic Ocean. Climate effects of selected processes are included as forcings, both direct and 1st indirect effect. The work is very valuable: marine aerosol background, especially aerosol size distribution, is not well constrained in climate models. While the analysis in the manuscript is rather standard, the paper is generally well written and results are presented in a clear way. Below are detailed comments on selected issues with the research itself. Some issues listed below should become more clear in the revised manuscript.

AC: Thank you for these comments. In response to this review, we have conducted revisions that improve the clarity of the presentation, strengthening the manuscript. Details are provided in our point-by-point responses below.

RC1: The study applies activation-type nucleation (l. 265) with linear function of sulfuric acid concentrations. The empirical activation nucleation coefficient (A=2*10^6 s-1) is retrieved in continental environments, and is known to include high variability even over land. As discussed in the same paragraph (l. 275), the role of marine organic compounds in nucleation remains unclear, which also has implications in using continental empirical coefficient A in marine environment. This might be very essential for the study, especially since ABLNUC seems to produce a significant AIE (Fig. 8).

AC1: Thank you for this comment about the empirical nucleation coefficient. We revised the manuscript to include the following discussion, "As well, the coefficient that we used for the surrogate activation-style nucleation parameterization was derived for a continental environment. The empirical ('A') value used by the parameterization appears to yield excessive NPF for the NAAMES marine environment. Activation-style nucleation was added in our simulations as a proxy for missing nucleation when the condensation sink is low, and conditions favor high oxidation rates. We acknowledge that this approach will miss variability in the timing and rates because it is a surrogate and not exactly the correct mechanism." (lines 519-525).

We also added the following clarification statement related to the AIE, "We caution that both the DRE and AIE calculations represent a relative contribution of the considered factors to climate effects in the North Atlantic. However, further work is needed to gain confidence in the absolute magnitudes. The activation-style nucleation, which we used as a proxy for the unknown nucleation

mechanisms above the marine boundary layer, adds uncertainty to the climate effects of this nucleation. Certainly, if MSOA is contributing directly to NPF, it would increase MSOA's climatic importance. However, we have little knowledge of the MSOA precursor species, their chemical lifetimes, and their role in NPF, so we did not explore these dimensions in the study." (lines 849-857).

Despite the noted uncertainty in activation nucleation coefficient, the revised text now more clearly indicates that simulation BASE (with the activation-type nucleation) yields acceptable model-measurement agreement, "For each season the mean model-measurement MFE across the parameters considered in Figs. 2 to 5 (BASE versus measurements, Table S2) is satisfactory (MFE ranges 0.43 to 0.50)" (lines 492-494). The text also now more clearly indicates that the model performance is unacceptable for noABLNUC, "Without the surrogate activation-style NPF scheme employed near and above the MBL top, the ternary NPF scheme in the MBL in simulation noABLNUC fails to simulate sufficient particle number, although vertical-profile campaign-median ammonium concentrations below 4 km altitude had acceptable agreement with observations (MFE ranges from 0.12 to 0.48, not shown). Figure 4 shows about a one-order-of-magnitude underprediction of N3 below about 2 km for noABLNUC. NoABLNUC has an unacceptable seasonal-mean model-measurement agreement across the measurement set (MFE ranges 0.68 to 0.78, Supplementary Table S2)" (lines 503-510).

The text was also revised to clarify that we consider this surrogate activation-style scheme to be a place-holder until related knowledge gaps are resolved, "The extra nucleation in the lower troposphere with the activation-type parameterization represents particle precursors that could have the same source as sulfuric acid. This approach may not capture the timing and magnitude of the variability in NPF correctly because the vapors participating in this nucleation are likely not just sulfuric acid. Future work is needed to better understand the nature of the nucleating species in the lower troposphere over the oceans" (lines 335-340).

RC2: Also, is the activation-type nucleation really active only between MBL-top and 2 km altitude (l. 265)? Why not through all levels in MBL?

AC2: Yes, in the original manuscript, we only had this nucleation scheme between the MBL-top and 2 km altitude because it was clear that there was an enhancement of N3-10 that we were not capturing in the model. This scheme was added as a proxy for the unknown mechanism. To address the reviewer's question about having the activation mechanism throughout the MBL, we added Supplementary Figs. S5-S8 and Supplementary Table S3. These figures and table show the impact of extending the activation-type nucleation throughout the MBL. This approach leads to over prediction of the particle number, surface area and volume (in the SMPS particle diameter size range of 10-282 nm) in the MBL.

The revised text clarifies that, "Extending the surrogate activation-style parameterization to the surface (Supplementary Figs. S5-S8 and Supplementary Table 3), leads to over prediction of the number of particles with diameters less than 50 nm in the MBL and yields higher MFEs (ranging from 0.20 to 0.56) than for simulation BASE, although the errors were not as large as those for noABLNUC. For the vertical profiles, this extra NPF extended into the MBL yields over prediction of N3, N10, and N3-N10. Aerosol surface area and volume (in the SMPS particle-diameter size

range of 10 nm - 282 nm) were also over predicted during the August/September declining phase, when the simulated temperature-dependent MSOA source was strongest, growing these extra new particles to larger sizes. These challenges highlight the relevance of ongoing research to better understand NPF in the marine environment" (lines 544-553).

We also revised the methods to clarify that all simulations do include nucleation in the MBL, "All simulations include particle nucleation in the boundary layer that is parameterized with the ternary (H_2SO_4-NH_3-H_2O) scheme of Napari et al. (2002), which was scaled by 10^{-5} to better match continental boundary-layer measurements (Westervelt et al., 2013)" (lines 315-317).

RC3: Although large-scale models have typically limited a separate nucleation mechanisms, such as activation-type nucleation to the BL, it seems even more unphysical to limit a mechanism to only a few (not well defined?) regions of the model system. Perhaps another mechanism/parameterization could better account for different regimes in the surface/BL/BL-top/2-km/free troposphere system.

AC3: In this study we tested the impact of added particle nucleation in the lower troposphere over the oceans, between the MBL top and 2 km. This was motivated by the occurrence of the largest measurement N3-N10 concentrations below 2 km (Fig. 4, phytoplankton bloom), and this enhancement being not captured by the model without the added nucleation. The revised text points out that "For the May/June 2016 climax transition (phytoplankton bloom maximum), there are enhancements in observed number concentration (N3, N10 and N3-N10) below about 2 km in the free troposphere, indicating NPF at these altitudes (Fig, 4). The MBL top ranged from about 0.5 to 2 km for the NAAMES cruises (Behrenfeld et al., 2019). The lower free tropospheric region near and above the MBL top is an important region for marine NPF. These altitudes above the MBL clouds are generally very clean, which favors NPF, and strongly sunlit, which favors the photochemical oxidative production of particle precursors for NPF" (lines 441-448).

However, the model-measurement agreement deteriorates when the parameterization was extended through the entire MBL, as indicated by the revised text that is quoted in AC2

We also revised the text to indicate the need for future work to better understand and parameterize NPF at various altitudes in the marine environment, "As well in the summertime, the simulations underpredict N3-N10 concentrations above 2 km, suggesting the need for future work to better understand the NPF processes at these levels, where the binary scheme of Vehkamaki et al. (2002) does not generate sufficient NPF" (lines 525-528).

RC4: The choice and reasoning behind MSOA emission parameters remains nonconclusive.
Five sets of two parameters for MSOA source are simulated, and size distributions are used in constraining the best possible parameter set (e.g. Fig. S1). I do not see that the information compiled in Figs. S1-S4, or even the statistics in Table S1, would convince the chosen source parameters as the best plausible set.

AC4: To address this concern, we revised Supplementary Figures S1-S4 and Supplementary Tables S1 and S2. Figures S1-S4 and Table S1 were revised to include a simulation with no MSOA, and a simulation with the chosen parameterization scaled up by a factor of 10. These revised figures and table provide clarification regarding the choice and reasoning behind the MSOA emission parameterization. This additional information supports that the chosen parameters are the best for the various emission schemes that we tried, have acceptable MFEs. and are physically plausible.

The related discussion to the main text was revised to state, "For the NAAMES MBL size distributions, the annual-mean model-measurement MFEs are acceptable (ranging from 0.23 – 0.38, lowest for BASE) for all temperature-dependent parameterizations that we tested, except for the factor-of-ten scaling up of the BASE MSOA parameterization (simulation 10x(70T-350), Supplementary Table S1, MFE of 0.75) and with the MSOA parameterization removed (simulation noMSOA, Supplementary Table S1, MFE of 0.63). While this source flux is reasonably constrained for our simulations, future work is needed to better understand and parameterize this source" (lines 588-594).

As well, the revised text states, "The vertical profiles are also sensitive to the MSOA parameterization (Supplementary Figs. S2-4). Between noMSOA and the various MSOA parameterizations that we tested, concentrations vary by up to a factor of about 2 for aerosol number (N3, N10, and N3-N10), SMPS-size-range (diameters 10 nm --282 nm) number, surface area, volume and also OM. Simulation noMSOA has relatively greater error in the mean across the entire measurement set for each season (MFE ranges from 0.53-0.68) relative to BASE (MFE ranges from 0.42-0.50) (Supplementary Table S2)" (lines 596-601).

We also added the following discussion about the plausibility of our MSOA parameterization, "Although the chosen MSOA parameterization reasonably represents the observations, major knowledge gaps remain regarding MSOA precursor species and their chemical lifetimes. While the nature of MSOA precursors is not well-understood, recent measurements suggest that these precursors could include a variety of chemical compounds. For example, measurements from the Arctic indicate that the organics in marine aerosols were not typical biogenic SOA but had a long-hydrocarbon chain implying a fatty acid type precursor (Willis et al., 2017). In other marine regions, isoprene (Ciuraru et al., 2015) and carboxylic acids (Chiu et al., 2017) may also be important. Given the limitations of current knowledge and the indications for a variety of MSOA precursors, the improved MFEs for BASE relative to noMSOA provide support for the employed MSOA parameterization" (lines 603-612).

RC5: Considering the amount of additional assumptions for MSOA, e.g. volatility and chemical processing (l. 321) as well as dismissing the effect on NPF, the uncertainty in simulated MSOA
and conclusions on the respective aerosol-cloud effects remains non-satisfactory.

AC5: We agree that there is much more work that needs to be done regarding the role of MSOA in this system. Certainly, if MSOA is contributing directly to NPF, it would increase MSOA's climactic importance. However, we have little knowledge of the MSOA precursor species, their chemical lifetimes, and their role in NPF, so we did not explore these dimensions in the study.

We consider that our study demonstrates acceptable model-measurement agreement for simulation BASE, such that our simulations can be employed to examine the potential role of MSOA on AIE. We added metrics as outlined in AC4 to support our use of simulation BASE, which includes MSOA. We also revised the text to highlight the need for future work as quoted in AC4 (lines 603-612).

As well, we added cautionary words about uncertainty in the magnitude of the AIE as quoted in AC1 (lines 849-857).

We also added the following cautionary statement in the conclusion, "Our study demonstrated acceptable model-measurement agreement for our base simulation, such that our simulations can be employed to examine the potential role and relative importance of the considered factors in the DRE and AIE. However, we caution that, further work is needed to gain confidence in the absolute magnitudes. In particular, the activation-style nucleation, which we used as a proxy for the unknown nucleation mechanism above the marine boundary layer, adds uncertainty to the climate effects of this nucleation" (lines 919-924).

RC6: One key factor when analyzing the role of nucleation or early growth is to constrain the
background aerosol, in this case sea spray aerosol, to have e.g. realistic sink described for NPF. According to l. 298, sea salt emissions are simulated according to Jaeglé et al. (2011). Jaeglé et al. (2011) compares several formulations of sea spray emission. Assuming this refers to the flux as a function of SST, Jaeglé et al. (2011) shows that this decreases global emissions from 5200 to 4600 Tg/yr when compared to Gong (2003), with clear reduction over study area. However, e.g. Regayre et al. (2020) used a massive amount of observations was to constrain a global model with Gong (2003) sea spray flux, and the process indicated that simulated sea spray flux was even a factor of 3 too low. Perhaps this result is not applicable to the study region used here, but some discussion on potential biases could be discussed in model description or in conclusions.

AC6: Thank you for this discussion about the role of sea spray aerosol. We have added an analysis of this species' role. We revised the manuscript and supplement to include additional simulations with no sea spray emissions (noSS) and with 3-fold scaling up of the sea spray emissions (3xSS). This additional analysis related to sea spray is included in the new Sect. 3.6 (lines 719-740).

We also added the following comment to the introduction to more clearly acknowledge potential biases, "Recent studies have highlighted knowledge gaps related to sea spray emissions, particularly as related to the submicron sizes (e.g. Bian et al., 2019; Regayre et al, 2020). Measurement and modeling studies are needed to better understand and simulate the size-resolved contribution of sea spray to the Northwest Atlantic MBL" (lines 87-90).

As well, we added the following text to the model description for clarification about the performance of our simulations, "Sea salt emissions follow Jaeglé et al. (2011). This temperature-dependent parameterization decreases global emissions relative to the Gong (2003)

parameterization. A coupled parameterization for primary organic aerosol from sea spray was not available for our aerosol size-resolved GEOS-Chem-TOMAS simulations, such that some sea spray organics could be misrepresented as sea salt, since all sea spray in our simulations is considered sea salt" (lines 287-291).

We added Supplementary Fig. S10, which shows the simulated sea spray mass concentrations for simulation BASE. The revised text now more clearly indicates that our simulations have a reasonable representation of the sea spray emissions, while commenting on potential biases as follows, "The simulated campaign-median MBL sea spray mass concentrations are within the measurement range of 3-8 μg m^{-3} d^{-1} found by Saliba et al. (2019) (Supplementary Fig. S10), despite the considerable uncertainties related to size-resolved sea spray emissions (e.g. Bian et al., 2019; Regayre et al. (2020)). Regayre et al. (2020) found that global sea spray emissions could be under predicted by a factor of 3 by the Gong (2003) parameterization. We conducted a simulation with factor-of-3 scaling of the sea spray emissions (Supplementary Figs. S11-S14, Supplementary Table S4) and found a decrease in MBL number concentrations, rather than an increase. This reduction occurred because the enhanced condensation sink from the additional sea spray emissions suppressed NPF. Our simulations use the Gong (2003) parameterization with a sea-surface-temperature-based scaling as described by Jaeglé et al. (2011), so are not directly comparable to the Regayre et al. (2020) findings. Nonetheless, these findings highlight the importance of ongoing work to improve size-resolved sea spray emissions parameterizations in models" (lines 727-739).

We added the following discussion related to the DRE attributed to sea spray, "Figure 7 indicates that the strongest calculated DRE is attributed to sea spray, which dominates the aerosol mass loading in the MBL. The sea spray DRE has a maximum during the 2018 March/April accumulating phase, which is a time of frequent synoptic scale storms with strong winds. Stormy conditions prevented the R/V Atlantis from travelling north of 45 ºN during this final NAAMES campaign" (lines 752-756).

We also added the following discussion related to the AIE attributed to sea spray, "In our simulations, sea spray has a lower contribution to aerosol number concentrations, among the factors considered, and as a result has the smallest AIEs. However, recent studies have pointed out that there are knowledge gaps related to the sea spray emissions parameterizations (e.g Bian et al., 2019; Regayre et al., 2020). Future work is needed to gain confidence in the magnitude of the AIE attributed to sea spray" (lines 843-847).

The revised conclusion also notes that, "This strong DRE attributed to sea spray highlights the importance of work to better constrain parameterizations for models" (lines 909-910).

RC7: The simulations are using a very coarse horizontal resolution, 4x5 degrees. Even while the observation/model comparison is using hourly output, there is no discussion on potential biases or sampling issues with large grid-scale.

AC7: Thank you for pointing out this omission. To address this concern, we revised the methods section to include the following discussion about the potential for biases and sampling issues as related to model grid-scale, "To manage computational expense, the simulations are necessarily

at a coarse resolution, which can bias model-measurement comparisons. However, these biases will be lower for remote marine regions such as the NAAMES study region than over land regions, which generally have greater spatial inhomogeneity. Representativeness errors were also reduced by limiting our model-measurement comparisons to campaign-median values" (lines 402-406).

RC8: Is there any horizontal interpolation performed when sampling the model data against flight/ship data?

AC8: Thank you for pointing out the need for clarification about our methodology for sampling the model. We added the following text to clarify the methods that we used for model sampling along the flight tracks, "For consideration of vertical profiles, we binned the measurement and simulation values using a 500 m height resolution, starting from the surface to 500 m as the first bin. Campaign-median values are calculated within each bin and plotted at the mid-point of the bin, starting at 250 m. During NAAMES, the lowest aircraft flight level altitude was around 150-200 m GPS altitude. We use a plane-flight diagnostic in the model to sample the simulation interpolated between grid-cell centers to the aircraft-flight-track position during the times when measurement data was available for each respective instrument. We find consistent results with bin resolutions of 250, 500 and 1000 m, giving support for our selected binning resolution. The vertical profiles show measurements and model output along the aircraft flight tracks only and do not include any measurements or model output for the ship track" (lines 376-385).

We also revised the text to clarify that, "All simulations are sampled coincidentally with the measurements using hourly output along the NAAMES aircraft and ship tracks within the respective model grid box, using the NAAMES campaigns' 1-minute-resolution navigation data" (lines 399-401).

Section 2:

Factors controlling marine aerosol size distributions and their climate effects over the Northwest Atlantic Ocean region

Betty Croft[1], Randall V. Martin[2,1], Richard H. Moore[3], Luke D. Ziemba[3], Ewan C. Crosbie[3,4], Hongyu Liu[5], Lynn M. Russell[6], Georges Saliba[6], Armin Wisthaler[7,8], Markus Müller[7], Arne Schiller[7], Martí Galí[9], Rachel Y.-W. Chang[1], Erin E. McDuffie[1,2], Kelsey R. Bilsback[10], and Jeffrey R. Pierce[10]

[1]Department of Physics and Atmospheric Science, Dalhousie University, Halifax, NS, Canada
[2]McKelvey School of Engineering, Washington University in St. Louis, St. Louis, MO, USA
[3]NASA Langley Research Center, Hampton, VA, USA
[4]Science Systems and Applications, Inc., Hampton, VA, USA
[5]National Institute of Aerospace, Hampton, VA, USA
[6]Scripps Institute of Oceanography, University of California, San Diego, La Jolla, CA, USA
[7]Institute for Ion Physics and Applied Physics, University of Innsbruck, Technikerstrasse 25, 6020 Innsbruck, Austria
[8]Department of Chemistry, University of Oslo, P.O. 1033 – Blindern, 0315 Oslo, Norway
[9]Barcelona Supercomputing Center (BSC)
[10]Department of Atmospheric Science, Colorado State University, Fort Collins, CO, USA
Correspondence to: Betty Croft (betty.croft@dal.ca)

Abstract.

Aerosols over Earth's remote and spatially extensive ocean surfaces have important influences on planetary climate. However, these aerosols and their effects remain poorly understood, in part due to the remoteness and limited observations over these regions. In this study, we seek to understand factors that shape marine aerosol size distributions and composition in the Northwest Atlantic Ocean region. We use the GEOS-Chem-TOMAS model to interpret measurements collected from ship and aircraft during the four seasonal campaigns of the North Atlantic Aerosols and Marine Ecosystems Study (NAAMES) conducted between 2015 and 2018. Observations from the NAAMES campaigns show enhancements in the campaign-median number of aerosols with

diameters larger than 3 nm in the lower troposphere (below 6 km), most pronounced during the phytoplankton bloom maxima (May/June) below 2 km in the free troposphere. Our simulations, combined with NAAMES ship and aircraft measurements, suggest several key factors that contribute to aerosol number and size in the Northwest Atlantic lower troposphere, with significant regional-mean (40-60 ºN, 20-50 ºW) aerosol-cloud albedo indirect effects (AIE) and direct radiative effects (DRE) during the phytoplankton bloom. These key factors and their associated simulated radiative effects in the region include: (1) particle formation near and above the marine boundary layer (MBL) top (AIE: -3.37 W m^{-2}, DRE: -0.62 W m^{-2}), (2) particle growth due to marine secondary organic aerosol (MSOA) as the nascent particles subside into the MBL, enabling them to become cloud-condensation-nuclei-size particles (AIE: -2.27 W m^{-2}, DRE: -0.10 W m^{-2}), (3) particle formation/growth due to the products of dimethyl sulfide, above/within the MBL (-1.29 W m^{-2}, DRE: -0.06 W m^{-2}), (4) ship emissions (AIE: -0.62 W m^{-2}, DRE: -0.05 W m^{-2}) and (5) primary sea spray emissions (AIE: +0.04 W m^{-2}, DRE: -0.79 W m^{-2}). Our results suggest that a synergy of particle formation in the lower troposphere (particularly near and above the MBL top), and growth by MSOA contributes strongly to cloud-condensation-nuclei-sized particles with significant regional radiative effects in the Northwest Atlantic. To gain confidence in radiative effect magnitudes, future work is needed to understand 1) the sources and temperature-dependence of condensable marine vapors forming MSOA, 2) primary sea spray emissions, and 3) the species that can form new particles in the lower troposphere and grow these particles as they descend into the marine boundary layer.

Deleted: total number concentration

Deleted: at atmospheric altitudes of about 1 km

Deleted: are

Deleted: above/

Deleted: and

Deleted: , with a maximum DRE of -1.37 W m^{-2} in the early springtime

Deleted: near the MBL top

Deleted: that

Deleted: F

Deleted: and to understand

Deleted: at the boundary layer top

1. Introduction

Marine atmospheric particles have important roles in Earth's climate system. Similar to particles in other regions, marine aerosols scatter and absorb solar radiation (Charlson et al., 1992), and modify cloud properties by acting as the seeds for cloud droplet formation (Boucher and Haywood, 2000; Lohmann and Feichter, 2005). Aerosols in the atmosphere's marine boundary layer (MBL) strongly influence the highly prevalent, low-altitude marine clouds, which have key climate cooling effects due to their reflection of incoming solar radiation (Wood, 2012; Chen et al., 2014). However, there remains high uncertainty about the magnitude of these aerosol effects (IPCC, 2013), due in part to limited understanding about the processes that control aerosols over Earth's expansive and remote ocean surfaces (Willis et al., 2018). Marine aerosols are strongly influenced

by natural, but poorly understood sources, making a large contribution to uncertainty in aerosol-climate effects (Carslaw et al., 2010; Carslaw et al., 2013). Limited observations of aerosols and their precursors over Earth's remote marine regions contribute to these knowledge gaps. In this study, we focus on investigation of several factors controlling the seasonal cycle of aerosol size and number and their resultant climate effects over the Northwest Atlantic Ocean.

Aerosol particles in the remote MBL have several seasonally varying sources (O'Dowd et al., 2004; Leck and Bigg, 2005; de Leeuw et al., 2011; Karl et al., 2012). Primary particles are emitted through wave breaking and bubble bursting processes that eject sea spray aerosols (SSA) of sea salt and organic composition (Russell et al., 2010; de Leeuw et al., 2011; Ovadnevaite et al., 2011; Gantt and Meskhidze, 2013; Prather et al., 2013; Hamacher-Barth et al., 2016; Brooks and Thornton, 2018). SSA have a not-yet-well-understood dependence on wind speed (Monahan et al., 1983; O'Dowd et al., 1997; Ovadnevaite et al., 2012; Grassian et al., 2015; Brooks and Thornton, 2018; Saliba et al., 2019) and sea surface temperature (Mårtensson et al., 2003; Jaeglé et al., 2011; Kasparian et al., 2017; Saliba et al., 2019). For the North Atlantic, observations indicate that primary SSA make a limited (less than 30%) contribution to cloud condensation nuclei (CCN) (Quinn et al., 2017, Zheng et al., 2018; Quinn et al., 2019) with no direct connection between SSA emissions and plankton ecosystems because the organic SSA appears to arise from the ocean's large pool of dissolved organic carbon (Quinn et al., 2014; Bates et al., 2020). SSA, however, could modify the CCN number that activate to form cloud droplets (Fossum et al., 2020), act as ice nuclei (Wilson et al., 2015; DeMott et al., 2016; Irish et al., 2017), and be more closely linked with biogenic activity in other regions (Ault et al., 2013; Cravigan et al., 2015; O'Dowd et al., 2015; Quinn et al., 2015; Wang et al., 2015; Schiffer et al., 2018; Christiansen et al., 2019; Cravigan et al., 2019). Recent studies have highlighted knowledge gaps related to sea spray emissions, particularly as related to the submicron sizes (e.g., Bian et al., 2019; Regayre et al, 2020). Measurement and modeling studies are needed to better understand and simulate the size-resolved contribution of sea spray to the Northwest Atlantic MBL.

For the North Atlantic, secondary aerosol of biogenic origin is observed to be an important seasonally varying contributor to marine particles and their growth to yield CCN (Sanchez et al., 2018). Marine secondary aerosol can arise from the condensation of a variety of marine-vapor-

oxidation products, which form and grow particles (Ceburnis et al., 2008; Rinaldi et al., 2010; Decesari et al., 2011). Formation of new aerosol particles in the marine environment is observed to be favored in clean atmospheric layers just below the marine inversion and also above the MBL top (Kazil et al., 2011; Takegawa et al., 2020). Newly formed particles, including those from the free troposphere can grow to CCN sizes (diameters larger than about 50 nm) through the condensation of available organic and sulfur-containing vapors on descent into the MBL (Korhonen et al., 2008). Once the particles reach CCN sizes, cloud processing (including aqueous phase aerosol production, and cloud droplet coagulation with other droplets and interstitial aerosols) also contributes to shaping the size distribution (Hoppel et al., 1986; Hoose et al., 2008; Pierce et al., 2015). For the North Atlantic MBL, entrainment of growing new particles formed in the relatively cleaner free troposphere is an important contributor to MBL particle number (Quinn et al., 2017; Sanchez et al., 2018; Zheng et al., 2018). In the pristine conditions of the summertime Arctic, both new particle formation (NPF) and growth (by condensation of organic and sulfur-containing vapors) are frequently observed within the boundary layer itself (Leaitch et al., 2013; Croft et al., 2016a; Willis et al., 2016; Collins et al., 2017; Burkart et al., 2017b). In addition to sulfuric acid, other vapors including amines, methane sulfonic acid (MSA), ammonia, and iodine all contribute to NPF in marine regions (O'Dowd, 2002; Facchini et al., 2008; Allan et al., 2015, Chen et al., 2016; Croft et al., 2016a; Dall´Osto et al., 2018). Interpretation of a combination of aircraft and ship-board observations with a size-resolved aerosol microphysics model is needed to develop understanding of the relative importance of near and above MBL top NPF as a contributor to aerosol size distributions in the Northwest Atlantic MBL.

Deleted: while descending in the MBL

Deleted: e-/

Deleted: near-

Deleted: -

Dimethyl sulfide (DMS) is one of the key contributors to secondary particle formation and growth that is released from the oceans as a result of marine biogenic activity (Lana et al., 2012a; Galí and Simó, 2015; Sanchez et al., 2018). The oxidation products of DMS include sulfuric acid and MSA (Barnes et al., 2006), which can form new particles and grow existing particles to sizes that can act as CCN (Hoffman et al., 2016; Hodshire et al., 2019). As well, hydroperoxymethyl thioformate (HPMTF) is a recently discovered DMS-oxidation product, which could also contribute to NPF and growth (Veres et al., 2020). The role of DMS in the climate system has undergone much debate since 1987 when the CLAW hypothesis proposed that DMS could act as a regulator in a warming

climate (Charlson et al., 1987). For the North Atlantic and Arctic, observations have linked DMS to the formation of aerosols during the times of phytoplankton blooms (Rempillo et al., 2011; Chang et al., 2011; Park et al., 2017; Sanchez et al., 2018; Abbatt et al., 2019; Quinn et al., 2019). As well, modelling studies have supported a role for DMS, linked to phytoplankton blooms, as a contributor to CCN number concentrations in the North Atlantic and Arctic MBLs (Woodhouse et al., 2013; Zheng et al., 2018; Ghahremaninezhad et al., 2019; Mahmood et al., 2019) and Southern Ocean MBL (Korhonen et al., 2008; McCoy et al., 2015; Revell et al., 2019). However, the extent to which DMS can act as a climate regulator remains unclear (Schwinger et al., 2017; Fiddes et al., 2018), and this role has been refuted (Quinn and Bates, 2011). Analysis of in situ observations of DMS and its products across the seasonal cycle of marine biogenic activity and in various ocean regions is needed to improve understanding related to the role of DMS in Earth's climate system.

Marine secondary organic aerosol (SOA) is another important contributor to sub-micron diameter marine aerosols, but is not well characterized (Rinaldi et al., 2010). The oceans are a source of a variety of organic vapors that could lead to SOA formation (O'Dowd and de Leeuw, 2007; Yassaa et al., 2008; Carpenter et al., 2012; Lana et al. 2012b; Hu et al., 2013; Carpenter and Nightingale, 2015; Kim et al., 2017; Rodríguez-Ros et al., 2020a). Oxygenated volatile organic compounds (OVOCs) recently linked to photochemical oxidative processes at the sea surface microlayer are possible contributors to marine SOA (Mungall et al., 2017). Isoprene and monoterpenes appear to make relatively minor contributions to marine SOA by mass, less than 1% for particles with diameters smaller than 10 µm at Cape Grim (Cui et al., 2019). The global, annual source of organic vapors from the oceans is highly uncertain, but current estimates are about 23 to 92 Tg C yr^{-1} (Brüggemann et al., 2018). Laboratory studies indicate that emissions of marine organic vapors increase with both temperature and incident radiation for temperatures up to about 26 °C (Meskhidze et al., 2015). Recent observations and modeling studies support a role for Arctic marine secondary organic aerosol (AMSOA) as a contributor to particle growth to CCN sizes (Burkart et al., 2017a; Collins et al., 2017; Willis et al, 2017; Willis et al., 2018; Tremblay et al., 2018; Leaitch et al., 2018; Croft et al., 2019; Abbatt et al., 2019). For the North Atlantic, organics are also found to make a large contribution to particle growth to CCN sizes (Sanchez et al., 2018; Zheng et al., 2020a). The result of the above-noted processes is a large and complex pool of organic

Deleted: .2

Deleted: 1.9

Deleted: .

aerosol in the marine environment with sources that vary seasonally and regionally (Cavalli et al., 2004; Decesari et al., 2011; Cravigan et al., 2015; Liu et al., 2018; Leaitch et al., 2018).

Anthropogenic activity is also an important source of aerosols over the portions of the Earth's oceans. For the North Atlantic, several previous studies (e.g., Savoie et al., 2002; Stohl et al., 2003; Huntrieser et al., 2005; Fast et al., 2016) found a key role for synoptic scale motions in lifting aerosols arising from North American continental emissions and transporting them in layers over the North Atlantic with intrusions into the MBL. As well, ship traffic is an important source of both particles and oxidants in the MBL (Corbett et al., 2007; Zanatta et al., 2019; Bilsback et al., in press). Ship emissions of nitrogen oxides have a significant control on levels of oxidants such as ozone, the hydroxyl radical (OH) and NO_3 in the MBL (Vinken et al., 2011; Holmes et al., 2014). In the remote MBL, both OH and NO_3 are key oxidants of DMS, along with natural-source halogens such as BrO, with an important role for multiphase chemistry (Chen et al., 2018). Interpretation of aerosol observations across several seasons is needed to better understand the relative contribution of ship emissions to marine particles in the Northwest Atlantic region.

In this study, as part of the Ocean Frontier Institute (www.oceanfrontierinstitute.com), we address the knowledge gaps that were identified above, concerning several key factors shaping Northwest Atlantic MBL aerosol size distributions and their seasonal cycle. We consider the role of (1) new particle formation in clean atmospheric layers near and above the MBL top, (2) particle growth by marine SOA (MSOA) on descent into the MBL, (3) DMS contributions, (4) ship traffic emissions and (5) primary sea spray emissions. Aerosol measurements from the North Atlantic Aerosols and Marine Ecosystems Study (NAAMES) (Behrenfeld et al., 2019) provide an excellent basis for addressing the role of these five factors in the Northwest Atlantic Ocean region. The NAAMES aircraft and ship campaigns were conducted during four phases of the Northwest Atlantic annual plankton cycle from 2015-2018. We interpret the NAAMES aerosol measurements using a state-of-the-science size-resolved global aerosol microphysics model, GEOS-Chem-TOMAS (www.geos-chem.org). Our synergistic approach in bringing together NAAMES measurements and size-resolved aerosol process modeling enables a unique consideration of several key factors shaping Northwest Atlantic MBL aerosol size distributions and their annual cycle. We also quantify the impact of these factors on aerosol radiative effects over the North Atlantic.

Deleted: submitted

Deleted: near/above

Deleted: &

Deleted: and

Deleted: our

The second section provides an overview of our measurement and modeling methodology. The third section presents results using the GEOS-Chem-TOMAS model to interpret NAAMES aerosol measurements and their seasonal cycle with a focus on the roles of near and above MBL top NPF, MSOA, DMS, sea spray, and ship emissions. We also quantify the direct and cloud-albedo indirect aerosol radiative effects attributed to each of these factors during the seasonal cycle. The final section gives our summary and outlook.

Deleted: above/near

Deleted: -

Deleted: -

2. Methodology

2.1 Aerosol measurements during the NAAMES campaigns

NAAMES campaigns were conducted during four key periods in the annual cycle of marine biogenic activity, namely: the winter transition (November 2015), the accumulating phase (March/April 2018), the climax transition (May/June 2016), and the declining phase (August/September 2017) (Behrenfeld et al., 2019). These periods are defined by shifts in net phytoplankton growth rates and span a wide range in phytoplankton biomass, here estimated from chlorophyll-*a* concentrations (Chl-*a*). The winter transition is characterized by the annual minimum in Chl-*a* concentrations (generally < 1 mg m^{-3}) and a shift to favor phytoplankton growth over loss as the increasing ocean mixed-layer depth leads to fewer encounters between phytoplankton and their grazers. The accumulation phase occurs in early springtime when increasing sunlight and decreasing ocean mixed layer depths promote increasing phytoplankton growth rates and concentrations (Chl-*a* between 1 and 2 mg m^{-3}). The climax transition is the time of the annual maximum in phytoplankton biomass (Chl-*a* between 2 and 9 mg m^{-3}) and marks the shift from positive to negative growth rates owing to high grazing rates and depletion of nutrients. The declining phase (Chl-*a* between 1 and 2 mg m^{-3}) occurs later in the summertime when the ocean mixed layer depth increases and incident sunlight decreases, leading to further declines in phytoplankton growth and concentrations. Behrenfeld et al. (2019) provide an overview of the four measurement campaigns, and further details about Chl-*a* during NAAMES. The R/V Atlantis cruise tracks and NASA C130 flight paths are shown in Figure 1. Due to aircraft mechanical problems, there were no flights in 2018 during the accumulating phase.

In this study, we examine the NAAMES size-resolved aerosol measurements (particle diameters 20 to 500 nm) from the Scanning Electrical Mobility Sizer (SEMS, Model 138, 2002, BMI, Hayward, CA) aboard the R/V Atlantis ship. Aerosol particles were isokinetically drawn through an inlet positioned 18 m above sea level (Bates et al. 2002) and were subsequently dried below 20% relative humidity using silica diffusion driers prior to sampling by the SEMS. Clean marine periods were identified with criteria of relative wind directions within 90° of the bow, condensation nuclei number concentrations less than 2000 cm^{-3}, ammonium and organic aerosol not covarying, ammonium < 100 ng m^{-3} and having back trajectories primarily over the ocean surface. We also consider aerosol size-resolved measurements (particle diameters 10 to 282 nm) from the Scanning Mobility Particle Sizer (SMPS, TSI Inc., Shoreview, MN) aboard the C130 aircraft. As well, we give attention to measurements of total particle number concentration from the Condensation Particle Counters (CPCs) with differing nominal lower detection diameters: 3 nm for the CPC 3025 (yielding N3 measurements) and 10 nm for the CPC 3772 (TSI Inc., St. Paul, MN) (yielding N10 measurements) aboard the C130 aircraft. We also consider submicron, non-refractory sulfate ($SO_4^=$) and organic mass (OM) concentrations from an Aerodyne High Resolution Time-of-Flight Aerosol Mass Spectrometer (HR-ToF-AMS, DeCarlo et al., 2006) and refractory black carbon from the Single Particle Soot Photometer (SP2, Schwarz et al., 2006) aboard the aircraft. HR-ToF-AMS and SP2 measurements are restricted to accumulation-mode aerosol (60-600 nm and 105-600 nm diameter, respectively). All aircraft observations are made behind a forward-facing, shrouded, solid diffuser inlet that efficiently transmits particles with aerodynamic diameter less than 5.0 µm to cabin-mounted instrumentation (McNaughton et al., 2007). Cloud-contaminated aerosol observations have been removed using a combination of wing-mounted cloud probe and relative humidity measurements. This filtering may possibly obscure some NPF events in proximity to clouds and remove some cloud-processed samples from the vertical profiles. Aerosol number and mass concentrations are reported at standard temperature and pressure. A Proton-Transfer-Reaction Time-of-Flight Mass Spectrometer (PTR-ToF-MS) (Müller et al, 2014; Schiller, 2018) was used aboard the NASA C-130 to measure volatile organic compounds including DMS and acetonitrile. Both observational and model data for periods where acetonitrile concentrations exceed 200 ppt are filtered out following Singh et al. (2012) to remove significant biomass burning contributions that are not the focus of this study.

Deleted: 0

2.2 GEOS-Chem-TOMAS model description

We use the GEOS-Chem model (v12.1.1) (http://www.geos-chem.org) coupled to the TwO Moment Aerosol Sectional (TOMAS) microphysics scheme (Adams and Seinfeld, 2002; Lee and Adams, 2012; Kodros and Pierce, 2017), with 15 sections, representing particle sizes from 3 nm to 10 µm. All simulations are at a 4° × 5° resolution with 47 vertical levels extending to 0.01 hPa. The meteorological fields are from the GEOS Forward Processing off-line fields (GEOS-FP; https://gmao.gsfc.nasa.gov/GMAO_products/). Our size-resolved aerosol simulations parameterize the processes of particle nucleation, coagulation, condensation, along with wet and dry deposition and include the in-cloud aerosol coagulation scheme of Pierce et al. (2015). Sulfate, organic and black carbon, sea salt, dust and aerosol water are simulated. TOMAS is coupled to the full tropospheric aerosol/chemistry scheme of GEOS-Chem. Wet deposition follows Liu et al. (2001), Wang et al. (2011) and Wang et al. (2014). To represent efficient wet removal by North Atlantic drizzle in October and November, we implement a fixed in-cloud removal efficiency of 0.001 s^{-1} in the lowest 2 km of the model atmosphere over the ice-free ocean and enable wet removal of sulfate and organic aerosol in clouds with temperatures between 237 K and 258 K. In all seasons, we use the GEOS-FP cloud fraction as the precipitation fraction in the model layers where precipitation occurs for a closer connection with the meteorological fields (Croft et al., 2016b; Luo et al., 2019; Luo et al., 2020). Dry deposition uses the resistance in series approach of Wesley (1989). Simulated gas-phase species are also removed by dry and wet deposition as described in Amos et al. (2012).

For emissions, we use the GEOS-Chem v 12.1.1 default setup for gas-phase and primary aerosol emissions. We use emissions from the Community Emissions Data System (CEDS) for global anthropogenic sources of NO_x, CO, SO_2, NH_3, non-methane VOCs, black carbon, and organic carbon, including from international shipping as a source of both primary and secondary particles. Primary particles are emitted with a lognormal distribution (Lee et al., 2013). The most recent CEDS emissions dataset extends to the year 2017, as described in McDuffie et al. (2020). In this work, monthly CEDS emission totals for each compound are spatially gridded by source sector, according to the 0.1° × 0.1° gridded EDGAR v4.2 emissions inventory (EC-JRC/PBL, 2012) and population, as described in Hoesly et al. (2018). To account for in-plume chemical processing of

Deleted: in this study

Deleted: All simulations in this study include pParticle nucleation in the boundary layer that is parameterized with the ternary (H_2SO_4-NH_3-H_2O) scheme of Napari et al. (2002), which was scaled by 10^{-5} to better match continental boundary-layer measurements (Westervelt et al., 2013). T and the binary (H_2SO_4-H_2O) scheme of Vehkamaki et al. (2002) is employed in the free troposphere at low NH_3 concentrations. Growth and loss of particles smaller than 3 nm are approximated following Kerminen et al. (2004). In our simulations, aAs a surrogate for unparameterized processes in the lower free troposphere and near the MBL top, we also employ an activation-type nucleation parameterization from the MBL top to about 2 km altitude. This activation-type scheme parameterizes nucleation rates as a linear function of sulfuric acid concentrations, using an empirical factor ($A = 2 \times 10^{-6}$ s^{-1}) (Kulmala et al., 2006; Sihto et al., 2006), and serves as a proxy representing severalthe following unknown/unparameterized mechanisms related to NPF. Pockets of very clean air with low condensation sink near MBL clouds, which favor new particle formation (Kazil et al., 2011), are not resolved by large-scale models such as ours, with grid boxes on the scale of 100s km^2. Efficient wet removal by drizzling MBL clouds contributes to these pristine conditions (Wood et al., 2017). As well, MBL clouds reflect ultraviolet (UV) radiation and create pockets of enhanced UV, which favors photochemical production of aerosol precursor vapors (Weber et al., 2001; Wehner et al., 2015), and are not resolved by our model. Additionally, the particle nucleating capacity of MSOA is unclear and particle formation parameterizations are not yet developed to represent NPF when several gas-phase precursors interact. These precursors include, but are not limited to, MSA (Chen et al., 2016), HPMTF (Veres et al., 2020), amines (Facchini et al., 2008), iodine (Allan et al., 2015), and other extremely low-volatility organic compounds (ELVOCs) (Riccobono et al., 2014). The extra nucleation in the lower troposphere with the activation-type parameterization represents particle precursors that could have the same source as sulfuric acid. This approach may not capture the timing and magnitude of the variability in NPF correctly because the vapors participating in this nucleation are likely not just sulfuric acid. Future work is needed to better understand the nature of the nucleating species in the lower troposphere over the oceans.¶
¶
¶

ship emissions, we use the PARANOX scheme of Holmes et al. (2014). CEDS emissions are overwritten over the United States by the National Emissions Inventory (NEI11) with updated scale factors for our simulation years (2015-2018). We calculated these factors based on emission data for these years from the United States Environmental Protection Agency. Over Canada, we use the Air Pollutant Emissions Inventory (APEI). The Global Fire Emissions Database (GFED4s) is used for biomass burning emissions (van der Werf et al., 2017) for the years 2015-2016, with GFED4s climatological values for 2017 and 2018 since exact-year emissions were not available when we conducted our simulations. Dust emissions are from the scheme of Zender et al. (2003). Sea salt emissions follow Jaeglé et al. (2011). This temperature-dependent parameterization decreases global emissions relative to the Gong (2003) parameterization. A coupled parameterization for primary organic aerosol from sea spray was not available for our aerosol size-resolved GEOS-Chem-TOMAS simulations, such that some sea spray organics could be misrepresented as sea salt, since all sea spray in our simulations is considered sea salt. Such primary organic emissions are expected to have no seasonal cycle when averaged over the NAAMES region (Bates et al., 2020).

Exchange of DMS between the ocean and atmosphere is parameterized using the default GEOS-Chem parameterization, which follows Johnson (2010), largely based on Nightingale et al. (2000a; 2000b). We use the 8-day mean satellite-retrieval seawater DMS dataset of Galí et al. (2019) developed using the methodology of Galí et al. (2018), for available years (2015 and 2016) for the region north of about 40 °N. The Lana et al. (2011) DMS climatology is used elsewhere. Terrestrial biogenic emissions are from MEGAN2.1 as described in Guenther et al. (2012). Following Croft et al. (2019), we add a source of MSOA coupled to the simple SOA scheme described in Pai et al. (2020). Emissions of MSOA-precursor vapors have been found to increase with temperature (Meskhidze et al., 2015; Rodríguez-Ros et al., 2020a; Rodríguez-Ros et al., 2020b). Here, we use a temperature-dependent simulated source of MSOA-precursor emissions (S_{MSOA}), S_{MSOA} = 70T + 350 μg m^{-2} d^{-1}, where T is atmospheric temperature (°C) at 2 m altitude. The values of 70 and 350 are found to yield acceptable model-measurement agreement for NAAMES campaign-median ship-track and aircraft measurements (Supplementary Figs. S1-S4 and Supplementary Tables S1 and S2). This simulated source of condensable vapors is emitted with a 50/50 split between vapors that are immediately available to form MSOA and vapors with 1-day aging prior to availability

Moved (insertion) [2]

Deleted: However, a recent global observation-based study by Regayre etal. (2020) suggested that the Gong (2003) parameterization might under-predict sea spray emissions by a factor of three. As result, the employed sea spray emissions could be biased low.

Moved up [2]: Dust emissions are from the scheme of Zender et al. (2003).

Deleted: ¶

Deleted: kg m^{-2} d^{-1}

Deleted: the

Deleted: aerosol size distributions

Deleted: The selected parameterization also yielded agreement generally within the 25th to 75th percentiles of measurements in the lowest 1 km of the atmosphere for the campaign-median vertical profiles of total aerosol number (diameters larger than 3 nm, 10 nm, and between 3 and 10 nm) and integrated SMPS number, as well as in the near-surface OM concentrations (Figs. S2-S4).

(and not susceptible to wet removal). MSOA contributes to particle growth in our simulations (in agreement with observational-based studies e.g., Sanchez et al., 2018; Zheng et al., 2020a), along with sulfuric acid, but since the particle nucleating abilities of MSOA are unclear, it does not contribute to new-particle formation.

All simulations include particle nucleation in the boundary layer that is parameterized with the ternary (H_2SO_4-NH_3-H_2O) scheme of Napari et al. (2002), which was scaled by 10^{-5} to better match continental boundary-layer measurements (Westervelt et al., 2013). The binary (H_2SO_4-H_2O) scheme of Vehkamaki et al. (2002) is employed in the free troposphere at low NH_3 concentrations. Growth and loss of particles smaller than 3 nm are approximated following Kerminen et al. (2004). In our simulations, as a surrogate for unparameterized processes in the lower free troposphere and near the MBL top, we also employ an activation-type nucleation parameterization from the MBL top to about 2 km altitude. This activation-type scheme parameterizes nucleation rates as a linear function of sulfuric acid concentrations, using an empirical factor ($A = 2 \times 10^{-6}$ s^{-1}) (Kulmala et al., 2006; Sihto et al., 2006), and serves as a proxy representing several unknown/unparameterized mechanisms related to NPF. Pockets of very clean air with low condensation sink near MBL clouds, which favor new particle formation (Kazil et al., 2011), are not resolved by large-scale models such as ours, with grid boxes on the scale of 100s km^2. Efficient wet removal by drizzling MBL clouds contributes to these pristine conditions (Wood et al., 2017). As well, MBL clouds reflect ultraviolet (UV) radiation and create pockets of enhanced UV, which favors photochemical production of aerosol precursor vapors (Weber et al., 2001; Wehner et al., 2015), that are not resolved by our model. Additionally, the particle nucleating capacity of MSOA is unclear and particle formation parameterizations are not yet developed to represent NPF when several gas-phase precursors interact. These precursors include, but are not limited to, MSA (Chen et al., 2016), HPMTF (Veres et al., 2020), amines (Facchini et al., 2008), iodine (Allan et al., 2015), and other extremely low-volatility organic compounds (ELVOCs) (Riccobono et al., 2014). The extra nucleation in the lower troposphere with the activation-type parameterization represents particle precursors that could have the same source as sulfuric acid. This approach may not capture the timing and magnitude of the variability in NPF correctly because the vapors participating in this nucleation are likely not just sulfuric acid. Future work is needed to better understand the nature of the nucleating species in the lower troposphere over the oceans.

Formatted: Justified

Deleted: in this study

Formatted: Font color: Text 1

We also conduct off-line radiative transfer calculations using the Rapid Radiative Transfer Model for Global Climate Models (RRTMG) (Iacono et al., 2008) to assess the direct radiative effect (DRE) and cloud-albedo aerosol indirect effect (AIE). The aerosol optical properties are calculated using the Mie code of Bohren and Hoffman (1983) to find the extinction efficiency, single scattering albedo, and asymmetry factor. Then, these optical properties, along with the monthly mean cloud fraction and surface albedo from the GEOS-FP meteorology fields, are input to the RRTMG to determine the change in top-of-the-atmosphere solar flux (DRE) between two simulations (our control simulation and one of the sensitivity simulations, Sect. 2.3). Our DRE calculations follow Kodros et al. (2016), with updates to include ammonium nitrate as described in Bilsback et al. (in press). All particles except black carbon are treated as internally mixed within each size section. We also calculate the cloud-albedo aerosol indirect effect (AIE) as described in Kodros et al. (2016), Croft et al. (2016a) and Ramnarine et al. (2019). The Abdul-Razzak and Ghan (2002) parameterization is used to calculate offline cloud droplet number concentrations (CDNC) using the aerosol mass and number concentrations from our simulations. We assume an updraft velocity of 0.5 m s^{-1} and the hygroscopicity parameters used by Kodros et al. (2016) and Kodros and Pierce (2017), assuming aerosol internal mixture, including ammonium nitrate following Bilsback et al. (in press). For each model grid box, we assume cloud droplet radii of 10 μm and perturb this value with the ratio of the monthly mean CDNC between two simulations (our control simulation and one of the sensitivity simulations, Sect. 2.3), assuming constant cloud liquid water content. The RRTMG is used to calculate the change in the top-of-the-atmosphere solar flux (AIE) due to changes in cloud droplet radii.

As one evaluation of simulation performance, we calculate the mean fractional error (MFE) of the 0^{th} to 3^{rd} moments between the simulated and observed MBL aerosol size distributions, following Boylan and Russell (2006) and using the same methodology as Hodshire et al. (2019) and Croft et al., (2019). The MFE is defined as a mean over the *N* aerosol size distribution moments,

$$\mathrm{MFE} = \frac{1}{N}\sum_{i=0}^{i=N-1}\frac{abs|C_m(i)-C_o(i)|}{(C_m(i)+C_o(i))/2} \quad (1)$$

Formatted: Font color: Text 1

Formatted: Font color: Text 1

Formatted: Font color: Text 1

Deleted: submitted

Deleted: submitted

where $C_m(i)$ is the integrated value of the i^{th} moment of the simulated aerosol size distribution and $C_o(i)$ is the integrated value of the i^{th} moment of the observed aerosol size distribution. The MFE can range from 0 to +2. We adopt the convention of Boylan and Russell (2006) to consider a MFE of 0.5 or less as acceptable.

For consideration of vertical profiles, we binned the measurement and simulation values using a 500 m height resolution, starting from the surface to 500 m as the first bin. Campaign-median values are calculated within each bin and plotted at the mid-point of the bin, starting at 250 m. During NAAMES, the lowest aircraft flight level altitude was around 150-200 m GPS altitude. We use a plane-flight diagnostic in the model to sample the simulation interpolated between grid-cell centers to the aircraft-flight-track position, during the times when measurement data was available for each respective instrument. We find consistent results with bin resolutions of 250, 500 and 1000 m, giving support for our selected binning resolution. The vertical profiles show measurements and model output along the aircraft flight tracks only and do not include any measurements or model output for the ship track. Vertical profile MFEs (Eq. 1) are calculated by summation over the altitude bins.

2.3 Summary of GEOS-Chem-TOMAS simulations

Table 1 summarizes the simulations conducted. Simulation BASE is our control simulation and includes all emissions and process parameterizations described above. We conduct five sensitivity simulations to examine the role of several key factors involved in shaping the aerosol distributions within the NAAMES study region. Simulation noABLNUC is the same as BASE, except without the sulfuric acid-dependent activation-type surrogate nucleation parameterization, which we implemented from the MBL top to about 2 km. Simulation noMSOA is the same as BASE, but without the source of temperature-dependent condensable marine organic vapors, forming MSOA. Simulation noDMS is the same as BASE, but without DMS. Simulation noSHIPS is the same as BASE, but without any ship emissions. Finally, simulation noSS is the same as BASE, but without any primary sea spray emissions. All simulations are sampled coincidentally with the measurements using hourly output along the NAAMES aircraft and ship tracks within the respective model grid boxes, using the NAAMES campaigns' 1-minute-resolution navigation data.

Deleted: A
Deleted: less than
Deleted: is
Deleted: considered
Deleted: (Boylan and Russell, 2006)
Formatted: Font color: Text 1
Formatted: Font color: Text 1
Formatted: Font color: Text 1
Deleted: ¶ ¶
Deleted: our
Deleted: Finally, s

To manage computational expense, the simulations are necessarily at a coarse resolution, which can bias model-measurement comparisons. However, these biases will be lower for remote marine regions such as the NAAMES study region than over land regions, which generally have greater spatial inhomogeneity. Representativeness errors were also reduced by limiting our model-measurement comparisons to campaign-median values.

3. Results and Discussion

3.1 Key features of aerosols observed during NAAMES

Aerosol observations made during the NAAMES campaigns were in four seasons, capturing different stages of the annual cycle of Northwest Atlantic marine biogenic activity (Behrenfeld et al., 2019). Figure 2 shows the campaign-median marine-influenced aerosol size distributions from SEMS (particle diameters 20-500 nm) for the four R/V Atlantis cruises. November 2015 (winter transition, bloom minima) is characterized by the lowest aerosol number concentrations. The peak of the Northwest Atlantic drizzle season occurs at this time, with efficient wet removal of accumulation-sized aerosol (diameters larger than about 50 to 100 nm) (Browse et al., 2012). As well, relative to other the seasons, marine biogenic emissions are low at this time of minimal phytoplankton biomass. The summertime observations during both May/June 2016 (climax transition, phytoplankton bloom maxima) and August/September 2017 (declining phase) are characterized by a weakly dominant Aitken mode (particle diameters < 100 nm). The winter transition (November 2015) and early spring accumulation phase observations (March/April 2018) are characterized by the dominance of accumulation-mode aerosols (particle diameters > 100 nm).

The vertical profiles of campaign-median integrated-SMPS (particle diameters of 10 to 282 nm) observations are shown in Fig. 3. There are several key features of the observed aerosol vertical profiles for the three NAAMES flight campaigns. These profiles exhibit several particle number maxima in the lower free troposphere below 6 km, including below 2 km during the May/June climax transition period. As shown in Fig. 3, aerosol surface area and volume are less at altitudes below about 3 km relative to altitudes above 3 km. This lower particle surface area at these altitudes favors NPF over growth of pre-existing particles as available vapors condense in these relatively

Deleted: .
Deleted: T
Deleted: ¶
Deleted: Bias
Deleted: particularly
Deleted: at about 1 km altitude
Deleted: However, as
Deleted: the
Deleted: have a relative minimum at about 1-2 km
Deleted: L
Deleted: new-particle formation

cleaner atmospheric layers (Kazil et al., 2011). Transport of aerosols (in part associated with continental emissions) contributes to particles in all seasons. Fast et al. (2016) characterized summertime North Atlantic transport layers in the free troposphere associated with synoptic-scale lifting. The late fall (November 2015, Fig.3) is characterized by the lowest aerosol number, surface and volume concentrations, similar to the findings shown in Fig. 2.

Figure 4 shows the vertical-profile campaign-median total particle number concentrations from CPCs, for aerosols with diameters larger than 3 nm (N3), larger than 10 nm (N10), and the difference between the two (N3-N10). For the May/June 2016 climax transition (phytoplankton bloom maximum), there are enhancements in observed number concentration (N3, N10 and N3-N10) below about 2 km in the free troposphere, indicating NPF at these altitudes (Fig. 4). The MBL top ranged from about 0.5 to 2 km for the NAAMES cruises (Behrenfeld et al., 2019). The lower free tropospheric region near and above the MBL top is an important region for marine NPF. These altitudes above the MBL clouds are generally very clean, which favors NPF, and strongly sunlit, which favors the photochemical oxidative production of particle precursors for NPF. Previous studies based on observations from other marine regions have also found a cloud-processed ultra-clean layer with weak condensation/coagulation sinks at about 1 km altitude, where NPF is favored (Kazil et al., 2011; Takegawa et al., 2020). Figure 4 also shows enhancements in the observed N3 and N10 concentrations below 6 km during the declining phase and winter transition (bloom minima). However, the total number concentration enhancements below 2 km are most pronounced during the phytoplankton bloom maximum, suggesting a connection between particle number and the level of marine biogenic activity.

$SO_4^=$ and OM are dominant non-refractory components of the submicron-diameter aerosols, and vertical profiles of campaign-median observations are shown on Fig. 5. During the summertime (May/June 2016, climax transition and August/September 2017, declining phase), the OM contribution exceeds that of $SO_4^=$ at most altitudes up to 6 km. Non-refractory $SO_4^=$ has its peak contribution during the climax transition season. This May/June phytoplankton bloom maxima period is the time of peak observed near-surface atmospheric DMS mixing ratios, as shown in Fig. 6. During the climax transition (bloom maxima), non-refractory $SO_4^=$ concentrations increase towards the surface, suggesting a marine surface source, similar to summertime Arctic marine

Moved (insertion) [1]
Deleted: is evident
Deleted:).
Deleted: at about 4-5 km altitude.
Deleted: This is similar to the altitude of North Atlantic transport layers found by
Moved up [1]: Fast et al. (2016).
Formatted: Left, Don't adjust space between Latin and Asian text, Don't adjust space between Asian text and numbers
Deleted: is a strong
Formatted: Font color: Auto
Deleted: and variability of sub-10 nm particles (N3-N10) between about 1 and 2 km altitude
Deleted: indicating
Formatted: Font color: Auto
Deleted: ,
Deleted: , right column
Deleted: his feature is near t
Deleted: op, which
Formatted: Font color: Auto
Deleted:
Deleted: several
Deleted: near and below 2 km during the summer months (climax transition and
Deleted:). There is a relatively weaker N3, N10 and N3-N10 enhancement at about 2-3 km during the
Deleted: These
Deleted: low-altitude
Deleted: for
Deleted: illustrating
Deleted: the
Deleted: close
Formatted: Font color: Accent 1, English (US)
Commented [RM4]: not at surface during May/June
Deleted: all

profile observations (Willis et al., 2017). Black carbon (BC) concentrations are also shown in Fig. 5 and have several peaks in the free troposphere in all seasons, consistent with a long-range transport source. Maximum BC concentrations are in May/June, likely associated with greater transport of anthropogenic continental pollution and biomass burning during this time, relative to other seasons. Springtime has also been associated with peak BC concentrations in the Arctic due to long-range transport (Sharma et al., 2004; Sharma et al., 2006; Fisher et al., 2010; Wang et al., 2011; Xu et al., 2017). All aerosol mass concentrations in the lowest 2 km of the atmosphere (Fig. 5) are lowest in the November 2015 winter transition, which is a time of efficient wet removal by drizzle (Browse et al., 2012; Wood et al., 2017), diminishing marine emissions due to diminishing phytoplankton biomass, and outbreaks of relatively less polluted polar air advected down the Labrador Strait (Behrenfeld et al., 2019). For the Arctic, the fall season has also been associated with a relative minimum in aerosol number concentrations (Tunved et al., 2013; Croft et al., 2016b).

The GEOS-Chem-TOMAS model (described in Sect. 2.2 and 2.3) is generally able to simulate the above-noted features of the aerosols over the Northwest Atlantic. Simulation BASE captures key aspects of the MBL size distributions including the minimum in aerosol number during the November winter transition, the weakly dominant Aitken mode during the May/June climax transition and August/September declining phase and the maximum in number of accumulation-mode particles (diameters greater than 100 nm) during the March/April accumulation phase, despite errors such as between 20-50 nm (Fig. 2). As well, the BASE simulation captures several lower tropospheric enhancements in particle number concentration, although the simulated altitude for the maximum is sometimes displaced and there are errors in the magnitude (Figs. 3 and 4). In the lowest 2 km of the atmosphere, $SO_4^=$, OM, and BC mass concentrations for simulation BASE are generally within the 25th to 75th measurement percentiles, except for BC and OM underpredictions in May/June 2016, and OM overprediction in November 2015. All simulated $SO_4^=$ presented in this study is non-sea-salt $SO_4^=$. Simulation BASE also captures that the near-surface $SO_4^=$ is greatest during the May/June climax transition and the near-surface OM has its maximum value during the August/September declining phase. For each season the mean MFE across the parameters considered in Figs. 2 to 5 (BASE versus measurements, Supplementary Table S2) is satisfactory (MFE ranges 0.43 to 0.50). In the next four sub-sections, we use the

Deleted: are highest

Deleted: for each NAAMES season

Deleted: peak

Deleted:

Deleted: the

Deleted: by a few 100 m

Deleted: In

GEOS-Chem-TOMAS BASE simulation, relative to a set of sensitivity simulations, to examine the potential of five key factors to shape aerosol size distributions in the Northwest Atlantic during four stages of the annual cycle of marine biogenic activity.

3.2 Role of new particle formation (NPF) in the lower troposphere

Our simulations (BASE relative to noABLNUC, Fig. 4) suggest that NPF near and above the MBL has a strong control on the development of the total particle number (N3) maxima, with peak magnitude during the phytoplankton bloom maxima in layers below 2 km. Without the surrogate NPF scheme employed near and above the MBL top, the ternary NPF scheme in the MBL in simulation noABLNUC fails to simulate sufficient particle number, although vertical-profile campaign-median ammonium concentrations below 4 km altitude had acceptable agreement with observations (MFE ranges from 0.12 to 0.48, not shown). Figure 4 shows about a one-order-of-magnitude underprediction of N3 below about 2 km for noABLNUC. NoABLNUC has an unacceptable seasonal-mean model-measurement agreement across the measurement set (MFE ranges from 0.66 to 0.78, Supplementary Table S2). Figure 3 also shows that NPF near and above the MBL top makes a significant contribution to simulated particle number concentrations for aerosol diameters of 10 to 282 nm in the lower troposphere, most strongly in the summertime (BASE relative to noABLNUC). There is little impact on aerosol mass concentrations for simulation noABLNUC relative to BASE (Fig. 5).

The simulated N3-N10 (Fig. 4) illustrates that representation of NPF is a challenge for models, because there are difficulties capturing the magnitude and altitudes of the N3-N10 maxima. These discrepancies reflect key knowledge gaps related to the species that can form new particles in the marine environment (e.g., Veres et al. 2020). As well, the coefficient that we used for the surrogate activation-style nucleation parameterization was derived for a continental environment. The empirical ('A') value used by the parameterization appears to yield excessive NPF for the NAAMES marine environment. Activation-style nucleation was added in our simulations as a proxy for missing nucleation when the condensation sink is low, and conditions favor high oxidation rates. We acknowledge that this approach will miss variability in the timing and rates because it is a surrogate and not exactly the correct mechanism. As well in the summertime, the

Deleted: our

Deleted: near the MBL top

Deleted: near/above the MBL

Deleted: near 1 km altitude

Deleted: . This is particularly evident when considering the N3-N10 concentrations in May/June (right column, Fig. 4).

Formatted: Font color: Auto

Formatted: Font color: Auto

Formatted: Font color: Auto

Formatted: Font color: Auto

Deleted: As well, n

Deleted: this

Deleted: st 2 km of the atmosphere

Deleted: May/June

Deleted: very

Deleted: great

Deleted: problems arise because there are

simulations underpredict N3-N10 concentrations above 2 km, suggesting the need for future work to better understand the NPF processes at these levels, where the binary scheme of Vehkamaki et al. (2002) does not generate sufficient NPF.

NPF also makes a very strong contribution to the simulated aerosol size distributions within the MBL near the ocean surface (BASE versus noABLNUC, Fig. 2). Although our simulations do include NPF within the MBL, simulated NPF occurs more strongly near and above the MBL top and the resultant particles grow by condensation of available vapors and cloud processing while descending into the MBL. This role for NPF is in agreement with previous studies including those of Clarke et al. (2013), Quinn et al. (2017), and Williamson et al. (2019). As a result, NPF from several altitudes above the ocean surface contributes to the near-ocean-surface particles, with diameters from 20 to 200 nm. NPF does occur in the MBL. However, those levels above the MBL clouds favor oxidative chemistry that yields particle precursors, particularly from the wide-spread and persistent DMS sources in the marine environment (Kazil et al., 2011). Table 2 shows that for all seasons, the surrogate nucleation (simulation BASE, MFEs ranging from 0.04 to 0.33) represents an improvement over simulation noABLNUC (without this surrogate NPF parameterization, MFEs ranging from 0.50 to 0.95).

Extending the surrogate activation-style parameterization to the surface (Supplementary Figs. S5-S8 and Supplementary Table 3), leads to overprediction of the number of particles with diameters less than 50 nm in the MBL and yields higher MFEs (ranging from 0.20 to 0.56) than for simulation BASE, although the errors were not as large as those for noABLNUC. For the vertical profiles, this extra NPF extended into the MBL yields overprediction of N3, N10, and N3-N10 below 1 km in all seasons. Aerosol surface area and volume (in the SMPS particle-diameter size range of 10 nm - 282 nm) were also over predicted during the August/September declining phase, when the simulated temperature-dependent MSOA source was strongest, growing these extra new particles to larger sizes. These challenges highlight the relevance of ongoing research to better understand NPF in the marine environment.

3.3 Role of particle growth by condensing marine organic vapors

Deleted: near/above the MBL top

Deleted: indirect

Deleted: In our simulations

Deleted: near and above the MBL top, then

Deleted: and the N3-N10 concentrations from measurements shown in Supplementary Figs. S15, S17 and S19…

Deleted: the MBL-top

Deleted: process

Deleted: indirectly

Deleted: but measurements suggest that stronger NPF occurs near and above the MBL top (Supplementary Figs. S15, S17 and S19)

Deleted: the MFE is acceptable (< 0.5, following Boylan and Russell, (2006)) with

Deleted:), and BASE

Formatted: Font color: Auto

Formatted: Font color: Auto

Formatted: Font color: Auto

Deleted: ¶

Condensing marine organic vapors forming MSOA are needed in our simulations (in addition to H_2SO_4) for sufficient particle growth to yield satisfactory model-measurement agreement for MBL size distributions (BASE versus noMSOA, Fig. 2). For simulation noMSOA, the model overpredicts the number of particles with diameters smaller than about 30 nm in the MBL. Due to insufficient particle growth of these sub-30 nm particles, the number of particles with diameters between about 30 to 200 nm is underpredicted by more than 50% for simulation noMSOA.

In our simulations, MSOA enables particle growth to CCN sizes (diameters of about 50 nm or larger). After particles reach CCN sizes, cloud processing can also contribute to simulated particle growth towards accumulation-mode particles (diameters of 100-1000 nm) due to aqueous-phase aerosol production. Other cloud processes include coagulation of cloud droplets with each other and with interstitial aerosols (Hoose et al., 2008; Pierce et al., 2015). Our simulations include the latter and aqueous-phase sulfate production. As clouds evaporate, cloud processing leads to development of the 'Hoppel minima' of the MBL aerosol size distributions (Hoppel et al., 1987), which is the minimum aerosol diameter that activates to form a cloud droplet (about 50-70 nm for the observations in Fig. 2). This minimum diameter is smallest in the winter transition (November 2015), suggesting that smaller particles activated under the clean condition of this season relative to the other seasons. As shown by Table 2, simulation noMSOA has an unacceptable annual-mean MFE of 0.63, larger than the MFE of 0.23 for simulation BASE, which includes particle growth due to MSOA.

The nature and flux of marine vapors forming MSOA are not well understood. As a result, we developed a simplistic MSOA parameterization for use in this study, such that the MSOA precursors vapor emissions are an increasing function of temperature. This approach yields a seasonal cycle, and is in agreement with the temperature dependence trend found by previous studies, including Meskhidze et al. (2015), Rodríguez-Ros et al. (2020a) and Rodríguez-Ros et al., 2020b). We find that the simulated NAAMES cruise-track median aerosol size distributions are sensitive to the coefficients used in the parameterization (S_{MSOA} = 70T - 350 $\mu g\ m^{-2}\ d^{-1}$) (Supplemental Figs. S1 and Table S1). For example, varying the temperature sensitivity between 50-100 and the intercept between 300-500 change the simulated number concentration of particles with diameters larger than 50 nm in the MBL by up to a factor of two, with the greatest sensitivity

Deleted: very

Deleted: However, future work is needed to examine the impact of this parameterization on the simulated aerosol number, size and seasonal cycle in other ocean regions. We caution that the current parameterization was developed for the NAAMES study region.

Deleted: kg m^{-2} d^{-1}

during the summertime (Supplemental Fig. S1). For the NAAMES MBL size distributions, the annual-mean model-measurement MFEs are acceptable (ranging from 0.23 – 0.38, lowest for BASE) for all temperature-dependent parameterizations that we tested, except for the factor-of-ten scaling up of the BASE MSOA parameterization (simulation 10x(70T-350), Supplementary Table S1, MFE of 0.75) and with the MSOA parameterization removed (simulation noMSOA, Supplementary Table S1, MFE of 0.63). While this source flux is reasonably constrained for our simulations, future work is needed to better understand and parameterize this source.

The vertical profiles are also sensitive to the MSOA parameterization (Supplementary Figs. S2-4). Between noMSOA and the various MSOA parameterizations that we tested, concentrations vary by up to a factor of about 2 for aerosol number (N3, N10, and N3-N10), SMPS-size-range (diameters 10 nm - 282 nm) number, surface area, volume and also OM. Simulation noMSOA has relatively greater error in the mean across the entire measurement set for each season (MFE ranges from 0.53-0.68) relative to BASE (MFE ranges from 0.42-0.50) (Supplementary Table S2).

Although the chosen MSOA parameterization reasonably represents the observations, major knowledge gaps remain regarding MSOA precursor species and their chemical lifetimes. While the nature of MSOA precursors is not well-understood, recent measurements suggest that these precursors could include a variety of chemical compounds. For example, measurements from the Arctic indicate that the organics in marine aerosols were not typical biogenic SOA but had a long-hydrocarbon chain implying a fatty acid type precursor (Willis et al., 2017). In other marine regions, isoprene (Ciuraru et al., 2015) and carboxylic acids (Chiu et al., 2017) may also be important. Given the limitations of current knowledge and the indications for a variety of MSOA precursors, the improved MFEs for BASE relative to noMSOA provide support for the employed MSOA parameterization.

The near-surface campaign-median climax transition and declining phase OM concentrations are within the 25th to 75th measurement percentiles for simulation BASE, and below the 25th percentile of the observations for simulation noMSOA (Fig. 5). On average over the lowest 2 km of the atmosphere during the May/June climax transition and August/September declining phase, simulation BASE relative to noMSOA indicates that MSOA contributes about 200-400 ng m^{-3} to

Formatted: Font color: Text 1
Formatted: Font color: Text 1
Formatted: Font color: Auto
Deleted: a
Formatted: Font color: Auto
Formatted: Font color: Auto
Formatted: Font color: Auto
Formatted: Font color: Auto
Deleted: -
Formatted: Font color: Auto
Formatted: Font color: Auto
Deleted: The vertical profiles also have a seasonally varying sensitivity of up to a factor of about 2 for aerosol number (N3, N10, and N3-N10), surface area, volume and OM on average in the lowest 2 km of the atmosphere (Supplemental Figs. S2-4).
Deleted: Based on current knowledge, we consider that
Deleted: is physically plausible. However,
Formatted: Font color: Auto
Deleted: , in addition to isoprene
Deleted: (Ciuraru et al. 2015)
Deleted: agreement of our flux within an order of measurement photosensitized isoprene fluxe
Deleted: we consider
Deleted: to be physically plausible

simulated OM. Saliba et al. (2020) suggest that MBL-measurement non-refractory OM during NAAMES clean marine periods provides a good estimate of MSOA. Their seasonal-average non-refractory OM of about 300-400 ng m^{-3} for the 2016 May/June climax transition (phytoplankton bloom maxima) and 2017 August/September declining phase is similar to our model result. This contribution is about 3- to 4-fold greater than the contribution upwards of 100 ng m^{-3} from previous studies, noted in Kim et al. (2017). The model-measurement agreement for OM for 2017 is influenced by significant biomass burning with high altitude emission injections during this time (Zheng et al., 2020b; Saliba et al., 2020). Errors in the simulated emissions due to use of a GFED climatological-year emissions and injection-height errors could account for some of the model-measurement bias at high altitudes. As well, despite our implementation of a filter to remove measurement and model samples with strong in-plume aerosol enhancements during times of high acetonitrile concentrations, some biomass burning influence still affects the presented vertical profiles. Below 500 m altitude, condensing organic vapors yielding MSOA also increase the simulated aerosol surface area and volume by a factor of about 2-3 in all seasons (noMSOA versus BASE, Fig. 3), to be slightly over the 75th percentile of the observations (Fig. 3). Surface area and volume results from the simulation are very sensitive to the size-distribution simulation near the 282 nm diameter cut-off that contributes to differences between these simulations.

Figure 4 demonstrates that MSOA has a feedback on NPF. With lower aerosol surface area and lower condensation sink (noMSOA), the N3 and N3-N10 below 2 km altitude are strongly overpredicted because NPF increases and a lack of growth to larger sizes impacts N3-N10. During November, the N3 and N3-N10 overprediction also occurs at altitudes above 2 km because MSOA has a relatively greater influence on aerosol surface area at those altitudes in this season (Fig. 3). In this less-polluted late fall season, the influence of MSOA is relatively stronger at higher altitudes than in other seasons. Model-measurement agreement improves for N3 and N3-N10 with the addition of MSOA (simulation BASE relative to noMSOA, Fig. 4). Kazil et al. (2011) also found that condensing vapors generate a condensation sink that moderates the level of NPF in the marine environment. As well, recent studies from the Arctic indicate a key contribution to particles from condensing marine organic vapors (Burkart et al., 2017a; Willis et al., 2017; Croft et al., 2019). The impact of MSOA on the simulated N10 vertical profiles is small. The cloud filtering, which

Deleted: submitted

Deleted: submitted

Deleted: ing

we applied to the model and measurement aerosol samples along the flight track, preferentially removes some of the cloud-processed samples, and contributes to this result.

3.4 Role of DMS

Figure 2 shows that DMS also has a control on the simulated MBL aerosol size distributions (BASE versus noDMS) for the four seasons of the NAAMES campaigns. The total simulated number of particles attributed to DMS is lowest during the phytoplankton bloom minima (winter, November 2015) and greater in other seasons. For example, for particle diameters at 40 nm, the DMS-related contribution to the size distribution (Fig. 2) is about 200-300 cm^{-3} in all seasons, except less than 50 cm^{-3} during the bloom minima. Sulfuric acid from the oxidation of DMS has a two-fold role in both NPF and in growing particles. However, as indicated by simulations noABLNUC and noMSOA relative to BASE (Fig. 2), the DMS contribution is in concert with both (1) a source of condensable marine organic vapors and (2) NPF near and above the MBL top. The contribution of DMS to MBL particles is consistent with the findings of many previous studies, including Chang et al. (2011), Ghahremaninezhad et al. (2016), Park et al. (2018), Sanchez et al. (2018), Mahmood et al. (2019), Quinn et al. (2019) and Veres et al. (2020).

Simulation noABLNUC relative to noDMS for the marine-influenced MBL size distributions (Fig. 2) suggests that anthropogenic influences make a contribution as a source of particle-precursor vapors for NPF, in addition to DMS. This relative contribution is particularly strong during the accumulation phase (March/April 2018). In our simulations, anthropogenic SO_2 is oxidized to H_2SO_4 and contributes to the particle precursors for NPF near and above the MBL top (in addition to DMS oxidation products), followed by particle growth on descent into the MBL. As a result, Fig. 2 shows a greater underprediction of aerosol number for simulation noABLNUC versus noDMS.

Figure 6 indicates that the simulated DMS is generally consistent (MFEs ranging from 0.12 to 0.26, Supplementary Table S2) with the observed DMS mixing ratio vertical profiles and their seasonal cycle for the NAAMES campaigns. DMS makes the strongest contribution to simulated sulfate mass concentrations in the lowest 2 km during the May/June climax transition, reducing

Deleted: significant

Deleted: relative impact

Deleted: of

Deleted: greatest

Deleted: e times of greater marine biogenic activity (May/June climax transition and August/September declining phase). …

Deleted: near/above

Deleted: &

Deleted: above/

Deleted: within 10-50% except during climax transition

model-measurement bias from about 40% to 10% (Fig. 5). Figures 3 and 4 suggest that in the lowest 2 km of the atmosphere, DMS contributes to both NPF and particle growth as there are increases in N3, N10, N3-N10, particle surface area and volume for simulations BASE versus noDMS. However, this behavior is co-dependent on conditions favorable to NPF near the MBL top and a source of MSOA.

3.5 Role of ship traffic emissions

Ship emissions are a source of primary and secondary particles, as well as a control on oxidants (Corbett et al., 2010; Vinken et al., 2011; Holmes et al., 2014). Our simulations suggest that ship emissions are also a control on the NAAMES-region MBL marine-influenced aerosol size distributions (Fig. 2, noSHIPS versus BASE). For example, for the simulated summertime MBL size distribution at particle diameters at 40 nm, about 100-200 particles cm^{-3} are attributed to ship emissions (Fig. 2). Table 2 shows that during the phytoplankton bloom and March/April accumulating phase, the noSHIPS simulation agrees more closely with the measurements than the BASE simulation, although both are within acceptable agreement (MFE < 0.5). These simulation challenges highlight the importance of future work to better understand the role of oxidants from ship emissions on particle production in the marine environment and to understand the size distribution of primary marine emissions.

Ship emissions make about a 50% contribution to the simulated sulfate campaign-median near-surface mass concentration in vertical profiles over the NAAMES study region (Fig. 5). For our simulations the impact of ship emissions on particle number is mostly limited to the lowest 2 km. Simulation BASE relative to noSHIPS suggest that about 10% of the N10 in the lowest 500 m of the atmosphere is attributed to ship emissions (Fig. 4). Figure 4 (right column) indicates that among the five factors considered by our sensitivity studies, ship emissions are among the smallest influence on the NPF. Major trans-Atlantic ship traffic routes (Corbett et al. (2007) are included in the NAAMES study region. Enhancements in observed benzene mixing ratios in the MBL relative to other long-lived tracers of anthropogenic emissions such as acetone (not associated with ship traffic) are observational evidence that ship emissions influence the study region (Supplementary Fig. S9).

Deleted: have
Deleted: modest
Deleted:), versus the factors discussed in the previous three sub-sections.
Deleted: our
Deleted: have
Deleted: (Fig. S5)
Deleted: (Fig. S6)

Figure 6 demonstrates that atmospheric DMS mixing ratios are also sensitive to ship emissions. This effect occurs because ship emissions are a control on oxidants in the MBL, and enhance OH and NO_3, which are chemical sinks of DMS. As a result, simulated DMS mixing ratios increase when ship emissions are removed. As ship traffic is expected to change in future years with changes to routes and regulations (Gilgen et al., 2018; Bilsback et al. (in press)), the relative importance of ship emissions in the North Atlantic MBL will likely change.

3.6 Role of sea spray

Figure 2 shows that simulated sea spray acts as a condensation sink in the MBL. Without sea spray emissions, there is an increase in the number of sub-200 nm diameter particles (simulation noSS relative to BASE). However, this relative increase in simulated number is less than that attributed to other factors considered in the previous sections. While not a strong contributor to particle number in our simulations, sea spray is the dominant contributor to aerosol mass.

The simulated campaign-median MBL sea spray mass concentrations are within the measurement range of 3-8 μg m^{-3} found by Saliba et al. (2019) (Supplementary Fig. S10), despite the considerable uncertainties related to size-resolved sea spray emissions (e.g., Bian et al., 2019; Regayre et al. (2020)). Regayre et al. (2020) found that global sea spray emissions could be under predicted by a factor of 3 by the Gong (2003) parameterization. We conducted a simulation with factor-of-3 scaling of the sea spray emissions (Supplementary Figs. S11-S14, Supplementary Table S4) and found a decrease in MBL number concentrations, rather than an increase. This reduction occurred because the enhanced condensation sink from the additional sea spray emissions suppressed NPF. Our simulations use the Gong (2003) parameterization with a sea-surface-temperature-based scaling as described by Jaeglé et al. (2011), so are not directly comparable to the Regayre et al. (2020) findings. Nonetheless, these findings highlight the importance of ongoing work to improve size-resolved sea spray emissions parameterizations in models. The direct radiative effect of this sea spray mass loading is examined in the following section.

Deleted: submitted

Formatted: Font: (Default) Times New Roman, Bold

Formatted: Font: Times New Roman

Formatted: Font: Times New Roman

Formatted: Font color: Auto

Formatted: Font color: Auto

Formatted: Font color: Auto

Formatted: Font color: Auto

Deleted: , although the model-measurement agreement was still acceptable (MFE < 0.5)

Formatted: Font color: Auto

Deleted: Overall

Formatted: Font color: Auto

Formatted: Font: Times New Roman

Formatted: Font: Times New Roman

3.7 Radiative effects attributed to NPF near MBL top, MSOA, DMS and ship emissions

Figure 7 shows the simulated two-month mean direct radiative effect (DRE) attributed to the five factors we consider, (1) NPF near and above the MBL top, (2) MSOA, (3) DMS, (4) ship emissions and (5) primary sea spray emissions and magnitude of the regional-mean DREs over a region of the North Atlantic (40-60 °N, 20-50 °W). We note that the radiative effects attributed to the separate factors are not linearly additive because the factors impact each other non-linearly. For example, turning off either MSOA or nucleation above the boundary layer would shut down the majority of the production of accumulation-mode particles in the MBL (Fig. 2) since these particles require both nucleation and growth. Hence, adding the radiative effects from these two factors would result in double counting some radiative effects. Figure 7 indicates that the strongest calculated DRE is attributed to sea spray, which dominates the aerosol mass loading in the MBL. The sea spray DRE has a maximum during the 2018 March/April accumulating phase, which is a time of frequent synoptic scale storms with strong winds. Stormy conditions prevented the R/V Atlantis from travelling north of 45 °N during this final NAAMES campaign.

The strongest DRE values attributed to the above boundary layer NPF, MSOA, DMS and ship emission factors are during the summer season (climax transition (bloom maxima) and declining phase). This result highlights the link between the level of marine biogenic activity and aerosol climate effects. The second strongest individual DRE is attributed to condensing marine organic vapors, yielding MSOA. In our simulations, MSOA contributes significantly to particle growth to diameters of about 100 to 200 nm, which can then interact directly with radiation (Fig. 2). This effect is greatest in the declining phase because we used a temperature-dependent parameterization and sea surface temperatures are warmest during the late summer. The DRE geographic distribution suggests an increasing role for MSOA towards southern latitudes, again due to the temperature-dependent parameterization. Further work is needed to examine the role of MSOA in the more southerly latitudes as we cannot explicitly test this result across the annual cycle with the NAAMES observations.

Among the factors considered, Figure 7 shows that during the time of the May/June phytoplankton bloom, the aerosols produced and grown by the oxidation products of DMS have the third strongest

Formatted: Font: Bold
Formatted: Normal, No bullets or numbering
Formatted: Font: Bold
Deleted: ly
Deleted: our
Deleted: near/above
Deleted: &
Deleted: and
Moved (insertion) [3]
Deleted: ¶
Deleted: four considered
Moved up [3]: Figure 7 indicates that the strongest calculated DRE is attributed to sea spray, which dominates the aerosol mass loading in the MBL. The sea spray DRE has a maximum during the 2018 March/April accumulating phase, which is a time of frequent synoptic scale storms with strong winds. Stormy conditions prevented the R/V Atlantis from travelling north of 45 °N during this final NAAMES campaign. ¶
Deleted: ¶
¶
Deleted: second

impact on the DRE, greatest over the regions where the bloom is located. The DRE is -0.10 Wm^{-2} over the region between 40-60 ºN and 20-50 ºW during the bloom maxima and diminishes to -0.005 Wm^{-2} during the bloom minima. This simulated impact of DMS relies in part on (1) conditions favoring NPF processes near and above the MBL top, and (2) growth by MSOA as the nascent DMS-related particles descend in the MBL. DMS (similar to MSOA) also contributes to the DRE over the continents as these vapors have a lifetime of about a day in our simulations and can be transported before their oxidation products are available for condensation. Once available for condensation, DMS products and MSOA contribute to growing particles (of both marine and continental origin) to sizes that can interact more strongly with radiation (diameters near 100 -200 nm). Particles arising from DMS grow during transport, and some particles may only reach sizes large enough to interact with radiation when they are over the continents.

The DRE attributed to the near and above MBL top NPF factor (Fig. 7, top row, ABLNUC) is strongest in summertime, during the May/June climax transition (bloom maxima) and August/September declining phase. Summertime is the season of the greatest photochemical production of particle precursors for NPF. In order to contribute to the DRE, this NPF factor acts in synergy with the other factors, particularly DMS as a source of particle precursors and MSOA for particle growth, such that during the May/June climax transition season the DREs for those factors dominate over the NPF factor (ABLNUC, Fig. 7).

The DREs for ship emissions have a similar geographic distribution as those for DMS. In these regions, major international ship traffic routes are coincident with regions of higher biogenic activity, enabling an interaction of biogenic and anthropogenic emissions. Ships enhance oxidant levels, which promote formation of biogenic aerosol precursors such as sulfuric acid and MSA that arise from oxidation of DMS. Condensing vapors of marine origin (such as DMS products and MSOA precursors) can also help to grow particles arising from ship emissions to sizes large enough to interact directly with radiation. As a result, the largest DRE attributed to ship emissions is during the phytoplankton bloom maxima. Figure 7 also suggests that ship emissions could contribute to the DRE over the continents. This effect occurs because ship emissions include particle precursors, oxidants, and primary particles that are transported and interact with continental pollution to form and grow particles to sizes that can interact with radiation over the

Deleted: above/

Deleted: above/near-

Deleted: -

Deleted: , which

continents as well as over the oceans. Figure 6 shows that there is a ship-emission-related control on atmospheric DMS mixing ratios, which increase when the ship-source oxidants are removed.

Figure 8 shows the calculated two-month mean cloud-albedo aerosol indirect effect (AIE) attributed to each of the same five factors that we considered for the DREs. The AIEs are about an order-of-magnitude larger than the calculated DRE for each respective factor with the exception of sea spray. The AIE is strongly controlled by changes to highly reflective MBL clouds, which are in turn very sensitive to the aerosol number concentrations (diameters larger than about 50 to 70 nm that can act as CCN), which are controlled by the MBL-related factors examined here. On the other hand, the DRE is relatively more sensitive to aerosol abundance in mid-tropospheric layers, which are less influenced by the considered processes.

The strongest simulated AIEs for all considered factors are during the May/June climax transition (Fig. 8). There is a strong synergy among all factors that reach their maxima during May/June when the effective combination of sources, photochemistry and particle production/growth processes peak. As well, during summertime, the magnitude of the AIE for all factors is greater in the more northward regions of the North Atlantic relative to more southerly latitudes. These more northerly regions are less influenced by continental pollution and have lower CCN concentrations, coupled with persistent low cloud cover. These conditions make these regions quite sensitive to the factors controlling MBL aerosol size distributions studied here.

In all seasons, we calculated a stronger AIE related to (1) NPF near and above the MBL top (ABLNUC, top row, Fig. 8) and (2) MSOA (contributor to particle growth) than to (1) DMS (2) ship emissions and (3) sea spray emissions. In our simulations, the major source of CCN-sized particles in the North Atlantic MBL during the summer is particle nucleation near and above the MBL top with growth by MSOA. Without either of these factors, the number concentration of CCN-sized particles in the simulations drops dramatically (Fig. 2). Hence, it is unsurprising that the largest simulated AIEs are due to these two factors during the summertime (climate transition and declining phase). The stronger AIEs attributed to NPF near and above the MBL top (Fig. 8, top row, ABLNUC) relative to DMS and ship emissions indicate that near and above MBL NPF in our simulations is controlled not only by the sulfuric acid from the oxidation of DMS or ship

Deleted: . ¶
We caution that these DRE calculations should be viewed as an examination of the relative contribution of the considered factors to climate effects in the North Atlantic. However, further work is needed to gain confidence in the absolute magnitudes.

Formatted: Font color: Text 1

Formatted: Font color: Text 1

Deleted: ly

Deleted: our

Deleted: near/above

Deleted: &

Deleted: and

Deleted: near/above

Deleted: &

Deleted: near/above

Deleted: &

Deleted: near/above

Deleted: &

Deleted: -

SO_2, but also arising from other sources, including SO_2 transported from continental sources. However, the maximum North Atlantic regional-mean AIE attributed to ship emissions (-0.62 W m^{-2} for the May/June climax transition) still exceeds the global mean effect of -0.155 W m^{-2} attributed to international shipping calculated by Jin et al. (2018), showing the strong location-dependence and seasonality of this factor. Ship emissions enhance the oxidation rate of DMS, such that the largest AIE attributed to ships occurs during the phytoplankton bloom due to increased particle formation/growth during this season.

In our simulations, sea spray has a lower contribution to aerosol number concentrations, among the factors considered, and as a result has the smallest AIEs. However, recent studies have pointed out that there are knowledge gaps related to the sea spray emissions parameterizations (e.g Bian et al., 2019; Regayrre et al., 2020). Future work is needed to gain confidence in the magnitude of the AIE attributed to sea spray.

We caution that both the DRE and AIE calculations represent a relative contribution of the considered factors to climate effects in the North Atlantic. However, further work is needed to gain confidence in the absolute magnitudes. The activation-style nucleation, which we used as a proxy for the unknown nucleation mechanisms above the marine boundary layer, contributes uncertainty to the climate effects of this nucleation. There is much more work that needs to be done regarding the role of MSOA in this system. Certainly, if MSOA is contributing directly to NPF, it would increase MSOA's climatic importance. However, we have little knowledge of the MSOA precursor species, their chemical lifetimes, and their role in NPF, so we did not explore these dimensions in the study. Like the DRE estimates, the separate AIEs are not linearly additive. Other aerosol indirect effects related to changes in cloud lifetime and precipitation are the subject of future work. In summary, these calculated DREs and AIEs suggest that aerosol-climate impacts for North Atlantic regions are controlled by a combination of strong biogenic and anthropogenic influences and that the nucleation near and above the MBL top contributes to important radiative effects.

4. Conclusions

Deleted: ¶

Deleted: Similar to the DRE, we consider that these AIE calculations indicate the relative importance of the considered factors, further work is needed to gain confidence in the absolute magnitudes.

Deleted: near/above

Deleted: &

Deleted: ¶

In this study, we examined aerosol size distribution and composition measurements from the NAAMES campaigns. These ship and aircraft campaigns took place over four separate stages of the annual cycle of marine biogenic activity in the Northwest Atlantic during 2015-2018. We used the GEOS-Chem-TOMAS model with size-resolved aerosol microphysics to interpret these NAAMES measurements. Observations in layers of the lower troposphere below 6 km showed enhancements in the campaign-median number concentration of particles with diameters between 3-10 nm. These enhancements indicated new particle formation, and were most pronounced during the May/June 2016 climax transition (phytoplankton bloom maxima) in the lowest 2 km of atmosphere, particularly near and just above the boundary layer top. This lower tropospheric region near and above the MBL top is a key region for marine NPF. This zone above the MBL clouds is generally very clean, which favors both NPF and strongly sunlit, which favors the photochemical oxidative production of particle precursors for NPF. The November 2015 winter transition (phytoplankton bloom minima) was characterized by the lowest particle number concentrations. During the summer months, OM, followed by sulfate mass concentrations made strong contributions the total aerosol loading in the lowest 2 km. However, sea spray dominated the MBL aerosol mass loading. Peak near-surface sulfate concentrations occurred in May/June during the phytoplankton bloom, whereas peak near-surface OM concentrations were in August/September. Campaign-median MBL aerosol size distributions were dominated by Aitken mode particles (diameters 10-100 nm) during the summertime (May/June climax transition and August/September declining phase). The larger accumulation mode particles were dominant in the November winter transition and March/April accumulation phase.

Our simulations suggested that a synergy of key factors contributed to Northwest Atlantic MBL aerosol size distributions, including (1) new particle formation near and above the MBL top; (2) growth of the newly formed particles by condensation of marine organic vapors, forming marine secondary organic aerosol (MSOA), which yields more abundant CCN-sized particles that descend into the MBL while continuing to grow and being subject to cloud processing (e.g., aqueous-phase aerosol production, which does not add to particle number); (3) DMS-oxidation products that contribute to particle formation and growth; (4) ship emissions, which are a source of primary and secondary particles and also contribute to atmospheric oxidants and (5) sea spray emissions, which also provide a condensation sink that suppresses particle formation. These findings are in

Deleted: tot

Deleted: al aerosol number concentrations (

Deleted: ,

Deleted: as well as greater than 3 and 10 nm) and variability near 1 km altitude,

Deleted: ive of

Deleted:

Formatted: Font color: Auto

Formatted: Font color: Text 1

Formatted: Font color: Text 1

Deleted: dominated

Deleted: (NPF)

Deleted: near/above

Deleted: &

Deleted: ,

Deleted: ,

Deleted: ,

Deleted: and

agreement with previous observational-based studies for the North Atlantic region (e.g., Sanchez et al., 2018; Zheng et al., 2020)

We calculated the aerosol direct (DRE) and cloud-albedo indirect (AIE) radiative effects over the North Atlantic attributed to five key factors controlling MBL aerosols. The cooling effects were about a factor of 10 larger for the AIEs than the respective DREs except for sea spray, which dominated the DRE. The strong AIE response was attributed to the strong sensitivity of the MBL cloud reflectivity to the MBL-related factors that we examined. Mid-tropospheric aerosol (altitude of transport of continental pollution) has a strong impact on the DRE and the factors that we considered had less impact at these altitudes. The maximum regional-mean (40-60 ºN, 20-50 ºW) DRE for our simulations was -1.37 W m^{-2}, attributed to sea spray during the March/April accumulating phase, which is a time of strong synoptic-scale storms in the Northwest Atlantic, enhancing wind-generated sea spray. This strong DRE attributed to sea spray highlights the importance of work to better constrain parameterizations for models. The second strongest DRE was connected to the temperature-dependent source of MSOA, which had a key role in growing simulated particles to large enough (diameters of 100-200 nm) to strongly reflect incoming solar radiation. The maximum AIE was -3.37 W m^{-2}, for the May/June climax transition phase (peak phytoplankton bloom). This AIE was related to the role MSOA in growing new particles to CCN sizes as they descend into the MBL and are subject to further growth in clouds after their formation near the MBL top. The AIE attributed to the NPF factor was nearly as large (-2.27 W m^{-2}) during May/June. The NPF and MSOA factors act in concert with each other and removal of either of these factors contributed to shutdown the production of cloud-condensation-nuclei-size particles. Our study demonstrated acceptable model-measurement agreement for our base simulation, such that our simulations can be employed to examine the *potential* role and relative importance of the considered factors in the DRE and AIE. However, we caution that further work is needed to gain confidence in the absolute magnitudes. In particular, the activation-style nucleation, which we used as a proxy for the unknown nucleation mechanism above the marine boundary layer, adds uncertainty to the climate effects of this nucleation

This study highlighted the importance of processes connected to both marine biogenic activity and anthropogenic activity in controlling aerosol size distributions in the Northwest Atlantic MBL. We

Deleted: our

Deleted: 0.26

Deleted: for

Deleted: August/September declining phase

Deleted: ot

Deleted: is

Deleted: Although o

Deleted: control

Deleted: ,

Deleted: . However,

Deleted: ,

identified key factors, which could be the focus of future work. Particularly, work is needed to better understand the nature, flux, and chemistry of marine organic vapors that can form MSOA. As well, work is needed to better understand the contributors to NPF near and above the MBL top. Further work is also needed to understand the interactions of the considered factors with cloud processing of aerosols and its relative importance in particle growth. As the Earth's climate changes and shipping traffic/regulations/routes change, work to understand the source strength of DMS, MSOA, shipping and sea spray emissions is highly relevant. Such work will bridge the knowledge gaps related to factors controlling aerosols in the marine MBL and their climate impacts.

Code and data availability. The NAAMES project website is at https://naames.larc.nasa.gov. The NAAMES airborne and ship datasets used in this paper are publicly available and permanently archived in the NASA Atmospheric Science Data Center (ASDC; https://doi.org/10.5067/Suborbital/NAAMES/DATA001) and the SeaWiFS Bio-Optical Archive and Storage System (SeaBASS; https://doi.org/10.5067/SeaBASS/NAAMES/DATA001). The ship datasets generated during and analyzed for NAAMES studies are also available in the UCSD Library Digital Collection repository, https://doi.org/10.6075/J04T6GJ6. The GEOS-Chem model is freely available for download at https://github.com/geoschem/geos-chem (last access 19 July 2020).

Supplement link.

Author contributions. BC, RVM and JRP designed the study. BC conducted the GEOS-Chem-TOMAS simulations, led the related analysis, and wrote the manuscript with contributions from all coauthors. RHM, ECC, and LDZ contributed the aerosol measurements from aboard the NASA C130 aircraft. AW, MM and AS contributed the gas-phase measurements from aboard the NASA C130 aircraft. LMR and GS contributed the aerosol measurements from aboard the R/V Atlantis. RYWC and HL contributed to the interpretation of model-measurement comparisons. EEM contributed the CEDS data set. KRB contributed to the off-line radiative calculations, MG contributed the satellite DMS data set.

Deleted: and

Competing interests. The authors declare that they have no conflict of interest.

Acknowledgements. BC, RVM and RYWC acknowledge research funding provided by the Ocean Frontier Institute, through an award from the Canada First Research Excellence Fund. JRP and KRB acknowledge funding support from the Monfort Excellence Fund, and the US Department of Energy's Atmospheric System Research, an Office of Science, Office of Biological and Environmental Research program, under grant DE-SC0019000. LMR and GS acknowledge funding support from NASA grant NNX15AE66G. RHM, ECC, LDZ, LMR, and GS acknowledge funding support from the NASA NAAMES EVS-2 project. HL acknowledges funding support from the NASA NAAMES mission and the National Institute of Aerospace's IRAD program. DMS measurements aboard the NASA C-130 during NAAMES were supported by the Austrian Federal Ministry for Transport, Innovation and Technology (bmvit) through the Austrian Space Applications Programme (ASAP) of the Austrian Research Promotion Agency (FFG). MM's participation in NAAMES 2016 was funded by the Tiroler Wissenschaftsfonds (grant # UNI-0404/1895). AS's participation in NAAMES 2017 was partly funded by National Institute of Aerospace (Task No 80LARC18F0031). MG acknowledges funding support from the Natural Sciences and Engineering Research Council of Canada through the NETCARE project of the Climate Change and Atmospheric Research Program. Tomas Mikoviny is acknowledged for technical support; Ionicon Analytik is acknowledged for instrumental support

References.

Abbatt, J. P. D., Leaitch, W. R., Aliabadi, A. A., Bertram, A. K., Blanchet, J.-P., Boivin-Rioux, A., Bozem, H., Burkart, J., Chang, R. Y. W., Charette, J., Chaubey, J. P., Christensen, R. J., Cirisan, A., Collins, D. B., Croft, B., Dionne, J., Evans, G. J., Fletcher, C. G., Galí, M., Ghahremaninezhad, R., Girard, E., Gong, W., Gosselin, M., Gourdal, M., Hanna, S. J., Hayashida, H., Herber, A. B., Hesaraki, S., Hoor, P., Huang, L., Hussherr, R., Irish, V. E., Keita, S. A., Kodros, J. K., Köllner, F., Kolonjari, F., Kunkel, D., Ladino, L. A., Law, K., Levasseur, M., Libois, Q., Liggio, J., Lizotte, M., Macdonald, K. M., Mahmood, R., Martin, R. V., Mason, R. H., Miller, L. A., Moravek, A., Mortenson, E., Mungall, E. L., Murphy, J. G.,

Namazi, M., Norman, A.-L., O'Neill, N. T., Pierce, J. R., Russell, L. M., Schneider, J., Schulz, H., Sharma, S., Si, M., Staebler, R. M., Steiner, N. S., Thomas, J. L., von Salzen, K., Wentzell, J. J. B., Willis, M. D., Wentworth, G. R., Xu, J.-W., and Yakobi-Hancock, J. D.: Overview paper: New insights into aerosol and climate in the Arctic, Atmos. Chem. Phys., 19, 2527–2560, https://doi.org/10.5194/acp-19-2527-2019, 2019.

Abdul-Razzak, H. and Ghan, S. J.: A parameterization of aerosol activation 3. Sectional representation, J. Geophys. Res., 107, 4026, doi:10.1029/2001JD000483, 2002.

Adams, P. J. and Seinfeld, J. H.: Predicting global aerosol size distributions in general circulation models, J. Geophys. Res., 107, 4370, doi:10.1029/2001JD001010, 2002.

Allan, J. D., Williams, P. I., Najera, J., Whitehead, J. D., Flynn, M. J., Taylor, J. W., Liu, D., Darbyshire, E., Carpenter, L. J., Chance, R., Andrews, S. J., Hackenberg, S. C. and McFiggans, G.: Iodine observed in new particle formation events in the Arctic atmosphere during ACCACIA, Atmos. Chem. Phys., 15(10), 5599–5609, doi:10.5194/acp-15-5599-2015, 2015.

Amos, H. M., Jacob, D. J., Holmes, C. D., Fisher, J. A., Wang, Q., Yantosca, R. M., Corbitt, E. S., Galarneau, E., Rutter, A. P., Gustin, M. S., Steffen, A., Schauer, J. J., Graydon, J. A., St Louis, V. L., Talbot, R. W., Edgerton, E. S., Zhang, Y. and Sunderland, E. M.: Gas-particle partitioning of atmospheric Hg(II) and its effect on global mercury deposition, Atmos. Chem. Phys., 12(1), 591–603, doi:10.5194/acp-12-591-2012, 2012.

Ault, A. P., Moffet, R. C., Baltrusaitis, J., Collins, D. B., Ruppel, M. J., Cuadra-Rodriguez, L. A., Zhao, D., Guasco, T. L., Ebben, C. J., Geiger, F. M., Bertram, T. H., Prather, K. A. and Grassian, V. H.: Size-Dependent Changes in Sea Spray Aerosol Composition and Properties with Different Seawater Conditions, Environ. Sci. Technol., 47(11), 5603–5612, doi:10.1021/es400416g, 2013.

Barnes, I., Hjorth, J. and Mihalapoulos, N.: Dimethyl sulfide and dimethyl sulfoxide and their oxidation in the atmosphere, Chem. Rev., 106(3), 940–975, doi:10.1021/cr020529+, 2006.

Bates, T. S., Coffman, D. J., Covert, D. S., Quinn, P. K.: Regional marine boundary layer aerosol size distributions in the Indian, Atlantic, and Pacific Oceans: A comparison of

Deleted: '

Formatted: Font color: Text 1

INDOEX measurements with ACE-1, ACE-2, and Aerosols99. J. Geophys. Res. Atmos., 107, D19, doi:10.1029/2001JD001174, 2002.

Bates, T. S., Quinn, P. K., Coffman, D. J., Johnson, J. E., Upchurch, L., Saliba, G. and Lewis, S.: Variability in Marine Plankton Ecosystems Are Not Observed in Freshly Emitted Sea Spray Aerosol Over the North Atlantic Ocean, Geophys. Res. Lett., doi:10.1029/2019GL085938, 2020.

Behrenfeld, M. J., Moore, R. H., Hostetler, C. A., Graff, J., Gaube, P., Russell, L. M., Chen, G., Doney, S. C., Giovannoni, S., Liu, H., Proctor, C., Bolaños, L. M., Baetge, N., Davie-Martin, C., Westberry, T. K., Bates, T. S., Bell, T. G., Bidle, K. D., Boss, E. S., Brooks, S. D., Cairns, B., Carlson, C., Halsey, K., Harvey, E. L., Hu, C., Karp-Boss, L., Kleb, M., Menden-Deuer, S., Morison, F., Quinn, P. K., Scarino, A. J., Anderson, B., Chowdhary, J., Crosbie, E., Ferrare, R., Hair, J. W., Hu, Y., Janz, S., Redemann, J., Saltzman, E., Shook, M., Siegel, D. A., Wisthaler, A., Martin, M. Y. and Ziemba, L.: The North Atlantic Aerosol and Marine Ecosystem Study (NAAMES): Science Motive and Mission Overview, Front. Mar. Sci., 6, 122, doi:10.3389/fmars.2019.00122, 2019.

Bian, H., Froyd, K., Murphy, D. M., Dibb, J., Darmenov, A., Chin, M., Colarco, P. R., da Silva, A., Kucsera, T. L., Schill, G., Yu, H., Bui, P., Doliner, M., Weinzierl, B. and Smirnov, A.: Observationally contrained analysis of sea salt aerosol in the marine atmosphere, Atmos. Chem. Phys., 19, 10773-10785, 2019.

Bilsback, K., Kerry, D., Croft, B., Ford, B., Jathar, S. H., Carter, E., Martin, R. V., and Pierce, J. R.: Beyond SO_2 reductions from shipping: Assessing the impact of NOx and carbonaceous particle controls on human health and climate, Environ. Res. Lett., in press https://doi.org/10.1088/1748-9326/abc718, 2020).

Boucher, O. and Haywood, J.: Estimates of the Direct and Indirect Radiative Forcing Due to Tropospheric Aerosols: A Review, Rev. Geophys., 34(4), 513–543, 2000.

Boylan, J. W. and Russell, A. G.: PM and light extinction model performance metrics, goals, and criteria for three-dimensional air quality models, Atmos. Environ., 40(26), 4946–4959, doi:10.1016/j.atmosenv.2005.09.087, 2006.

Formatted: Normal (Web)

Formatted: Font: Times New Roman, 12 pt

Deleted: (in review)

Deleted: ¶

Formatted: Font color: Auto, English (CAN), Check spelling and grammar

Formatted: Font color: Auto

Formatted: Indent: Left: 0 cm, Hanging: 2.54 cm

Deleted: ¶

Formatted: Font color: Auto

Formatted: Normal (Web), Widow/Orphan control, Adjust space between Latin and Asian text, Adjust space between Asian text and numbers

1356 Brooks, S. D. and Thornton, D. C. O.: Marine Aerosols and Clouds, Ann. Rev. Mar. Sci., 10(1),
1357 289–313, doi:10.1146/annurev-marine-121916-063148, 2018.
1358 Browse, J., Carslaw, K. S., Arnold, S. R., Pringle, K. and Boucher, O.: The scavenging processes
1359 controlling the seasonal cycle in Arctic sulphate and black carbon aerosol, Atmos.
1360 Chem. Phys., 12(15), 6775–6798, doi:10.5194/acp-12-6775-2012, 2012.
1361 Brüggemann, M., Hayeck, N. and George, C.: Interfacial photochemistry at the ocean surface is a
1362 global source of organic vapors and aerosols, Nat. Commun., 1–8,
1363 doi:10.1038/s41467-018-04528-7, 2018.
1364 Burkart, J., Hodshire, A. L., Mungall, E. L., Pierce, J. R., Collins, D. B., Ladino, L. A., Lee, A. K.
1365 Y., Irish, V., Wentzell, J. J. B., Liggio, J., Papakyriakou, T., Murphy, J. and Abbatt,
1366 J.: Organic Condensation and Particle Growth to CCN Sizes in the Summertime
1367 Marine Arctic Is Driven by Materials More Semivolatile Than at Continental Sites,
1368 Geophys. Res. Lett., 44(20), 10,725-10,734, doi:10.1002/2017GL075671, 2017a.
1369 Burkart, J., Willis, M. D., Bozem, H., Thomas, J. L., Law, K., Hoor, P., Aliabadi, A. A., Köllner,
1370 F., Schneider, J., Herber, A., Abbatt, J. P. D. and Leaitch, W. R.: Summertime
1371 observations of elevated levels of ultrafine particles in the high Arctic marine
1372 boundary layer, Atmos. Chem. Phys., 17(8), 5515–5535, doi:10.5194/acp-17-5515-
1373 2017, 2017b.
1374 Carpenter, L. J. and Nightingale, P. D.: Chemistry and Release of Gases from the Surface Ocean,
1375 Chem. Rev., 115(10), 4015–4034, doi:10.1021/cr5007123, 2015.
1376 Carpenter, L. J., Archer, S. D. and Beale, R.: Ocean-atmosphere trace gas exchange, Chem. Soc.
1377 Rev., 41(19), 6473–6506, doi:10.1039/c2cs35121h, 2012.
1378 Carslaw, K. S., Boucher, O., Spracklen, D. V., Mann, G. W., Rae, J. G. L., Woodward, S., and
1379 Kulmala, M.: A review of natural aerosol interactions and feedbacks within the
1380 Earth system, Atmos. Chem. Phys., 10, 1701–1737, https://doi.org/10.5194/acp-
1381 10-1701-2010, 2010.
1382 Carslaw, K. S., Lee, L. A., Reddington, C. L., Pringle, K. J., Rap, A., Forster, P. M., Mann, G. W.,
1383 Spracklen, D. V, Woodhouse, M. T., Regayre, L. A. and Pierce, J. R.: Large
1384 contribution of natural aerosols to uncertainty in indirect forcing, Nature, 503, 67
1385 [online] Available from: http://dx.doi.org/10.1038/nature12674, 2013.
1386 Cavalli, F., Facchini, M. C., Decesari, S., Mircea, M., Emblico, L., Fuzzi, S., Ceburnis, D., Yoon,

Y. J., O'Dowd, C., Putaud, J. P. and Dell'Acqua, A.: Advances in characterization of size-resolved organic matter in marine aerosol over the North Atlantic, J. Geophys. Res. D Atmos., 109(24), 1–14, doi:10.1029/2004JD005137, 2004.

Ceburnis, D., O'Dowd, C., Jennings, G. S., Facchini, M. C., Emblico, L., Decesari, S., Fuzzi, S. and Sakalys, J.: Marine aerosol chemistry gradients : Elucidating primary and secondary processes and fluxes, Geophys. Res. Lett., 35(2), 1–5, doi:10.1029/2008GL033462, 2008.

Chang, R. Y. W., Sjostedt, S. J., Pierce, J. R., Papakyriakou, T. N., Scarratt, M. G., Michaud, S., Levasseur, M., Leaitch, W. R. and Abbatt, J. P. D.: Relating atmospheric and oceanic DMS levels to particle nucleation events in the Canadian Arctic, J. Geophys. Res. Atmos., 116(21), 1–10, doi:10.1029/2011JD015926, 2011.

Charlson, R. J., Lovelock, J. E., Andreae, M. O. and Warren, S. G.: Oceanic phytoplankton, atmospheric sulphur, cloud albedo and climate, Nature, 326(6114), 655–661, doi:10.1038/326655a0, 1987.

Charlson, R. J., Schwartz, S. E., Hales, J. M., Cess, R. D., Coakley, J. A., Hansen, J. E. and Hofmann, D. J.: Climate Forcing by Anthropogenic Aerosols, Science (80), 255(5043), 423–430 [online] Available from: http://science.sciencemag.org/content/255/5043/423.abstract, 1992.

Chen, H., Varner, M. E., Gerber, R. B. and Finlayson-Pitts, B. J.: Reactions of Methanesulfonic Acid with Amines and Ammonia as a Source of New Particles in Air, J. Phys. Chem. B, 120(8), 1526–1536, doi:10.1021/acs.jpcb.5b07433, 2016.

Chen, Q., Sherwen, T., Evans, M. and Alexander, B.: DMS oxidation and sulfur aerosol formation in the marine troposphere : a focus on reactive halogen and multiphase chemistry, Atmos. Chem. Phys., 18, 13617–13637, 2018.

Chen, Y.-C., Christensen, M. W., Stephens, G. L. and Seinfeld, J. H.: Satellite-based estimate of global aerosol–cloud radiative forcing by marine warm clouds, Nat. Geosci., 7(9), 643–646, doi:10.1038/ngeo2214, 2014.

Christiansen, S., Salter, M. E., Gorokhova, E., Nguyen, Q. T. and Bilde M.: Sea spray aerosol formation: Results on the role of air entrainment, water temperature and phytoplankton biomass, Environ. Sci. Technol., 53, 13107-13116, 2019.

Chiu, R., Tinel, L., Gonzalez, L., Ciuraru, R., Bernard, F., George, C., and Volkamer R.: UV

photochemistry of carboxylic acids at the air-sea boundary: A relevant source of glyoxal and other oxygenated VOC in the marine atmosphere, Geophys. Res. Lett., 44, 1079–1087, doi:10.1002/2016GL071240, 2017.

Ciuraru, R., Fine, L., van Pinxteren, M., D'Anna, B., Herrmann, H., and George, C.: Unravelling new processes at interfaces: Photochemical isoprene production at the sea surface, Environ. Sci. Technol., 49(22), 13,199–13,205, doi:10.1021/acs.est.5b02388, 2015.

Collins, D. B., Burkart, J., Chang, R. Y.-W., Lizotte, M., Boivin-Rioux, A., Blais, M., Mungall, E. L., Boyer, M., Irish, V. E., Massé, G., Kunkel, D., Tremblay, J.-É., Papakyriakou, T., Bertram, A. K., Bozem, H., Gosselin, M., Levasseur, M., and Abbatt, J. P. D.: Frequent ultrafine particle formation and growth in Canadian Arctic marine and coastal environments, Atmos. Chem. Phys., 17, 13119–13138, https://doi.org/10.5194/acp-17-13119-2017, 2017.

Corbett, J. J., Winebrake, J. J., Green, E. H., Kasibhatla, P., Eyring, V. and Lauer, A.: Mortality from Ship Emissions: A Global Assessment, Environ. Sci. Technol., 41(24), 8512–8518, doi:10.1021/es071686z, 2007.

Corbett, J. J., Lack, D. A., Winebrake, J. J., Harder, S., Silberman, J. A., and Gold, M.: Arctic shipping emissions inventories and future scenarios, Atmos. Chem. Phys., 10, 9689–9704, https://doi.org/10.5194/acp-10-9689-2010, 2010.

Cravigan, L. T., Ristovski, Z., Modini, R. L., Keywood, M. D., and Gras, J. L.: Observation of sea-salt fraction in sub-100 nm diameter particles at Cape Grim, J. Geophys. Res. Atmos., 120, 1848–1864, doi:10.1002/2014JD022601, 2015

Cravigan, L. T., Mallet, M. D., Vaattovaara, P., Harvey, M. J., Law, C. S., Modini, R. L., Russell, L. M., Stelcer, E., Cohen, D. D., Olsen, G., Safi, K., Burrell, T. J. and Ristovski, Z.: Sea spray aerosol organic enrichment , water uptake and surface tension effects, Atmos. Chem. Phys., 20, 7955–7977, https://doi.org/10.5194/acp-20-7955-2020, 2020.

Croft, B., Wentworth, G. R., Martin, R. V, Leaitch, W. R., Murphy, J. G., Murphy, B. N., Kodros, J. K., Abbatt, J. P. D. and Pierce, J. R.: Contribution of Arctic seabird-colony ammonia to atmospheric particles and cloud-albedo radiative effect, Nat. Commun., 7, 13444, doi:10.1038/ncomms13444, 2016a.

Formatted: Font: 12 pt, Font color: Text 1

Formatted: Font: 12 pt, Font color: Text 1

Formatted: Don't adjust space between Latin and Asian text, Don't adjust space between Asian text and numbers

Formatted: Font: 12 pt, Font color: Text 1

Formatted: Font: 12 pt, Font color: Text 1

Formatted: Font: 12 pt, Font color: Text 1

Formatted: Font: 12 pt, Font color: Text 1

Formatted: Font: 12 pt, Font color: Text 1

Formatted: Font color: Text 1

Formatted: Font: 12 pt, Font color: Text 1

Formatted: Font color: Text 1

Formatted: Font: English (US), Pattern: Clear

1449 Croft, B., Martin, R. V., Richard Leaitch, W., Tunved, P., Breider, T. J., D'Andrea, S. D. and
1450 Pierce, J. R.: Processes controlling the annual cycle of Arctic aerosol number and
1451 size distributions, Atmos. Chem. Phys., 16(6), 3665–3682, doi:10.5194/acp-16-
1452 3665-2016, 2016b.
1453 Croft, B., Martin, R. V., Leaitch, W. R., Burkart, J., Chang, R. Y.-W., Collins, D. B., Hayes, P. L.,
1454 Hodshire, A. L., Huang, L., Kodros, J. K., Moravek, A., Mungall, E. L., Murphy,
1455 J. G., Sharma, S., Tremblay, S., Wentworth, G. R., Willis, M. D., Abbatt, J. P. D.
1456 and Pierce, J. R.: Arctic marine secondary organic aerosol contributes significantly
1457 to summertime particle size distributions in the Canadian Arctic Archipelago,
1458 Atmos. Chem. Phys., 19(5), 2787–2812, doi:10.5194/acp-19-2787-2019, 2019.
1459 Cui, T., Green, H. S., Selleck, P. W., Zhang, Z., Brien, R. E. O., Gold, A., Keywood, M., Kroll, J.
1460 H. and Surratt, J. D.: Chemical Characterization of Isoprene- and Monoterpene-
1461 Derived Secondary Organic Aerosol Tracers in Remote Marine Aerosols over a
1462 Quarter Century, doi:10.1021/acsearthspacechem.9b00061, 2019.
1463 Dall´Osto, M., Simo, R., Harrison, R. M., Beddows, D. C. S., Saiz-Lopez, A., Lange, R., Skov,
1464 H., Nøjgaard, J. K., Nielsen, I. E. and Massling, A.: Abiotic and biotic sources
1465 influencing spring new particle formation in North East Greenland, Atmos.
1466 Environ., 190(July), 126–134, doi:10.1016/J.ATMOSENV.2018.07.019, 2018.
1467 DeCarlo, P. F., Kimmel, J. R., Trimborn, A., Northway, M. J., Jayne, J. T., Aiken, A. C., Gonin,
1468 M., Fuhrer, K., Horvath, T., Docherty, K. S., Worsnop, D. R., and Jimenez, J. L.:
1469 Field-deployable, high-resolution, time-of-flight aerosol mass spectrometer,
1470 Analytical Chemistry 78, (24), 8281-8289, 2006.
1471 Decesari, S., Finessi, E., Rinaldi, M., Paglione, M., Fuzzi, S., Stephanou, E. G., Tziaras, T., Spyros,
1472 A., Ceburnis, D., O'Dowd, C., Osto, M. D., Harrison, R. M., Allan, J., Coe, H. and
1473 Facchini, M. C.: Primary and secondary marine organic aerosols over the North
1474 Atlantic Ocean during the MAP experiment, J. Geophys. Res., 116, D22210, 1–21,
1475 doi:10.1029/2011JD016204, 2011.
1476 de Leeuw, G., Andreas, E. L., Anguelova, M. D., Fairall, C. W., Lewis, E. R., O'Dowd, C., Schulz,
1477 M., and Schwartz, S. E.: Production flux of sea spray aerosol, Rev. Geophys., 49,
1478 RG2001, https://doi.org/10.1029/2010RG000349, 2011.
1479 DeMott, P. J., Hill, T. C. J., McCluskey, C. S., Prather, K. A., Collins, D. B., Sullivan, R. C.,

Ruppel, M. J., Mason, R. H., Irish, V. E. and Lee, T.: Sea spray aerosol as a unique source of ice nucleating particles, Proc. Natl. Acad. Sci., 113(21), 5797–5803 [online] Available from: http://www.pnas.org/content/113/21/5797.full.pdf, 2016.

EC-JRC/PBL: Emission Database for Global Atmospheric Research (EDGAR), release EDGAR v4.2 FT2012, http://edgar.jrc.ec.europa.eu (last access: 15 January 2018), 2012.

Facchini, M. C., Decesari, S., Rinaldi, M., Carbone, C., Finessi, E., Mircea, M., Fuzzi, S., Moretti, F., Tagliavini, E., Ceburnis, D. and O'Dowd, C.: Important Source of Marine Secondary Organic Aerosol from Biogenic Amines, Environ. Sci. Technol., 42(24), 9116–9121, doi:10.1021/es8018385, 2008.

Fast, J. D., Berg, L. K., Zhang, K., Easter, R. C., Ferrare, R. A., Hair, J. W., Hostetler, C. A., Liu, Y., Ortega, I., Sedlacek III, A., Shilling, J. E., Shrivastava, M., Springston, S. T., Tomlinson, Jason, M., Rainer, V., Wilson, J., Zaveri, R. A. and Zelenyuk, A.: Model representations of aerosol layers transported from North America over the Atlantic Ocean during the Two-Column Aerosol Project, J. Geophys. Res. Atmos., 121, 9814–9848, doi:10.1002/2016JD025248, 2016.

Fiddes, S. L., Woodhouse, M. T., Nicholls, Z., Lane, T. P. and Schofield, R.: Cloud, precipitation and radiation responses to large perturbations in global dimethyl sulfide, Atmos. Chem. Phys., 18, 10177–10198, https://doi.org/10.5194/acp-18-10177-2018, 2018.

Fisher, J. A., Jacob, D. J., Purdy, M. T., Kopacz, M., Le Sager, P., Carouge, C., Holmes, C. D., Yantosca, R. M., Batchelor, R. L., Strong, K., Diskin, G. S., Fuelberg, H. E., Holloway, J. S., Hyer, E. J., McMillan, W. W., Warner, J., Streets, D. G., Zhang, Q., Wang, Y. and Wu, S.: Source attribution and interannual variability of Arctic pollution in spring constrained by aircraft (ARCTAS, ARCPAC) and satellite (AIRS) observations of carbon monoxide, Atmos. Chem. Phys., 10(3), 977–996, doi:10.5194/acp-10-977-2010, 2010.

Fossum, K.N., Ovadnevaite, J., Ceburnis, D. Preißler, J., Snider, J. R., Huang, R. J., Zuend, A. and O'Dowd, C.: Sea-spray regulates sulfate cloud droplet activation over oceans, NPJ Clim. Atmos. Sci., 3, 14, https://doi.org/10.1038/s41612-020-0116-2, 2020.

1508 Galí, M., and Simó, R.: A meta-analysis of oceanic DMS and DMSP cycling processes:
1509 Disentangling the summer paradox, Global Biogeochem. Cycles, 29, 496–515,
1510 doi:10.1002/2014GB004940, 2015.
1511 Galí, M., Levasseur, M., Devred, E., Simó, R. and Babin, M.: Sea-surface dimethylsulfide (DMS)
1512 concentration from satellite data at global and regional scales, Biogeosciences, 15,
1513 3497–3519, https://doi.org/10.5194/bg-15-3497-2018, 2018.
1514 Galí, M., Devred, E., Babin, M. and Levasseur, M.: Decadal increase in Arctic dimethylsulfide
1515 emission, Proc. Natl. Acad. Sci., 116(39), 19311–19317,
1516 doi:10.1073/pnas.1904378116, 2019.
1517 Gantt, B. and Meskhidze, N.: The physical and chemical characteristics of marine primary organic
1518 aerosol: A review, Atmos. Chem. Phys., 13(8), 3979–3996, doi:10.5194/acp-13-
1519 3979-2013, 2013.
1520 Ghahremaninezhad, R., Norman, A. L., Abbatt, J. P. D., Levasseur, M. and Thomas, J. L.:
1521 Biogenic, anthropogenic and sea salt sulfate size-segregated aerosols in the Arctic
1522 summer, Atmos. Chem. Phys., 16(8), 5191–5202, doi:10.5194/acp-16-5191-2016,
1523 2016.
1524 Ghahremaninezhad, R., Gong, W., Galí, M., Norman, A., Beagley, S. R., Akingunola, A., Zheng,
1525 Q., Lupu, A., Lizotte, M., Levasseur, M. and Leaitch, W. R.: Dimethyl sulfide and
1526 its role in aerosol formation and growth in the Arctic summer – a modelling study,
1527 Atmos. Chem. Phys., 19, 14455–14476, https://doi.org/10.5194/acp-19-14455-
1528 2019, 2019.
1529 Gilgen, A., Ting, W., Huang, K., Ickes, L., Neubauer, D. and Lohmann, U.: How important are
1530 future marine and shipping aerosol emissions in a warming Arctic summer and
1531 autumn ?, Atmos. Chem. Phys., 18, 10521–10555, https://doi.org/10.5194/acp-18-
1532 10521-2018, 2018.
1533 Gong, S. L.: A parameterization of sea-salt aerosol source function for sub- and super-micron
1534 particles, J. Geophys. Res., 17(4), 1097, doi:10.1029/2003GB002079, 2003.
1535 Grassian, V. H., Quinn, P. K., Collins, D. B., Bates, T. S. and Prather, K. A.: Chemistry and Related
1536 Properties of Freshly Emitted Sea Spray Aerosol, Chem. Rev., 115(10), 4383–
1537 4399, doi:10.1021/cr500713g, 2015.
1538 Hamacher-Barth, E., Leck, C. and Jansson, K.: Size-resolved morphological properties of the high

Formatted: Font color: Auto

1539 Arctic summer aerosol during ASCOS-2008, Atmos. Chem. Phys., 16, 6577–6593,
1540 doi:10.5194/acp-16-6577-2016, 2016.
1541 Hodshire, A. L., Campuzano-jost, P., Kodros, J. K., Croft, B., Nault, B. A., Schroder, J. C.,
1542 Jimenez, J. L. and Pierce, J. R.: The potential role of methanesulfonic acid (MSA
1543) in aerosol formation and growth and the associated radiative forcings, Atmos.
1544 Chem. Phys., 19, 3137-3160, https://doi.org/10.5194/acp-19-3137-2019 , 2019.
1545 Hoesly, R. M., Smith, S. J., Feng, L., Klimont, Z., Janssens-Maenhout, G., Pitkanen, T., Seibert,
1546 J. J., Vu, L., Andres, R. J., 1010 Bolt, R. M., Bond, T. C., Dawidowski, L., Kholod,
1547 N., Kurokawa, J. I., Li, M., Liu, L., Lu, Z., Moura, M. C. P., O'Rourke, P. R., and
1548 Zhang, Q.: Historical (1750–2014) anthropogenic emissions of reactive gases and
1549 aerosols from the Community Emissions Data System (CEDS), Geosci. Model
1550 Dev., 11, 369-408, 10.5194/gmd-11-369-2018, 2018.
1551 Hoffman, E. H., Tilgner, A., Schrödner, R., Bräuer, P., Wolke, R. and Herrmann, H.: An advanced
1552 modeling study on the impacts and atmospheric implications of multiphase
1553 dimethyl sulfide chemistry, Proc. Natl., Acad. Sci., 113, (42), 11776-11781,
1554 https://doi.org/10.1073/pnas.1606320113, 2016.
1555 Holmes, C. D., Prather, M. J. and Vinken, G. C. M.: The climate impact of ship NO x emissions :
1556 an improved estimate accounting for plume chemistry, Atmos. Chem. Phys., 14,
1557 6801–6812, doi:10.5194/acp-14-6801-2014, 2014.
1558 Hoose, C., Lohmann, U., Bennartz, R., Croft, B., Lesins, G.: Global simulations of aerosol
1559 processing in clouds, Atmos. Chem. Phus., 8, 6939–6963, 2008.
1560 Hoppel, W. A., G. M. Frick, and R. E. Larson (1986), Effect of nonprecipitating clouds on the
1561 aerosol size distribution in the marine boundary layer, Geophys. Res. Lett., 13(1),
1562 125–128, doi:10.1029/GL013i002p00125, 1987.
1563 Hu, Q.-H., Xie, Z.-Q., Wang, X.-M., Kang, H., He, Q.-F. and Zhang, P.: Secondary organic
1564 aerosols over oceans via oxidation of isoprene and monoterpenes from Arctic to
1565 Antarctic, Sci. Rep., 3, 2280, doi:10.1038/srep02280, 2013.
1566 Huntrieser, H., Heland, J., Schlager, H., Forster, C., Stohl, A., Aufmhoff, H., Arnold, F., Scheel,
1567 H. E., Campana, M., Gilge, S., Eixmann, R. and Cooper, O.: Intercontinental air
1568 pollution transport from North America to Europe : Experimental evidence from
1569 airborne measurements and surface observations, J. Geophys. Res., 110, D01305,

doi:10.1029/2004JD005045, 2005.

Iacono, M. J., Delamere, J. S., Mlawer, E. J., Shephard, M. W., Clough, S. A. and Collins, W. D.: Radiative forcing by long-lived greenhouse gases: Calculations with the AER radiative transfer models, J. Geophys. Res. Atmos., 113(13), D13103, doi:10.1029/2008JD009944, 2008.

IPCC, 2013: *Climate Change 2013: The Physical Science Basis. Contribution of Working Group I to the Fifth Assessment Report of the Intergovernmental Panel on Climate Change* [Stocker, T.F., D. Qin, G.-K. Plattner, M. Tignor, S.K. Allen, J. Boschung, A. Nauels, Y. Xia, V. Bex and P.M. Midgley (eds.)]. Cambridge University Press, Cambridge, United Kingdom and New York, NY, USA, 1535 pp.

Irish, V. E., Elizondo, P., Chen, J., Chou, C., Charette, J., Lizotte, M., Ladino, L. A., Wilson, T. W., Gosselin, M., Murray, B. J., Polishchuk, E., Abbatt, J. P. D., Miller, L. A., and Bertram, A. K.: Ice-nucleating particles in Canadian Arctic sea-surface microlayer and bulk seawater, Atmos. Chem. Phys., 17, 10583–10595, https://doi.org/10.5194/acp-17-10583-2017, 2017.

Jaeglé, L., Quinn, P. K., Bates, T. S., Alexander, B. and Lin, J. T.: Global distribution of sea salt aerosols: New constraints from in situ and remote sensing observations, Atmos. Chem. Phys., 11(7), 3137–3157, doi:10.5194/acp-11-3137-2011, 2011.

Jin, Q., Grandey, B. S., Rothenberg, D., Avramov, A. and Wang, C.: Impacts on cloud radiative effects induced by coexisting aerosols converted from international shipping and maritime DMS emissions, Atmos. Chem. Phys., 18, 16793–16808, https://doi.org/10.5194/acp-18-16793-2018, 2018.

Johnson, M. T.: A numerical scheme to calculate temperature and salinity dependent air-water transfer velocities for any gas, Ocean Sci., 6(4), 913–932, doi:10.5194/os-6-913-2010, 2010.

Karl, M., Leck, C., Gross, A. and Pirjola, L.: A study of new particle formation in the marine boundary layer over the central Arctic Ocean using a flexible multicomponent aerosol dynamic model, Tellus, Ser. B Chem. Phys. Meteorol., 64(1), 1–24, doi:10.3402/tellusb.v64i0.17158, 2012.

Kasparian, J., Hassler, C., Ibelings, B., Berti, N., Bigorre, S., Djambazova, V., Gascon-diez, E., Giuliani, G., Houlmann, R., Kiselev, D., Laborie, P. De, Le, A., Magouroux, T., Neri, T., Palomino, D., Pfändler, S., Ray, N., Sousa, G., Staedler, D., Tettamanti,

F., Wolf, J. and Beniston, M.: Assessing the Dynamics of Organic Aerosols over the North Atlantic Ocean, Sci. Rep., 7, 45476, doi:10.1038/srep45476, 2017.

Kazil, J., Wang, H., Feingold, G., Clarke, A. D., Snider, J. R. and Bandy, A. R.: and Physics Modeling chemical and aerosol processes in the transition from closed to open cells during VOCALS-REx, Atmos. Chem. Phys., 11, 7491–7514, doi:10.5194/acp-11-7491-2011, 2011.

Kerminen, V. M., Anttila, T., Lehtinen, K. E. J. and Kulmala, M.: Parameterization for atmospheric new-particle formation: Application to a system involving sulfuric acid and condensable water-soluble organic vapors, Aerosol Sci. Technol., 38(10), 1001–1008, doi:10.1080/027868290519085, 2004.

Kim, M. J., Novak, G. A., Zoerb, M. C., Yang, M., Blomquist, B. W., Huebert, B. J., Cappa, C. D. and Bertram, T. H.: Air-Sea exchange of biogenic volatile organic compounds and the impact on aerosol particle size distributions, Geophys. Res. Lett., 44(8), 3887–3896, doi:10.1002/2017GL072975, 2017.

Kodros, J. K., Cucinotta, R., Ridley, D. A., Wiedinmyer, C. and Pierce, J. R.: The aerosol radiative effects of uncontrolled combustion of domestic waste, Atmos. Chem. Phys., 16(11), 6771–6784, doi:10.5194/acp-16-6771-2016, 2016.

Kodros, J. K. and Pierce, J. R.: Important global and regional differences in aerosol cloud-albedo effect estimates between simulations with and without prognostic aerosol microphysics, J. Geophys. Res., 122(7), 4003–4018, doi:10.1002/2016JD025886, 2017.

Korhonen, H., Carslaw, K. S., Spracklen, D. V, Mann, G. W. and Woodhouse, M. T.: Influence of oceanic dimethyl sulfide emissions on cloud condensation nuclei concentrations and seasonality over the remote Southern Hemisphere oceans: A global model study, J. Geophys. Res. Atmos., 113(D15), doi:10.1029/2007JD009718, 2008

Kuang, C., Senum, G. I., Dedrick, J., Leaitch, W. R., Lubin, D., Aiken, A. C., Springston, S. R., Uin, J., Russell, L. M. and Liu, J.: High summertime aerosol organic functional group concentrations from marine and seabird sources at Ross Island, Antarctica, during AWARE, Atmos. Chem. Phys., 18(12), 8571–8587, doi:10.5194/acp-18-8571-2018, 2018.

Kulmala, M., Lehtinen, K. E. J., and Laaksonen, A.: Cluster activation theory as an explanation of the linear dependence between formation rate of 3nm particles and sulphuric acid concentration, Atmos. Chem. Phys., 6, 787–793, https://doi.org/10.5194/acp-6-787-2006, 2006.

Lana, A., Bell, T. G., Simó, R., Vallina, S. M., Ballabrera-Poy, J., Kettle, A. J., Dachs, J., Bopp, L., Saltzman, E. S., Stefels, J., Johnson, J. E. and Liss, P. S.: An updated climatology of surface dimethlysulfide concentrations and emission fluxes in the global ocean, Global Biogeochem. Cycles, 25(1), 1–17, doi:10.1029/2010GB003850, 2011.

Lana, A., Simó, R., Vallina, S. M. and Dachs, J.: Re-examination of global emerging patterns of ocean DMS concentration, Biogeochemistry, 110(1), 173–182, doi:10.1007/s10533-011-9677-9, 2012a.

Lana, A., Simó, R., Vallina, S. M., and Dachs, J.: Potential for a biogenic influence on cloud microphysics over the ocean: a correlation study with satellite-derived data, Atmos. Chem. Phys., 12, 7977–7993, https://doi.org/10.5194/acp-12-7977-2012, 2012b.

Lapina, K., Heald, C. L., Spracklen, D. V., Arnold, S. R., Allan, J. D., Coe, H., McFiggans, G., Zorn, S. R., Drewnick, F., Bates, T. S., Hawkins, L. N., Russell, L. M., Smirnov, A., O'Dowd, C. D., and Hind, A. J.: Investigating organic aerosol loading in the remote marine environment, Atmos. Chem. Phys., 11, 8847–8860, https://doi.org/10.5194/acp-11-8847-2011, 2011

Leaitch, W. R., Sharma, S., Huang, L., Toom-Sauntry, D., Chivulescu, A., Macdonald, A. M., von Salzen, K., Pierce, J. R., Bertram, A. K., Schroder, J. C., Shantz, N. C., Chang, R. Y.-W. and Norman, A.-L.: Dimethyl sulfide control of the clean summertime Arctic aerosol and cloud, Elem. Sci. Anthr., 1, 000017, doi:10.12952/journal.elementa.000017, 2013.

Leaitch, R. W., Russell, L. M., Liu, J., Kolonjari, F., Toom, D., Huang, L., Sharma, S., Chivulescu, A., Veber, D. and Zhang, W.: Organic functional groups in the submicron aerosol at 82.5 degrees N, 62.5 degrees W from 2012 to 2014, Atmos. Chem. Phys., 18, 3269–3287, doi:10.5194/acp-18-3269-2018, 2018.

Leck, C. and Bigg, E. K.: Source and evolution of the marine aerosol—A new perspective, Geophys. Res. Lett., 32(19), doi:10.1029/2005GL023651, 2005.

Deleted: ¶

1665 Lee, Y. H. and Adams, P. J.: A fast and efficient version of the TwO-Moment Aerosol Sectional
1666 (TOMAS) global aerosol microphysics model, Aerosol Sci. Technol., 46(6), 678–
1667 689, doi:10.1080/02786826.2011.643259, 2012.
1668 Lee, Y. H., Pierce, J. R., and Adams, P. J.: Representation of nucleation mode microphysics in a
1669 global aerosol model with sectional microphysics, Geosci. Model Dev., 6, 1221–
1670 1232, https://doi.org/10.5194/gmd-6-1221-2013, 2013.
1671 Liu, H., Jacob, D. J., Bey, I. and Yantosca, R. M.: Constraints from210Pb and7Be on wet
1672 deposition and transport in a global three-dimensional chemical tracer model driven
1673 by assimilated meteorological fields, J. Geophys. Res. Atmos., 106(D11), 12109–
1674 12128, doi:10.1029/2000JD900839, 2001.
1675 Lohmann, U. and Feichter, J.: Global indirect aerosol effects: a review, Atmos. Chem. Phys., 5(3),
1676 715–737, doi:10.5194/acp-5-715-2005, 2005.
1677 Luo, G., Yu, F. and Schwab, J.: Revised treatment of wet scavenging processes dramatically
1678 improves GEOS-Chem 12 . 0 . 0 simulations of surface nitric acid, nitrate, and
1679 ammonium over the United States, Geosci. Model. Dev., 12, 3439–3447,
1680 doi.10.5194/gmd-12-3439-2019, 2019.
1681 Luo, G., Yu, F. and Moch, J. M.: Further improvement of wet process treatments in GEOS-Chem
1682 v12 . 6 . 0 : impact on global distributions of aerosols and aerosol precursors,
1683 Geosci. Model Dev., 2879–2903, 2020.
1684 Mahmood, R., Salzen, K. Von, Norman, A., Galí, M. and Levasseur, M.: Sensitivity of Arctic
1685 sulfate aerosol and clouds to changes in future surface seawater dimethylsulfide
1686 concentrations, Atmos. Chem. Phys., 19, 6419–6435, https://doi.org/10.5194/acp-
1687 19-6419-2019, 2019.
1688 Mårtensson, E. M., Nilsson, E. D., de Leeuw, G., Cohen, L. H. and Hansson, H.-C.: Laboratory
1689 simulations and parameterization of the primary marine aerosol production, J.
1690 Geophys. Res. Atmos., 108(D9), n/a-n/a, doi:10.1029/2002JD002263, 2003.
1691 McCoy, D. T., Burrows, S. M., Wood, R., Grosvenor, D. P., Elliott, S. M., Ma, P.-L., Rasch, P. J.
1692 and Hartmann, D. L.: Natural aerosols explain seasonal and spatial patterns of
1693 Southern Ocean cloud albedo, Sci. Adv., 1(6), e1500157,
1694 doi:10.1126/sciadv.1500157, 2015.

McDuffie, E. E., Smith, S. J., O'Rourke, P., Tibrewal, K., Venkataraman, C., Marais, E. A., Zheng, B., Crippa, M., Brauer, M., and Martin, R. V.: A global anthropogenic emission inventory of atmospheric pollutants from sector- and fuel-specific sources (1970–2017): An application of the Community Emissions Data System (CEDS), Earth Syst. Sci. Data Discuss., https://doi.org/10.5194/essd-2020-103, in review, 2020.

McNaughton, C. S., Clarke, A. D., Howell, S. G., Pinkerton, M., Anderson, B., Thornhill, L., Hudgins, C., et al.: Results from the DC-8 Inlet Characterization Experiment (DICE): Airborne versus surface sampling of mineral dust and sea salt aerosols, Aerosol Sci. Tech. 41, (2). 136-159, 2007.

Meskhidze, N., Sabolis, A., Reed, R. and Kamykowski, D.: Quantifying environmental stress-induced emissions of algal isoprene and monoterpenes using laboratory measurements, Biogeosciences, 12, 637–651, doi:10.5194/bg-12-637-2015, 2015.

Monahan, E. C., Fairall, C. W., Davidson, K. L., and Boyle, P. J.: Observed inter-relations between 10m winds, ocean whitecaps and marine aerosols, Q. J. Roy. Meteor. Soc., 109, 379–392, 1983.

Müller, M., Mikoviny, T., Feil, S., Haidacher, S., Hanel, G., Hartungen, E., Jordan, A., Märk, L., Mutschlechner, P., Schottkowsky, R., Sulzer, P., Crawford, J. H., and Wisthaler, A.: A compact PTR-ToF-MS instrument for airborne measurements of VOCs at high spatio-temporal resolution, Atmos. Meas. Tech. 7, 3763-3772, doi:10.5194/amt-7-3763-2014, 2014.

Mungall, E. L., Abbatt, J. P. D., Wentzell, J. J. B., Lee, A. K. Y., Thomas, J. L., Blais, M., Gosselin, M., Miller, L. A., Papakyriakou, T., Willis, M. D. and Liggio, J.: Microlayer source of oxygenated volatile organic compounds in the summertime marine Arctic boundary layer, Proc. Natl. Acad. Sci., 114(24), 6203–6208, doi:10.1073/pnas.1620571114, 2017.

Napari, I., Noppel, M., Vehkamaki, H. and Kulmala, M.: Parametrization of ternary nucleation rates for H2SO4-NH3-H2O vapors, J. Geophys. Res. Atmos., 107(19), 2–7, doi:10.1029/2002JD002132, 2002.

Nightingale, P. D., Liss, P. S. and Schlosser, P.: Measurements of air-sea gas transfer during an open ocean algal bloom, Geophys. Res. Lett., 27(14), 2117–2120, doi:10.1029/2000GL011541, 2000a.

Nightingale, P. D., Malin, G., Law, C. S., Watson, A. J., Liss, P. S., Liddicoat, M. I., Boutin, J. and Upstill-Goddard, R. C.: In situ evaluation of air-sea gas exchange parameterizations using novel conservative and volatile tracers, Global Biogeochem. Cycles, 14(1), 373–387, doi:10.1029/1999GB900091, 2000b.

O'Dowd, C. D., Smith, M. H., Consterdine, I. E., Lowe, J. A.: Marine aerosol, sea-salt, and the marine sulphur cycle: A short review. Atmos. Environ. 31, 73–80 (1997)

O'Dowd, C. D.: Marine aerosol formation from biogenic iodine emissions, Nature, 417(June), 1–5, doi:10.1038/nature00775, 2002.

O' Dowd, C. D., Facchini, M. C., Cavalli, F., Ceburnis, D., Mircea, M., Decesari, S., Fuzzi, S., Yoon, Y. J. and Putaud, J.: Biogenically driven organic contribution to marine aerosol, Nature, 431(7009), 676-680, https://doi.org/10.1038/nature02959, 2004

O'Dowd, C. D. and de Leeuw, G.: Marine aerosol production : a review of the current knowledge, Phil. Trans. R. Soc. A, 1(May), 1753–1774, doi:10.1098/rsta.2007.2043, 2007.

O'Dowd, C. D., Ceburnis, D., Ovadnevaite, J., Bialek, J., Stengel, D. B., Zacharias, M., Nitschke, U., Connan, S., Rinaldi, M., Fuzzi, S., Decesari, S., Facchini, M. C., Marullo, S., Santoleri, R., Anno, A. D., Corinaldesi, C., Tangherlini, M. and Danovaro, R.: Connecting marine productivity to sea-spray via nanoscale biological processes : Phytoplankton Dance or Death Disco ?, Sci. Rep, 5(May), 14883, 1–11, doi:10.1038/srep14883, 2015.

Ovadnevaite, J., Ceburnis, D., Martucci, G., Bialek, J., Monahan, C., Rinaldi, M., Facchini, M. C., Berresheim, H., Worsnop, D. R. and O'Dowd, C.: Primary marine organic aerosol : A dichotomy of low hygroscopicity and high CCN activity, Geophys. Res. Lett., 38, L21806 1–5, doi:10.1029/2011GL048869, 2011.

Ovadnevaite, J., Ceburnis, D., Canagaratna, M., Berresheim, H., Bialek, J., Martucci, G., Worsnop, D. R. and Dowd, C. O.: On the effect of wind speed on submicron sea salt mass concentrations and source fluxes, J. Geophys. Res.,, 117, D16201, 1–11, doi:10.1029/2011JD017379, 2012.

Pai, S. J., Heald, C. L., Pierce, J. R., Farina, S. C., Marais, E. A., Jimenez, J. L., Campuzano-jost, P., Nault, B. A., Middlebrook, A. M., Coe, H., Shilling, J. E., Bahreini, R., Dingle, J. H. and Vu, K.: An evaluation of global organic aerosol schemes using airborne observations, Atmos. Chem. Phys., 20 , 2637–2665, https://doi.org/10.5194/acp-

20-2637-2020, 2020.

Park, K.-T., Jang, S., Lee, K., Yoon, Y. J., Kim, M.-S., Park, K., Cho, H.-J., Kang, J.-H., Udisti, R., Lee, B.-Y. and Shin, K.-H.: Observational evidence for the formation of DMS-derived aerosols during Arctic phytoplankton blooms, Atmos. Chem. Phys., 17(15), 9665–9675, doi:https://doi.org/10.5194/acp-17-9665-2017, 2017.

Park, K.-T., Lee, K., Kim, T.-W., Yoon, Y. J., Jang, E.-H., Jang, S., Lee, B.-Y. and Hermansen, O.: Atmospheric DMS in the Arctic Ocean and Its Relation to Phytoplankton Biomass, Global Biogeochem. Cycles, 32(3), 351–359, doi:10.1002/2017GB005805, 2018.

Pierce, J. R., Croft, B., Kodros, J. K., D'Andrea, S. D. and Martin, R. V.: The importance of interstitial particle scavenging by cloud droplets in shaping the remote aerosol size distribution and global aerosol-climate effects, Atmos. Chem. Phys., 15(11), 6147–6158, doi:10.5194/acp-15-6147-2015, 2015.

Prather, K. A., Bertram, T. H., Grassian, V. H., Deane, G. B., Stokes, M. D., DeMott, P. J., Aluwihare, L. I., Palenik, B. P., Azam, F., Seinfeld, J. H., Moffet, R. C., Molina, M. J., Cappa, C. D., Geiger, F. M., Roberts, G. C., Russell, L. M., Ault, A. P., Baltrusaitis, J., Collins, D. B., Corrigan, C. E., Cuadra-Rodriguez, L. A., Ebben, C. J., Forestieri, S. D., Guasco, T. L., Hersey, S. P., Kim, M. J., Lambert, W. F., Modini, R. L., Mui, W., Pedler, B. E., Ruppel, M. J., Ryder, O. S., Schoepp, N. G., Sullivan, R. C. and Zhao, D.: Bringing the ocean into the laboratory to probe the chemical complexity of sea spray aerosol, Proc. Natl. Acad. Sci., 110(19), 7550–7555, doi:10.1073/pnas.1300262110, 2013.

Quinn, P. K. and Bates, T. S.: The case against climate regulation via oceanic phytoplankton sulphur emissions, Nature, 480(7375), 51–56, doi:10.1038/nature10580, 2011.

Quinn, P. K., Bates, T. S., Schulz, K. S., Coffman, D. J., Frossard, A. A., Russell, L. M., Keene, W. C. and Kieber, D. J.: Contribution of sea surface carbon pool to organic matter enrichment in sea spray aerosol, Nat. Geosci., 7(3), 228–232, doi:10.1038/ngeo2092, 2014.

Quinn, P. K., Collins, D. B., Grassian, V. H., Prather, K. A. and Bates, T. S.: Chemistry and Related Properties of Freshly Emitted Sea Spray Aerosol, Chem. Rev., 115(10), 4383–4399, doi:10.1021/cr500713g, 2015.

Quinn, P. K., Coffman, D. J., Johnson, J. E., Upchurch, L. M. and Bates, T. S.: Small fraction of marine cloud condensation nuclei made up of sea spray aerosol, Nat. Geosci., 10(9), 674–679, doi:10.1038/ngeo3003, 2017.

Quinn, P. K., Bates, T. S., Coffman, D. J., Upchurch, L., Johnson, J. E., Moore, R. and Ziemba, L.: Seasonal Variations in Western North Atlantic Remote Marine Aerosol Properties, J. Geophys. Res., Atmos., 124, 14,240–14,261. https://doi.org/10.1029/2019JD031740, 2019.

Park, K.-T., Lee, K., Kim, T.-W., Yoon, Y. J., Jang, E.-H., Jang, S., Lee, B.-Y. and Hermansen, O.: Atmospheric DMS in the Arctic Ocean and Its Relation to Phytoplankton Biomass, Global Biogeochem. Cycles, 32(3), 351–359, doi:10.1002/2017GB005805, 2018.

Ramnarine, E., Kodros, J. K., Hodshire, A. L., Lonsdale, C. R., Alvarado, M. J. and Pierce, J. R.: Effects of near-source coagulation of biomass burning aerosols on global predictions of aerosol size distributions and implications for aerosol radiative effects, Atmos. Chem. Phys., 19, 6561–6577, https://doi.org/10.5194/acp-19-6561-2019, 2019.

Regayre, L. A., Schmale, J., Johnson, J. S., Tatzelt, C., Baccarini, A., Henning, S., Yoshioka, M., Stratmann, F., Gysel-Beer, M., Grosvenor, D. P., and Carslaw, K. S.: The value of remote marine aerosol measurements for constraining radiative forcing uncertainty, Atmos. Chem. Phys., 20, 10063–10072, https://doi.org/10.5194/acp-20-10063-2020, 2020.

Rempillo, O., Seguin, A. M., Norman, A.-L., Scarratt, M., Michaud, S., Chang, R., Sjostedt, S., Abbatt, J., Else, B., Papakyriakou, T., Sharma, S., Grasby, S. and Levasseur, M.: Dimethyl sulfide air-sea fluxes and biogenic sulfur as a source of new aerosols in the Arctic fall, J. Geophys. Res. Atmos., 116, (D100S04), doi:10.1029/2011JD016336, 2011.

Revell, L. E., Kremser, S., Hartery, S., Harvey, M., Mulcahy, J. P., Williams, J., Morgenstern, O., Mcdonald, A. J., Varma, V., Bird, L. and Schuddeboom, A.: The sensitivity of Southern Ocean aerosols and cloud microphysics to sea spray and sulfate aerosol production in the HadGEM3-GA7 . 1 chemistry – climate model, Atmos. Chem. Phys., 19, 15447–15466, https://doi.org/10.5194/acp-19-15447-2019, 2019.

Formatted: Font: Times New Roman, 12 pt

Formatted: Justified

Formatted: Font color: Auto

1843 Riccobono, F., Schobesberger, S., Scott, C. E., Dommen, J., Ortega, I. K., Rondo, L., Almeida, J.,
1844 Amorim, A., Bianchi, F., Breitenlechner, M., David, A., Downard, A., Dunne, E.
1845 M., Duplissy, J., Ehrhart, S., Flagan, R. C., Franchin, A., Hansel, A., Junninen, H.,
1846 Kajos, M., Keskinen, H., Kupc, A., Kupiainen, O., Kürten, A., Kurtén, T., Kvashin,
1847 A. N., Laaksonen, A., Lehtipalo, K., Makhmutov, V., Mathot, S., Nieminen, T.,
1848 Olenius, T., Onnela, A., Petäjä, T., Praplan, A. P., Santos, F. D., Schallhart, S.,
1849 Seinfeld, J. H., Sipilä, M., Spracklen, D. V, Stozhkov, Y., Stratmann, F., Tomé, A.,
1850 Tsagkogeorgas, G., Vaattovaara, P., Vehkamäki, H., Viisanen, Y., Vrtala, A.,
1851 Wagner, P. E., Weingartner, E., Wex, H., Wimmer, D., Carslaw, K. S., Curtius, J.,
1852 Donahue, N. M., Kirkby, J., Kulmala, M., Worsnop, D. R., Baltensperger, U. U. .,
1853 Schobesberger, S., Scott, C. E., Dommen, J., Ortega, I. K., Rondo, L., Almeida, J.,
1854 Amorim, A., Bianchi, F., Breitenlechner, M., David, A., Downard, A., Dunne, E.
1855 M., Duplissy, J., Ehrhart, S., Flagan, R. C., Franchin, A., Hansel, A., Junninen, H.,
1856 Kajos, M., Keskinen, H., Kupc, A., Kürten, A., Kvashin, A. N., Laaksonen, A.,
1857 Lehtipalo, K., Makhmutov, V., Mathot, S., Nieminen, T., Onnela, A., Petäjä, T.,
1858 Praplan, A. P., Santos, F. D., Schallhart, S., Seinfeld, J. H., Sipilä, M., Spracklen,
1859 D. V, Stozhkov, Y., Stratmann, F., Tomé, A., Tsagkogeorgas, G., et al.: Oxidation
1860 Products of Biogenic Emissions Contribute to Nucleation of Atmospheric Particles,
1861 Science, 344(May), 717–721 [online] Available from:
1862 http://www.sciencemag.org/content/344/6185/717.abstract, doi:
1863 10.1126/science.1243527, 2014.
1864 Rinaldi, M., Decesari, S., Finessi, E., Giulianelli, L., Carbone, C., Fuzzi, S., O'Dowd, C., Ceburnis,
1865 D. and Facchini, M. C.: Primary and Secondary Organic Marine Aerosol and
1866 Oceanic Biological Activity: Recent Results and New Perspectives for Future
1867 Studies, Adv. Meteorol., 2010, 1–10, doi:10.1155/2010/310682, 2010.
1868 Rodríguez-Ros, P., Cortés, P., Robinson, C. M., Nunes, S., Hassler, C., Royer, S., Estrada, M. and
1869 Simó, R.: Distribution and Drivers of Marine Isoprene Concentration across the
1870 Southern Ocean, Atmosphere, 11, 556, 1–19, doi:10.3390/atmos11060556, 2020a.
1871 Rodriguez-Ros, P., Galí, M., Cortés, P., Robinson, C. M., Antoine, D., Wohl, C., Yang, M. and
1872 Simó, R.: Remote Sensing Retrieval of Isoprene Concentrations in the Southern
1873 Ocean Geophys. Res. Lett., 47, e2020GL087888, 1–10,

doi:10.1029/2020GL087888, 2020b.

Russell, L. M., Hawkins, L. N., Frossard, A. A., Quinn, P. K. and Bates, T. S.: Carbohydrate-like composition of submicron atmospheric particles and their production from ocean bubble bursting, Proc. Natl. Acad. Sci., 107(15), 6652-6657, doi:10.1073/pnas.0908905107, 2010.

Saliba, G., Chen, C., Lewis, S., Russell, L. M., Rivellini, L., Lee, A. K. Y., Carlson, C. A. and Behrenfeld, M. J.: Factors driving the seasonal and hourly variability of sea-spray aerosol number in the North Atlantic, Proc, Nat. Acad. Sci., 116(41), 20309–20314, doi:10.1073/pnas.1907574116, 2019.

Saliba, G., Chen, C., Lewis, S., Russell, L. M., Quinn, P. K., Bates, T. S., Bell, T. G., Lawler, M.J., Saltzman, E. S., Sanchez, K. J., Moore, R., Shook, M., Rivellini, L-H, Lee, A. K. Y. Baetge, N., Carlson, C. A. and Behrenfeld, M. J.: Seasonal differences and variability of concentrations, chemical composition, and cloud condensation nuclei of marine aerosol over the North Atlantic, 125, e2020JD033145. https://doi.org/10.1029/2020JD033145, 2020.

Sanchez, K. J., Chen, C.-L., Russell, L. M., Betha, R., Liu, J., Price, D. J., Massoli, P., Ziemba, L. D., Crosbie, E. C., Moore, R. H., Müller, M., Schiller, S. A., Wisthaler, A., Lee, A. K. Y., Quinn, P. K., Bates, T. S., Porter, J., Bell, T. G., Saltzman, E. S., Vaillancourt, R. D. and Behrenfeld, M. J.: Substantial Seasonal Contribution of Observed Biogenic Sulfate Particles to Cloud Condensation Nuclei, Sci. Rep., 8(1), 3235, doi:10.1038/s41598-018-21590-9, 2018.

Savoie, D. L., R. Arimoto, W. C. Keene, J. M. Prospero, R. A. Duce, and J. N. Galloway, Marine biogenic and anthropogenic contributions to non-sea-salt sulfate in the marine boundary layer over the North Atlantic Ocean, J. Geophys. Res., 107(D18), 4356, doi:10.1029/2001JD000970, 2002

Schwarz, J. P., Gao, R. S., Fahey, D. W., Thomson, D. S., Watts, L. A., Wilson, J. C., Reeves, J. M., Darbeheshti, M., Baumgardner, D. G., Kok, G. L., Chung, S. H., Schulz, M., Hendricks, J., Lauer, A., Ka, B. and Slowik, J. G.: Single-particle measurements of midlatitude black carbon and light-scattering aerosols from the boundary layer to the lower stratosphere, J. Geophys. Res. Atmos., 111, D216207, 1–15, doi:10.1029/2006JD007076, 2006.

Formatted: Widow/Orphan control

Deleted:

Deleted: .

Deleted: ,

Deleted: L

Formatted: Font: 12 pt

Formatted: Font: 12 pt

Deleted: submitted (

Deleted:)

Formatted: Font: Font color: Custom Color(RGB(35,31,32)), Check spelling and grammar

1911 Schiffer, J. M., Mael, L. E., Prather, K. A., Amaro, R. E. and Grassian, V. H.: Sea Spray Aerosol:
1912 Where Marine Biology Meets Atmospheric Chemistry, ACS Cent. Sci., 4, 1617-
1913 1623 doi:10.1021/acscentsci.8b00674, 2018.
1914 Schiller, S. A. P.: Flugzeuggestützte Messung flüchtiger organischer Verbindungen über dem
1915 Nordatlantik mittels PTR-ToF-MS, Master Thesis (*in German*), Universität
1916 Innsbruck (2018)
1917 Schwinger, J., Tjiputra, J., Goris, N., Six, K. D., Kirkevåg, A., Seland, Ø., Heinze, C. and Ilyina,
1918 T.: Amplification of global warming through pH dependence of DMS production
1919 simulated with a fully coupled Earth system model, Biogeosciences, 14, 3633–
1920 3648, https://doi.org/10.5194/bg-14-3633-2017, 2017.
1921 Sharma, S., Lavoué, D., Cachier, H., Barrie, L. A. and Gong, S. L.: Long-term trends of the black
1922 carbon concentrations in the Canadian Arctic, J. Geophys. Res. Atmos., 109,
1923 (D15203), doi:10.1029/2003JD004331, 2004.
1924 Sharma, S., Andrews, E., Barrie, L. A., Ogren, J. A. and Lavoué, D.: Variations and sources of the
1925 equivalent black carbon in the high Arctic revealed by long-term observations at
1926 Alert and Barrow: 1989–2003, J. Geophys. Res. Atmos., 111, (D14208),
1927 doi:10.1029/2005JD006581, 2006.
1928 Sihto, S., Kulmala, M., Kerminen, V., Maso, M. D. and Petäjä, T., Riipinen, I., Korhonen, H.,
1929 Arnold, F., Janson, R., Boy, M., Laaksonen, A. and Lehtinen, K. E. J.: Atmospheric
1930 sulphuric acid and aerosol formation : implications from atmospheric
1931 measurements for nucleation and early growth mechanisms, Atmos. Chem. Phys.,
1932 6, 4079–4091, www.atmos-chem-phys.net/6/4079/2006/, 2006.
1933 Singh, H. B., Cai, C., Kaduwela, A., Weinheimer, A. and Wisthaler, A.: Interactions of fire
1934 emissions and urban pollution over California : Ozone formation and air quality
1935 simulations, Atmos. Environ., 56, 45–51, doi:10.1016/j.atmosenv.2012.03.046,
1936 2012.
1937 Stohl, A., Forster, C., Eckhardt, S., Spichtinger, N., Huntrieser, H., Heland, J., Schlager, H.,
1938 Wilhelm, S., Arnold, F. and Cooper, O.: A backward modeling study of
1939 intercontinental pollution transport using aircraft measurements, J. Geophys. Res.,
1940 108, D12, 4370, doi:10.1029/2002JD002862, 2003.

Takegawa, N., Seto, T., Moteki, N., Koike, M., Oshima, N., Adachi, K., Kita, K., Takami, A. and Kondo, Y.: Enhanced New Particle Formation Above the Marine Boundary Layer Over the Yellow Sea : Potential Impacts on Cloud Condensation Nuclei, J. Geophys. Res. Atmos., 125, e2019JD031448, 1–17, doi:10.1029/2019JD031448, 2020.

Tremblay, S., Picard, J.-C., Bachelder, J. O., Lutsch, E., Strong, K., Fogal, P., Leaitch, W. R., Sharma, S., Kolonjari, F., Cox, C. J., Chang, R. Y.-W. and Hayes, P. L.: Characterization of aerosol growth events over Ellesmere Island during summers of 2015 and 2016, Atmos. Chem. Phys., 19, 5589-5604, https://doi.org/10.5194/acp-19-5589-2019, 2019.

Tunved, P., Ström, J. and Krejci, R.: Arctic aerosol life cycle: Linking aerosol size distributions observed between 2000 and 2010 with air mass transport and precipitation at Zeppelin station, Ny-Ålesund, Svalbard, Atmos. Chem. Phys., 13(7), 3643–3660, doi:10.5194/acp-13-3643-2013, 2013.

van der Werf, G. R., Randerson, J. T., Giglio, L., Van Leeuwen, T. T., Chen, Y., Rogers, B. M., Mu, M., Van Marle, M. J. E., Morton, D. C., Collatz, G. J., Yokelson, R. J. and Kasibhatla, P. S.: Global fire emissions estimates during 1997-2016, Earth Syst. Sci. Data, 9(2), 697–720, doi:10.5194/essd-9-697-2017, 2017.

Vehkamäki, H., Kulmala, M., Napari, I., Lehtinen, K. E. J., Timmreck, C., Noppel, M. and Laaksonen, A.: An improved parameterization for sulfuric acid – water nucleation rates for tropospheric and stratospheric conditions, J. Geophys. Res., 107, D22, 4622, 1–10, doi:10.1029/2002JD002184, 2002.

Veres, P. R., Neuman, J. A., Bertram, T. H., Assaf, E. and Wolfe, G. M.: Global airborne sampling reveals a previously unobserved dimethyl sulfide oxidation mechanism in the marine atmosphere, Proc.Natl, Acad. Sci., 117(9), 4505–4510, doi:10.1073/pnas.1919344117, 2020.

Vinken, G. C. M., Boersma, K. F., Jacob, D. J., Meijer, E. W.: Accounting for non-linear chemistry of ship plumes in the GEOS-Chem global chemistry transport model, Atmos. Chem. Phys., 11, 11707–11722, doi:10.5194/acp-11-11707-2011, 2011.

Wang, Q., Jacob, D. J., Fisher, J. A., Mao, J., Leibensperger, E. M., Carouge, C. C., Le Sager, P., Kondo, Y., Jimenez, J. L., Cubison, M. J. and Doherty, S. J.: Sources of

carbonaceous aerosols and deposited black carbon in the Arctic in winter-spring: Implications for radiative forcing, Atmos. Chem. Phys., 11, 12453–12473, doi:10.5194/acp-11-12453-2011, 2011.

Wang, Q., Jacob, D. J., Spackman, J. R., Perring, A. E., Schwarz, J. P., Moteki, N., Marais, E. A., Ge, C., Wang, J. and Barrett, S. R. H.: Global budget and radiative forcing of black carbon aerosol : Constraints from pole-to-pole (HIPPO) observations across the Pacific, J. Geophys. Res., 119, 195–206, doi:10.1002/2013JD020824, 2014.

Wang, X., Sultana, C. M., Trueblood, J., Hill, T. C. J., Malfatti, F., Lee, C., Laskina, O., Moore, K. A., Beall, C. M., McCluskey, C. S., Cornwell, G. C., Zhou, Y., Cox, J. L., Pendergraft, M. A., Santander, M. V., Bertram, T. H., Cappa, C. D., Azam, F., DeMott, P. J., Grassian, V. H. and Prather, K. A.: Microbial control of sea spray aerosol composition: A tale of two blooms, ACS Cent. Sci., 1(3), 124–131, doi:10.1021/acscentsci.5b00148, 2015.

Weber, R. J., Chen, G., Davis, D. D., Mauldin, R. L., Tanner, D. J., Clarke, A. D., Thornton, D. C. and Bandy, A. R.: Measurements of enhanced H_2SO_4 and 3-4 nm particles near a frontal cloud during the First Aerosol Characterization Experiment (ACE 1), J. Geophys. Res., 106, (D20),24 107 - 24117, 2001.

Wehner, B., Werner, F., Ditas, F., Shaw, R. A., Kulmala, M. and Siebert, H.: Observations of new particle formation in enhanced UV irradiance zones near cumulus clouds, Atmos. Chem. Phys., 11701–11711, doi:10.5194/acp-15-11701-2015, 2015.

Wesley, M. L.: Parameterization of surface resistances to gaseous deposition in regional-scale numerical models, Atmos. Environ., 23, 1293-1304, 1989.

Westervelt, D. M.: Formation and growth of nucleated particles into cloud condensation nuclei : model – measurement comparison, Atmos. Chem. Phys., 13, 7645–7663, doi:10.5194/acp-13-7645-2013, 2013.

Willis, M. D., Burkart, J., Thomas, J. L., Köllner, F., Schneider, J., Bozem, H., Hoor, P. M., Aliabadi, A. A., Schulz, H., Herber, A. B., Leaitch, W. R. and Abbatt, J. P. D.: Growth of nucleation mode particles in the summertime Arctic: A case study, Atmos. Chem. Phys., 16(12), 7663–7679, doi:10.5194/acp-16-7663-2016, 2016.

Willis, M. D., Köllner, F., Burkart, J., Bozem, H., Thomas, J. L., Schneider, J., Aliabadi, A. A., Hoor, P. M., Schulz, H., Herber, A. B., Leaitch, W. R. and Abbatt, J. P. D.:

Evidence for marine biogenic influence on summertime Arctic aerosol, Geophys. Res. Lett., 44(12), 6460–6470, doi:10.1002/2017GL073359, 2017.

Willis, M. D., Leaitch, W. R. and Abbatt, J. P. D.: Processes Controlling the Composition and Abundance of Arctic Aerosol, Reviews of Geophysics, 56, 621-671, doi:10.1029/2018RG000602, 2018.

Wood, R.: Stratocumulus Clouds, Mon. Weather Rev., 140, 2373–2423, doi:10.1175/MWR-D-11-00121.1, 2012.

Wilson, T. W., Ladino, L. A., Alpert, P. A., Breckels, M. N., Brooks, I. M., Browse, J., Burrows, S. M., Carslaw, K. S., Huffman, J. A., Judd, C., Kilthau, W. P., Mason, R. H., McFiggans, G., Miller, L. A., Najera, J. J., Polishchuk, E., Rae, S., Schiller, C. L., Si, M., Temprado, J. V., Whale, T. F., Wong, J. P. S., Wurl, O., Yakobi-Hancock, J. D., Abbatt, J. P. D., Aller, J. Y., Bertram, A. K., Knopf, D. A. and Murray, B. J.: A marine biogenic source of atmospheric ice-nucleating particles, Nature, 525(7568), 234–238, doi:10.1038/nature14986, 2015.

Wood, R., Stemmler, J. D., Rémillard, J. and Jefferson, A.: Low-CCN concentration air masses over the eastern North Atlantic : Seasonality , meteorology , and drivers, J. Geophys. Res. Atmos., 122, 1203-1223, doi:10.1002/2016JD025557, 2017.

Woodhouse, M. T., Mann, G. W., Carslaw, K. S. and Boucher, O.: Sensitivity of cloud condensation nuclei to regional changes in dimethyl-sulphide emissions, Atmos. Chem. Phys., 13(5), 2723–2733, doi:https://doi.org/10.5194/acp-13-2723-2013, 2013.

Xu, J. W., Martin, R. V., Morrow, A., Sharma, S., Huang, L., Richard Leaitch, W., Burkart, J., Schulz, H., Zanatta, M., Willis, M. D., Henze, D. K., Lee, C. J., Herber, A. B. and Abbatt, J. P. D.: Source attribution of Arctic black carbon constrained by aircraft and surface measurements, Atmos. Chem. Phys., 17(19), 11971–11989, doi:10.5194/acp-17-11971-2017, 2017.

Yassaa, N., Peeken, I., Zöllner, E., Bluhm, K., Arnold, S., Spracklan, D. and Williams, J: Evidence for marine production of monoterpenes, Environ. Chem., 5, 391–401, doi:10.1071/EN08047, 2008.

Zanatta, M., Bozem, H., Köllner, F., Schneider, J., Hoor, P., Faria, J. De, Petzold, A., Bundke, U., Staebler, R. M., Schulz, H., Herber, A. B., Zanatta, M., Bozem, H., Köllner, F.,

Schneider, J., Hoor, P., Faria, J. De, Petzold, A., Bundke, U., Hayden, K., Staebler, R. M., Schulz, H. and Herber, A. B..: Airborne survey of trace gases amd aerosol over the Southern Baltic Sea: from clean marine boundary layer to shipping corridor effect, Tellus B Chem. Phys. Meteorol., 72(1), 1–24, doi:10.1080/16000889.2019.1695349, 2019.

Zender, C. S., Bian, H. and Newman, D.: Mineral Dust Entrainment and Deposition (DEAD) model: Description and 1990s dust climatology, J. Geophys. Res., 108(D14), 4416, doi:10.1029/2002JD002775, 2003.

Zhang, H. F., Worton, D. R., Lewandowski, M., Ortega, J., Rubitschun, C. L., Park, J. H., Kristensen, K., Campuzano-Jost, P., Day, D. A., Jimenez, J. L., Jaoui, M., Offenberg, J. H., Kleindienst, T. E., Gilman, J., Kuster, W. C., de Gouw, J., Park, C., Schade, G. W., Frossard, A. A., Russell, L., Kaser, L., Jud, W., Hansel, A., Cappellin, L., Karl, T., Glasius, M., Guenther, A., Goldstein, A. H., Seinfeld, J. H., Gold, A., Kamens, R. M. and Surratt, J. D.: Organosulfates as Tracers for Secondary Organic Aerosol (SOA) Formation from 2-Methyl-3-Buten-2-ol (MBO) in the Atmosphere, Environ. Sci. Technol., 46(17), 9437–9446, doi:10.1021/es301648z, 2012.

Zheng, G., Wang, Y., Aiken, A. C., Gallo, F., Jensen, M. P., Kollias, P., Kuang, C., Luke, E., Springston, S., Uin, J., Wood, R. and Wang, J.: Marine boundary layer aerosol in the eastern North Atlantic : seasonal variations and key controlling processes, Atmos. Chem. Phys., 18, 17615–17635, https://doi.org/10.5194/acp-18-17615-2018, 2018.

Zheng, G., Kuang, C., Uin, J., Watson, T., and Wang, J.: Large contribution of organics to condensational growth and formation of cloud condensation nuclei (CCN) in remote marine boundary layer, Atmos. Chem. Phys. Discuss., https://doi.org/10.5194/acp-2020-625, in review, 2020a.

Zheng, G., Sedlacek, A. J., Aiken, A. C., Feng, Y., Watson, T. B., Raveh-rubin, S., Uin, J., Lewis, E. R. and Wang, J.: Long-range transported North American wild fire aerosols observed in marine boundary layer of eastern North Atlantic, Environ. Int., 139(March), 105680, doi:10.1016/j.envint.2020.105680, 2020b.

Figures and tables

Deleted: ¶

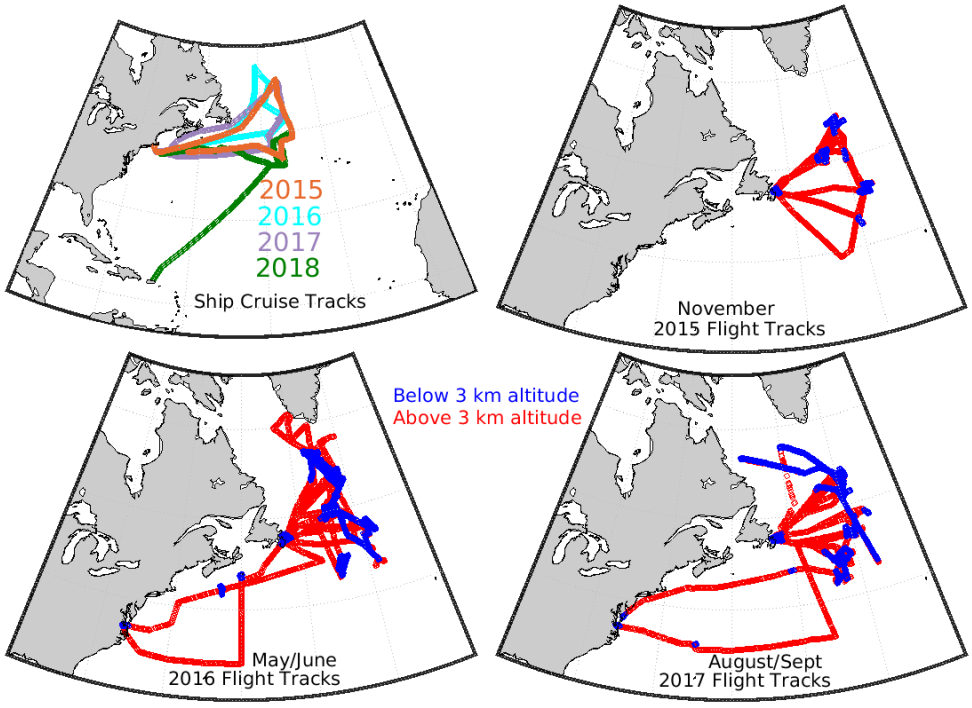

Figure 1: Cruise and aircraft tracks for the 2015-2018 NAAMES campaigns. Flight altitudes below 3 km are color-coded in medium blue and above 3 km in red. Ship tracks campaigns are color-coded for each year as shown by the legend, and as follows: Orange: November 2015 winter transition (bloom minima); Cyan: May/June 2016 climax transition (bloom maxima); Purple: August/September 2017 declining phase; Green: March/April 2018 accumulation phase.

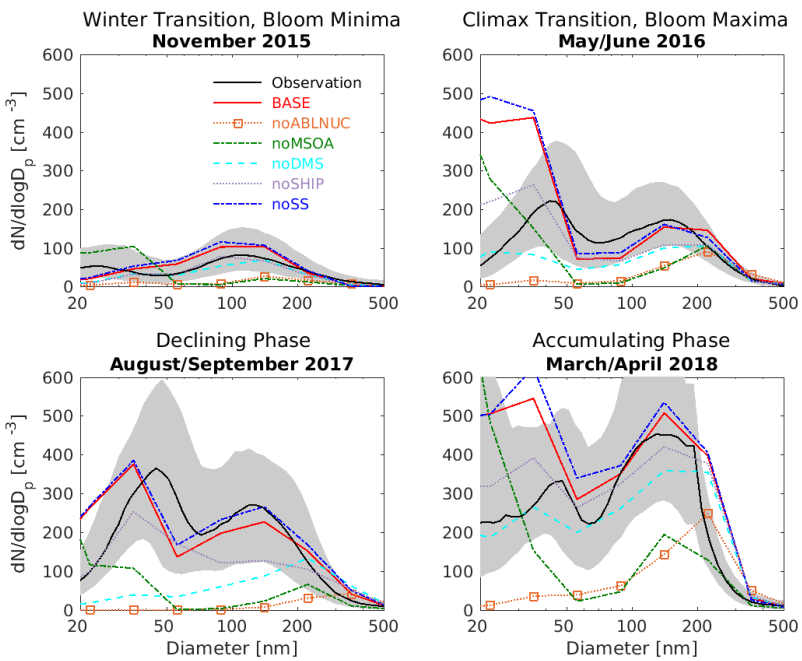

Figure 2: NAAMES cruise-track campaign-median marine boundary layer aerosol size distributions from marine-influenced SEMS (particle diameters 20-500 nm) observations (black, with 25th to 75th percentiles in grey) and for the six GEOS-Chem-TOMAS simulations as described in Table 1 (color-coded as shown in legend).

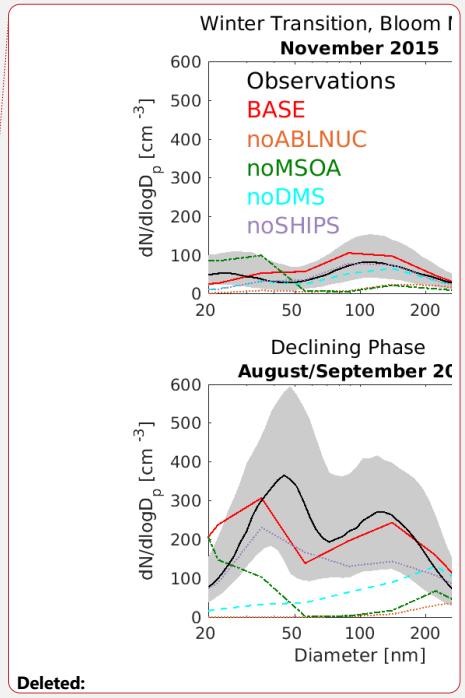

Deleted:

Deleted: five

Deleted: Linestyles: Solid: Observations, BASE; Dotted: noABLNUC, noSHIPS; Dash-dot: noMSOA; Dashed: noDMS.¶

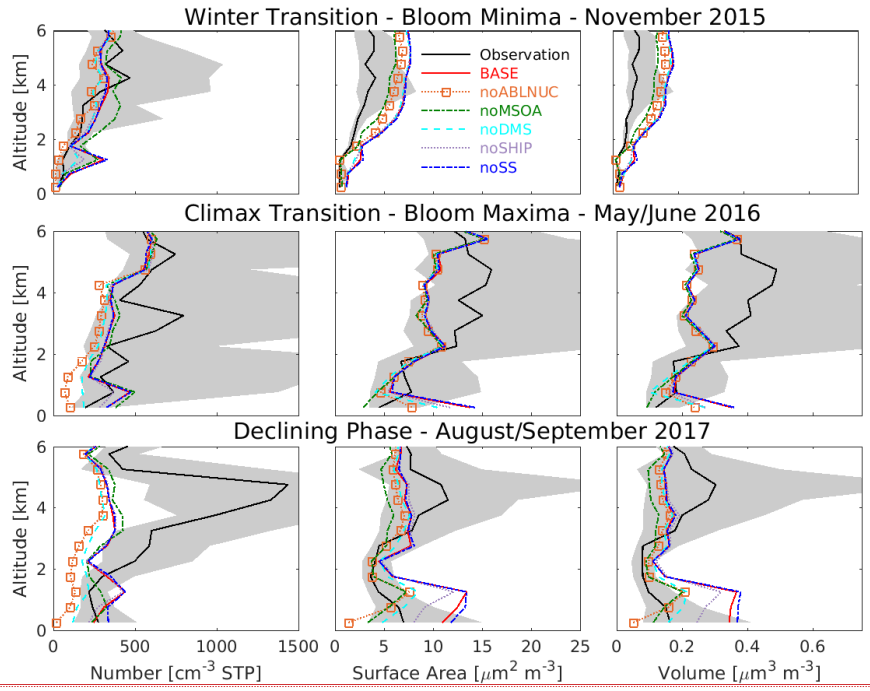

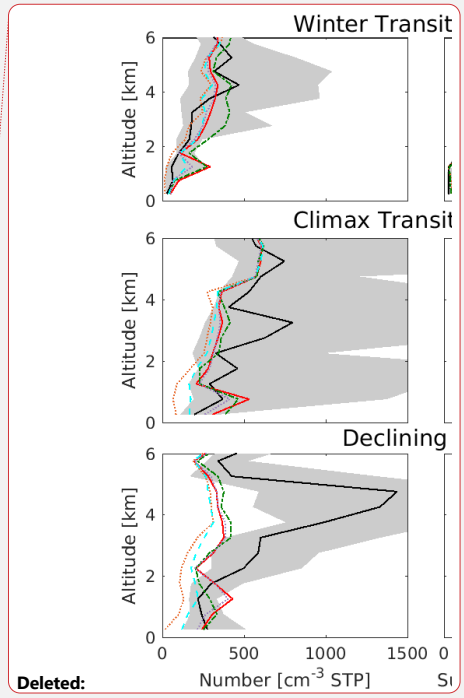

Figure 3: Vertical profiles of NAAMES campaign-median integrated SMPS observations aboard aircraft at standard temperature and pressure (STP) for particles with diameters of 10 to 282 nm (black, with 25th-75th percentiles in grey) and for the six GEOS-Chem-TOMAS simulations described in Table 1 (color-coded as shown in legend). All measurement and model output is binned at 500 m resolution and campaign-median values plotted at the mid-point of each bin starting at 250 m above the surface. Lines show linear interpolation between these values.

Deleted: five

Deleted: Linestyles: Solid: Observations, BASE; Dotted: noABLNUC, noSHIPS; Dash-dot: noMSOA; Dashed: noDMS….

Deleted: ¶

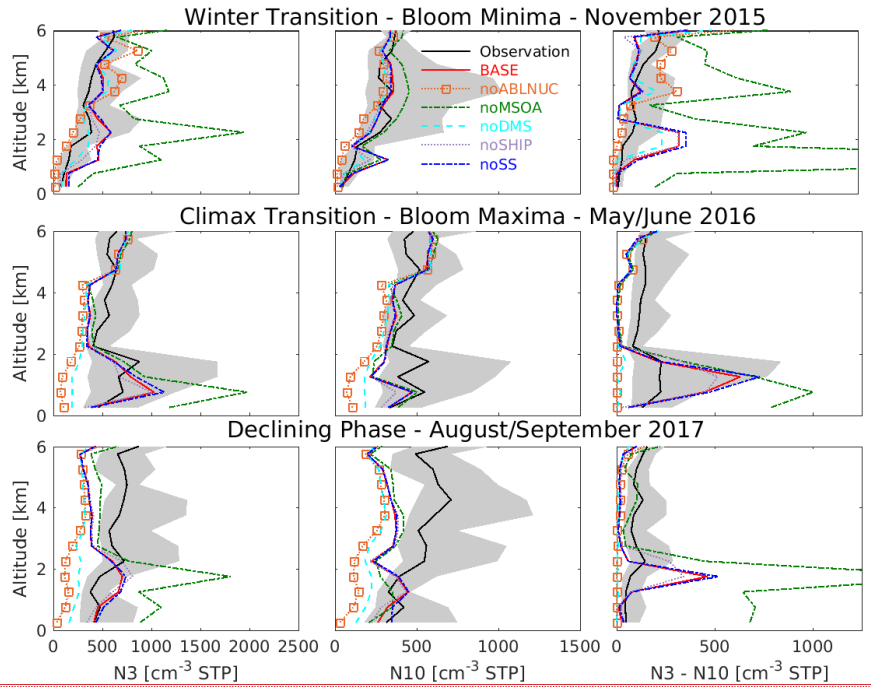

Figure 4: Vertical profiles of NAAMES campaign-median total number concentrations for particles with diameters larger than 3 nm (N3), 10 nm (N10) and between 3 to 10 nm (N3-N10) from CPC observations aboard aircraft at standard temperature and pressure (STP) (black, with 25th-75th percentiles in grey) and for the six GEOS-Chem-TOMAS simulations described in Table 1 (color-coded as shown in legend). All measurement and model output is binned at 500 m resolution and campaign-median values are plotted at the mid-point of each bin starting at 250 m above the surface. Lines show linear interpolation between these values.

Deleted:

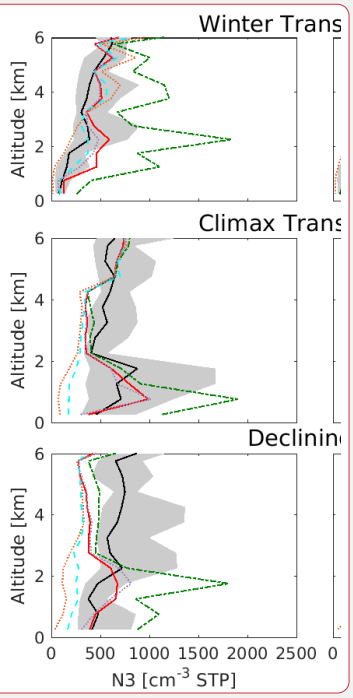

Deleted: five

Deleted:

Deleted: Linestyles: Solid: Observations, BASE; Dotted: noABLNUC, noSHIPS; Dash-dot: noMSOA; Dashed: noDMS….

Deleted: ¶

Deleted: →¶

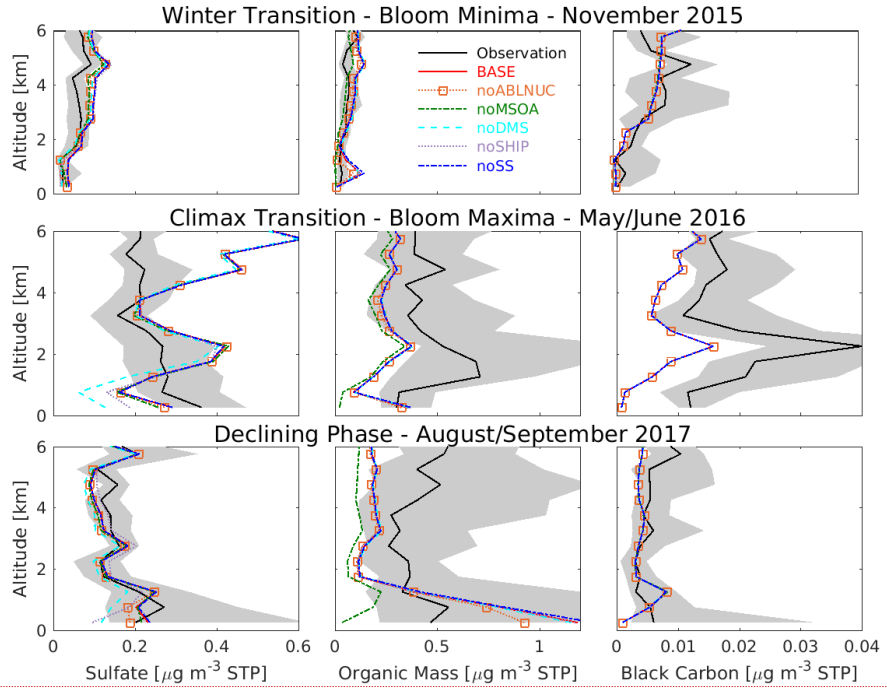

Figure 5: Vertical profiles of NAAMES campaign-median aerosol non-refractory sulfate and organic mass concentrations at standard temperature and pressure (STP) from Aerosol Mass Spectrometer and refractory black carbon from Single Particle Soot Photometer observations aboard aircraft (black, with 25th-75th percentiles in grey) and for the six GEOS-Chem-TOMAS simulations described in Table 1 (color-coded as shown in legend). Simulated sulfate shown is non-sea-salt-sulfate. All measurement and model output is binned at 500 m resolution and campaign-median values are plotted at the mid-point of each bin starting at 250 m above the surface. Lines show linear interpolation between these values.

Deleted:

Formatted: Justified, Line spacing: 1.5 lines

Deleted: five

Deleted: Linestyles: Solid: Observations, BASE; Dotted: noABLNUC, noSHIPS; Dash-dot: noMSOA; Dashed: noDMS….

Deleted: .

Deleted: ¶

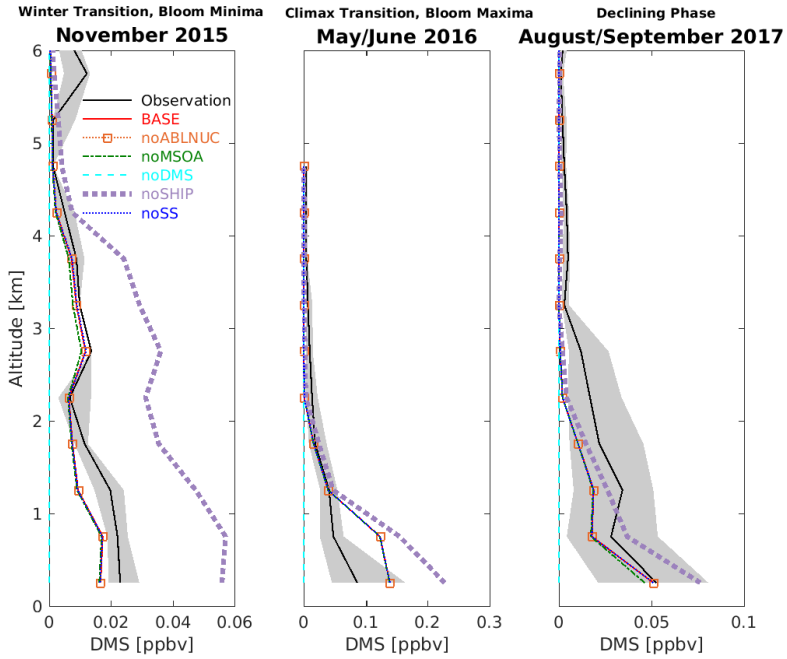

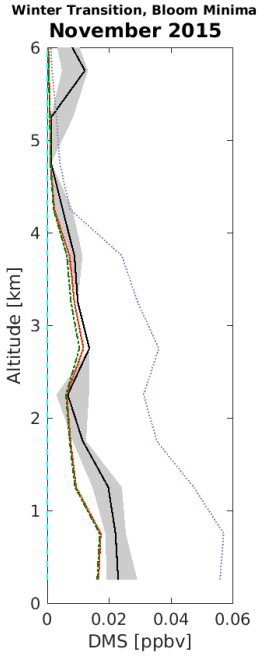

Deleted:

Figure 6: Vertical profiles of NAAMES cruise-track campaign-median observed dimethyl sulfide (DMS) mixing ratios (black, 25th-75th percentiles in grey) from aboard aircraft and for the six GEOS-Chem-TOMAS simulations described in Table 1 (color-coded as shown in legend). Simulations BASE, noABLNUC, noMSOA and noSS are nearly coincident. All measurement and model output is binned at 500 m resolution and campaign-median values plotted at the mid-point of each bin starting at 250 m above the surface. Lines show linear interpolation between these values. Note the horizontal scale change between panels.

Deleted: five

Deleted: and

Deleted: Linestyles: Solid: Observations, BASE; Dotted: noABLNUC, noSHIPS; Dash-dot: noMSOA; Dashed: noDMS.…

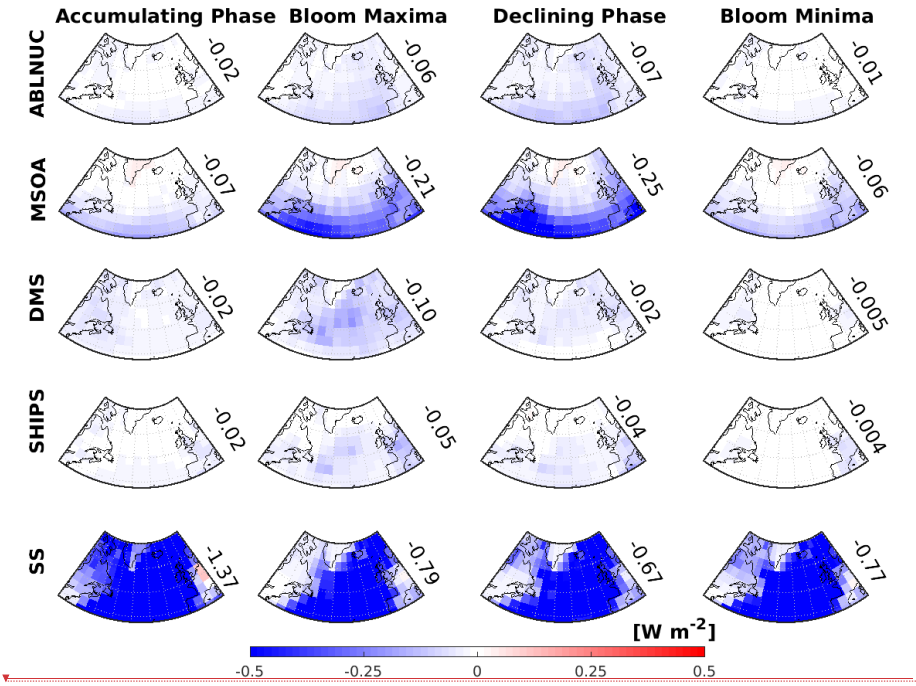

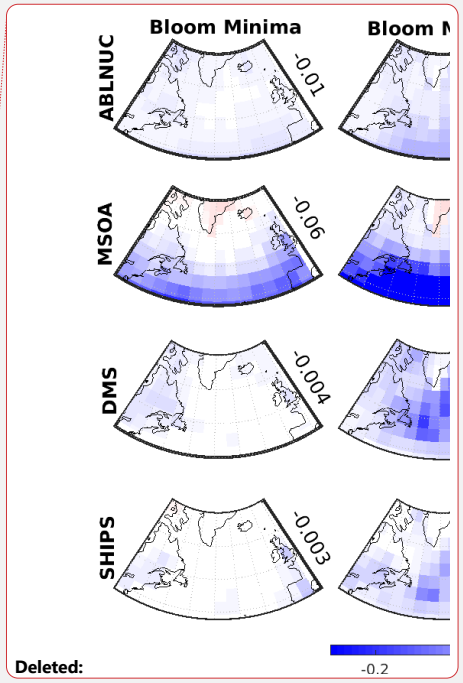

Figure 7: GEOS-Chem-TOMAS-simulated two-monthly-mean aerosol direct radiative effect (DRE) attributed to five key factors. Top row: Above boundary layer particle nucleation (ABLNUC); Second row: Particle growth by marine secondary organic aerosol (MSOA); Third row: Particle formation/growth due to DMS-oxidation products (DMS); Fourth row: Shipping emissions contribution to particles (SHIPS); Bottom row: Sea spray (SS). DREs are in columns for the following time periods, March/April 2018 (Accumulating Phase), May/June 2016 (Climax Transition, Bloom Maxima), August/September 2017 (Declining Phase), and October/November 2015 (Winter Transition, Bloom Minima). DREs for ABLNUC, MSOA, DMS, SHIPS, and SS are calculated using the differences in the top-of-the-atmosphere solar flux between simulation BASE and respective sensitivity simulations (noABLNUC, noMSOA, noDMS, noSHIPS, noSS). Values shown are area-weighted-mean DREs over the region bounded by 40-60 ºN, 20-50 ºW.

Deleted: our

Deleted: Bottom

Deleted: October/November 2015 (Winter Transition, Bloom Minima)…

Deleted: March/April 2018 (Accumulating Phase)

Deleted: S and

Deleted: ¶

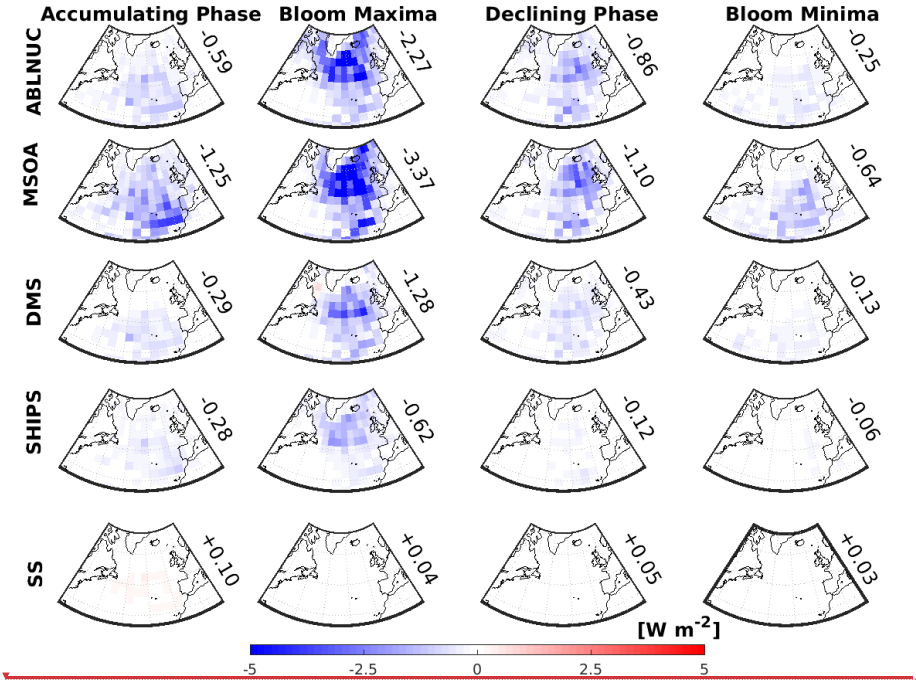

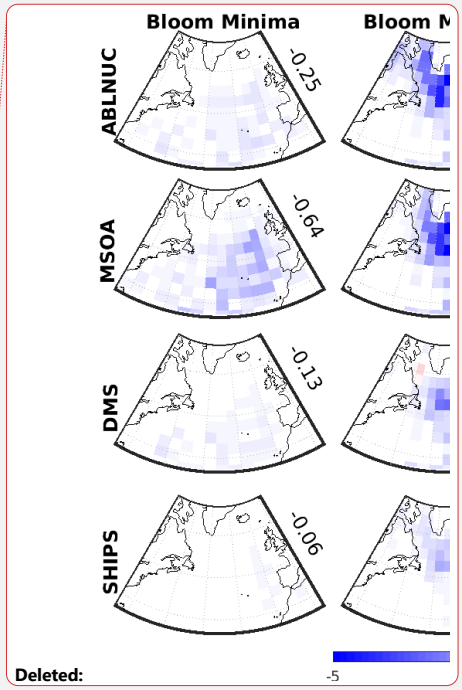

Deleted:

Figure 8: GEOS-Chem-TOMAS-simulated two-monthly-mean aerosol cloud-albedo indirect radiative effect (AIE) attributed to five key factors. Top row: Above boundary layer particle nucleation (ABLNUC); Second row: Particle growth by marine secondary organic aerosol (MSOA); Third row: Particle formation/growth due to DMS-oxidation products (DMS); Fourth row: Shipping emissions contribution to particles (SHIPS); Bottom row: Sea spray (SS). AIEs are in columns for the following time periods, March/April 2018 (Accumulating Phase), May/June 2016 (Climax Transition, Bloom Maxima), August/September 2017 (Declining Phase), and October/November 2015 (Winter Transition, Bloom Minima). AIEs for ABLNUC, MSOA, DMS, SHIPS, and SS are calculated using the differences in the top-of-the-atmosphere solar flux between simulation BASE and respective sensitivity simulations (noABLNUC, noMSOA, noDMS, noSHIPS, noSS). Values shown are area-weighted-mean AIEs over the region bounded by 40-60 ºN, 20-50 ºW.

Deleted: our

Deleted: Bottom

Deleted: October/November 2015 (Winter Transition, Bloom Minima)…

Deleted: March/April 2018 (Accumulating Phase

Deleted: and

Deleted: ¶
¶

Simulation	Description
BASE	Control simulation with GEOS-Chem-TOMAS model (GCT12.1.1) as described in Sect. 2.2
noABLNUC	Same as BASE, excluding the surrogate activation-type particle nucleation parameterization above the marine boundary layer to about 2 km altitude, as described in Sect. 2.2
noMSOA	Same as BASE, excluding the temperature-dependent marine organic vapors, forming marine secondary organic aerosol (MSOA)
noDMS	Same as BASE, excluding all emissions of DMS
noSHIPS	Same as BASE, excluding all ship emissions
noSS	Same as BASE, excluding all sea spray emissions

Table 1: GEOS-Chem-TOMAS simulation acronyms. Simulations and methodology are described in detail in Sect. 2.2 and 2.3.

Simulation	Nov 2015 Bloom Minima	May/June 2016 Bloom Maxima	Aug/Sept 2017 Declining Phase	Mar/Apr 2018 Accumulating	Annual Mean
BASE	0.20	0.33	0.04	0.28	0.21
noABLNUC	0.95	0.51	0.89	0.50	0.71
noMSOA	0.76	0.31	0.84	0.59	0.63
noDMS	0.44	0.27	0.43	0.06	0.30
noSHIPS	0.31	0.13	0.23	0.21	0.22
noSS	0.31	0.24	0.12	0.28	0.24

Table 2: Mean fractional error (MFE) between observations and the six GEOS-Chem-TOMAS simulations described in Sect. 2.2 and Table 1 for the ship-track campaign-median aerosol size distributions shown in Fig. 2.

Section 3:

Deleted: 17
Deleted: 40
Deleted: 12
Deleted: 31
Deleted: 3
Deleted: 84
Deleted: 53
Deleted: 7
Deleted: 44
Deleted: 66
Deleted: 6
Deleted: 3
Deleted: 3
Deleted: 3
Deleted: 0
Deleted: 11
Deleted: 29
Deleted: five

Factors controlling marine aerosol size distributions and their climate effects over the Northwest Atlantic Ocean region

Betty Croft[1], Randall V. Martin[2,1], Richard H. Moore[3], Luke D. Ziemba[3], Ewan C. Crosbie[3,4], Hongyu Liu[5], Lynn M. Russell[6], Georges Saliba[6], Armin Wisthaler[7,8], Markus Müller[7], Arne Schiller[7], Martí Galí[9], Rachel Y.-W. Chang[1], Erin E. McDuffie[1,2], Kelsey R. Bilsback[10], and Jeffrey R. Pierce[10]

[1]Department of Physics and Atmospheric Science, Dalhousie University, Halifax, NS, Canada
[2]McKelvey School of Engineering, Washington University in St. Louis, St. Louis, MO, USA
[3]NASA Langley Research Center, Hampton, VA, USA
[4]Science Systems and Applications, Inc., Hampton, VA, USA
[5]National Institute of Aerospace, Hampton, VA, USA
[6]Scripps Institute of Oceanography, University of California, San Diego, La Jolla, CA, USA
[7]Institute for Ion Physics and Applied Physics, University of Innsbruck, Technikerstrasse 25, 6020 Innsbruck, Austria
[8]Department of Chemistry, University of Oslo, P.O. 1033 – Blindern, 0315 Oslo, Norway
[9]Barcelona Supercomputing Center (BSC)
[10]Department of Atmospheric Science, Colorado State University, Fort Collins, CO, USA
Correspondence to: Betty Croft (betty.croft@dal.ca)

Abstract.

Aerosols over Earth's remote and spatially extensive ocean surfaces have important influences on planetary climate. However, these aerosols and their effects remain poorly understood, in part due to the remoteness and limited observations over these regions. In this study, we seek to understand factors that shape marine aerosol size distributions and composition in the Northwest Atlantic Ocean region. We use the GEOS-Chem-TOMAS model to interpret measurements collected from ship and aircraft during the four seasonal campaigns of the North Atlantic Aerosols and Marine Ecosystems Study (NAAMES) conducted between 2015 and 2018. Observations from the NAAMES campaigns show enhancements in the campaign-median number of aerosols with

diameters larger than 3 nm in the lower troposphere (below 6 km), most pronounced during the phytoplankton bloom maxima (May/June) below 2 km in the free troposphere. Our simulations, combined with NAAMES ship and aircraft measurements, suggest several key factors that contribute to aerosol number and size in the Northwest Atlantic lower troposphere, with significant regional-mean (40-60 ^{o}N, 20-50 ^{o}W) aerosol-cloud albedo indirect effects (AIE) and direct radiative effects (DRE) during the phytoplankton bloom. These key factors and their associated simulated radiative effects in the region include: (1) particle formation near and above the marine boundary layer (MBL) top (AIE: -3.37 W m^{-2}, DRE: -0.62 W m^{-2}), (2) particle growth due to marine secondary organic aerosol (MSOA) as the nascent particles subside into the MBL, enabling them to become cloud-condensation-nuclei-size particles (AIE: -2.27 W m^{-2}, DRE: -0.10 W m^{-2}), (3) particle formation/growth due to the products of dimethyl sulfide, above/within the MBL (-1.29 W m^{-2}, DRE: -0.06 W m^{-2}), (4) ship emissions (AIE: -0.62 W m^{-2}, DRE: -0.05 W m^{-2}) and (5) primary sea spray emissions (AIE: +0.04 W m^{-2}, DRE: -0.79 W m^{-2}). Our results suggest that a synergy of particle formation in the lower troposphere (particularly near and above the MBL top) and growth by MSOA contributes strongly to cloud-condensation-nuclei-sized particles with significant regional radiative effects in the Northwest Atlantic. To gain confidence in radiative effect magnitudes, future work is needed to understand 1) the sources and temperature-dependence of condensable marine vapors forming MSOA, 2) primary sea spray emissions, and 3) the species that can form new particles in the lower troposphere and grow these particles as they descend into the marine boundary layer.

5. Introduction

Marine atmospheric particles have important roles in Earth's climate system. Similar to particles in other regions, marine aerosols scatter and absorb solar radiation (Charlson et al., 1992), and modify cloud properties by acting as the seeds for cloud droplet formation (Boucher and Haywood, 2000; Lohmann and Feichter, 2005). Aerosols in the atmosphere's marine boundary layer (MBL) strongly influence the highly prevalent, low-altitude marine clouds, which have key climate cooling effects due to their reflection of incoming solar radiation (Wood, 2012; Chen et al., 2014). However, there remains high uncertainty about the magnitude of these aerosol effects (IPCC, 2013), due in part to limited understanding about the processes that control aerosols over Earth's expansive and remote ocean surfaces (Willis et al., 2018). Marine aerosols are strongly influenced

by natural, but poorly understood sources, making a large contribution to uncertainty in aerosol-climate effects (Carslaw et al., 2010; Carslaw et al., 2013). Limited observations of aerosols and their precursors over Earth's remote marine regions contribute to these knowledge gaps. In this study, we focus on investigation of several factors controlling the seasonal cycle of aerosol size and number and their resultant climate effects over the Northwest Atlantic Ocean.

Aerosol particles in the remote MBL have several seasonally varying sources (O'Dowd et al., 2004; Leck and Bigg, 2005; de Leeuw et al., 2011; Karl et al., 2012). Primary particles are emitted through wave breaking and bubble bursting processes that eject sea spray aerosols (SSA) of sea salt and organic composition (Russell et al., 2010; de Leeuw et al., 2011; Ovadnevaite et al., 2011; Gantt and Meskhidze, 2013; Prather et al., 2013; Hamacher-Barth et al., 2016; Brooks and Thornton, 2018). SSA have a not-yet-well-understood dependence on wind speed (Monahan et al., 1983; O'Dowd et al., 1997; Ovadnevaite et al., 2012; Grassian et al., 2015; Brooks and Thornton, 2018; Saliba et al., 2019) and sea surface temperature (Mårtensson et al., 2003; Jaeglé et al., 2011; Kasparian et al., 2017; Saliba et al., 2019). For the North Atlantic, observations indicate that primary SSA make a limited (less than 30%) contribution to cloud condensation nuclei (CCN) (Quinn et al., 2017, Zheng et al., 2018; Quinn et al., 2019) with no direct connection between SSA emissions and plankton ecosystems because the organic SSA appears to arise from the ocean's large pool of dissolved organic carbon (Quinn et al., 2014; Bates et al., 2020). SSA, however, could modify the CCN number that activate to form cloud droplets (Fossum et al., 2020), act as ice nuclei (Wilson et al., 2015; DeMott et al., 2016; Irish et al., 2017), and be more closely linked with biogenic activity in other regions (Ault et al., 2013; Cravigan et al., 2015; O'Dowd et al., 2015; Quinn et al., 2015; Wang et al., 2015; Schiffer et al., 2018; Christiansen et al., 2019; Cravigan et al., 2019). Recent studies have highlighted knowledge gaps related to sea spray emissions, particularly as related to the submicron sizes (e.g., Bian et al., 2019; Regayre et al, 2020). Measurement and modeling studies are needed to better understand and simulate the size-resolved contribution of sea spray to the Northwest Atlantic MBL.

For the North Atlantic, secondary aerosol of biogenic origin is observed to be an important seasonally varying contributor to marine particles and their growth to yield CCN (Sanchez et al., 2018). Marine secondary aerosol can arise from the condensation of a variety of marine-vapor-

oxidation products, which form and grow particles (Ceburnis et al., 2008; Rinaldi et al., 2010; Decesari et al., 2011). Formation of new aerosol particles in the marine environment is observed to be favored in clean atmospheric layers just below the marine inversion and also above the MBL top (Kazil et al., 2011; Takegawa et al., 2020). Newly formed particles, including those from the free troposphere can grow to CCN sizes (diameters larger than about 50 nm) through the condensation of available organic and sulfur-containing vapors on descent into the MBL (Korhonen et al., 2008). Once the particles reach CCN sizes, cloud processing (including aqueous phase aerosol production, and cloud droplet coagulation with other droplets and interstitial aerosols) also contributes to shaping the size distribution (Hoppel et al., 1986; Hoose et al., 2008; Pierce et al., 2015). For the North Atlantic MBL, entrainment of growing new particles formed in the relatively cleaner free troposphere is an important contributor to MBL particle number (Quinn et al., 2017; Sanchez et al., 2018; Zheng et al., 2018). In the pristine conditions of the summertime Arctic, both new particle formation (NPF) and growth (by condensation of organic and sulfur-containing vapors) are frequently observed within the boundary layer itself (Leaitch et al., 2013; Croft et al., 2016a; Willis et al., 2016; Collins et al., 2017; Burkart et al., 2017b). In addition to sulfuric acid, other vapors including amines, methane sulfonic acid (MSA), ammonia, and iodine all contribute to NPF in marine regions (O'Dowd, 2002; Facchini et al., 2008; Allan et al., 2015, Chen et al., 2016; Croft et al., 2016a; Dall´Osto et al., 2018). Interpretation of a combination of aircraft and ship-board observations with a size-resolved aerosol microphysics model is needed to develop understanding of the relative importance of near and above MBL top NPF as a contributor to aerosol size distributions in the Northwest Atlantic MBL.

Dimethyl sulfide (DMS) is one of the key contributors to secondary particle formation and growth that is released from the oceans as a result of marine biogenic activity (Lana et al., 2012a; Galí and Simó, 2015; Sanchez et al., 2018). The oxidation products of DMS include sulfuric acid and MSA (Barnes et al., 2006), which can form new particles and grow existing particles to sizes that can act as CCN (Hoffman et al., 2016; Hodshire et al., 2019). As well, hydroperoxymethyl thioformate (HPMTF) is a recently discovered DMS-oxidation product, which could also contribute to NPF and growth (Veres et al., 2020). The role of DMS in the climate system has undergone much debate since 1987 when the CLAW hypothesis proposed that DMS could act as a regulator in a warming

climate (Charlson et al., 1987). For the North Atlantic and Arctic, observations have linked DMS to the formation of aerosols during the times of phytoplankton blooms (Rempillo et al., 2011; Chang et al., 2011; Park et al., 2017; Sanchez et al., 2018; Abbatt et al., 2019; Quinn et al., 2019). As well, modelling studies have supported a role for DMS, linked to phytoplankton blooms, as a contributor to CCN number concentrations in the North Atlantic and Arctic MBLs (Woodhouse et al., 2013; Zheng et al., 2018; Ghahremaninezhad et al., 2019; Mahmood et al., 2019) and Southern Ocean MBL (Korhonen et al., 2008; McCoy et al., 2015; Revell et al., 2019). However, the extent to which DMS can act as a climate regulator remains unclear (Schwinger et al., 2017; Fiddes et al., 2018), and this role has been refuted (Quinn and Bates, 2011). Analysis of in situ observations of DMS and its products across the seasonal cycle of marine biogenic activity and in various ocean regions is needed to improve understanding related to the role of DMS in Earth's climate system.

Marine secondary organic aerosol (SOA) is another important contributor to sub-micron diameter marine aerosols, but is not well characterized (Rinaldi et al., 2010). The oceans are a source of a variety of organic vapors that could lead to SOA formation (O'Dowd and de Leeuw, 2007; Yassaa et al., 2008; Carpenter et al., 2012; Lana et al. 2012b; Hu et al., 2013; Carpenter and Nightingale, 2015; Kim et al., 2017; Rodríguez-Ros et al., 2020a). Oxygenated volatile organic compounds (OVOCs) recently linked to photochemical oxidative processes at the sea surface microlayer are possible contributors to marine SOA (Mungall et al., 2017). Isoprene and monoterpenes appear to make relatively minor contributions to marine SOA by mass, less than 1% for particles with diameters smaller than 10 μm at Cape Grim (Cui et al., 2019). The global, annual source of organic vapors from the oceans is highly uncertain, but current estimates are about 23 to 92 Tg C yr^{-1} (Brüggemann et al., 2018). Laboratory studies indicate that emissions of marine organic vapors increase with both temperature and incident radiation for temperatures up to about 26 ^{o}C (Meskhidze et al., 2015). Recent observations and modeling studies support a role for Arctic marine secondary organic aerosol (AMSOA) as a contributor to particle growth to CCN sizes (Burkart et al., 2017a; Collins et al., 2017; Willis et al, 2017; Willis et al., 2018; Tremblay et al., 2018; Leaitch et al., 2018; Croft et al., 2019; Abbatt et al., 2019). For the North Atlantic, organics are also found to make a large contribution to particle growth to CCN sizes (Sanchez et al., 2018; Zheng et al., 2020a). The result of the above-noted processes is a large and complex pool of organic

aerosol in the marine environment with sources that vary seasonally and regionally (Cavalli et al., 2004; Decesari et al., 2011; Cravigan et al., 2015; Liu et al., 2018; Leaitch et al., 2018).

Anthropogenic activity is also an important source of aerosols over the portions of the Earth's oceans. For the North Atlantic, several previous studies (e.g., Savoie et al., 2002; Stohl et al., 2003; Huntrieser et al., 2005; Fast et al., 2016) found a key role for synoptic scale motions in lifting aerosols arising from North American continental emissions and transporting them in layers over the North Atlantic with intrusions into the MBL. As well, ship traffic is an important source of both particles and oxidants in the MBL (Corbett et al., 2007; Zanatta et al., 2019; Bilsback et al., in press). Ship emissions of nitrogen oxides have a significant control on levels of oxidants such as ozone, the hydroxyl radical (OH) and NO_3 in the MBL (Vinken et al., 2011; Holmes et al., 2014). In the remote MBL, both OH and NO_3 are key oxidants of DMS, along with natural-source halogens such as BrO, with an important role for multiphase chemistry (Chen et al., 2018). Interpretation of aerosol observations across several seasons is needed to better understand the relative contribution of ship emissions to marine particles in the Northwest Atlantic region.

In this study, as part of the Ocean Frontier Institute (www.oceanfrontierinstitute.com), we address the knowledge gaps that were identified above, concerning several key factors shaping Northwest Atlantic MBL aerosol size distributions and their seasonal cycle. We consider the role of (1) new particle formation in clean atmospheric layers near and above the MBL top, (2) particle growth by marine SOA (MSOA) on descent into the MBL, (3) DMS contributions, (4) ship traffic emissions and (5) primary sea spray emissions. Aerosol measurements from the North Atlantic Aerosols and Marine Ecosystems Study (NAAMES) (Behrenfeld et al., 2019) provide an excellent basis for addressing the role of these five factors in the Northwest Atlantic Ocean region. The NAAMES aircraft and ship campaigns were conducted during four phases of the Northwest Atlantic annual plankton cycle from 2015-2018. We interpret the NAAMES aerosol measurements using a state-of-the-science size-resolved global aerosol microphysics model, GEOS-Chem-TOMAS (www.geos-chem.org). Our synergistic approach in bringing together NAAMES measurements and size-resolved aerosol process modeling enables a unique consideration of several key factors shaping Northwest Atlantic MBL aerosol size distributions and their annual cycle. We also quantify the impact of these factors on aerosol radiative effects over the North Atlantic.

The second section provides an overview of our measurement and modeling methodology. The third section presents results using the GEOS-Chem-TOMAS model to interpret NAAMES aerosol measurements and their seasonal cycle with a focus on the roles of near and above MBL top NPF, MSOA, DMS, sea spray, and ship emissions. We also quantify the direct and cloud-albedo indirect aerosol radiative effects attributed to each of these factors during the seasonal cycle. The final section gives our summary and outlook.

6. Methodology

2.1 Aerosol measurements during the NAAMES campaigns

NAAMES campaigns were conducted during four key periods in the annual cycle of marine biogenic activity, namely: the winter transition (November 2015), the accumulating phase (March/April 2018), the climax transition (May/June 2016), and the declining phase (August/September 2017) (Behrenfeld et al., 2019). These periods are defined by shifts in net phytoplankton growth rates and span a wide range in phytoplankton biomass, here estimated from chlorophyll-*a* concentrations (Chl-*a*). The winter transition is characterized by the annual minimum in Chl-*a* concentrations (generally < 1 mg m^{-3}) and a shift to favor phytoplankton growth over loss as the increasing ocean mixed-layer depth leads to fewer encounters between phytoplankton and their grazers. The accumulation phase occurs in early springtime when increasing sunlight and decreasing ocean mixed layer depths promote increasing phytoplankton growth rates and concentrations (Chl-*a* between 1 and 2 mg m^{-3}). The climax transition is the time of the annual maximum in phytoplankton biomass (Chl-*a* between 2 and 9 mg m^{-3}) and marks the shift from positive to negative growth rates owing to high grazing rates and depletion of nutrients. The declining phase (Chl-*a* between 1 and 2 mg m^{-3}) occurs later in the summertime when the ocean mixed layer depth increases and incident sunlight decreases, leading to further declines in phytoplankton growth and concentrations. Behrenfeld et al. (2019) provide an overview of the four measurement campaigns, and further details about Chl-*a* during NAAMES. The R/V Atlantis cruise tracks and NASA C130 flight paths are shown in Figure 1. Due to aircraft mechanical problems, there were no flights in 2018 during the accumulating phase.

In this study, we examine the NAAMES size-resolved aerosol measurements (particle diameters 20 to 500 nm) from the Scanning Electrical Mobility Sizer (SEMS, Model 138, 2002, BMI, Hayward, CA) aboard the R/V Atlantis ship. Aerosol particles were isokinetically drawn through an inlet positioned 18 m above sea level (Bates et al. 2002) and were subsequently dried below 20% relative humidity using silica diffusion driers prior to sampling by the SEMS. Clean marine periods were identified with criteria of relative wind directions within 90^{o} of the bow, condensation nuclei number concentrations less than 2000 cm^{-3}, ammonium and organic aerosol not covarying, ammonium < 100 ng m^{-3} and having back trajectories primarily over the ocean surface. We also consider aerosol size-resolved measurements (particle diameters 10 to 282 nm) from the Scanning Mobility Particle Sizer (SMPS, TSI Inc., Shoreview, MN) aboard the C130 aircraft. As well, we give attention to measurements of total particle number concentration from the Condensation Particle Counters (CPCs) with differing nominal lower detection diameters: 3 nm for the CPC 3025 (yielding N3 measurements) and 10 nm for the CPC 3772 (TSI Inc., St. Paul, MN) (yielding N10 measurements) aboard the C130 aircraft. We also consider submicron, non-refractory sulfate ($SO_4^{=}$) and organic mass (OM) concentrations from an Aerodyne High Resolution Time-of-Flight Aerosol Mass Spectrometer (HR-ToF-AMS, DeCarlo et al., 2006) and refractory black carbon from the Single Particle Soot Photometer (SP2, Schwarz et al., 2006) aboard the aircraft. HR-ToF-AMS and SP2 measurements are restricted to accumulation-mode aerosol (60-600 nm and 105-600 nm diameter, respectively). All aircraft observations are made behind a forward-facing, shrouded, solid diffuser inlet that efficiently transmits particles with aerodynamic diameter less than 5.0 μm to cabin-mounted instrumentation (McNaughton et al., 2007). Cloud-contaminated aerosol observations have been removed using a combination of wing-mounted cloud probe and relative humidity measurements. This filtering may possibly obscure some NPF events in proximity to clouds and remove some cloud-processed samples from the vertical profiles. Aerosol number and mass concentrations are reported at standard temperature and pressure. A Proton-Transfer-Reaction Time-of-Flight Mass Spectrometer (PTR-ToF-MS) (Müller et al, 2014; Schiller, 2018) was used aboard the NASA C-130 to measure volatile organic compounds including DMS and acetonitrile. Both observational and model data for periods where acetonitrile concentrations exceed 200 ppt are filtered out following Singh et al. (2012) to remove significant biomass burning contributions that are not the focus of this study.

2.2 GEOS-Chem-TOMAS model description

We use the GEOS-Chem model (v12.1.1) (http://www.geos-chem.org) coupled to the TwO Moment Aerosol Sectional (TOMAS) microphysics scheme (Adams and Seinfeld, 2002; Lee and Adams, 2012; Kodros and Pierce, 2017), with 15 sections, representing particle sizes from 3 nm to 10 µm. All simulations are at a $4^o \times 5^o$ resolution with 47 vertical levels extending to 0.01 hPa. The meteorological fields are from the GEOS Forward Processing off-line fields (GEOS-FP; https://gmao.gsfc.nasa.gov/GMAO_products/). Our size-resolved aerosol simulations parameterize the processes of particle nucleation, coagulation, condensation, along with wet and dry deposition and include the in-cloud aerosol coagulation scheme of Pierce et al. (2015). Sulfate, organic and black carbon, sea salt, dust and aerosol water are simulated. TOMAS is coupled to the full tropospheric aerosol/chemistry scheme of GEOS-Chem. Wet deposition follows Liu et al. (2001), Wang et al. (2011) and Wang et al. (2014). To represent efficient wet removal by North Atlantic drizzle in October and November, we implement a fixed in-cloud removal efficiency of 0.001 s^{-1} in the lowest 2 km of the model atmosphere over the ice-free ocean and enable wet removal of sulfate and organic aerosol in clouds with temperatures between 237 K and 258 K. In all seasons, we use the GEOS-FP cloud fraction as the precipitation fraction in the model layers where precipitation occurs for a closer connection with the meteorological fields (Croft et al., 2016b; Luo et al., 2019; Luo et al., 2020). Dry deposition uses the resistance in series approach of Wesley (1989). Simulated gas-phase species are also removed by dry and wet deposition as described in Amos et al. (2012).

For emissions, we use the GEOS-Chem v 12.1.1 default setup for gas-phase and primary aerosol emissions. We use emissions from the Community Emissions Data System (CEDS) for global anthropogenic sources of NO_x, CO, SO_2, NH_3, non-methane VOCs, black carbon, and organic carbon, including from international shipping as a source of both primary and secondary particles. Primary particles are emitted with a lognormal distribution (Lee et al., 2013). The most recent CEDS emissions dataset extends to the year 2017, as described in McDuffie et al. (2020). In this work, monthly CEDS emission totals for each compound are spatially gridded by source sector, according to the $0.1° \times 0.1°$ gridded EDGAR v4.2 emissions inventory (EC-JRC/PBL, 2012) and population, as described in Hoesly et al. (2018). To account for in-plume chemical processing of

ship emissions, we use the PARANOX scheme of Holmes et al. (2014). CEDS emissions are overwritten over the United States by the National Emissions Inventory (NEI11) with updated scale factors for our simulation years (2015-2018). We calculated these factors based on emission data for these years from the United States Environmental Protection Agency. Over Canada, we use the Air Pollutant Emissions Inventory (APEI). The Global Fire Emissions Database (GFED4s) is used for biomass burning emissions (van der Werf et al., 2017) for the years 2015-2016, with GFED4s climatological values for 2017 and 2018 since exact-year emissions were not available when we conducted our simulations. Dust emissions are from the scheme of Zender et al. (2003). Sea salt emissions follow Jaeglé et al. (2011). This temperature-dependent parameterization decreases global emissions relative to the Gong (2003) parameterization. A coupled parameterization for primary organic aerosol from sea spray was not available for our aerosol size-resolved GEOS-Chem-TOMAS simulations, such that some sea spray organics could be misrepresented as sea salt, since all sea spray in our simulations is considered sea salt. Such primary organic emissions are expected to have no seasonal cycle when averaged over the NAAMES region (Bates et al., 2020).

Exchange of DMS between the ocean and atmosphere is parameterized using the default GEOS-Chem parameterization, which follows Johnson (2010), largely based on Nightingale et al. (2000a; 2000b). We use the 8-day mean satellite-retrieval seawater DMS dataset of Galí et al. (2019) developed using the methodology of Galí et al. (2018), for available years (2015 and 2016) for the region north of about 40 ^{o}N. The Lana et al. (2011) DMS climatology is used elsewhere. Terrestrial biogenic emissions are from MEGAN2.1 as described in Guenther et al. (2012). Following Croft et al. (2019), we add a source of MSOA coupled to the simple SOA scheme described in Pai et al. (2020). Emissions of MSOA-precursor vapors have been found to increase with temperature (Meskhidze et al., 2015; Rodríguez-Ros et al., 2020a; Rodríguez-Ros et al., 2020b). Here, we use a temperature-dependent simulated source of MSOA-precursor emissions (S_{MSOA}), $S_{MSOA} = 70T + 350$ μg m^{-2} d^{-1}, where T is atmospheric temperature (^{o}C) at 2 m altitude. The values of 70 and 350 are found to yield acceptable model-measurement agreement for NAAMES campaign-median ship-track and aircraft measurements (Supplementary Figs. S1-S4 and Supplementary Tables S1 and S2). This simulated source of condensable vapors is emitted with a 50/50 split between vapors that are immediately available to form MSOA and vapors with 1-day aging prior to availability

(and not susceptible to wet removal). MSOA contributes to particle growth in our simulations (in agreement with observational-based studies e.g., Sanchez et al., 2018; Zheng et al., 2020a), along with sulfuric acid, but since the particle nucleating abilities of MSOA are unclear, it does not contribute to new-particle formation.

All simulations include particle nucleation in the boundary layer that is parameterized with the ternary (H_2SO_4-NH_3-H_2O) scheme of Napari et al. (2002), which was scaled by 10^{-5} to better match continental boundary-layer measurements (Westervelt et al., 2013). The binary (H_2SO_4-H_2O) scheme of Vehkamaki et al. (2002) is employed in the free troposphere at low NH_3 concentrations. Growth and loss of particles smaller than 3 nm are approximated following Kerminen et al. (2004). In our simulations, as a surrogate for unparameterized processes in the lower free troposphere and near the MBL top, we also employ an activation-type nucleation parameterization from the MBL top to about 2 km altitude. This activation-type scheme parameterizes nucleation rates as a linear function of sulfuric acid concentrations, using an empirical factor ($A = 2 \times 10^{-6}\ s^{-1}$) (Kulmala et al., 2006; Sihto et al., 2006), and serves as a proxy representing several unknown/unparameterized mechanisms related to NPF. Pockets of very clean air with low condensation sink near MBL clouds, which favor new particle formation (Kazil et al., 2011), are not resolved by large-scale models such as ours, with grid boxes on the scale of 100s km^2. Efficient wet removal by drizzling MBL clouds contributes to these pristine conditions (Wood et al., 2017). As well, MBL clouds reflect ultraviolet (UV) radiation and create pockets of enhanced UV, which favors photochemical production of aerosol precursor vapors (Weber et al., 2001; Wehner et al., 2015), that are not resolved by our model. Additionally, the particle nucleating capacity of MSOA is unclear and particle formation parameterizations are not yet developed to represent NPF when several gas-phase precursors interact. These precursors include, but are not limited to, MSA (Chen et al., 2016), HPMTF (Veres et al., 2020), amines (Facchini et al., 2008), iodine (Allan et al., 2015), and other extremely low-volatility organic compounds (ELVOCs) (Riccobono et al., 2014). The extra nucleation in the lower troposphere with the activation-type parameterization represents particle precursors that could have the same source as sulfuric acid. This approach may not capture the timing and magnitude of the variability in NPF correctly because the vapors participating in this nucleation are likely not just sulfuric acid. Future work is needed to better understand the nature of the nucleating species in the lower troposphere over the oceans.

We also conduct off-line radiative transfer calculations using the Rapid Radiative Transfer Model for Global Climate Models (RRTMG) (Iacono et al., 2008) to assess the direct radiative effect (DRE) and cloud-albedo aerosol indirect effect (AIE). The aerosol optical properties are calculated using the Mie code of Bohren and Hoffman (1983) to find the extinction efficiency, single scattering albedo, and asymmetry factor. Then, these optical properties, along with the monthly mean cloud fraction and surface albedo from the GEOS-FP meteorology fields, are input to the RRTMG to determine the change in top-of-the-atmosphere solar flux (DRE) between two simulations (our control simulation and one of the sensitivity simulations, Sect. 2.3). Our DRE calculations follow Kodros et al. (2016), with updates to include ammonium nitrate as described in Bilsback et al. (in press). All particles except black carbon are treated as internally mixed within each size section. We also calculate the cloud-albedo aerosol indirect effect (AIE) as described in Kodros et al. (2016), Croft et al. (2016a) and Ramnarine et al. (2019). The Abdul-Razzak and Ghan (2002) parameterization is used to calculate offline cloud droplet number concentrations (CDNC) using the aerosol mass and number concentrations from our simulations. We assume an updraft velocity of 0.5 m s^{-1} and the hygroscopicity parameters used by Kodros et al. (2016) and Kodros and Pierce (2017), assuming aerosol internal mixture, including ammonium nitrate following Bilsback et al. (in press). For each model grid box, we assume cloud droplet radii of 10 μm and perturb this value with the ratio of the monthly mean CDNC between two simulations (our control simulation and one of the sensitivity simulations, Sect. 2.3), assuming constant cloud liquid water content. The RRTMG is used to calculate the change in the top-of-the-atmosphere solar flux (AIE) due to changes in cloud droplet radii.

As one evaluation of simulation performance, we calculate the mean fractional error (MFE) of the 0^{th} to 3^{rd} moments between the simulated and observed MBL aerosol size distributions, following Boylan and Russell (2006) and using the same methodology as Hodshire et al. (2019) and Croft et al., (2019). The MFE is defined as a mean over the *N* aerosol size distribution moments,

$$\mathrm{MFE} = \frac{1}{N}\sum_{i=0}^{i=N-1}\frac{abs|C_m(i)-C_o(i)|}{(C_m(i)+C_o(i))/2} \quad (1)$$

where $C_m(i)$ is the integrated value of the i^{th} moment of the simulated aerosol size distribution and $C_o(i)$ is the integrated value of the i^{th} moment of the observed aerosol size distribution. The MFE can range from 0 to +2. We adopt the convention of Boylan and Russell (2006) to consider a MFE of 0.5 or less as acceptable.

For consideration of vertical profiles, we binned the measurement and simulation values using a 500 m height resolution, starting from the surface to 500 m as the first bin. Campaign-median values are calculated within each bin and plotted at the mid-point of the bin, starting at 250 m. During NAAMES, the lowest aircraft flight level altitude was around 150-200 m GPS altitude. We use a plane-flight diagnostic in the model to sample the simulation interpolated between grid-cell centers to the aircraft-flight-track position, during the times when measurement data was available for each respective instrument. We find consistent results with bin resolutions of 250, 500 and 1000 m, giving support for our selected binning resolution. The vertical profiles show measurements and model output along the aircraft flight tracks only and do not include any measurements or model output for the ship track. Vertical profile MFEs (Eq. 1) are calculated by summation over the altitude bins.

2.3 Summary of GEOS-Chem-TOMAS simulations

Table 1 summarizes the simulations conducted. Simulation BASE is our control simulation and includes all emissions and process parameterizations described above. We conduct five sensitivity simulations to examine the role of several key factors involved in shaping the aerosol distributions within the NAAMES study region. Simulation noABLNUC is the same as BASE, except without the sulfuric acid-dependent activation-type surrogate nucleation parameterization, which we implemented from the MBL top to about 2 km. Simulation noMSOA is the same as BASE, but without the source of temperature-dependent condensable marine organic vapors, forming MSOA. Simulation noDMS is the same as BASE, but without DMS. Simulation noSHIPS is the same as BASE, but without any ship emissions. Finally, simulation noSS is the same as BASE, but without any primary sea spray emissions. All simulations are sampled coincidentally with the measurements using hourly output along the NAAMES aircraft and ship tracks within the respective model grid boxes, using the NAAMES campaigns' 1-minute-resolution navigation data.

To manage computational expense, the simulations are necessarily at a coarse resolution, which can bias model-measurement comparisons. However, these biases will be lower for remote marine regions such as the NAAMES study region than over land regions, which generally have greater spatial inhomogeneity. Representativeness errors were also reduced by limiting our model-measurement comparisons to campaign-median values.

7. Results and Discussion

7.1 Key features of aerosols observed during NAAMES

Aerosol observations made during the NAAMES campaigns were in four seasons, capturing different stages of the annual cycle of Northwest Atlantic marine biogenic activity (Behrenfeld et al., 2019). Figure 2 shows the campaign-median marine-influenced aerosol size distributions from SEMS (particle diameters 20-500 nm) for the four R/V Atlantis cruises. November 2015 (winter transition, bloom minima) is characterized by the lowest aerosol number concentrations. The peak of the Northwest Atlantic drizzle season occurs at this time, with efficient wet removal of accumulation-sized aerosol (diameters larger than about 50 to 100 nm) (Browse et al., 2012). As well, relative to other the seasons, marine biogenic emissions are low at this time of minimal phytoplankton biomass. The summertime observations during both May/June 2016 (climax transition, phytoplankton bloom maxima) and August/September 2017 (declining phase) are characterized by a weakly dominant Aitken mode (particle diameters < 100 nm). The winter transition (November 2015) and early spring accumulation phase observations (March/April 2018) are characterized by the dominance of accumulation-mode aerosols (particle diameters > 100 nm).

The vertical profiles of campaign-median integrated-SMPS (particle diameters of 10 to 282 nm) observations are shown in Fig. 3. There are several key features of the observed aerosol vertical profiles for the three NAAMES flight campaigns. These profiles exhibit several particle number maxima in the lower free troposphere below 6 km, including below 2 km during the May/June climax transition period. As shown in Fig. 3, aerosol surface area and volume are less at altitudes below about 3 km relative to altitudes above 3 km. This lower particle surface area at these altitudes favors NPF over growth of pre-existing particles as available vapors condense in these relatively

cleaner atmospheric layers (Kazil et al., 2011). Transport of aerosols (in part associated with continental emissions) contributes to particles in all seasons. Fast et al. (2016) characterized summertime North Atlantic transport layers in the free troposphere associated with synoptic-scale lifting. The late fall (November 2015, Fig.3) is characterized by the lowest aerosol number, surface and volume concentrations, similar to the findings shown in Fig. 2.

Figure 4 shows the vertical-profile campaign-median total particle number concentrations from CPCs, for aerosols with diameters larger than 3 nm (N3), larger than 10 nm (N10), and the difference between the two (N3-N10). For the May/June 2016 climax transition (phytoplankton bloom maximum), there are enhancements in observed number concentration (N3, N10 and N3-N10) below about 2 km in the free troposphere, indicating NPF at these altitudes (Fig. 4). The MBL top ranged from about 0.5 to 2 km for the NAAMES cruises (Behrenfeld et al., 2019). The lower free tropospheric region near and above the MBL top is an important region for marine NPF. These altitudes above the MBL clouds are generally very clean, which favors NPF, and strongly sunlit, which favors the photochemical oxidative production of particle precursors for NPF. Previous studies based on observations from other marine regions have also found a cloud-processed ultra-clean layer with weak condensation/coagulation sinks at about 1 km altitude, where NPF is favored (Kazil et al., 2011; Takegawa et al., 2020). Figure 4 also shows enhancements in the observed N3 and N10 concentrations below 6 km during the declining phase and winter transition (bloom minima). However, the total number concentration enhancements below 2 km are most pronounced during the phytoplankton bloom maximum, suggesting a connection between particle number and the level of marine biogenic activity.

$SO_4^=$ and OM are dominant non-refractory components of the submicron-diameter aerosols, and vertical profiles of campaign-median observations are shown on Fig. 5. During the summertime (May/June 2016, climax transition and August/September 2017, declining phase), the OM contribution exceeds that of $SO_4^=$ at most altitudes up to 6 km. Non-refractory $SO_4^=$ has its peak contribution during the climax transition season. This May/June phytoplankton bloom maxima period is the time of peak observed near-surface atmospheric DMS mixing ratios, as shown in Fig. 6. During the climax transition (bloom maxima), non-refractory $SO_4^=$ concentrations increase towards the surface, suggesting a marine surface source, similar to summertime Arctic marine

Commented [RM5]: not at surface during May/June

profile observations (Willis et al., 2017). Black carbon (BC) concentrations are also shown in Fig. 5 and have several peaks in the free troposphere in all seasons, consistent with a long-range transport source. Maximum BC concentrations are in May/June, likely associated with greater transport of anthropogenic continental pollution and biomass burning during this time, relative to other seasons. Springtime has also been associated with peak BC concentrations in the Arctic due to long-range transport (Sharma et al., 2004; Sharma et al., 2006; Fisher et al., 2010; Wang et al., 2011; Xu et al., 2017). All aerosol mass concentrations in the lowest 2 km of the atmosphere (Fig. 5) are lowest in the November 2015 winter transition, which is a time of efficient wet removal by drizzle (Browse et al., 2012; Wood et al., 2017), diminishing marine emissions due to diminishing phytoplankton biomass, and outbreaks of relatively less polluted polar air advected down the Labrador Strait (Behrenfeld et al., 2019). For the Arctic, the fall season has also been associated with a relative minimum in aerosol number concentrations (Tunved et al., 2013; Croft et al., 2016b).

The GEOS-Chem-TOMAS model (described in Sect. 2.2 and 2.3) is generally able to simulate the above-noted features of the aerosols over the Northwest Atlantic. Simulation BASE captures key aspects of the MBL size distributions including the minimum in aerosol number during the November winter transition, the weakly dominant Aitken mode during the May/June climax transition and August/September declining phase and the maximum in number of accumulation-mode particles (diameters greater than 100 nm) during the March/April accumulation phase, despite errors such as between 20-50 nm (Fig. 2). As well, the BASE simulation captures several lower tropospheric enhancements in particle number concentration, although the simulated altitude for the maximum is sometimes displaced and there are errors in the magnitude (Figs. 3 and 4). In the lowest 2 km of the atmosphere, $SO_4^=$, OM, and BC mass concentrations for simulation BASE are generally within the 25^{th} to 75^{th} measurement percentiles, except for BC and OM underpredictions in May/June 2016, and OM overprediction in November 2015. All simulated $SO_4^=$ presented in this study is non-sea-salt $SO_4^=$. Simulation BASE also captures that the near-surface $SO_4^=$ is greatest during the May/June climax transition and the near-surface OM has its maximum value during the August/September declining phase. For each season the mean MFE across the parameters considered in Figs. 2 to 5 (BASE versus measurements, Supplementary Table S2) is satisfactory (MFE ranges 0.43 to 0.50). In the next four sub-sections, we use the

GEOS-Chem-TOMAS BASE simulation, relative to a set of sensitivity simulations, to examine the potential of five key factors to shape aerosol size distributions in the Northwest Atlantic during four stages of the annual cycle of marine biogenic activity.

7.2 Role of new particle formation (NPF) in the lower troposphere

Our simulations (BASE relative to noABLNUC, Fig. 4) suggest that NPF near and above the MBL has a strong control on the development of the total particle number (N3) maxima, with peak magnitude during the phytoplankton bloom maxima in layers below 2 km. Without the surrogate NPF scheme employed near and above the MBL top, the ternary NPF scheme in the MBL in simulation noABLNUC fails to simulate sufficient particle number, although vertical-profile campaign-median ammonium concentrations below 4 km altitude had acceptable agreement with observations (MFE ranges from 0.12 to 0.48, not shown). Figure 4 shows about a one-order-of-magnitude underprediction of N3 below about 2 km for noABLNUC. NoABLNUC has an unacceptable seasonal-mean model-measurement agreement across the measurement set (MFE ranges from 0.66 to 0.78, Supplementary Table S2). Figure 3 also shows that NPF near and above the MBL top makes a significant contribution to simulated particle number concentrations for aerosol diameters of 10 to 282 nm in the lower troposphere, most strongly in the summertime (BASE relative to noABLNUC). There is little impact on aerosol mass concentrations for simulation noABLNUC relative to BASE (Fig. 5).

The simulated N3-N10 (Fig. 4) illustrates that representation of NPF is a challenge for models, because there are difficulties capturing the magnitude and altitudes of the N3-N10 maxima. These discrepancies reflect key knowledge gaps related to the species that can form new particles in the marine environment (e.g., Veres et al. 2020). As well, the coefficient that we used for the surrogate activation-style nucleation parameterization was derived for a continental environment. The empirical ('A') value used by the parameterization appears to yield excessive NPF for the NAAMES marine environment. Activation-style nucleation was added in our simulations as a proxy for missing nucleation when the condensation sink is low, and conditions favor high oxidation rates. We acknowledge that this approach will miss variability in the timing and rates because it is a surrogate and not exactly the correct mechanism. As well in the summertime, the

simulations underpredict N3-N10 concentrations above 2 km, suggesting the need for future work to better understand the NPF processes at these levels, where the binary scheme of Vehkamaki et al. (2002) does not generate sufficient NPF.

NPF also makes a very strong contribution to the simulated aerosol size distributions within the MBL near the ocean surface (BASE versus noABLNUC, Fig. 2). Although our simulations do include NPF within the MBL, simulated NPF occurs more strongly near and above the MBL top and the resultant particles grow by condensation of available vapors and cloud processing while descending into the MBL. This role for NPF is in agreement with previous studies including those of Clarke et al. (2013), Quinn et al. (2017), and Williamson et al. (2019). As a result, NPF from several altitudes above the ocean surface contributes to the near-ocean-surface particles, with diameters from 20 to 200 nm. NPF does occur in the MBL. However, those levels above the MBL clouds favor oxidative chemistry that yields particle precursors, particularly from the wide-spread and persistent DMS sources in the marine environment (Kazil et al., 2011). Table 2 shows that for all seasons, the surrogate nucleation (simulation BASE, MFEs ranging from 0.04 to 0.33) represents an improvement over simulation noABLNUC (without this surrogate NPF parameterization, MFEs ranging from 0.50 to 0.95).

Extending the surrogate activation-style parameterization to the surface (Supplementary Figs. S5-S8 and Supplementary Table 3), leads to overprediction of the number of particles with diameters less than 50 nm in the MBL and yields higher MFEs (ranging from 0.20 to 0.56) than for simulation BASE, although the errors were not as large as those for noABLNUC. For the vertical profiles, this extra NPF extended into the MBL yields overprediction of N3, N10, and N3-N10 below 1 km in all seasons. Aerosol surface area and volume (in the SMPS particle-diameter size range of 10 nm - 282 nm) were also over predicted during the August/September declining phase, when the simulated temperature-dependent MSOA source was strongest, growing these extra new particles to larger sizes. These challenges highlight the relevance of ongoing research to better understand NPF in the marine environment.

7.3 Role of particle growth by condensing marine organic vapors

557 Condensing marine organic vapors forming MSOA are needed in our simulations (in addition to
558 H_2SO_4) for sufficient particle growth to yield satisfactory model-measurement agreement for MBL
559 size distributions (BASE versus noMSOA, Fig. 2). For simulation noMSOA, the model
560 overpredicts the number of particles with diameters smaller than about 30 nm in the MBL. Due to
561 insufficient particle growth of these sub-30 nm particles, the number of particles with diameters
562 between about 30 to 200 nm is underpredicted by more than 50% for simulation noMSOA.
563
564 In our simulations, MSOA enables particle growth to CCN sizes (diameters of about 50 nm or
565 larger). After particles reach CCN sizes, cloud processing can also contribute to simulated particle
566 growth towards accumulation-mode particles (diameters of 100-1000 nm) due to aqueous-phase
567 aerosol production. Other cloud processes include coagulation of cloud droplets with each other
568 and with interstitial aerosols (Hoose et al., 2008; Pierce et al., 2015). Our simulations include the
569 latter and aqueous-phase sulfate production. As clouds evaporate, cloud processing leads to
570 development of the 'Hoppel minima' of the MBL aerosol size distributions (Hoppel et al., 1987),
571 which is the minimum aerosol diameter that activates to form a cloud droplet (about 50-70 nm for
572 the observations in Fig. 2). This minimum diameter is smallest in the winter transition (November
573 2015), suggesting that smaller particles activated under the clean condition of this season relative
574 to the other seasons. As shown by Table 2, simulation noMSOA has an unacceptable annual-mean
575 MFE of 0.63, larger than the MFE of 0.23 for simulation BASE, which includes particle growth
576 due to MSOA.
577
578 The nature and flux of marine vapors forming MSOA are not well understood. As a result, we
579 developed a simplistic MSOA parameterization for use in this study, such that the MSOA
580 precursors vapor emissions are an increasing function of temperature. This approach yields a
581 seasonal cycle, and is in agreement with the temperature dependence trend found by previous
582 studies, including Meskhidze et al. (2015), Rodríguez-Ros et al. (2020a) and Rodríguez-Ros et al.,
583 2020b). We find that the simulated NAAMES cruise-track median aerosol size distributions are
584 sensitive to the coefficients used in the parameterization (S_{MSOA} = 70T - 350 μg m^{-2} d^{-1})
585 (Supplemental Figs. S1 and Table S1). For example, varying the temperature sensitivity between
586 50-100 and the intercept between 300-500 change the simulated number concentration of particles
587 with diameters larger than 50 nm in the MBL by up to a factor of two, with the greatest sensitivity

588 during the summertime (Supplemental Fig. S1). For the NAAMES MBL size distributions, the
589 annual-mean model-measurement MFEs are acceptable (ranging from 0.23 – 0.38, lowest for
590 BASE) for all temperature-dependent parameterizations that we tested, except for the factor-of-
591 ten scaling up of the BASE MSOA parameterization (simulation 10x(70T-350), Supplementary
592 Table S1, MFE of 0.75) and with the MSOA parameterization removed (simulation noMSOA,
593 Supplementary Table S1, MFE of 0.63). While this source flux is reasonably constrained for our
594 simulations, future work is needed to better understand and parameterize this source.
595
596 The vertical profiles are also sensitive to the MSOA parameterization (Supplementary Figs. S2-
597 4). Between noMSOA and the various MSOA parameterizations that we tested, concentrations
598 vary by up to a factor of about 2 for aerosol number (N3, N10, and N3-N10), SMPS-size-range
599 (diameters 10 nm - 282 nm) number, surface area, volume and also OM. Simulation noMSOA has
600 relatively greater error in the mean across the entire measurement set for each season (MFE ranges
601 from 0.53-0.68) relative to BASE (MFE ranges from 0.42-0.50) (Supplementary Table S2).
602
603 Although the chosen MSOA parameterization reasonably represents the observations, major
604 knowledge gaps remain regarding MSOA precursor species and their chemical lifetimes. While
605 the nature of MSOA precursors is not well-understood, recent measurements suggest that these
606 precursors could include a variety of chemical compounds. For example, measurements from the
607 Arctic indicate that the organics in marine aerosols were not typical biogenic SOA but had a long-
608 hydrocarbon chain implying a fatty acid type precursor (Willis et al., 2017). In other marine
609 regions, isoprene (Ciuraru et al., 2015) and carboxylic acids (Chiu et al., 2017) may also be
610 important. Given the limitations of current knowledge and the indications for a variety of MSOA
611 precursors, the improved MFEs for BASE relative to noMSOA provide support for the employed
612 MSOA parameterization.
613
614 The near-surface campaign-median climax transition and declining phase OM concentrations are
615 within the 25^{th} to 75^{th} measurement percentiles for simulation BASE, and below the 25^{th} percentile
616 of the observations for simulation noMSOA (Fig. 5). On average over the lowest 2 km of the
617 atmosphere during the May/June climax transition and August/September declining phase,
618 simulation BASE relative to noMSOA indicates that MSOA contributes about 200-400 ng m^{-3} to

simulated OM. Saliba et al. (2020) suggest that MBL-measurement non-refractory OM during NAAMES clean marine periods provides a good estimate of MSOA. Their seasonal-average non-refractory OM of about 300-400 ng m^{-3} for the 2016 May/June climax transition (phytoplankton bloom maxima) and 2017 August/September declining phase is similar to our model result. This contribution is about 3- to 4-fold greater than the contribution upwards of 100 ng m^{-3} from previous studies, noted in Kim et al. (2017). The model-measurement agreement for OM for 2017 is influenced by significant biomass burning with high altitude emission injections during this time (Zheng et al., 2020b; Saliba et al., 2020). Errors in the simulated emissions due to use of a GFED climatological-year emissions and injection-height errors could account for some of the model-measurement bias at high altitudes. As well, despite our implementation of a filter to remove measurement and model samples with strong in-plume aerosol enhancements during times of high acetonitrile concentrations, some biomass burning influence still affects the presented vertical profiles. Below 500 m altitude, condensing organic vapors yielding MSOA also increase the simulated aerosol surface area and volume by a factor of about 2-3 in all seasons (noMSOA versus BASE, Fig. 3), to be slightly over the 75th percentile of the observations (Fig. 3). Surface area and volume results from the simulation are very sensitive to the size-distribution simulation near the 282 nm diameter cut-off that contributes to differences between these simulations.

Figure 4 demonstrates that MSOA has a feedback on NPF. With lower aerosol surface area and lower condensation sink (noMSOA), the N3 and N3-N10 below 2 km altitude are strongly overpredicted because NPF increases and a lack of growth to larger sizes impacts N3-N10. During November, the N3 and N3-N10 overprediction also occurs at altitudes above 2 km because MSOA has a relatively greater influence on aerosol surface area at those altitudes in this season (Fig. 3). In this less-polluted late fall season, the influence of MSOA is relatively stronger at higher altitudes than in other seasons. Model-measurement agreement improves for N3 and N3-N10 with the addition of MSOA (simulation BASE relative to noMSOA, Fig. 4). Kazil et al. (2011) also found that condensing vapors generate a condensation sink that moderates the level of NPF in the marine environment. As well, recent studies from the Arctic indicate a key contribution to particles from condensing marine organic vapors (Burkart et al., 2017a; Willis et al., 2017; Croft et al., 2019). The impact of MSOA on the simulated N10 vertical profiles is small. The cloud filtering, which

649 we applied to the model and measurement aerosol samples along the flight track, preferentially
650 removes some of the cloud-processed samples, and contributes to this result.
651
652 **7.4 Role of DMS**
653
654 Figure 2 shows that DMS also has a control on the simulated MBL aerosol size distributions
655 (BASE versus noDMS) for the four seasons of the NAAMES campaigns. The total simulated
656 number of particles attributed to DMS is lowest during the phytoplankton bloom minima (winter,
657 November 2015) and greater in other seasons. For example, for particle diameters at 40 nm, the
658 DMS-related contribution to the size distribution (Fig. 2) is about 200-300 cm^{-3} in all seasons,
659 except less than 50 cm^{-3} during the bloom minima. Sulfuric acid from the oxidation of DMS has a
660 two-fold role in both NPF and in growing particles. However, as indicated by simulations
661 noABLNUC and noMSOA relative to BASE (Fig. 2), the DMS contribution is in concert with
662 both (1) a source of condensable marine organic vapors and (2) NPF near and above the MBL top.
663 The contribution of DMS to MBL particles is consistent with the findings of many previous
664 studies, including Chang et al. (2011), Ghahremaninezhad et al. (2016), Park et al. (2018), Sanchez
665 et al. (2018), Mahmood et al. (2019), Quinn et al. (2019) and Veres et al. (2020).
666
667 Simulation noABLNUC relative to noDMS for the marine-influenced MBL size distributions (Fig.
668 2) suggests that anthropogenic influences make a contribution as a source of particle-precursor
669 vapors for NPF, in addition to DMS. This relative contribution is particularly strong during the
670 accumulation phase (March/April 2018). In our simulations, anthropogenic SO_2 is oxidized to
671 H_2SO_4 and contributes to the particle precursors for NPF near and above the MBL top (in addition
672 to DMS oxidation products), followed by particle growth on descent into the MBL. As a result,
673 Fig. 2 shows a greater underprediction of aerosol number for simulation noABLNUC versus
674 noDMS.
675
676 Figure 6 indicates that the simulated DMS is generally consistent (MFEs ranging from 0.12 to
677 0.26, Supplementary Table S2) with the observed DMS mixing ratio vertical profiles and their
678 seasonal cycle for the NAAMES campaigns. DMS makes the strongest contribution to simulated
679 sulfate mass concentrations in the lowest 2 km during the May/June climax transition, reducing

model-measurement bias from about 40% to 10% (Fig. 5). Figures 3 and 4 suggest that in the lowest 2 km of the atmosphere, DMS contributes to both NPF and particle growth as there are increases in N3, N10, N3-N10, particle surface area and volume for simulations BASE versus noDMS. However, this behavior is co-dependent on conditions favorable to NPF near the MBL top and a source of MSOA.

7.5 Role of ship traffic emissions

Ship emissions are a source of primary and secondary particles, as well as a control on oxidants (Corbett et al., 2010; Vinken et al., 2011; Holmes et al., 2014). Our simulations suggest that ship emissions are also a control on the NAAMES-region MBL marine-influenced aerosol size distributions (Fig. 2, noSHIPS versus BASE). For example, for the simulated summertime MBL size distribution at particle diameters at 40 nm, about 100-200 particles cm^{-3} are attributed to ship emissions (Fig. 2). Table 2 shows that during the phytoplankton bloom and March/April accumulating phase, the noSHIPS simulation agrees more closely with the measurements than the BASE simulation, although both are within acceptable agreement (MFE < 0.5). These simulation challenges highlight the importance of future work to better understand the role of oxidants from ship emissions on particle production in the marine environment and to understand the size distribution of primary marine emissions.

Ship emissions make about a 50% contribution to the simulated sulfate campaign-median near-surface mass concentration in vertical profiles over the NAAMES study region (Fig. 5). For our simulations the impact of ship emissions on particle number is mostly limited to the lowest 2 km. Simulation BASE relative to noSHIPS suggest that about 10% of the N10 in the lowest 500 m of the atmosphere is attributed to ship emissions (Fig. 4). Figure 4 (right column) indicates that among the five factors considered by our sensitivity studies, ship emissions are among the smallest influence on the NPF. Major trans-Atlantic ship traffic routes (Corbett et al. (2007) are included in the NAAMES study region. Enhancements in observed benzene mixing ratios in the MBL relative to other long-lived tracers of anthropogenic emissions such as acetone (not associated with ship traffic) are observational evidence that ship emissions influence the study region (Supplementary Fig. S9).

Figure 6 demonstrates that atmospheric DMS mixing ratios are also sensitive to ship emissions. This effect occurs because ship emissions are a control on oxidants in the MBL, and enhance OH and NO_3, which are chemical sinks of DMS. As a result, simulated DMS mixing ratios increase when ship emissions are removed. As ship traffic is expected to change in future years with changes to routes and regulations (Gilgen et al., 2018; Bilsback et al. (in press)), the relative importance of ship emissions in the North Atlantic MBL will likely change.

7.6 Role of sea spray

Figure 2 shows that simulated sea spray acts as a condensation sink in the MBL. Without sea spray emissions, there is an increase in the number of sub-200 nm diameter particles (simulation noSS relative to BASE). However, this relative increase in simulated number is less than that attributed to other factors considered in the previous sections. While not a strong contributor to particle number in our simulations, sea spray is the dominant contributor to aerosol mass.

The simulated campaign-median MBL sea spray mass concentrations are within the measurement range of 3-8 μg m^{-3} found by Saliba et al. (2019) (Supplementary Fig. S10), despite the considerable uncertainties related to size-resolved sea spray emissions (e.g., Bian et al., 2019; Regayre et al. (2020)). Regayre et al. (2020) found that global sea spray emissions could be under predicted by a factor of 3 by the Gong (2003) parameterization. We conducted a simulation with factor-of-3 scaling of the sea spray emissions (Supplementary Figs. S11-S14, Supplementary Table S4) and found a decrease in MBL number concentrations, rather than an increase. This reduction occurred because the enhanced condensation sink from the additional sea spray emissions suppressed NPF. Our simulations use the Gong (2003) parameterization with a sea-surface-temperature-based scaling as described by Jaeglé et al. (2011), so are not directly comparable to the Regayre et al. (2020) findings. Nonetheless, these findings highlight the importance of ongoing work to improve size-resolved sea spray emissions parameterizations in models. The direct radiative effect of this sea spray mass loading is examined in the following section.

3.7 Radiative effects attributed to NPF near MBL top, MSOA, DMS and ship emissions

Figure 7 shows the simulated two-month mean direct radiative effect (DRE) attributed to the five factors we consider, (1) NPF near and above the MBL top, (2) MSOA, (3) DMS, (4) ship emissions and (5) primary sea spray emissions and magnitude of the regional-mean DREs over a region of the North Atlantic (40-60 ^{o}N, 20-50 ^{o}W). We note that the radiative effects attributed to the separate factors are not linearly additive because the factors impact each other non-linearly. For example, turning off either MSOA or nucleation above the boundary layer would shut down the majority of the production of accumulation-mode particles in the MBL (Fig. 2) since these particles require both nucleation and growth. Hence, adding the radiative effects from these two factors would result in double counting some radiative effects. Figure 7 indicates that the strongest calculated DRE is attributed to sea spray, which dominates the aerosol mass loading in the MBL. The sea spray DRE has a maximum during the 2018 March/April accumulating phase, which is a time of frequent synoptic scale storms with strong winds. Stormy conditions prevented the R/V Atlantis from travelling north of 45 ^{o}N during this final NAAMES campaign.

The strongest DRE values attributed to the above boundary layer NPF, MSOA, DMS and ship emission factors are during the summer season (climax transition (bloom maxima) and declining phase). This result highlights the link between the level of marine biogenic activity and aerosol climate effects. The second strongest individual DRE is attributed to condensing marine organic vapors, yielding MSOA. In our simulations, MSOA contributes significantly to particle growth to diameters of about 100 to 200 nm, which can then interact directly with radiation (Fig. 2). This effect is greatest in the declining phase because we used a temperature-dependent parameterization and sea surface temperatures are warmest during the late summer. The DRE geographic distribution suggests an increasing role for MSOA towards southern latitudes, again due to the temperature-dependent parameterization. Further work is needed to examine the role of MSOA in the more southerly latitudes as we cannot explicitly test this result across the annual cycle with the NAAMES observations.

Among the factors considered, Figure 7 shows that during the time of the May/June phytoplankton bloom, the aerosols produced and grown by the oxidation products of DMS have the third strongest

773 impact on the DRE, greatest over the regions where the bloom is located. The DRE is -0.10 Wm^{-2}
774 over the region between 40-60 ºN and 20-50 ºW during the bloom maxima and diminishes to -
775 0.005 Wm^{-2} during the bloom minima. This simulated impact of DMS relies in part on (1)
776 conditions favoring NPF processes near and above the MBL top, and (2) growth by MSOA as the
777 nascent DMS-related particles descend in the MBL. DMS (similar to MSOA) also contributes to
778 the DRE over the continents as these vapors have a lifetime of about a day in our simulations and
779 can be transported before their oxidation products are available for condensation. Once available
780 for condensation, DMS products and MSOA contribute to growing particles (of both marine and
781 continental origin) to sizes that can interact more strongly with radiation (diameters near 100 -200
782 nm). Particles arising from DMS grow during transport, and some particles may only reach sizes
783 large enough to interact with radiation when they are over the continents.
784
785 The DRE attributed to the near and above MBL top NPF factor (Fig. 7, top row, ABLNUC) is
786 strongest in summertime, during the May/June climax transition (bloom maxima) and
787 August/September declining phase. Summertime is the season of the greatest photochemical
788 production of particle precursors for NPF. In order to contribute to the DRE, this NPF factor acts
789 in synergy with the other factors, particularly DMS as a source of particle precursors and MSOA
790 for particle growth, such that during the May/June climax transition season the DREs for those
791 factors dominate over the NPF factor (ABLNUC, Fig. 7).
792
793 The DREs for ship emissions have a similar geographic distribution as those for DMS. In these
794 regions, major international ship traffic routes are coincident with regions of higher biogenic
795 activity, enabling an interaction of biogenic and anthropogenic emissions. Ships enhance oxidant
796 levels, which promote formation of biogenic aerosol precursors such as sulfuric acid and MSA
797 that arise from oxidation of DMS. Condensing vapors of marine origin (such as DMS products
798 and MSOA precursors) can also help to grow particles arising from ship emissions to sizes large
799 enough to interact directly with radiation. As a result, the largest DRE attributed to ship emissions
800 is during the phytoplankton bloom maxima. Figure 7 also suggests that ship emissions could
801 contribute to the DRE over the continents. This effect occurs because ship emissions include
802 particle precursors, oxidants, and primary particles that are transported and interact with
803 continental pollution to form and grow particles to sizes that can interact with radiation over the

804 continents as well as over the oceans. Figure 6 shows that there is a ship-emission-related control
805 on atmospheric DMS mixing ratios, which increase when the ship-source oxidants are removed.
806
807 Figure 8 shows the calculated two-month mean cloud-albedo aerosol indirect effect (AIE)
808 attributed to each of the same five factors that we considered for the DREs. The AIEs are about an
809 order-of-magnitude larger than the calculated DRE for each respective factor with the exception
810 of sea spray. The AIE is strongly controlled by changes to highly reflective MBL clouds, which
811 are in turn very sensitive to the aerosol number concentrations (diameters larger than about 50 to
812 70 nm that can act as CCN), which are controlled by the MBL-related factors examined here. On
813 the other hand, the DRE is relatively more sensitive to aerosol abundance in mid-tropospheric
814 layers, which are less influenced by the considered processes.
815
816 The strongest simulated AIEs for all considered factors are during the May/June climax transition
817 (Fig. 8). There is a strong synergy among all factors that reach their maxima during May/June
818 when the effective combination of sources, photochemistry and particle production/growth
819 processes peak. As well, during summertime, the magnitude of the AIE for all factors is greater in
820 the more northward regions of the North Atlantic relative to more southerly latitudes. These more
821 northerly regions are less influenced by continental pollution and have lower CCN concentrations,
822 coupled with persistent low cloud cover. These conditions make these regions quite sensitive to
823 the factors controlling MBL aerosol size distributions studied here.
824
825 In all seasons, we calculated a stronger AIE related to (1) NPF near and above the MBL top
826 (ABLNUC, top row, Fig. 8) and (2) MSOA (contributor to particle growth) than to (1) DMS (2)
827 ship emissions and (3) sea spray emissions. In our simulations, the major source of CCN-sized
828 particles in the North Atlantic MBL during the summer is particle nucleation near and above the
829 MBL top with growth by MSOA. Without either of these factors, the number concentration of
830 CCN-sized particles in the simulations drops dramatically (Fig. 2). Hence, it is unsurprising that
831 the largest simulated AIEs are due to these two factors during the summertime (climate transition
832 and declining phase). The stronger AIEs attributed to NPF near and above the MBL top (Fig. 8,
833 top row, ABLNUC) relative to DMS and ship emissions indicate that near and above MBL NPF
834 in our simulations is controlled not only by the sulfuric acid from the oxidation of DMS or ship

SO_2, but also arising from other sources, including SO_2 transported from continental sources. However, the maximum North Atlantic regional-mean AIE attributed to ship emissions (-0.62 W m^{-2} for the May/June climax transition) still exceeds the global mean effect of -0.155 W m^{-2} attributed to international shipping calculated by Jin et al. (2018), showing the strong location-dependence and seasonality of this factor. Ship emissions enhance the oxidation rate of DMS, such that the largest AIE attributed to ships occurs during the phytoplankton bloom due to increased particle formation/growth during this season.

In our simulations, sea spray has a lower contribution to aerosol number concentrations, among the factors considered, and as a result has the smallest AIEs. However, recent studies have pointed out that there are knowledge gaps related to the sea spray emissions parameterizations (e.g Bian et al., 2019; Regayrre et al., 2020). Future work is needed to gain confidence in the magnitude of the AIE attributed to sea spray.

We caution that both the DRE and AIE calculations represent a relative contribution of the considered factors to climate effects in the North Atlantic. However, further work is needed to gain confidence in the absolute magnitudes. The activation-style nucleation, which we used as a proxy for the unknown nucleation mechanisms above the marine boundary layer, contributes uncertainty to the climate effects of this nucleation. There is much more work that needs to be done regarding the role of MSOA in this system. Certainly, if MSOA is contributing directly to NPF, it would increase MSOA's climatic importance. However, we have little knowledge of the MSOA precursor species, their chemical lifetimes, and their role in NPF, so we did not explore these dimensions in the study. Like the DRE estimates, the separate AIEs are not linearly additive. Other aerosol indirect effects related to changes in cloud lifetime and precipitation are the subject of future work. In summary, these calculated DREs and AIEs suggest that aerosol-climate impacts for North Atlantic regions are controlled by a combination of strong biogenic and anthropogenic influences and that the nucleation near and above the MBL top contributes to important radiative effects.

8. Conclusions

In this study, we examined aerosol size distribution and composition measurements from the NAAMES campaigns. These ship and aircraft campaigns took place over four separate stages of the annual cycle of marine biogenic activity in the Northwest Atlantic during 2015-2018. We used the GEOS-Chem-TOMAS model with size-resolved aerosol microphysics to interpret these NAAMES measurements. Observations in layers of the lower troposphere below 6 km showed enhancements in the campaign-median number concentration of particles with diameters between 3-10 nm. These enhancements indicated new particle formation, and were most pronounced during the May/June 2016 climax transition (phytoplankton bloom maxima) in the lowest 2 km of atmosphere, particularly near and just above the boundary layer top. This lower tropospheric region near and above the MBL top is a key region for marine NPF. This zone above the MBL clouds is generally very clean, which favors both NPF and strongly sunlit, which favors the photochemical oxidative production of particle precursors for NPF. The November 2015 winter transition (phytoplankton bloom minima) was characterized by the lowest particle number concentrations. During the summer months, OM, followed by sulfate mass concentrations made strong contributions the total aerosol loading in the lowest 2 km. However, sea spray dominated the MBL aerosol mass loading. Peak near-surface sulfate concentrations occurred in May/June during the phytoplankton bloom, whereas peak near-surface OM concentrations were in August/September. Campaign-median MBL aerosol size distributions were dominated by Aitken mode particles (diameters 10-100 nm) during the summertime (May/June climax transition and August/September declining phase). The larger accumulation mode particles were dominant in the November winter transition and March/April accumulation phase.

Our simulations suggested that a synergy of key factors contributed to Northwest Atlantic MBL aerosol size distributions, including (1) new particle formation near and above the MBL top; (2) growth of the newly formed particles by condensation of marine organic vapors, forming marine secondary organic aerosol (MSOA), which yields more abundant CCN-sized particles that descend into the MBL while continuing to grow and being subject to cloud processing (e.g., aqueous-phase aerosol production, which does not add to particle number); (3) DMS-oxidation products that contribute to particle formation and growth; (4) ship emissions, which are a source of primary and secondary particles and also contribute to atmospheric oxidants and (5) sea spray emissions, which also provide a condensation sink that suppresses particle formation. These findings are in

agreement with previous observational-based studies for the North Atlantic region (e.g., Sanchez et al., 2018; Zheng et al., 2020)

We calculated the aerosol direct (DRE) and cloud-albedo indirect (AIE) radiative effects over the North Atlantic attributed to five key factors controlling MBL aerosols. The cooling effects were about a factor of 10 larger for the AIEs than the respective DREs except for sea spray, which dominated the DRE. The strong AIE response was attributed to the strong sensitivity of the MBL cloud reflectivity to the MBL-related factors that we examined. Mid-tropospheric aerosol (altitude of transport of continental pollution) has a strong impact on the DRE and the factors that we considered had less impact at these altitudes. The maximum regional-mean (40-60 ^{o}N, 20-50 ^{o}W) DRE for our simulations was -1.37 W m^{-2}, attributed to sea spray during the March/April accumulating phase, which is a time of strong synoptic-scale storms in the Northwest Atlantic, enhancing wind-generated sea spray. This strong DRE attributed to sea spray highlights the importance of work to better constrain parameterizations for models. The second strongest DRE was connected to the temperature-dependent source of MSOA, which had a key role in growing simulated particles to large enough (diameters of 100-200 nm) to strongly reflect incoming solar radiation. The maximum AIE was -3.37 W m^{-2}, for the May/June climax transition phase (peak phytoplankton bloom). This AIE was related to the role MSOA in growing new particles to CCN sizes as they descend into the MBL and are subject to further growth in clouds after their formation near the MBL top. The AIE attributed to the NPF factor was nearly as large (-2.27 W m^{-2}) during May/June. The NPF and MSOA factors act in concert with each other and removal of either of these factors contributed to shutdown the production of cloud-condensation-nuclei-size particles. Our study demonstrated acceptable model-measurement agreement for our base simulation, such that our simulations can be employed to examine the *potential* role and relative importance of the considered factors in the DRE and AIE. However, we caution that further work is needed to gain confidence in the absolute magnitudes. In particular, the activation-style nucleation, which we used as a proxy for the unknown nucleation mechanism above the marine boundary layer, adds uncertainty to the climate effects of this nucleation

This study highlighted the importance of processes connected to both marine biogenic activity and anthropogenic activity in controlling aerosol size distributions in the Northwest Atlantic MBL. We

identified key factors, which could be the focus of future work. Particularly, work is needed to better understand the nature, flux, and chemistry of marine organic vapors that can form MSOA. As well, work is needed to better understand the contributors to NPF near and above the MBL top. Further work is also needed to understand the interactions of the considered factors with cloud processing of aerosols and its relative importance in particle growth. As the Earth's climate changes and shipping traffic/regulations/routes change, work to understand the source strength of DMS, MSOA, shipping and sea spray emissions is highly relevant. Such work will bridge the knowledge gaps related to factors controlling aerosols in the marine MBL and their climate impacts.

Code and data availability. The NAAMES project website is at https://naames.larc.nasa.gov. The NAAMES airborne and ship datasets used in this paper are publicly available and permanently archived in the NASA Atmospheric Science Data Center (ASDC; https://doi.org/10.5067/Suborbital/NAAMES/DATA001) and the SeaWiFS Bio-Optical Archive and Storage System (SeaBASS; https://doi.org/10.5067/SeaBASS/NAAMES/DATA001). The ship datasets generated during and analyzed for NAAMES studies are also available in the UCSD Library Digital Collection repository, https://doi.org/10.6075/J04T6GJ6. The GEOS-Chem model is freely available for download at https://github.com/geoschem/geos-chem (last access 19 July 2020).

Supplement link.

Author contributions. BC, RVM and JRP designed the study. BC conducted the GEOS-Chem-TOMAS simulations, led the related analysis, and wrote the manuscript with contributions from all coauthors. RHM, ECC, and LDZ contributed the aerosol measurements from aboard the NASA C130 aircraft. AW, MM and AS contributed the gas-phase measurements from aboard the NASA C130 aircraft. LMR and GS contributed the aerosol measurements from aboard the R/V Atlantis. RYWC and HL contributed to the interpretation of model-measurement comparisons. EEM contributed the CEDS data set. KRB contributed to the off-line radiative calculations, MG contributed the satellite DMS data set.

Competing interests. The authors declare that they have no conflict of interest.

Acknowledgements. BC, RVM and RYWC acknowledge research funding provided by the Ocean Frontier Institute, through an award from the Canada First Research Excellence Fund. JRP and KRB acknowledge funding support from the Monfort Excellence Fund, and the US Department of Energy's Atmospheric System Research, an Office of Science, Office of Biological and Environmental Research program, under grant DE-SC0019000. LMR and GS acknowledge funding support from NASA grant NNX15AE66G. RHM, ECC, LDZ, LMR, and GS acknowledge funding support from the NASA NAAMES EVS-2 project. HL acknowledges funding support from the NASA NAAMES mission and the National Institute of Aerospace's IRAD program. DMS measurements aboard the NASA C-130 during NAAMES were supported by the Austrian Federal Ministry for Transport, Innovation and Technology (bmvit) through the Austrian Space Applications Programme (ASAP) of the Austrian Research Promotion Agency (FFG). MM's participation in NAAMES 2016 was funded by the Tiroler Wissenschaftsfonds (grant # UNI-0404/1895). AS's participation in NAAMES 2017 was partly funded by National Institute of Aerospace (Task No 80LARC18F0031). MG acknowledges funding support from the Natural Sciences and Engineering Research Council of Canada through the NETCARE project of the Climate Change and Atmospheric Research Program. Tomas Mikoviny is acknowledged for technical support; Ionicon Analytik is acknowledged for instrumental support

References.

Abbatt, J. P. D., Leaitch, W. R., Aliabadi, A. A., Bertram, A. K., Blanchet, J.-P., Boivin-Rioux, A., Bozem, H., Burkart, J., Chang, R. Y. W., Charette, J., Chaubey, J. P., Christensen, R. J., Cirisan, A., Collins, D. B., Croft, B., Dionne, J., Evans, G. J., Fletcher, C. G., Galí, M., Ghahremaninezhad, R., Girard, E., Gong, W., Gosselin, M., Gourdal, M., Hanna, S. J., Hayashida, H., Herber, A. B., Hesaraki, S., Hoor, P., Huang, L., Hussherr, R., Irish, V. E., Keita, S. A., Kodros, J. K., Köllner, F., Kolonjari, F., Kunkel, D., Ladino, L. A., Law, K., Levasseur, M., Libois, Q., Liggio, J., Lizotte, M., Macdonald, K. M., Mahmood, R., Martin, R. V., Mason, R. H., Miller, L. A., Moravek, A., Mortenson, E., Mungall, E. L., Murphy, J. G.,

990 Namazi, M., Norman, A.-L., O'Neill, N. T., Pierce, J. R., Russell, L. M., Schneider,
991 J., Schulz, H., Sharma, S., Si, M., Staebler, R. M., Steiner, N. S., Thomas, J. L., von
992 Salzen, K., Wentzell, J. J. B., Willis, M. D., Wentworth, G. R., Xu, J.-W., and
993 Yakobi-Hancock, J. D.: Overview paper: New insights into aerosol and climate in
994 the Arctic, Atmos. Chem. Phys., 19, 2527–2560, https://doi.org/10.5194/acp-19-
995 2527-2019, 2019.
996 Abdul-Razzak, H. and Ghan, S. J.: A parameterization of aerosol activation 3. Sectional
997 representation, J. Geophys. Res., 107, 4026, doi:10.1029/2001JD000483, 2002.
998 Adams, P. J. and Seinfeld, J. H.: Predicting global aerosol size distributions in general circulation
999 models, J. Geophys. Res., 107, 4370, doi:10.1029/2001JD001010, 2002.
1000 Allan, J. D., Williams, P. I., Najera, J., Whitehead, J. D., Flynn, M. J., Taylor, J. W., Liu, D.,
1001 Darbyshire, E., Carpenter, L. J., Chance, R., Andrews, S. J., Hackenberg, S. C. and
1002 McFiggans, G.: Iodine observed in new particle formation events in the Arctic
1003 atmosphere during ACCACIA, Atmos. Chem. Phys., 15(10), 5599–5609,
1004 doi:10.5194/acp-15-5599-2015, 2015.
1005 Amos, H. M., Jacob, D. J., Holmes, C. D., Fisher, J. A., Wang, Q., Yantosca, R. M., Corbitt, E. S.,
1006 Galarneau, E., Rutter, A. P., Gustin, M. S., Steffen, A., Schauer, J. J., Graydon, J.
1007 A., St Louis, V. L., Talbot, R. W., Edgerton, E. S., Zhang, Y. and Sunderland, E.
1008 M.: Gas-particle partitioning of atmospheric Hg(II) and its effect on global mercury
1009 deposition, Atmos. Chem. Phys., 12(1), 591–603, doi:10.5194/acp-12-591-2012,
1010 2012.
1011 Ault, A. P., Moffet, R. C., Baltrusaitis, J., Collins, D. B., Ruppel, M. J., Cuadra-Rodriguez, L. A.,
1012 Zhao, D., Guasco, T. L., Ebben, C. J., Geiger, F. M., Bertram, T. H., Prather, K. A.
1013 and Grassian, V. H.: Size-Dependent Changes in Sea Spray Aerosol Composition
1014 and Properties with Different Seawater Conditions, Environ. Sci. Technol., 47(11),
1015 5603–5612, doi:10.1021/es400416g, 2013.
1016 Barnes, I., Hjorth, J. and Mihalapoulos, N.: Dimethyl sulfide and dimethyl sulfoxide and their
1017 oxidation in the atmosphere, Chem. Rev., 106(3), 940–975,
1018 doi:10.1021/cr020529+, 2006.
1019 Bates, T. S., Coffman, D. J., Covert, D. S., Quinn, P. K.: Regional marine boundary layer aerosol
1020 size distributions in the Indian, Atlantic, and Pacific Oceans: A comparison of

INDOEX measurements with ACE-1, ACE-2, and Aerosols99. J. Geophys. Res. Atmos., 107, D19, doi:10.1029/2001JD001174, 2002.

Bates, T. S., Quinn, P. K., Coffman, D. J., Johnson, J. E., Upchurch, L., Saliba, G. and Lewis, S.: Variability in Marine Plankton Ecosystems Are Not Observed in Freshly Emitted Sea Spray Aerosol Over the North Atlantic Ocean, Geophys. Res. Lett., doi:10.1029/2019GL085938, 2020.

Behrenfeld, M. J., Moore, R. H., Hostetler, C. A., Graff, J., Gaube, P., Russell, L. M., Chen, G., Doney, S. C., Giovannoni, S., Liu, H., Proctor, C., Bolaños, L. M., Baetge, N., Davie-Martin, C., Westberry, T. K., Bates, T. S., Bell, T. G., Bidle, K. D., Boss, E. S., Brooks, S. D., Cairns, B., Carlson, C., Halsey, K., Harvey, E. L., Hu, C., Karp-Boss, L., Kleb, M., Menden-Deuer, S., Morison, F., Quinn, P. K., Scarino, A. J., Anderson, B., Chowdhary, J., Crosbie, E., Ferrare, R., Hair, J. W., Hu, Y., Janz, S., Redemann, J., Saltzman, E., Shook, M., Siegel, D. A., Wisthaler, A., Martin, M. Y. and Ziemba, L.: The North Atlantic Aerosol and Marine Ecosystem Study (NAAMES): Science Motive and Mission Overview, Front. Mar. Sci., 6, 122, doi:10.3389/fmars.2019.00122, 2019.

Bian, H., Froyd, K., Murphy, D. M., Dibb, J., Darmenov, A., Chin, M., Colarco, P. R., da Silva, A., Kucsera, T. L., Schill, G., Yu, H., Bui, P., Doliner, M., Weinzierl, B. and Smirnov, A.: Observationally contrained analysis of sea salt aerosol in the marine atmosphere, Atmos. Chem. Phys., 19, 10773-10785, 2019.

Bilsback, K., Kerry, D., Croft, B., Ford, B., Jathar, S. H., Carter, E., Martin, R. V., and Pierce, J. R.: Beyond SO_2 reductions from shipping: Assessing the impact of NOx and carbonaceous particle controls on human health and climate, Environ. Res. Lett., . in press https://doi.org/10.1088/1748-9326/abc718 , 2020).

Boucher, O. and Haywood, J.: Estimates of the Direct and Indirect Radiative Forcing Due to Tropospheric Aerosols: A Review, Rev. Geophys., 34(4), 513–543, 2000.

Boylan, J. W. and Russell, A. G.: PM and light extinction model performance metrics, goals, and criteria for three-dimensional air quality models, Atmos. Environ., 40(26), 4946–4959, doi:10.1016/j.atmosenv.2005.09.087, 2006.

Brooks, S. D. and Thornton, D. C. O.: Marine Aerosols and Clouds, Ann. Rev. Mar. Sci., 10(1), 289–313, doi:10.1146/annurev-marine-121916-063148, 2018.

Browse, J., Carslaw, K. S., Arnold, S. R., Pringle, K. and Boucher, O.: The scavenging processes controlling the seasonal cycle in Arctic sulphate and black carbon aerosol, Atmos. Chem. Phys., 12(15), 6775–6798, doi:10.5194/acp-12-6775-2012, 2012.

Brüggemann, M., Hayeck, N. and George, C.: Interfacial photochemistry at the ocean surface is a global source of organic vapors and aerosols, Nat. Commun., 1–8, doi:10.1038/s41467-018-04528-7, 2018.

Burkart, J., Hodshire, A. L., Mungall, E. L., Pierce, J. R., Collins, D. B., Ladino, L. A., Lee, A. K. Y., Irish, V., Wentzell, J. J. B., Liggio, J., Papakyriakou, T., Murphy, J. and Abbatt, J.: Organic Condensation and Particle Growth to CCN Sizes in the Summertime Marine Arctic Is Driven by Materials More Semivolatile Than at Continental Sites, Geophys. Res. Lett., 44(20), 10,725-10,734, doi:10.1002/2017GL075671, 2017a.

Burkart, J., Willis, M. D., Bozem, H., Thomas, J. L., Law, K., Hoor, P., Aliabadi, A. A., Köllner, F., Schneider, J., Herber, A., Abbatt, J. P. D. and Leaitch, W. R.: Summertime observations of elevated levels of ultrafine particles in the high Arctic marine boundary layer, Atmos. Chem. Phys., 17(8), 5515–5535, doi:10.5194/acp-17-5515-2017, 2017b.

Carpenter, L. J. and Nightingale, P. D.: Chemistry and Release of Gases from the Surface Ocean, Chem. Rev., 115(10), 4015–4034, doi:10.1021/cr5007123, 2015.

Carpenter, L. J., Archer, S. D. and Beale, R.: Ocean-atmosphere trace gas exchange, Chem. Soc. Rev., 41(19), 6473–6506, doi:10.1039/c2cs35121h, 2012.

Carslaw, K. S., Boucher, O., Spracklen, D. V., Mann, G. W., Rae, J. G. L., Woodward, S., and Kulmala, M.: A review of natural aerosol interactions and feedbacks within the Earth system, Atmos. Chem. Phys., 10, 1701–1737, https://doi.org/10.5194/acp-10-1701-2010, 2010.

Carslaw, K. S., Lee, L. A., Reddington, C. L., Pringle, K. J., Rap, A., Forster, P. M., Mann, G. W., Spracklen, D. V, Woodhouse, M. T., Regayre, L. A. and Pierce, J. R.: Large contribution of natural aerosols to uncertainty in indirect forcing, Nature, 503, 67 [online] Available from: http://dx.doi.org/10.1038/nature12674, 2013.

Cavalli, F., Facchini, M. C., Decesari, S., Mircea, M., Emblico, L., Fuzzi, S., Ceburnis, D., Yoon,

Y. J., O'Dowd, C., Putaud, J. P. and Dell'Acqua, A.: Advances in characterization of size-resolved organic matter in marine aerosol over the North Atlantic, J. Geophys. Res. D Atmos., 109(24), 1–14, doi:10.1029/2004JD005137, 2004.

Ceburnis, D., O'Dowd, C., Jennings, G. S., Facchini, M. C., Emblico, L., Decesari, S., Fuzzi, S. and Sakalys, J.: Marine aerosol chemistry gradients : Elucidating primary and secondary processes and fluxes, Geophys. Res. Lett., 35(2), 1–5, doi:10.1029/2008GL033462, 2008.

Chang, R. Y. W., Sjostedt, S. J., Pierce, J. R., Papakyriakou, T. N., Scarratt, M. G., Michaud, S., Levasseur, M., Leaitch, W. R. and Abbatt, J. P. D.: Relating atmospheric and oceanic DMS levels to particle nucleation events in the Canadian Arctic, J. Geophys. Res. Atmos., 116(21), 1–10, doi:10.1029/2011JD015926, 2011.

Charlson, R. J., Lovelock, J. E., Andreae, M. O. and Warren, S. G.: Oceanic phytoplankton, atmospheric sulphur, cloud albedo and climate, Nature, 326(6114), 655–661, doi:10.1038/326655a0, 1987.

Charlson, R. J., Schwartz, S. E., Hales, J. M., Cess, R. D., Coakley, J. A., Hansen, J. E. and Hofmann, D. J.: Climate Forcing by Anthropogenic Aerosols, Science (80), 255(5043), 423–430 [online] Available from: http://science.sciencemag.org/content/255/5043/423.abstract, 1992.

Chen, H., Varner, M. E., Gerber, R. B. and Finlayson-Pitts, B. J.: Reactions of Methanesulfonic Acid with Amines and Ammonia as a Source of New Particles in Air, J. Phys. Chem. B, 120(8), 1526–1536, doi:10.1021/acs.jpcb.5b07433, 2016.

Chen, Q., Sherwen, T., Evans, M. and Alexander, B.: DMS oxidation and sulfur aerosol formation in the marine troposphere : a focus on reactive halogen and multiphase chemistry, Atmos. Chem. Phys., 18, 13617–13637, 2018.

Chen, Y.-C., Christensen, M. W., Stephens, G. L. and Seinfeld, J. H.: Satellite-based estimate of global aerosol–cloud radiative forcing by marine warm clouds, Nat. Geosci., 7(9), 643–646, doi:10.1038/ngeo2214, 2014.

Christiansen, S., Salter, M. E., Gorokhova, E., Nguyen, Q. T. and Bilde M.: Sea spray aerosol formation: Results on the role of air entrainment, water temperature and phytoplankton biomass, Environ. Sci. Technol., 53, 13107-13116, 2019.

Chiu, R., Tinel, L., Gonzalez, L., Ciuraru, R., Bernard, F., George, C., and Volkamer R.: UV

photochemistry of carboxylic acids at the air-sea boundary: A relevant source of glyoxal and other oxygenated VOC in the marine atmosphere, Geophys. Res. Lett., 44, 1079–1087, doi:10.1002/2016GL071240, 2017.

Ciuraru, R., Fine, L., van Pinxteren, M., D'Anna, B., Herrmann, H., and George, C.: Unravelling new processes at interfaces: Photochemical isoprene production at the sea surface, Environ. Sci. Technol., 49(22), 13,199–13,205, doi:10.1021/acs.est.5b02388, 2015.

Collins, D. B., Burkart, J., Chang, R. Y.-W., Lizotte, M., Boivin-Rioux, A., Blais, M., Mungall, E. L., Boyer, M., Irish, V. E., Massé, G., Kunkel, D., Tremblay, J.-É., Papakyriakou, T., Bertram, A. K., Bozem, H., Gosselin, M., Levasseur, M., and Abbatt, J. P. D.: Frequent ultrafine particle formation and growth in Canadian Arctic marine and coastal environments, Atmos. Chem. Phys., 17, 13119–13138, https://doi.org/10.5194/acp-17-13119-2017, 2017.

Corbett, J. J., Winebrake, J. J., Green, E. H., Kasibhatla, P., Eyring, V. and Lauer, A.: Mortality from Ship Emissions: A Global Assessment, Environ. Sci. Technol., 41(24), 8512–8518, doi:10.1021/es071686z, 2007.

Corbett, J. J., Lack, D. A., Winebrake, J. J., Harder, S., Silberman, J. A., and Gold, M.: Arctic shipping emissions inventories and future scenarios, Atmos. Chem. Phys., 10, 9689–9704, https://doi.org/10.5194/acp-10-9689-2010, 2010.

Cravigan, L. T., Ristovski, Z., Modini, R. L., Keywood, M. D., and Gras, J. L.: Observation of sea-salt fraction in sub-100 nm diameter particles at Cape Grim, J. Geophys. Res. Atmos., 120, 1848–1864, doi:10.1002/2014JD022601, 2015

Cravigan, L. T., Mallet, M. D., Vaattovaara, P., Harvey, M. J., Law, C. S., Modini, R. L., Russell, L. M., Stelcer, E., Cohen, D. D., Olsen, G., Safi, K., Burrell, T. J. and Ristovski, Z.: Sea spray aerosol organic enrichment , water uptake and surface tension effects, Atmos. Chem. Phys., 20, 7955–7977, https://doi.org/10.5194/acp-20-7955-2020, 2020.

Croft, B., Wentworth, G. R., Martin, R. V, Leaitch, W. R., Murphy, J. G., Murphy, B. N., Kodros, J. K., Abbatt, J. P. D. and Pierce, J. R.: Contribution of Arctic seabird-colony ammonia to atmospheric particles and cloud-albedo radiative effect, Nat. Commun., 7, 13444, doi:10.1038/ncomms13444, 2016a.

1143 Croft, B., Martin, R. V., Richard Leaitch, W., Tunved, P., Breider, T. J., D'Andrea, S. D. and
1144 Pierce, J. R.: Processes controlling the annual cycle of Arctic aerosol number and
1145 size distributions, Atmos. Chem. Phys., 16(6), 3665–3682, doi:10.5194/acp-16-
1146 3665-2016, 2016b.
1147 Croft, B., Martin, R. V., Leaitch, W. R., Burkart, J., Chang, R. Y.-W., Collins, D. B., Hayes, P. L.,
1148 Hodshire, A. L., Huang, L., Kodros, J. K., Moravek, A., Mungall, E. L., Murphy,
1149 J. G., Sharma, S., Tremblay, S., Wentworth, G. R., Willis, M. D., Abbatt, J. P. D.
1150 and Pierce, J. R.: Arctic marine secondary organic aerosol contributes significantly
1151 to summertime particle size distributions in the Canadian Arctic Archipelago,
1152 Atmos. Chem. Phys., 19(5), 2787–2812, doi:10.5194/acp-19-2787-2019, 2019.
1153 Cui, T., Green, H. S., Selleck, P. W., Zhang, Z., Brien, R. E. O., Gold, A., Keywood, M., Kroll, J.
1154 H. and Surratt, J. D.: Chemical Characterization of Isoprene- and Monoterpene-
1155 Derived Secondary Organic Aerosol Tracers in Remote Marine Aerosols over a
1156 Quarter Century, doi:10.1021/acsearthspacechem.9b00061, 2019.
1157 Dall´Osto, M., Simo, R., Harrison, R. M., Beddows, D. C. S., Saiz-Lopez, A., Lange, R., Skov,
1158 H., Nøjgaard, J. K., Nielsen, I. E. and Massling, A.: Abiotic and biotic sources
1159 influencing spring new particle formation in North East Greenland, Atmos.
1160 Environ., 190(July), 126–134, doi:10.1016/J.ATMOSENV.2018.07.019, 2018.
1161 DeCarlo, P. F., Kimmel, J. R., Trimborn, A., Northway, M. J., Jayne, J. T., Aiken, A. C., Gonin,
1162 M., Fuhrer, K., Horvath, T., Docherty, K. S., Worsnop, D. R., and Jimenez, J. L.:
1163 Field-deployable, high-resolution, time-of-flight aerosol mass spectrometer,
1164 Analytical Chemistry 78, (24), 8281-8289, 2006.
1165 Decesari, S., Finessi, E., Rinaldi, M., Paglione, M., Fuzzi, S., Stephanou, E. G., Tziaras, T., Spyros,
1166 A., Ceburnis, D., O'Dowd, C., Osto, M. D., Harrison, R. M., Allan, J., Coe, H. and
1167 Facchini, M. C.: Primary and secondary marine organic aerosols over the North
1168 Atlantic Ocean during the MAP experiment, J. Geophys. Res., 116, D22210, 1–21,
1169 doi:10.1029/2011JD016204, 2011.
1170 de Leeuw, G., Andreas, E. L., Anguelova, M. D., Fairall, C. W., Lewis, E. R., O'Dowd, C., Schulz,
1171 M., and Schwartz, S. E.: Production flux of sea spray aerosol, Rev. Geophys., 49,
1172 RG2001, https://doi.org/10.1029/2010RG000349, 2011.
1173 DeMott, P. J., Hill, T. C. J., McCluskey, C. S., Prather, K. A., Collins, D. B., Sullivan, R. C.,

1174 Ruppel, M. J., Mason, R. H., Irish, V. E. and Lee, T.: Sea spray aerosol as a unique
1175 source of ice nucleating particles, Proc. Natl. Acad. Sci., 113(21), 5797–5803
1176 [online] Available from: http://www.pnas.org/content/113/21/5797.full.pdf, 2016.
1177 EC-JRC/PBL: Emission Database for Global Atmospheric Research (EDGAR), release EDGAR
1178 v4.2 FT2012, http://edgar.jrc.ec.europa.eu (last access: 15 January 2018), 2012.
1179 Facchini, M. C., Decesari, S., Rinaldi, M., Carbone, C., Finessi, E., Mircea, M., Fuzzi, S., Moretti,
1180 F., Tagliavini, E., Ceburnis, D. and O'Dowd, C.: Important Source of Marine
1181 Secondary Organic Aerosol from Biogenic Amines, Environ. Sci. Technol., 42(24),
1182 9116–9121, doi:10.1021/es8018385, 2008.
1183 Fast, J. D., Berg, L. K., Zhang, K., Easter, R. C., Ferrare, R. A., Hair, J. W., Hostetler, C. A., Liu,
1184 Y., Ortega, I., Sedlacek III, A., Shilling, J. E., Shrivastava, M., Springston, S. T.,
1185 Tomlinson, Jason, M., Rainer, V., Wilson, J., Zaveri, R. A. and Zelenyuk, A.:
1186 Model representations of aerosol layers transported from North America over the
1187 Atlantic Ocean during the Two-Column Aerosol Project, J. Geophys. Res. Atmos.,
1188 121, 9814–9848, doi:10.1002/2016JD025248, 2016.
1189 Fiddes, S. L., Woodhouse, M. T., Nicholls, Z., Lane, T. P. and Schofield, R.: Cloud, precipitation
1190 and radiation responses to large perturbations in global dimethyl sulfide, Atmos.
1191 Chem. Phys., 18, 10177–10198, https://doi.org/10.5194/acp-18-10177-2018, 2018.
1192 Fisher, J. A., Jacob, D. J., Purdy, M. T., Kopacz, M., Le Sager, P., Carouge, C., Holmes, C. D.,
1193 Yantosca, R. M., Batchelor, R. L., Strong, K., Diskin, G. S., Fuelberg, H. E.,
1194 Holloway, J. S., Hyer, E. J., McMillan, W. W., Warner, J., Streets, D. G., Zhang,
1195 Q., Wang, Y. and Wu, S.: Source attribution and interannual variability of Arctic
1196 pollution in spring constrained by aircraft (ARCTAS, ARCPAC) and satellite
1197 (AIRS) observations of carbon monoxide, Atmos. Chem. Phys., 10(3), 977–996,
1198 doi:10.5194/acp-10-977-2010, 2010.
1199 Fossum, K.N., Ovadnevaite, J., Ceburnis, D. Preißler, J., Snider, J. R., Huang, R. J., Zuend, A. and
1200 O'Dowd, C.: Sea-spray regulates sulfate cloud droplet activation over oceans, NPJ
1201 Clim. Atmos. Sci., 3, 14, https://doi.org/10.1038/s41612-020-0116-2, 2020.

1202 Galí, M., and Simó, R.: A meta-analysis of oceanic DMS and DMSP cycling processes:
1203 Disentangling the summer paradox, Global Biogeochem. Cycles, 29, 496–515,
1204 doi:10.1002/2014GB004940, 2015.
1205 Galí, M., Levasseur, M., Devred, E., Simó, R. and Babin, M.: Sea-surface dimethylsulfide (DMS)
1206 concentration from satellite data at global and regional scales, Biogeosciences, 15,
1207 3497–3519, https://doi.org/10.5194/bg-15-3497-2018, 2018.
1208 Galí, M., Devred, E., Babin, M. and Levasseur, M.: Decadal increase in Arctic dimethylsulfide
1209 emission, Proc. Natl. Acad. Sci., 116(39), 19311–19317,
1210 doi:10.1073/pnas.1904378116, 2019.
1211 Gantt, B. and Meskhidze, N.: The physical and chemical characteristics of marine primary organic
1212 aerosol: A review, Atmos. Chem. Phys., 13(8), 3979–3996, doi:10.5194/acp-13-
1213 3979-2013, 2013.
1214 Ghahremaninezhad, R., Norman, A. L., Abbatt, J. P. D., Levasseur, M. and Thomas, J. L.:
1215 Biogenic, anthropogenic and sea salt sulfate size-segregated aerosols in the Arctic
1216 summer, Atmos. Chem. Phys., 16(8), 5191–5202, doi:10.5194/acp-16-5191-2016,
1217 2016.
1218 Ghahremaninezhad, R., Gong, W., Galí, M., Norman, A., Beagley, S. R., Akingunola, A., Zheng,
1219 Q., Lupu, A., Lizotte, M., Levasseur, M. and Leaitch, W. R.: Dimethyl sulfide and
1220 its role in aerosol formation and growth in the Arctic summer – a modelling study,
1221 Atmos. Chem. Phys., 19, 14455–14476, https://doi.org/10.5194/acp-19-14455-
1222 2019, 2019.
1223 Gilgen, A., Ting, W., Huang, K., Ickes, L., Neubauer, D. and Lohmann, U.: How important are
1224 future marine and shipping aerosol emissions in a warming Arctic summer and
1225 autumn ?, Atmos. Chem. Phys., 18, 10521–10555, https://doi.org/10.5194/acp-18-
1226 10521-2018, 2018.
1227 Gong, S. L.: A parameterization of sea-salt aerosol source function for sub- and super-micron
1228 particles, J. Geophys. Res., 17(4), 1097, doi:10.1029/2003GB002079, 2003.
1229 Grassian, V. H., Quinn, P. K., Collins, D. B., Bates, T. S. and Prather, K. A.: Chemistry and Related
1230 Properties of Freshly Emitted Sea Spray Aerosol, Chem. Rev., 115(10), 4383–
1231 4399, doi:10.1021/cr500713g, 2015.
1232 Hamacher-Barth, E., Leck, C. and Jansson, K.: Size-resolved morphological properties of the high

1233 Arctic summer aerosol during ASCOS-2008, Atmos. Chem. Phys., 16, 6577–6593,
1234 doi:10.5194/acp-16-6577-2016, 2016.
1235 Hodshire, A. L., Campuzano-jost, P., Kodros, J. K., Croft, B., Nault, B. A., Schroder, J. C.,
1236 Jimenez, J. L. and Pierce, J. R.: The potential role of methanesulfonic acid (MSA
1237) in aerosol formation and growth and the associated radiative forcings, Atmos.
1238 Chem. Phys., 19, 3137-3160, https://doi.org/10.5194/acp-19-3137-2019 , 2019.
1239 Hoesly, R. M., Smith, S. J., Feng, L., Klimont, Z., Janssens-Maenhout, G., Pitkanen, T., Seibert,
1240 J. J., Vu, L., Andres, R. J., 1010 Bolt, R. M., Bond, T. C., Dawidowski, L., Kholod,
1241 N., Kurokawa, J. I., Li, M., Liu, L., Lu, Z., Moura, M. C. P., O'Rourke, P. R., and
1242 Zhang, Q.: Historical (1750–2014) anthropogenic emissions of reactive gases and
1243 aerosols from the Community Emissions Data System (CEDS), Geosci. Model
1244 Dev., 11, 369-408, 10.5194/gmd-11-369-2018, 2018.
1245 Hoffman, E. H., Tilgner, A., Schrödner, R., Bräuer, P., Wolke, R. and Herrmann, H.: An advanced
1246 modeling study on the impacts and atmospheric implications of multiphase
1247 dimethyl sulfide chemistry, Proc. Natl., Acad. Sci., 113, (42), 11776-11781,
1248 https://doi.org/10.1073/pnas.1606320113, 2016.
1249 Holmes, C. D., Prather, M. J. and Vinken, G. C. M.: The climate impact of ship NO x emissions :
1250 an improved estimate accounting for plume chemistry, Atmos. Chem. Phys., 14,
1251 6801–6812, doi:10.5194/acp-14-6801-2014, 2014.
1252 Hoose, C., Lohmann, U., Bennartz, R., Croft, B., Lesins, G.: Global simulations of aerosol
1253 processing in clouds, Atmos. Chem. Phus., 8, 6939–6963, 2008.
1254 Hoppel, W. A., G. M. Frick, and R. E. Larson (1986), Effect of nonprecipitating clouds on the
1255 aerosol size distribution in the marine boundary layer, Geophys. Res. Lett., 13(1),
1256 125–128, doi:10.1029/GL013i002p00125, 1987.
1257 Hu, Q.-H., Xie, Z.-Q., Wang, X.-M., Kang, H., He, Q.-F. and Zhang, P.: Secondary organic
1258 aerosols over oceans via oxidation of isoprene and monoterpenes from Arctic to
1259 Antarctic, Sci. Rep., 3, 2280, doi:10.1038/srep02280, 2013.
1260 Huntrieser, H., Heland, J., Schlager, H., Forster, C., Stohl, A., Aufmhoff, H., Arnold, F., Scheel,
1261 H. E., Campana, M., Gilge, S., Eixmann, R. and Cooper, O.: Intercontinental air
1262 pollution transport from North America to Europe : Experimental evidence from
1263 airborne measurements and surface observations, J. Geophys. Res., 110, D01305,

doi:10.1029/2004JD005045, 2005.

Iacono, M. J., Delamere, J. S., Mlawer, E. J., Shephard, M. W., Clough, S. A. and Collins, W. D.: Radiative forcing by long-lived greenhouse gases: Calculations with the AER radiative transfer models, J. Geophys. Res. Atmos., 113(13), D13103, doi:10.1029/2008JD009944, 2008.

IPCC, 2013: *Climate Change 2013: The Physical Science Basis. Contribution of Working Group I to the Fifth Assessment Report of the Intergovernmental Panel on Climate Change* [Stocker, T.F., D. Qin, G.-K. Plattner, M. Tignor, S.K. Allen, J. Boschung, A. Nauels, Y. Xia, V. Bex and P.M. Midgley (eds.)]. Cambridge University Press, Cambridge, United Kingdom and New York, NY, USA, 1535 pp.

Irish, V. E., Elizondo, P., Chen, J., Chou, C., Charette, J., Lizotte, M., Ladino, L. A., Wilson, T. W., Gosselin, M., Murray, B. J., Polishchuk, E., Abbatt, J. P. D., Miller, L. A., and Bertram, A. K.: Ice-nucleating particles in Canadian Arctic sea-surface microlayer and bulk seawater, Atmos. Chem. Phys., 17, 10583–10595, https://doi.org/10.5194/acp-17-10583-2017, 2017.

Jaeglé, L., Quinn, P. K., Bates, T. S., Alexander, B. and Lin, J. T.: Global distribution of sea salt aerosols: New constraints from in situ and remote sensing observations, Atmos. Chem. Phys., 11(7), 3137–3157, doi:10.5194/acp-11-3137-2011, 2011.

Jin, Q., Grandey, B. S., Rothenberg, D., Avramov, A. and Wang, C.: Impacts on cloud radiative effects induced by coexisting aerosols converted from international shipping and maritime DMS emissions, Atmos. Chem. Phys., 18, 16793–16808, https://doi.org/10.5194/acp-18-16793-2018, 2018.

Johnson, M. T.: A numerical scheme to calculate temperature and salinity dependent air-water transfer velocities for any gas, Ocean Sci., 6(4), 913–932, doi:10.5194/os-6-913-2010, 2010.

Karl, M., Leck, C., Gross, A. and Pirjola, L.: A study of new particle formation in the marine boundary layer over the central Arctic Ocean using a flexible multicomponent aerosol dynamic model, Tellus, Ser. B Chem. Phys. Meteorol., 64(1), 1–24, doi:10.3402/tellusb.v64i0.17158, 2012.

Kasparian, J., Hassler, C., Ibelings, B., Berti, N., Bigorre, S., Djambazova, V., Gascon-diez, E., Giuliani, G., Houlmann, R., Kiselev, D., Laborie, P. De, Le, A., Magouroux, T., Neri, T., Palomino, D., Pfändler, S., Ray, N., Sousa, G., Staedler, D., Tettamanti,

F., Wolf, J. and Beniston, M.: Assessing the Dynamics of Organic Aerosols over the North Atlantic Ocean, Sci. Rep., 7, 45476, doi:10.1038/srep45476, 2017.

Kazil, J., Wang, H., Feingold, G., Clarke, A. D., Snider, J. R. and Bandy, A. R.: and Physics Modeling chemical and aerosol processes in the transition from closed to open cells during VOCALS-REx, Atmos. Chem. Phys., 11, 7491–7514, doi:10.5194/acp-11-7491-2011, 2011.

Kerminen, V. M., Anttila, T., Lehtinen, K. E. J. and Kulmala, M.: Parameterization for atmospheric new-particle formation: Application to a system involving sulfuric acid and condensable water-soluble organic vapors, Aerosol Sci. Technol., 38(10), 1001–1008, doi:10.1080/027868290519085, 2004.

Kim, M. J., Novak, G. A., Zoerb, M. C., Yang, M., Blomquist, B. W., Huebert, B. J., Cappa, C. D. and Bertram, T. H.: Air-Sea exchange of biogenic volatile organic compounds and the impact on aerosol particle size distributions, Geophys. Res. Lett., 44(8), 3887–3896, doi:10.1002/2017GL072975, 2017.

Kodros, J. K., Cucinotta, R., Ridley, D. A., Wiedinmyer, C. and Pierce, J. R.: The aerosol radiative effects of uncontrolled combustion of domestic waste, Atmos. Chem. Phys., 16(11), 6771–6784, doi:10.5194/acp-16-6771-2016, 2016.

Kodros, J. K. and Pierce, J. R.: Important global and regional differences in aerosol cloud-albedo effect estimates between simulations with and without prognostic aerosol microphysics, J. Geophys. Res., 122(7), 4003–4018, doi:10.1002/2016JD025886, 2017.

Korhonen, H., Carslaw, K. S., Spracklen, D. V, Mann, G. W. and Woodhouse, M. T.: Influence of oceanic dimethyl sulfide emissions on cloud condensation nuclei concentrations and seasonality over the remote Southern Hemisphere oceans: A global model study, J. Geophys. Res. Atmos., 113(D15), doi:10.1029/2007JD009718, 2008

Kuang, C., Senum, G. I., Dedrick, J., Leaitch, W. R., Lubin, D., Aiken, A. C., Springston, S. R., Uin, J., Russell, L. M. and Liu, J.: High summertime aerosol organic functional group concentrations from marine and seabird sources at Ross Island, Antarctica, during AWARE, Atmos. Chem. Phys., 18(12), 8571–8587, doi:10.5194/acp-18-8571-2018, 2018.

1327 Kulmala, M., Lehtinen, K. E. J., and Laaksonen, A.: Cluster activation theory as an explanation of
1328 the linear dependence between formation rate of 3nm particles and sulphuric acid
1329 concentration, Atmos. Chem. Phys., 6, 787–793, https://doi.org/10.5194/acp-6-
1330 787-2006, 2006.
1331 Lana, A., Bell, T. G., Simó, R., Vallina, S. M., Ballabrera-Poy, J., Kettle, A. J., Dachs, J., Bopp,
1332 L., Saltzman, E. S., Stefels, J., Johnson, J. E. and Liss, P. S.: An updated
1333 climatology of surface dimethlysulfide concentrations and emission fluxes in the
1334 global ocean, Global Biogeochem. Cycles, 25(1), 1–17,
1335 doi:10.1029/2010GB003850, 2011.
1336 Lana, A., Simó, R., Vallina, S. M. and Dachs, J.: Re-examination of global emerging patterns of
1337 ocean DMS concentration, Biogeochemistry, 110(1), 173–182,
1338 doi:10.1007/s10533-011-9677-9, 2012a.
1339 Lana, A., Simó, R., Vallina, S. M., and Dachs, J.: Potential for a biogenic influence on cloud
1340 microphysics over the ocean: a correlation study with satellite-derived data, Atmos.
1341 Chem. Phys., 12, 7977–7993, https://doi.org/10.5194/acp-12-7977-2012, 2012b.
1342 Lapina, K., Heald, C. L., Spracklen, D. V., Arnold, S. R., Allan, J. D., Coe, H., McFiggans, G.,
1343 Zorn, S. R., Drewnick, F., Bates, T. S., Hawkins, L. N., Russell, L. M., Smirnov,
1344 A., O'Dowd, C. D., and Hind, A. J.: Investigating organic aerosol loading in the
1345 remote marine environment, Atmos. Chem. Phys., 11, 8847–8860,
1346 https://doi.org/10.5194/acp-11-8847-2011, 2011
1347 Leaitch, W. R., Sharma, S., Huang, L., Toom-Sauntry, D., Chivulescu, A., Macdonald, A. M., von
1348 Salzen, K., Pierce, J. R., Bertram, A. K., Schroder, J. C., Shantz, N. C., Chang, R.
1349 Y.-W. and Norman, A.-L.: Dimethyl sulfide control of the clean summertime Arctic
1350 aerosol and cloud, Elem. Sci. Anthr., 1, 000017,
1351 doi:10.12952/journal.elementa.000017, 2013.
1352 Leaitch, R. W., Russell, L. M., Liu, J., Kolonjari, F., Toom, D., Huang, L., Sharma, S., Chivulescu,
1353 A., Veber, D. and Zhang, W.: Organic functional groups in the submicron aerosol
1354 at 82.5 degrees N, 62.5 degrees W from 2012 to 2014, Atmos. Chem. Phys., 18,
1355 3269–3287, doi:10.5194/acp-18-3269-2018, 2018.
1356 Leck, C. and Bigg, E. K.: Source and evolution of the marine aerosol—A new perspective,
1357 Geophys. Res. Lett., 32(19), doi:10.1029/2005GL023651, 2005.

1358 Lee, Y. H. and Adams, P. J.: A fast and efficient version of the TwO-Moment Aerosol Sectional
1359 (TOMAS) global aerosol microphysics model, Aerosol Sci. Technol., 46(6), 678–
1360 689, doi:10.1080/02786826.2011.643259, 2012.
1361 Lee, Y. H., Pierce, J. R., and Adams, P. J.: Representation of nucleation mode microphysics in a
1362 global aerosol model with sectional microphysics, Geosci. Model Dev., 6, 1221–
1363 1232, https://doi.org/10.5194/gmd-6-1221-2013, 2013.
1364 Liu, H., Jacob, D. J., Bey, I. and Yantosca, R. M.: Constraints from210Pb and7Be on wet
1365 deposition and transport in a global three-dimensional chemical tracer model driven
1366 by assimilated meteorological fields, J. Geophys. Res. Atmos., 106(D11), 12109–
1367 12128, doi:10.1029/2000JD900839, 2001.
1368 Lohmann, U. and Feichter, J.: Global indirect aerosol effects: a review, Atmos. Chem. Phys., 5(3),
1369 715–737, doi:10.5194/acp-5-715-2005, 2005.
1370 Luo, G., Yu, F. and Schwab, J.: Revised treatment of wet scavenging processes dramatically
1371 improves GEOS-Chem 12 . 0 . 0 simulations of surface nitric acid, nitrate, and
1372 ammonium over the United States, Geosci. Model. Dev., 12, 3439–3447,
1373 doi.10.5194/gmd-12-3439-2019, 2019.
1374 Luo, G., Yu, F. and Moch, J. M.: Further improvement of wet process treatments in GEOS-Chem
1375 v12 . 6 . 0 : impact on global distributions of aerosols and aerosol precursors,
1376 Geosci. Model Dev., 2879–2903, 2020.
1377 Mahmood, R., Salzen, K. Von, Norman, A., Galí, M. and Levasseur, M.: Sensitivity of Arctic
1378 sulfate aerosol and clouds to changes in future surface seawater dimethylsulfide
1379 concentrations, Atmos. Chem. Phys., 19, 6419–6435, https://doi.org/10.5194/acp-
1380 19-6419-2019, 2019.
1381 Mårtensson, E. M., Nilsson, E. D., de Leeuw, G., Cohen, L. H. and Hansson, H.-C.: Laboratory
1382 simulations and parameterization of the primary marine aerosol production, J.
1383 Geophys. Res. Atmos., 108(D9), n/a-n/a, doi:10.1029/2002JD002263, 2003.
1384 McCoy, D. T., Burrows, S. M., Wood, R., Grosvenor, D. P., Elliott, S. M., Ma, P.-L., Rasch, P. J.
1385 and Hartmann, D. L.: Natural aerosols explain seasonal and spatial patterns of
1386 Southern Ocean cloud albedo, Sci. Adv., 1(6), e1500157,
1387 doi:10.1126/sciadv.1500157, 2015.

McDuffie, E. E., Smith, S. J., O'Rourke, P., Tibrewal, K., Venkataraman, C., Marais, E. A., Zheng, B., Crippa, M., Brauer, M., and Martin, R. V.: A global anthropogenic emission inventory of atmospheric pollutants from sector- and fuel-specific sources (1970–2017): An application of the Community Emissions Data System (CEDS), Earth Syst. Sci. Data Discuss., https://doi.org/10.5194/essd-2020-103, in review, 2020.

McNaughton, C. S., Clarke, A. D., Howell, S. G., Pinkerton, M., Anderson, B., Thornhill, L., Hudgins, C., et al.: Results from the DC-8 Inlet Characterization Experiment (DICE): Airborne versus surface sampling of mineral dust and sea salt aerosols, Aerosol Sci. Tech. 41, (2). 136-159, 2007.

Meskhidze, N., Sabolis, A., Reed, R. and Kamykowski, D.: Quantifying environmental stress-induced emissions of algal isoprene and monoterpenes using laboratory measurements, Biogeosciences, 12, 637–651, doi:10.5194/bg-12-637-2015, 2015.

Monahan, E. C., Fairall, C. W., Davidson, K. L., and Boyle, P. J.: Observed inter-relations between 10m winds, ocean whitecaps and marine aerosols, Q. J. Roy. Meteor. Soc., 109, 379–392, 1983.

Müller, M., Mikoviny, T., Feil, S., Haidacher, S., Hanel, G., Hartungen, E., Jordan, A., Märk, L., Mutschlechner, P., Schottkowsky, R., Sulzer, P., Crawford, J. H., and Wisthaler, A.: A compact PTR-ToF-MS instrument for airborne measurements of VOCs at high spatio-temporal resolution, Atmos. Meas. Tech. 7, 3763-3772, doi:10.5194/amt-7-3763-2014, 2014.

Mungall, E. L., Abbatt, J. P. D., Wentzell, J. J. B., Lee, A. K. Y., Thomas, J. L., Blais, M., Gosselin, M., Miller, L. A., Papakyriakou, T., Willis, M. D. and Liggio, J.: Microlayer source of oxygenated volatile organic compounds in the summertime marine Arctic boundary layer, Proc. Natl. Acad. Sci., 114(24), 6203–6208, doi:10.1073/pnas.1620571114, 2017.

Napari, I., Noppel, M., Vehkamaki, H. and Kulmala, M.: Parametrization of ternary nucleation rates for H2SO4-NH3-H2O vapors, J. Geophys. Res. Atmos., 107(19), 2–7, doi:10.1029/2002JD002132, 2002.

Nightingale, P. D., Liss, P. S. and Schlosser, P.: Measurements of air-sea gas transfer during an open ocean algal bloom, Geophys. Res. Lett., 27(14), 2117–2120, doi:10.1029/2000GL011541, 2000a.

1443 Nightingale, P. D., Malin, G., Law, C. S., Watson, A. J., Liss, P. S., Liddicoat, M. I., Boutin, J.
1444 and Upstill-Goddard, R. C.: In situ evaluation of air-sea gas exchange
1445 parameterizations using novel conservative and volatile tracers, Global
1446 Biogeochem. Cycles, 14(1), 373–387, doi:10.1029/1999GB900091, 2000b.
1447 O'Dowd, C. D., Smith, M. H., Consterdine, I. E., Lowe, J. A.: Marine aerosol, sea-salt, and the
1448 marine sulphur cycle: A short review. Atmos. Environ. 31, 73–80 (1997)
1449 O'Dowd, C. D.: Marine aerosol formation from biogenic iodine emissions, Nature, 417(June), 1–
1450 5, doi:10.1038/nature00775, 2002.
1451 O' Dowd, C. D., Facchini, M. C., Cavalli, F., Ceburnis, D., Mircea, M., Decesari, S., Fuzzi, S.,
1452 Yoon, Y. J. and Putaud, J.: Biogenically driven organic contribution to marine
1453 aerosol, Nature, 431(7009), 676-680, https://doi.org/10.1038/nature02959, 2004
1454 O'Dowd, C. D. and de Leeuw, G.: Marine aerosol production : a review of the current knowledge,
1455 Phil. Trans. R. Soc. A, 1(May), 1753–1774, doi:10.1098/rsta.2007.2043, 2007.
1456 O'Dowd, C. D., Ceburnis, D., Ovadnevaite, J., Bialek, J., Stengel, D. B., Zacharias, M., Nitschke,
1457 U., Connan, S., Rinaldi, M., Fuzzi, S., Decesari, S., Facchini, M. C., Marullo, S.,
1458 Santoleri, R., Anno, A. D., Corinaldesi, C., Tangherlini, M. and Danovaro, R.:
1459 Connecting marine productivity to sea-spray via nanoscale biological processes :
1460 Phytoplankton Dance or Death Disco ?, Sci. Rep, 5(May), 14883, 1–11,
1461 doi:10.1038/srep14883, 2015.
1462 Ovadnevaite, J., Ceburnis, D., Martucci, G., Bialek, J., Monahan, C., Rinaldi, M., Facchini, M. C.,
1463 Berresheim, H., Worsnop, D. R. and O'Dowd, C.: Primary marine organic aerosol :
1464 A dichotomy of low hygroscopicity and high CCN activity, Geophys. Res. Lett.,
1465 38, L21806 1–5, doi:10.1029/2011GL048869, 2011.
1466 Ovadnevaite, J., Ceburnis, D., Canagaratna, M., Berresheim, H., Bialek, J., Martucci, G., Worsnop,
1467 D. R. and Dowd, C. O.: On the effect of wind speed on submicron sea salt mass
1468 concentrations and source fluxes, J. Geophys. Res.,, 117, D16201, 1–11,
1469 doi:10.1029/2011JD017379, 2012.
1470 Pai, S. J., Heald, C. L., Pierce, J. R., Farina, S. C., Marais, E. A., Jimenez, J. L., Campuzano-jost,
1471 P., Nault, B. A., Middlebrook, A. M., Coe, H., Shilling, J. E., Bahreini, R., Dingle,
1472 J. H. and Vu, K.: An evaluation of global organic aerosol schemes using airborne
1473 observations, Atmos. Chem. Phys., 20 , 2637–2665, https://doi.org/10.5194/acp-

20-2637-2020, 2020.

Park, K.-T., Jang, S., Lee, K., Yoon, Y. J., Kim, M.-S., Park, K., Cho, H.-J., Kang, J.-H., Udisti, R., Lee, B.-Y. and Shin, K.-H.: Observational evidence for the formation of DMS-derived aerosols during Arctic phytoplankton blooms, Atmos. Chem. Phys., 17(15), 9665–9675, doi:https://doi.org/10.5194/acp-17-9665-2017, 2017.

Park, K.-T., Lee, K., Kim, T.-W., Yoon, Y. J., Jang, E.-H., Jang, S., Lee, B.-Y. and Hermansen, O.: Atmospheric DMS in the Arctic Ocean and Its Relation to Phytoplankton Biomass, Global Biogeochem. Cycles, 32(3), 351–359, doi:10.1002/2017GB005805, 2018.

Pierce, J. R., Croft, B., Kodros, J. K., D'Andrea, S. D. and Martin, R. V.: The importance of interstitial particle scavenging by cloud droplets in shaping the remote aerosol size distribution and global aerosol-climate effects, Atmos. Chem. Phys., 15(11), 6147–6158, doi:10.5194/acp-15-6147-2015, 2015.

Prather, K. A., Bertram, T. H., Grassian, V. H., Deane, G. B., Stokes, M. D., DeMott, P. J., Aluwihare, L. I., Palenik, B. P., Azam, F., Seinfeld, J. H., Moffet, R. C., Molina, M. J., Cappa, C. D., Geiger, F. M., Roberts, G. C., Russell, L. M., Ault, A. P., Baltrusaitis, J., Collins, D. B., Corrigan, C. E., Cuadra-Rodriguez, L. A., Ebben, C. J., Forestieri, S. D., Guasco, T. L., Hersey, S. P., Kim, M. J., Lambert, W. F., Modini, R. L., Mui, W., Pedler, B. E., Ruppel, M. J., Ryder, O. S., Schoepp, N. G., Sullivan, R. C. and Zhao, D.: Bringing the ocean into the laboratory to probe the chemical complexity of sea spray aerosol, Proc. Natl. Acad. Sci., 110(19), 7550–7555, doi:10.1073/pnas.1300262110, 2013.

Quinn, P. K. and Bates, T. S.: The case against climate regulation via oceanic phytoplankton sulphur emissions, Nature, 480(7375), 51–56, doi:10.1038/nature10580, 2011.

Quinn, P. K., Bates, T. S., Schulz, K. S., Coffman, D. J., Frossard, A. A., Russell, L. M., Keene, W. C. and Kieber, D. J.: Contribution of sea surface carbon pool to organic matter enrichment in sea spray aerosol, Nat. Geosci., 7(3), 228–232, doi:10.1038/ngeo2092, 2014.

Quinn, P. K., Collins, D. B., Grassian, V. H., Prather, K. A. and Bates, T. S.: Chemistry and Related Properties of Freshly Emitted Sea Spray Aerosol, Chem. Rev., 115(10), 4383–4399, doi:10.1021/cr500713g, 2015.

1505 Quinn, P. K., Coffman, D. J., Johnson, J. E., Upchurch, L. M. and Bates, T. S.: Small fraction of
1506 marine cloud condensation nuclei made up of sea spray aerosol, Nat. Geosci., 10(9),
1507 674–679, doi:10.1038/ngeo3003, 2017.
1508 Quinn, P. K., Bates, T. S., Coffman, D. J., Upchurch, L., Johnson, J. E., Moore, R. and Ziemba,
1509 L.: Seasonal Variations in Western North Atlantic Remote Marine Aerosol
1510 Properties, J. Geophys. Res., Atmos., 124, 14,240–14,261.
1511 https://doi.org/10.1029/2019JD031740, 2019.
1512 Park, K.-T., Lee, K., Kim, T.-W., Yoon, Y. J., Jang, E.-H., Jang, S., Lee, B.-Y. and Hermansen,
1513 O.: Atmospheric DMS in the Arctic Ocean and Its Relation to Phytoplankton
1514 Biomass, Global Biogeochem. Cycles, 32(3), 351–359,
1515 doi:10.1002/2017GB005805, 2018.
1516 Ramnarine, E., Kodros, J. K., Hodshire, A. L., Lonsdale, C. R., Alvarado, M. J. and Pierce, J. R.:
1517 Effects of near-source coagulation of biomass burning aerosols on global
1518 predictions of aerosol size distributions and implications for aerosol radiative
1519 effects, Atmos. Chem. Phys., 19, 6561–6577, https://doi.org/10.5194/acp-19-
1520 6561-2019, 2019.
1521 Regayre, L. A., Schmale, J., Johnson, J. S., Tatzelt, C., Baccarini, A., Henning, S., Yoshioka, M.,
1522 Stratmann, F., Gysel-Beer, M., Grosvenor, D. P., and Carslaw, K. S.: The value of
1523 remote marine aerosol measurements for constraining radiative forcing uncertainty,
1524 Atmos. Chem. Phys., 20, 10063–10072, https://doi.org/10.5194/acp-20-10063-
1525 2020, 2020.
1526 Rempillo, O., Seguin, A. M., Norman, A.-L., Scarratt, M., Michaud, S., Chang, R., Sjostedt, S.,
1527 Abbatt, J., Else, B., Papakyriakou, T., Sharma, S., Grasby, S. and Levasseur, M.:
1528 Dimethyl sulfide air-sea fluxes and biogenic sulfur as a source of new aerosols in
1529 the Arctic fall, J. Geophys. Res. Atmos., 116, (D100S04),
1530 doi:10.1029/2011JD016336, 2011.
1531 Revell, L. E., Kremser, S., Hartery, S., Harvey, M., Mulcahy, J. P., Williams, J., Morgenstern, O.,
1532 Mcdonald, A. J., Varma, V., Bird, L. and Schuddeboom, A.: The sensitivity of
1533 Southern Ocean aerosols and cloud microphysics to sea spray and sulfate aerosol
1534 production in the HadGEM3-GA7 . 1 chemistry – climate model, Atmos. Chem.
1535 Phys., 19, 15447–15466, https://doi.org/10.5194/acp-19-15447-2019, 2019.

Riccobono, F., Schobesberger, S., Scott, C. E., Dommen, J., Ortega, I. K., Rondo, L., Almeida, J., Amorim, A., Bianchi, F., Breitenlechner, M., David, A., Downard, A., Dunne, E. M., Duplissy, J., Ehrhart, S., Flagan, R. C., Franchin, A., Hansel, A., Junninen, H., Kajos, M., Keskinen, H., Kupc, A., Kupiainen, O., Kürten, A., Kurtén, T., Kvashin, A. N., Laaksonen, A., Lehtipalo, K., Makhmutov, V., Mathot, S., Nieminen, T., Olenius, T., Onnela, A., Petäjä, T., Praplan, A. P., Santos, F. D., Schallhart, S., Seinfeld, J. H., Sipilä, M., Spracklen, D. V, Stozhkov, Y., Stratmann, F., Tomé, A., Tsagkogeorgas, G., Vaattovaara, P., Vehkamäki, H., Viisanen, Y., Vrtala, A., Wagner, P. E., Weingartner, E., Wex, H., Wimmer, D., Carslaw, K. S., Curtius, J., Donahue, N. M., Kirkby, J., Kulmala, M., Worsnop, D. R., Baltensperger, U. U. ., Schobesberger, S., Scott, C. E., Dommen, J., Ortega, I. K., Rondo, L., Almeida, J., Amorim, A., Bianchi, F., Breitenlechner, M., David, A., Downard, A., Dunne, E. M., Duplissy, J., Ehrhart, S., Flagan, R. C., Franchin, A., Hansel, A., Junninen, H., Kajos, M., Keskinen, H., Kupc, A., Kürten, A., Kvashin, A. N., Laaksonen, A., Lehtipalo, K., Makhmutov, V., Mathot, S., Nieminen, T., Onnela, A., Petäjä, T., Praplan, A. P., Santos, F. D., Schallhart, S., Seinfeld, J. H., Sipilä, M., Spracklen, D. V, Stozhkov, Y., Stratmann, F., Tomé, A., Tsagkogeorgas, G., et al.: Oxidation Products of Biogenic Emissions Contribute to Nucleation of Atmospheric Particles, Science, 344(May), 717–721 [online] Available from: http://www.sciencemag.org/content/344/6185/717.abstract, doi: 10.1126/science.1243527, 2014.

Rinaldi, M., Decesari, S., Finessi, E., Giulianelli, L., Carbone, C., Fuzzi, S., O'Dowd, C., Ceburnis, D. and Facchini, M. C.: Primary and Secondary Organic Marine Aerosol and Oceanic Biological Activity: Recent Results and New Perspectives for Future Studies, Adv. Meteorol., 2010, 1–10, doi:10.1155/2010/310682, 2010.

Rodríguez-Ros, P., Cortés, P., Robinson, C. M., Nunes, S., Hassler, C., Royer, S., Estrada, M. and Simó, R.: Distribution and Drivers of Marine Isoprene Concentration across the Southern Ocean, Atmosphere, 11, 556, 1–19, doi:10.3390/atmos11060556, 2020a.

Rodriguez-Ros, P., Galí, M., Cortés, P., Robinson, C. M., Antoine, D., Wohl, C., Yang, M. and Simó, R.: Remote Sensing Retrieval of Isoprene Concentrations in the Southern Ocean Geophys. Res. Lett., 47, e2020GL087888, 1–10,

doi:10.1029/2020GL087888, 2020b.

Russell, L. M., Hawkins, L. N., Frossard, A. A., Quinn, P. K. and Bates, T. S.: Carbohydrate-like composition of submicron atmospheric particles and their production from ocean bubble bursting, Proc. Natl. Acad. Sci., 107(15), 6652-6657, doi:10.1073/pnas.0908905107, 2010.

Saliba, G., Chen, C., Lewis, S., Russell, L. M., Rivellini, L., Lee, A. K. Y., Carlson, C. A. and Behrenfeld, M. J.: Factors driving the seasonal and hourly variability of sea-spray aerosol number in the North Atlantic, Proc, Nat. Acad. Sci., 116(41), 20309–20314, doi:10.1073/pnas.1907574116, 2019.

Saliba, G., Chen, C., Lewis, S., Russell, L. M., Quinn, P. K., Bates, T. S., Bell, T. G., Lawler, M.J., Saltzman, E. S., Sanchez, K. J., Moore, R., Shook, M., Rivellini, L-H., Lee, A. K. Y. Baetge, N., Carlson, C. A. and Behrenfeld, M. J.: Seasonal differences and variability of concentrations, chemical composition, and cloud condensation nuclei of marine aerosol over the North Atlantic, 125, e2020JD033145. https://doi.org/10.1029/2020JD033145, 2020.

Sanchez, K. J., Chen, C.-L., Russell, L. M., Betha, R., Liu, J., Price, D. J., Massoli, P., Ziemba, L. D., Crosbie, E. C., Moore, R. H., Müller, M., Schiller, S. A., Wisthaler, A., Lee, A. K. Y., Quinn, P. K., Bates, T. S., Porter, J., Bell, T. G., Saltzman, E. S., Vaillancourt, R. D. and Behrenfeld, M. J.: Substantial Seasonal Contribution of Observed Biogenic Sulfate Particles to Cloud Condensation Nuclei, Sci. Rep., 8(1), 3235, doi:10.1038/s41598-018-21590-9, 2018.

Savoie, D. L., R. Arimoto, W. C. Keene, J. M. Prospero, R. A. Duce, and J. N. Galloway, Marine biogenic and anthropogenic contributions to non-sea-salt sulfate in the marine boundary layer over the North Atlantic Ocean, J. Geophys. Res., 107(D18), 4356, doi:10.1029/2001JD000970, 2002

Schwarz, J. P., Gao, R. S., Fahey, D. W., Thomson, D. S., Watts, L. A., Wilson, J. C., Reeves, J. M., Darbeheshti, M., Baumgardner, D. G., Kok, G. L., Chung, S. H., Schulz, M., Hendricks, J., Lauer, A., Ka, B. and Slowik, J. G.: Single-particle measurements of midlatitude black carbon and light-scattering aerosols from the boundary layer to the lower stratosphere, J. Geophys. Res. Atmos., 111, D216207, 1–15, doi:10.1029/2006JD007076, 2006.

1598 Schiffer, J. M., Mael, L. E., Prather, K. A., Amaro, R. E. and Grassian, V. H.: Sea Spray Aerosol:
1599 Where Marine Biology Meets Atmospheric Chemistry, ACS Cent. Sci., 4, 1617-
1600 1623 doi:10.1021/acscentsci.8b00674, 2018.
1601 Schiller, S. A. P.: Flugzeuggestützte Messung flüchtiger organischer Verbindungen über dem
1602 Nordatlantik mittels PTR-ToF-MS, Master Thesis (*in German*), Universität
1603 Innsbruck (2018)
1604 Schwinger, J., Tjiputra, J., Goris, N., Six, K. D., Kirkevåg, A., Seland, Ø., Heinze, C. and Ilyina,
1605 T.: Amplification of global warming through pH dependence of DMS production
1606 simulated with a fully coupled Earth system model, Biogeosciences, 14, 3633–
1607 3648, https://doi.org/10.5194/bg-14-3633-2017, 2017.
1608 Sharma, S., Lavoué, D., Cachier, H., Barrie, L. A. and Gong, S. L.: Long-term trends of the black
1609 carbon concentrations in the Canadian Arctic, J. Geophys. Res. Atmos., 109,
1610 (D15203), doi:10.1029/2003JD004331, 2004.
1611 Sharma, S., Andrews, E., Barrie, L. A., Ogren, J. A. and Lavoué, D.: Variations and sources of the
1612 equivalent black carbon in the high Arctic revealed by long-term observations at
1613 Alert and Barrow: 1989–2003, J. Geophys. Res. Atmos., 111, (D14208),
1614 doi:10.1029/2005JD006581, 2006.
1615 Sihto, S., Kulmala, M., Kerminen, V., Maso, M. D. and Petäjä, T., Riipinen, I., Korhonen, H.,
1616 Arnold, F., Janson, R., Boy, M., Laaksonen, A. and Lehtinen, K. E. J.: Atmospheric
1617 sulphuric acid and aerosol formation : implications from atmospheric
1618 measurements for nucleation and early growth mechanisms, Atmos. Chem. Phys.,
1619 6, 4079–4091, www.atmos-chem-phys.net/6/4079/2006/, 2006.
1620 Singh, H. B., Cai, C., Kaduwela, A., Weinheimer, A. and Wisthaler, A.: Interactions of fire
1621 emissions and urban pollution over California : Ozone formation and air quality
1622 simulations, Atmos. Environ., 56, 45–51, doi:10.1016/j.atmosenv.2012.03.046,
1623 2012.
1624 Stohl, A., Forster, C., Eckhardt, S., Spichtinger, N., Huntrieser, H., Heland, J., Schlager, H.,
1625 Wilhelm, S., Arnold, F. and Cooper, O.: A backward modeling study of
1626 intercontinental pollution transport using aircraft measurements, J. Geophys. Res.,
1627 108, D12, 4370, doi:10.1029/2002JD002862, 2003.

1628 Takegawa, N., Seto, T., Moteki, N., Koike, M., Oshima, N., Adachi, K., Kita, K., Takami, A. and
1629 Kondo, Y.: Enhanced New Particle Formation Above the Marine Boundary Layer
1630 Over the Yellow Sea : Potential Impacts on Cloud Condensation Nuclei, J.
1631 Geophys. Res. Atmos., 125, e2019JD031448, 1–17, doi:10.1029/2019JD031448,
1632 2020.
1633 Tremblay, S., Picard, J.-C., Bachelder, J. O., Lutsch, E., Strong, K., Fogal, P., Leaitch, W. R.,
1634 Sharma, S., Kolonjari, F., Cox, C. J., Chang, R. Y.-W. and Hayes, P. L.:
1635 Characterization of aerosol growth events over Ellesmere Island during summers
1636 of 2015 and 2016, Atmos. Chem. Phys., 19, 5589-
1637 5604, https://doi.org/10.5194/acp-19-5589-2019, 2019.
1638 Tunved, P., Ström, J. and Krejci, R.: Arctic aerosol life cycle: Linking aerosol size distributions
1639 observed between 2000 and 2010 with air mass transport and precipitation at
1640 Zeppelin station, Ny-Ålesund, Svalbard, Atmos. Chem. Phys., 13(7), 3643–3660,
1641 doi:10.5194/acp-13-3643-2013, 2013.
1642 van der Werf, G. R., Randerson, J. T., Giglio, L., Van Leeuwen, T. T., Chen, Y., Rogers, B. M.,
1643 Mu, M., Van Marle, M. J. E., Morton, D. C., Collatz, G. J., Yokelson, R. J. and
1644 Kasibhatla, P. S.: Global fire emissions estimates during 1997-2016, Earth Syst.
1645 Sci. Data, 9(2), 697–720, doi:10.5194/essd-9-697-2017, 2017.
1646 Vehkamäki, H., Kulmala, M., Napari, I., Lehtinen, K. E. J., Timmreck, C., Noppel, M. and
1647 Laaksonen, A.: An improved parameterization for sulfuric acid – water nucleation
1648 rates for tropospheric and stratospheric conditions, J. Geophys. Res., 107, D22,
1649 4622, 1–10, doi:10.1029/2002JD002184, 2002.
1650 Veres, P. R., Neuman, J. A., Bertram, T. H., Assaf, E. and Wolfe, G. M.: Global airborne sampling
1651 reveals a previously unobserved dimethyl sulfide oxidation mechanism in the
1652 marine atmosphere, Proc.Natl, Acad. Sci., 117(9), 4505–4510,
1653 doi:10.1073/pnas.1919344117, 2020.
1654 Vinken, G. C. M., Boersma, K. F., Jacob, D. J., Meijer, E. W.: Accounting for non-linear chemistry
1655 of ship plumes in the GEOS-Chem global chemistry transport model, Atmos.
1656 Chem. Phys., 11, 11707–11722, doi:10.5194/acp-11-11707-2011, 2011.
1657 Wang, Q., Jacob, D. J., Fisher, J. A., Mao, J., Leibensperger, E. M., Carouge, C. C., Le Sager, P.,
1658 Kondo, Y., Jimenez, J. L., Cubison, M. J. and Doherty, S. J.: Sources of

carbonaceous aerosols and deposited black carbon in the Arctic in winter-spring: Implications for radiative forcing, Atmos. Chem. Phys., 11, 12453–12473, doi:10.5194/acp-11-12453-2011, 2011.

Wang, Q., Jacob, D. J., Spackman, J. R., Perring, A. E., Schwarz, J. P., Moteki, N., Marais, E. A., Ge, C., Wang, J. and Barrett, S. R. H.: Global budget and radiative forcing of black carbon aerosol : Constraints from pole-to-pole (HIPPO) observations across the Pacific, J. Geophys. Res., 119, 195–206, doi:10.1002/2013JD020824, 2014.

Wang, X., Sultana, C. M., Trueblood, J., Hill, T. C. J., Malfatti, F., Lee, C., Laskina, O., Moore, K. A., Beall, C. M., McCluskey, C. S., Cornwell, G. C., Zhou, Y., Cox, J. L., Pendergraft, M. A., Santander, M. V., Bertram, T. H., Cappa, C. D., Azam, F., DeMott, P. J., Grassian, V. H. and Prather, K. A.: Microbial control of sea spray aerosol composition: A tale of two blooms, ACS Cent. Sci., 1(3), 124–131, doi:10.1021/acscentsci.5b00148, 2015.

Weber, R. J., Chen, G., Davis, D. D., Mauldin, R. L., Tanner, D. J., Clarke, A. D., Thornton, D. C. and Bandy, A. R.: Measurements of enhanced H_2SO_4 and 3-4 nm particles near a frontal cloud during the First Aerosol Characterization Experiment (ACE 1), J. Geophys. Res., 106, (D20),24 107 - 24117, 2001.

Wehner, B., Werner, F., Ditas, F., Shaw, R. A., Kulmala, M. and Siebert, H.: Observations of new particle formation in enhanced UV irradiance zones near cumulus clouds, Atmos. Chem. Phys., 11701–11711, doi:10.5194/acp-15-11701-2015, 2015.

Wesley, M. L.: Parameterization of surface resistances to gaseous deposition in regional-scale numerical models, Atmos. Environ., 23, 1293-1304, 1989.

Westervelt, D. M.: Formation and growth of nucleated particles into cloud condensation nuclei : model – measurement comparison, Atmos. Chem. Phys., 13, 7645–7663, doi:10.5194/acp-13-7645-2013, 2013.

Willis, M. D., Burkart, J., Thomas, J. L., Köllner, F., Schneider, J., Bozem, H., Hoor, P. M., Aliabadi, A. A., Schulz, H., Herber, A. B., Leaitch, W. R. and Abbatt, J. P. D.: Growth of nucleation mode particles in the summertime Arctic: A case study, Atmos. Chem. Phys., 16(12), 7663–7679, doi:10.5194/acp-16-7663-2016, 2016.

Willis, M. D., Köllner, F., Burkart, J., Bozem, H., Thomas, J. L., Schneider, J., Aliabadi, A. A., Hoor, P. M., Schulz, H., Herber, A. B., Leaitch, W. R. and Abbatt, J. P. D.:

1690 Evidence for marine biogenic influence on summertime Arctic aerosol, Geophys.
1691 Res. Lett., 44(12), 6460–6470, doi:10.1002/2017GL073359, 2017.
1692 Willis, M. D., Leaitch, W. R. and Abbatt, J. P. D.: Processes Controlling the Composition and
1693 Abundance of Arctic Aerosol, Reviews of Geophysics, 56, 621-671,
1694 doi:10.1029/2018RG000602, 2018.
1695 Wood, R.: Stratocumulus Clouds, Mon. Weather Rev., 140, 2373–2423, doi:10.1175/MWR-D-11-
1696 00121.1, 2012.
1697 Wilson, T. W., Ladino, L. A., Alpert, P. A., Breckels, M. N., Brooks, I. M., Browse, J., Burrows,
1698 S. M., Carslaw, K. S., Huffman, J. A., Judd, C., Kilthau, W. P., Mason, R. H.,
1699 McFiggans, G., Miller, L. A., Najera, J. J., Polishchuk, E., Rae, S., Schiller, C. L.,
1700 Si, M., Temprado, J. V., Whale, T. F., Wong, J. P. S., Wurl, O., Yakobi-Hancock,
1701 J. D., Abbatt, J. P. D., Aller, J. Y., Bertram, A. K., Knopf, D. A. and Murray, B. J.:
1702 A marine biogenic source of atmospheric ice-nucleating particles, Nature,
1703 525(7568), 234–238, doi:10.1038/nature14986, 2015.
1704 Wood, R., Stemmler, J. D., Rémillard, J. and Jefferson, A.: Low-CCN concentration air masses
1705 over the eastern North Atlantic : Seasonality , meteorology , and drivers, J.
1706 Geophys. Res. Atmos., 122, 1203-1223, doi:10.1002/2016JD025557, 2017.
1707 Woodhouse, M. T., Mann, G. W., Carslaw, K. S. and Boucher, O.: Sensitivity of cloud
1708 condensation nuclei to regional changes in dimethyl-sulphide emissions, Atmos.
1709 Chem. Phys., 13(5), 2723–2733, doi:https://doi.org/10.5194/acp-13-2723-2013,
1710 2013.
1711 Xu, J. W., Martin, R. V., Morrow, A., Sharma, S., Huang, L., Richard Leaitch, W., Burkart, J.,
1712 Schulz, H., Zanatta, M., Willis, M. D., Henze, D. K., Lee, C. J., Herber, A. B. and
1713 Abbatt, J. P. D.: Source attribution of Arctic black carbon constrained by aircraft
1714 and surface measurements, Atmos. Chem. Phys., 17(19), 11971–11989,
1715 doi:10.5194/acp-17-11971-2017, 2017.
1716 Yassaa, N., Peeken, I., Zöllner, E., Bluhm, K., Arnold, S., Spracklan, D. and Williams, J: Evidence
1717 for marine production of monoterpenes, Environ. Chem., 5, 391–401,
1718 doi:10.1071/EN08047, 2008.
1719 Zanatta, M., Bozem, H., Köllner, F., Schneider, J., Hoor, P., Faria, J. De, Petzold, A., Bundke, U.,
1720 Staebler, R. M., Schulz, H., Herber, A. B., Zanatta, M., Bozem, H., Köllner, F.,

Schneider, J., Hoor, P., Faria, J. De, Petzold, A., Bundke, U., Hayden, K., Staebler, R. M., Schulz, H. and Herber, A. B..: Airborne survey of trace gases amd aerosol over the Southern Baltic Sea: from clean marine boundary layer to shipping corridor effect, Tellus B Chem. Phys. Meteorol., 72(1), 1–24, doi:10.1080/16000889.2019.1695349, 2019.

Zender, C. S., Bian, H. and Newman, D.: Mineral Dust Entrainment and Deposition (DEAD) model: Description and 1990s dust climatology, J. Geophys. Res., 108(D14), 4416, doi:10.1029/2002JD002775, 2003.

Zhang, H. F., Worton, D. R., Lewandowski, M., Ortega, J., Rubitschun, C. L., Park, J. H., Kristensen, K., Campuzano-Jost, P., Day, D. A., Jimenez, J. L., Jaoui, M., Offenberg, J. H., Kleindienst, T. E., Gilman, J., Kuster, W. C., de Gouw, J., Park, C., Schade, G. W., Frossard, A. A., Russell, L., Kaser, L., Jud, W., Hansel, A., Cappellin, L., Karl, T., Glasius, M., Guenther, A., Goldstein, A. H., Seinfeld, J. H., Gold, A., Kamens, R. M. and Surratt, J. D.: Organosulfates as Tracers for Secondary Organic Aerosol (SOA) Formation from 2-Methyl-3-Buten-2-ol (MBO) in the Atmosphere, Environ. Sci. Technol., 46(17), 9437–9446, doi:10.1021/es301648z, 2012.

Zheng, G., Wang, Y., Aiken, A. C., Gallo, F., Jensen, M. P., Kollias, P., Kuang, C., Luke, E., Springston, S., Uin, J., Wood, R. and Wang, J.: Marine boundary layer aerosol in the eastern North Atlantic : seasonal variations and key controlling processes, Atmos. Chem. Phys., 18, 17615–17635, https://doi.org/10.5194/acp-18-17615-2018, 2018.

Zheng, G., Kuang, C., Uin, J., Watson, T., and Wang, J.: Large contribution of organics to condensational growth and formation of cloud condensation nuclei (CCN) in remote marine boundary layer, Atmos. Chem. Phys. Discuss., https://doi.org/10.5194/acp-2020-625, in review, 2020a.

Zheng, G., Sedlacek, A. J., Aiken, A. C., Feng, Y., Watson, T. B., Raveh-rubin, S., Uin, J., Lewis, E. R. and Wang, J.: Long-range transported North American wild fire aerosols observed in marine boundary layer of eastern North Atlantic, Environ. Int., 139(March), 105680, doi:10.1016/j.envint.2020.105680, 2020b.

Figures and tables

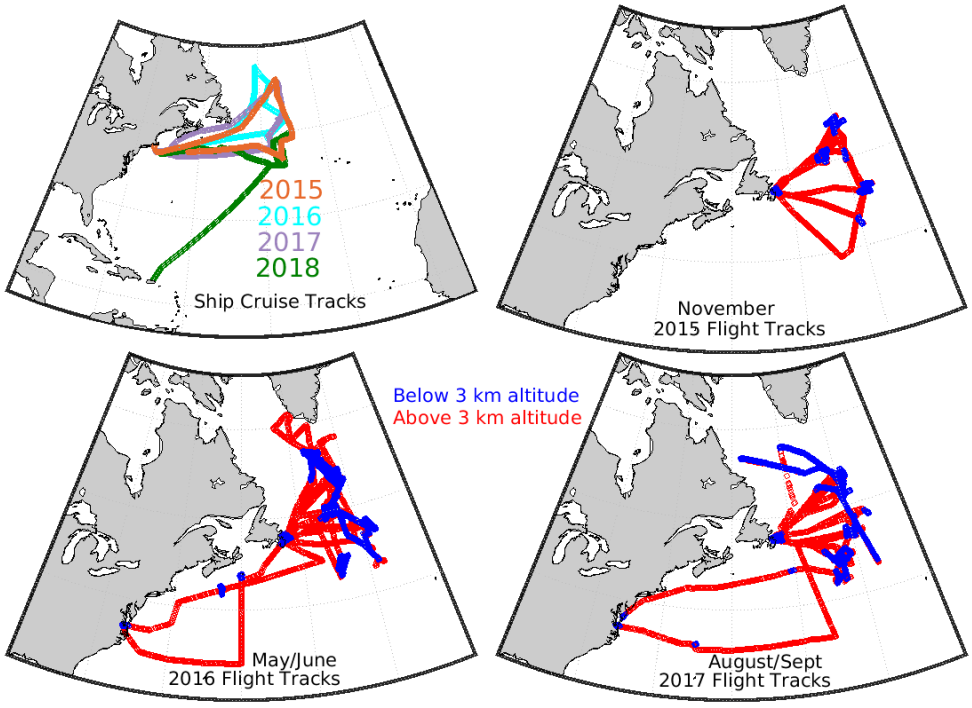

Figure 1: Cruise and aircraft tracks for the 2015-2018 NAAMES campaigns. Flight altitudes below 3 km are color-coded in medium blue and above 3 km in red. Ship tracks campaigns are color-coded for each year as shown by the legend, and as follows: Orange: November 2015 winter transition (bloom minima); Cyan: May/June 2016 climax transition (bloom maxima); Purple: August/September 2017 declining phase; Green: March/April 2018 accumulation phase.

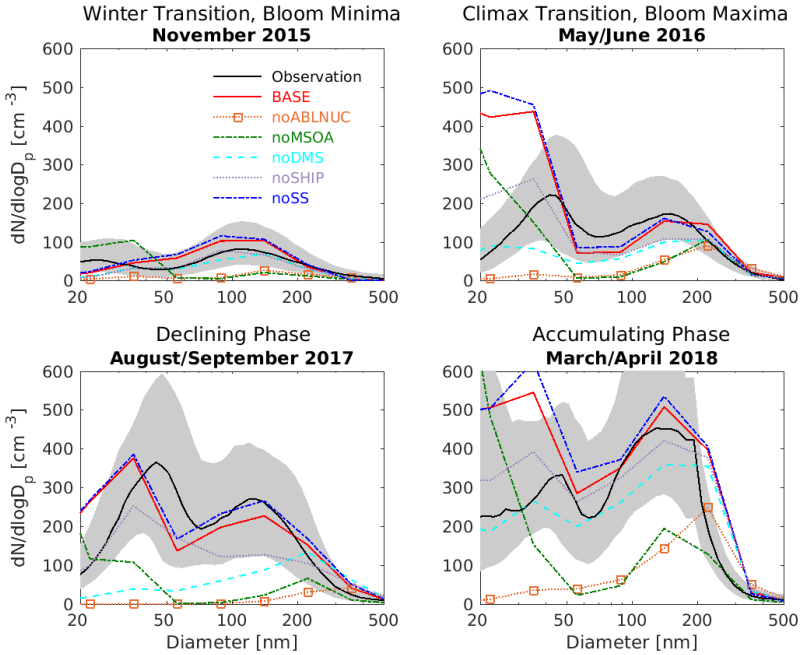

Figure 2: NAAMES cruise-track campaign-median marine boundary layer aerosol size distributions from marine-influenced SEMS (particle diameters 20-500 nm) observations (black, with 25th to 75th percentiles in grey) and for the six GEOS-Chem-TOMAS simulations as described in Table 1 (color-coded as shown in legend).

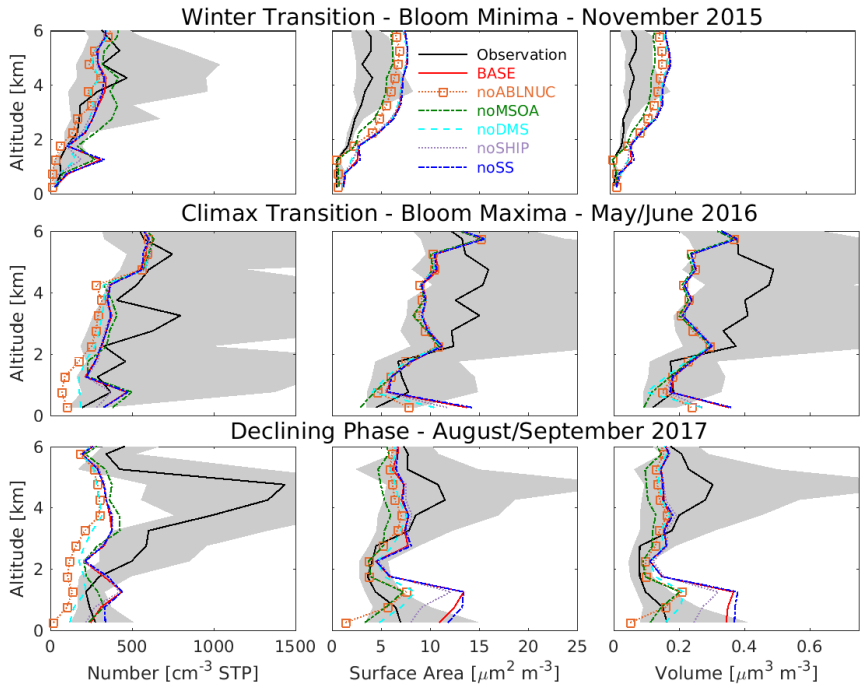

Figure 3: Vertical profiles of NAAMES campaign-median integrated SMPS observations aboard aircraft at standard temperature and pressure (STP) for particles with diameters of 10 to 282 nm (black, with 25th-75th percentiles in grey) and for the six GEOS-Chem-TOMAS simulations described in Table 1 (color-coded as shown in legend). All measurement and model output is binned at 500 m resolution and campaign-median values plotted at the mid-point of each bin starting at 250 m above the surface. Lines show linear interpolation between these values.

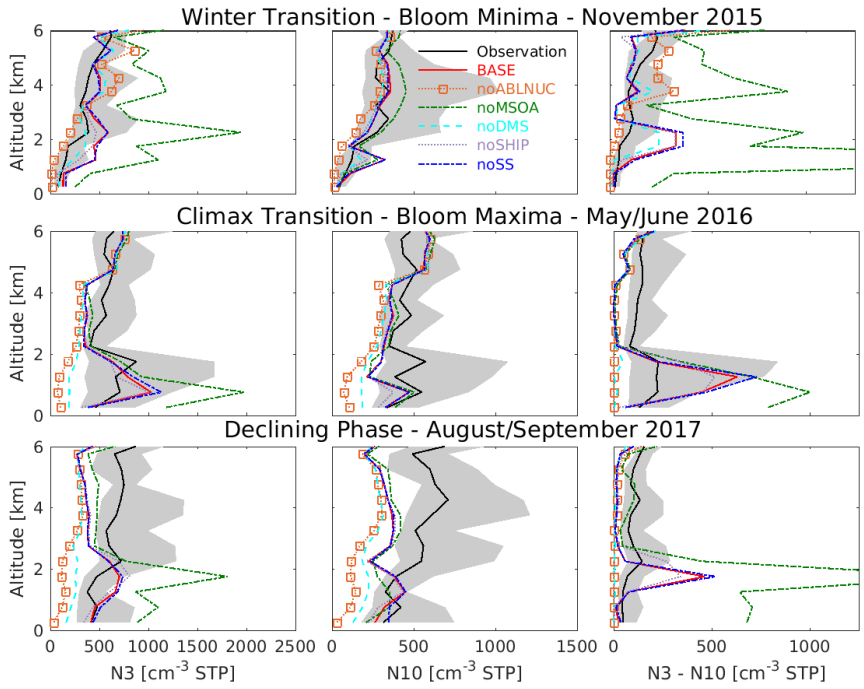

Figure 4: Vertical profiles of NAAMES campaign-median total number concentrations for particles with diameters larger than 3 nm (N3), 10 nm (N10) and between 3 to 10 nm (N3-N10) from CPC observations aboard aircraft at standard temperature and pressure (STP) (black, with 25th-75th percentiles in grey) and for the six GEOS-Chem-TOMAS simulations described in Table 1 (color-coded as shown in legend). All measurement and model output is binned at 500 m resolution and campaign-median values are plotted at the mid-point of each bin starting at 250 m above the surface. Lines show linear interpolation between these values.

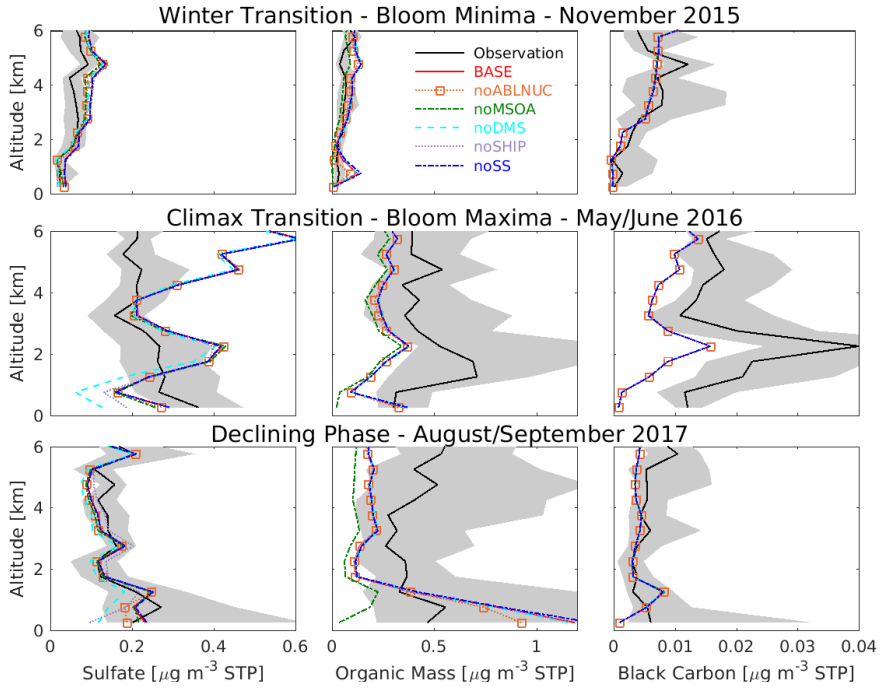

Figure 5: Vertical profiles of NAAMES campaign-median aerosol non-refractory sulfate and organic mass concentrations at standard temperature and pressure (STP) from Aerosol Mass Spectrometer and refractory black carbon from Single Particle Soot Photometer observations aboard aircraft (black, with 25th-75th percentiles in grey) and for the six GEOS-Chem-TOMAS simulations described in Table 1 (color-coded as shown in legend). Simulated sulfate shown is non-sea-salt-sulfate. All measurement and model output is binned at 500 m resolution and campaign-median values are plotted at the mid-point of each bin starting at 250 m above the surface. Lines show linear interpolation between these values.

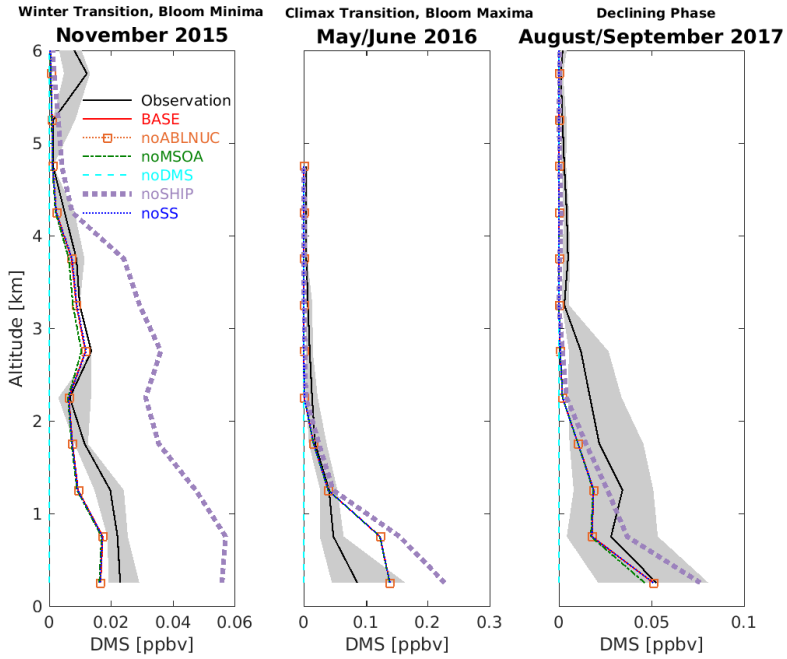

Figure 6: Vertical profiles of NAAMES cruise-track campaign-median observed dimethyl sulfide (DMS) mixing ratios (black, 25th-75th percentiles in grey) from aboard aircraft and for the six GEOS-Chem-TOMAS simulations described in Table 1 (color-coded as shown in legend). Simulations BASE, noABLNUC, noMSOA and noSS are nearly coincident. All measurement and model output is binned at 500 m resolution and campaign-median values plotted at the mid-point of each bin starting at 250 m above the surface. Lines show linear interpolation between these values. Note the horizontal scale change between panels.

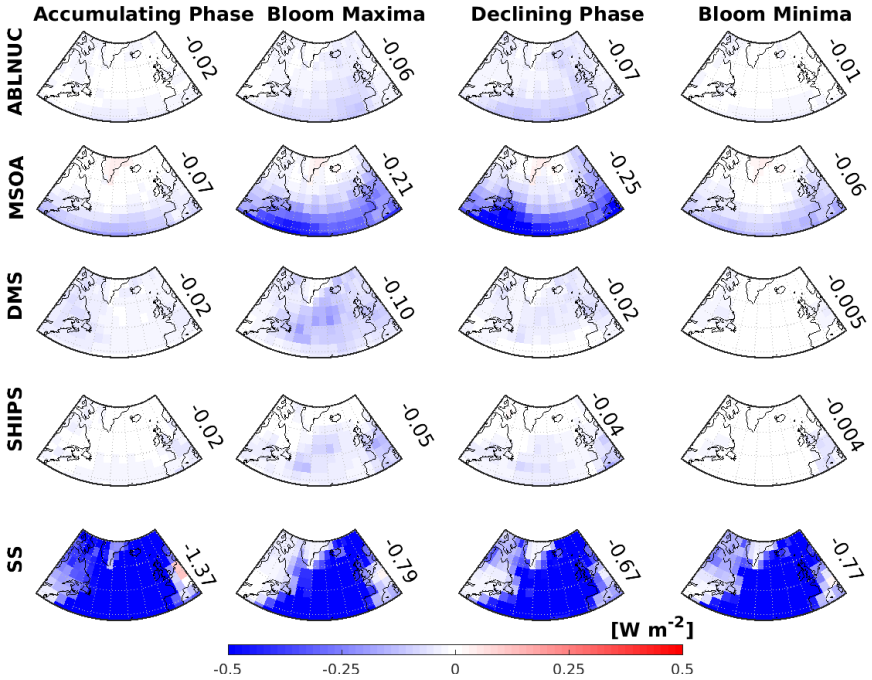

Figure 7: GEOS-Chem-TOMAS-simulated two-monthly-mean aerosol direct radiative effect (DRE) attributed to five key factors. Top row: Above boundary layer particle nucleation (ABLNUC); Second row: Particle growth by marine secondary organic aerosol (MSOA); Third row: Particle formation/growth due to DMS-oxidation products (DMS); Fourth row: Shipping emissions contribution to particles (SHIPS); Bottom row: Sea spray (SS). DREs are in columns for the following time periods, March/April 2018 (Accumulating Phase), May/June 2016 (Climax Transition, Bloom Maxima), August/September 2017 (Declining Phase), and October/November 2015 (Winter Transition, Bloom Minima). DREs for ABLNUC, MSOA, DMS, SHIPS, and SS are calculated using the differences in the top-of-the-atmosphere solar flux between simulation BASE and respective sensitivity simulations (noABLNUC, noMSOA, noDMS, noSHIPS, noSS). Values shown are area-weighted-mean DREs over the region bounded by 40-60 ^{o}N, 20-50 ^{o}W.

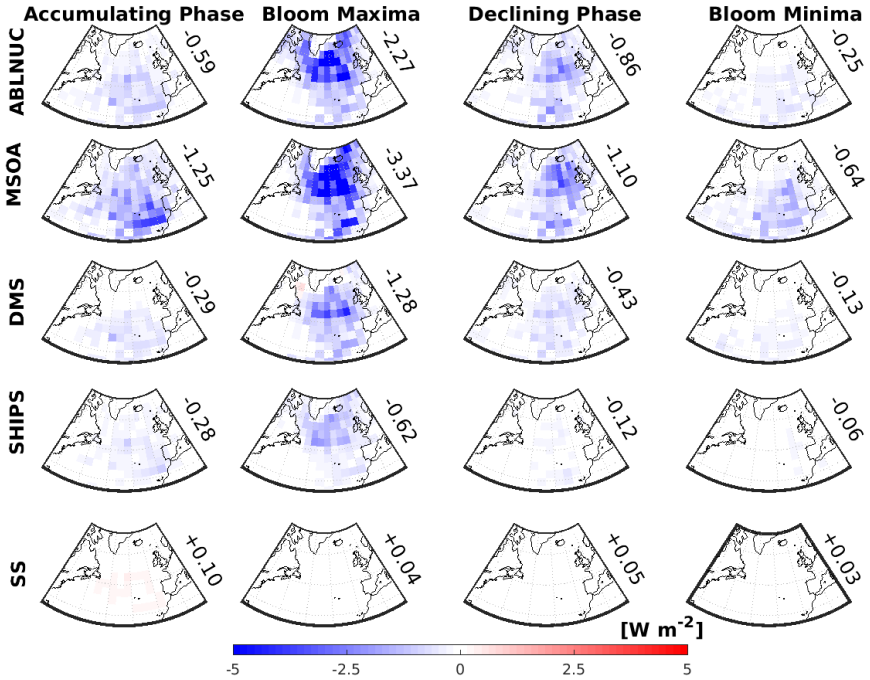

Figure 8: GEOS-Chem-TOMAS-simulated two-monthly-mean aerosol cloud-albedo indirect radiative effect (AIE) attributed to five key factors. Top row: Above boundary layer particle nucleation (ABLNUC); Second row: Particle growth by marine secondary organic aerosol (MSOA); Third row: Particle formation/growth due to DMS-oxidation products (DMS); Fourth row: Shipping emissions contribution to particles (SHIPS); Bottom row: Sea spray (SS). AIEs are in columns for the following time periods, March/April 2018 (Accumulating Phase), May/June 2016 (Climax Transition, Bloom Maxima), August/September 2017 (Declining Phase), and October/November 2015 (Winter Transition, Bloom Minima). AIEs for ABLNUC, MSOA, DMS, SHIPS, and SS are calculated using the differences in the top-of-the-atmosphere solar flux between simulation BASE and respective sensitivity simulations (noABLNUC, noMSOA, noDMS, noSHIPS, noSS). Values shown are area-weighted-mean AIEs over the region bounded by 40-60 ^{o}N, 20-50 ^{o}W.

Simulation	Description
BASE	Control simulation with GEOS-Chem-TOMAS model (GCT12.1.1) as described in Sect. 2.2
noABLNUC	Same as BASE, excluding the surrogate activation-type particle nucleation parameterization above the marine boundary layer to about 2 km altitude, as described in Sect. 2.2
noMSOA	Same as BASE, excluding the temperature-dependent marine organic vapors, forming marine secondary organic aerosol (MSOA)
noDMS	Same as BASE, excluding all emissions of DMS
noSHIPS	Same as BASE, excluding all ship emissions
noSS	Same as BASE, excluding all sea spray emissions

Table 1: GEOS-Chem-TOMAS simulation acronyms. Simulations and methodology are described in detail in Sect. 2.2 and 2.3.

Simulation	Nov 2015 Bloom Minima	May/June 2016 Bloom Maxima	Aug/Sept 2017 Declining Phase	Mar/Apr 2018 Accumulating	Annual Mean
BASE	0.20	0.33	0.04	0.28	0.21
noABLNUC	0.95	0.51	0.89	0.50	0.71
noMSOA	0.76	0.31	0.84	0.59	0.63
noDMS	0.44	0.27	0.43	0.06	0.30
noSHIPS	0.31	0.13	0.23	0.21	0.22
noSS	0.31	0.24	0.12	0.28	0.24

Table 2: Mean fractional error (MFE) between observations and the six GEOS-Chem-TOMAS simulations described in Sect. 2.2 and Table 1 for the ship-track campaign-median aerosol size distributions shown in Fig. 2.

Commented [RM6]: Best stated in text to avoid repetition

Section 4:

Supplementary information for:

Factors controlling marine aerosol size distributions and their climate effects over the Northwest Atlantic Ocean region

Betty Croft[1], Randall V. Martin[2,1], Richard H. Moore[3], Luke D. Ziemba[3], Ewan C. Crosbie[3,4], Hongyu Liu[5], Lynn M. Russell[6], Georges Saliba[6], Armin Wisthaler[7,8], Markus Müller[7], Arne Schiller[7], Martí Galí[9], Rachel Y.-W. Chang[1], Erin E. McDuffie[1,2], Kelsey R. Bilsback[10], and Jeffrey R. Pierce[10]

[1]Department of Physics and Atmospheric Science, Dalhousie University, Halifax, NS, Canada
[2]McKelvey School of Engineering, Washington University in St. Louis, St. Louis, MO, USA
[3]NASA Langley Research Center, Hampton, VA, USA
[4]Science Systems and Applications, Inc., Hampton, VA, USA
[5]National Institute of Aerospace, Hampton, VA, USA
[6]Scripps Institute of Oceanography, University of California, San Diego, La Jolla, CA, USA
[7]Institute for Ion Physics and Applied Physics, University of Innsbruck, Technikerstrasse 25, 6020 Innsbruck, Austria
[8]Department of Chemistry, University of Oslo, P.O. 1033 – Blindern, 0315 Oslo, Norway
[9]Barcelona Supercomputing Center (BSC)
[10]Department of Atmospheric Science, Colorado State University, Fort Collins, CO, USA
Correspondence to: Betty Croft (betty.croft@dal.ca)

Section S1: Role of MSOA The simulated marine organic vapor source flux for MOSA precursors was tuned to yield an acceptable annual-mean mean fractional error (MFE, 0.5 or less, Boylan and Russell, 2006) between NAAMES campaign-median measurements and simulations (described in Sect. 2). The simulated MBL aerosol size distributions for a set of sources fluxes are shown in Supplementary Fig. S1. Supplementary Table S1 shows the MFEs for this set of source fluxes. Among this set of source fluxes, we found the lowest annual mean MFE for the source flux of 70T-350 (T in ^{o}C and flux in $\mu g\ m^{-2}\ d^{-1}$). We caution that this tuning was specific for the NAAMES region and for a certain GEOS-Chem-TOMAS model configuration. As a result, this source flux may not perform as well in other models, other GEOS-Chem versions and other regions.

All of the temperature dependent parameterizations shown (Supplementary Fig.S1) had acceptable annual mean MFEs for the MBL size distributions, with the exception of 1) the simulation with the factor-of-ten scaling up of the flux that was used in BASE (10x(70T-350)) and 2) the simulation without condensable marine organic vapors (noMSOA). We consider that the order of magnitude of the flux was reasonably constrained for the purposes of this study under the various emission schemes that we tried. However, our findings suggest that further work is needed to better constrain the flux of marine organic vapors.

The selected parameterization also yielded agreement within the 25th to 75th percentiles for the campaign-median vertical profiles in the lowest 1 km for total aerosol number (N3, N10 and N3-N10) and integrated SMPS number, and near-surface OM concentrations (Supplementary Figs. S2-S4). Supplementary Fig. S2 shows slight overprediction outside of these percentiles for the integrated SMPS surface area and volume below 2 km. For the vertical profiles, the mean MFEs across the measurement set were acceptable for the BASE simulation with the 70T-350 source flux and unacceptable for noMSOA (Supplementary Table 2).

Section S2: Mean fractional errors The MFEs for the for all panels of Figs. 2 through 6 in the main text are shown in Supplementary Table S2. For vertical profiles, the MFEs are calculated using a summation (Eq. 1) over the altitude bins.

Section S3: Role of new particle formation A sensitivity simulation with the surrogate nucleation parameterization extended to the surface layer (BASE+BLNUC) increased simulated particle number in the MBL relative to BASE, worsening agreement with measurements (Supplementary Figs. S5-S8 and Supplementary Table S3).

Section S4: Role of ship emissions We found enhancements in benzene relative to other tracers, such as acetone, which have anthropogenic sources but not associated with ship emissions (Supplementary Fig. S9). These findings are supportive of the study region being influenced by ship emissions.

Section S5: Role of sea spray. Simulated campaign-median sea spray mass concentrations (Supplementary Fig. S10) were within the 3-8 in $\mu g\ m^{-3}$ range with a maximum for NAAMES in March/April 2018, which is in agreement with measurements reported by Saliba et al. (2019). Sensitivity studies with no sea spray and sea spray scaled up by a factor of 3 were conducted. In terms of simulated particle number, the factor-of-3 scaling up of sea spray made a stronger contribution as a condensation sink, suppressing the total particle number in the MBL (Supplementary Figs. S11-S14 and Supplementary Table S4).

Section S1: Role of MSOA

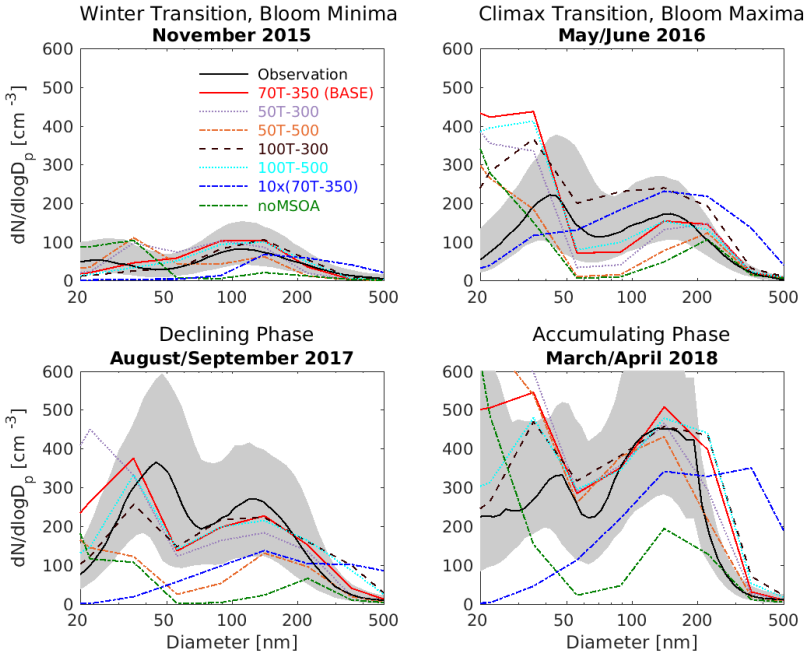

Figure S1: NAAMES cruise-track campaign-median marine boundary layer aerosol size distributions from marine-influenced SEMS observations (black, with 25th to 75th percentiles in grey) and for seven GEOS-Chem-TOMAS simulations with different assumptions for the temperature dependence of the flux of condensable organic vapors (color-coded as shown in legend, flux in μg m^{-2} d^{-1} and T in ^{o}C).

Marine organic vapor source	Nov 2015 Bloom Minima	May/June 2016 Bloom Maxima	Aug/Sept 2017 Declining Phase	Mar/Apr 2018 Accumulating	Annual Mean
70T-350 (BASE)	0.20	0.33	0.04	0.28	0.23
50T-300	0.34	0.22	0.22	0.21	0.25
50T-500	0.55	0.20	0.56	0.23	0.38
100T-300	0.11	0.54	0.26	0.33	0.31
100T-500	0.13	0.30	0.19	0.31	0.27
noMSOA	0.76	0.31	0.84	0.59	0.63
10x(70T-350)	0.87	0.80	0.73	0.60	0.75

Table S1: Mean fractional error (MFE) between observations and seven GEOS-Chem-TOMAS simulations for the ship-track campaign-median aerosol size distributions shown in Supplementary Fig. S1 (T in ^{o}C and source flux in $\mu g\ m^{-2}\ d^{-1}$).

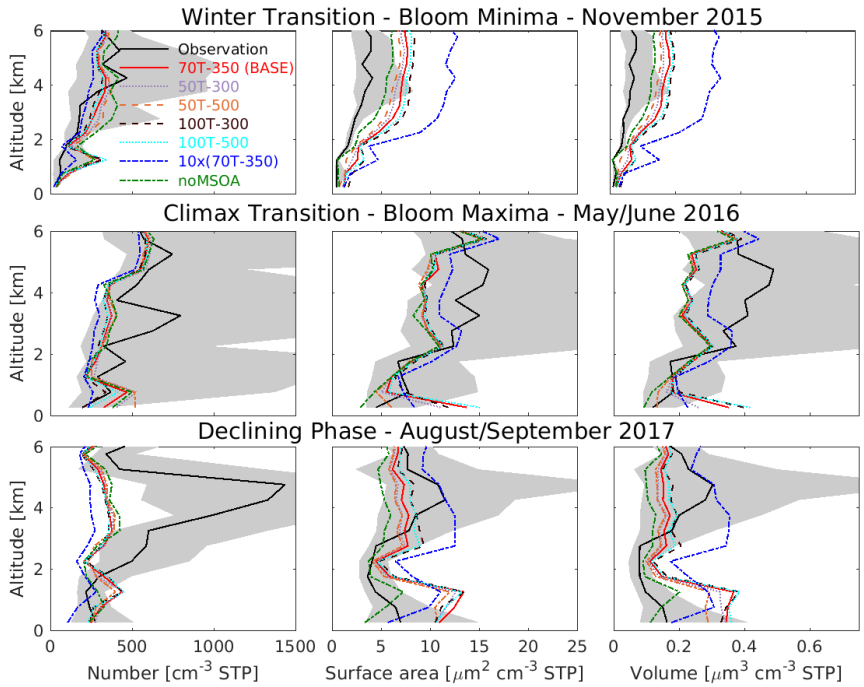

Figure S2: Vertical profiles of NAAMES campaign-median integrated SMPS observations at standard temperature and pressure (STP) for particles with diameters of 10 to 282 nm (black, with 25th-75th percentiles in grey) and at STP for seven GEOS-Chem-TOMAS simulations with different assumptions for the temperature dependence of the flux of condensable marine organic vapors (color-coded as shown in legend, flux in µg m^{-2} d^{-1} and T in ^{o}C). All measurement and model output are binned at 500 m resolution and campaign-median values plotted at the mid-point of each bin starting at 250 m above the surface. Lines show linear interpolation between these values.

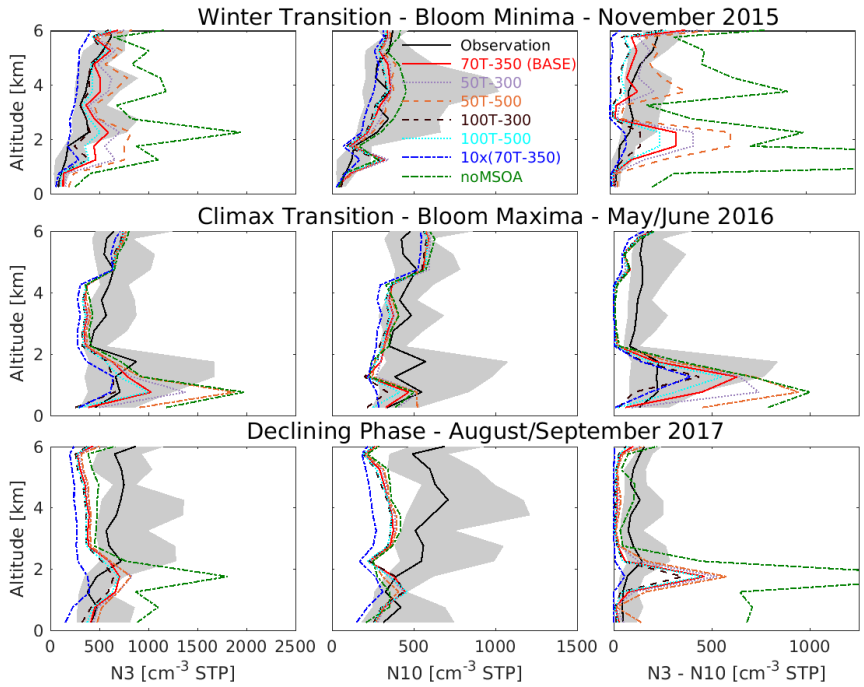

Figure S3: Vertical profiles of NAAMES campaign-median total number concentrations for particles with diameters larger than 3 nm (N3), 10 nm (N10) and between 3 to 10 nm (N3-N10) from CPC observations at standard temperature and pressure (STP) (black, with 25th-75th percentiles in grey) and at STP for seven GEOS-Chem-TOMAS simulations with different assumptions for the temperature dependence of the flux of condensable marine organic vapors (color-coded as shown in legend, flux in μg m^{-2} d^{-1} and T in ^{o}C). All measurement and model output are binned at 500 m resolution and campaign-median values plotted at the mid-point of each bin starting at 250 m above the surface. Lines show linear interpolation between these values.

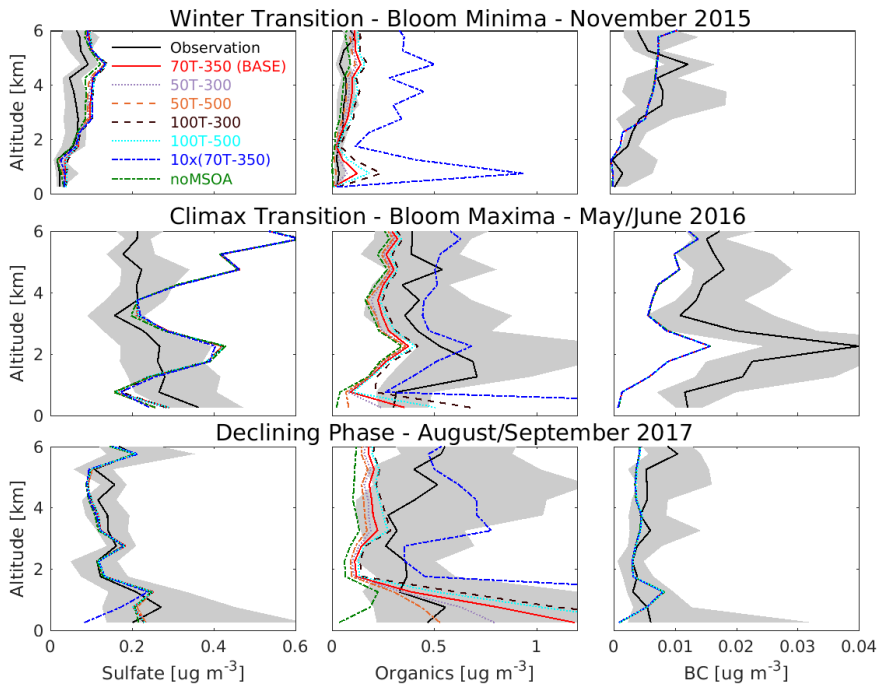

Figure S4: Vertical profiles of NAAMES campaign-median aerosol non-refractory sulfate and organic mass concentrations from Aerosol Mass Spectrometer and refractory black carbon from SP2 observations at standard temperature and pressure (STP) (black, with 25th-75th percentiles in grey) and at STP for seven GEOS-Chem-TOMAS simulations with different assumptions for the temperature dependence of the flux of marine condensable organic vapors (color-coded as shown in legend, flux in μg m^{-2} d^{-1} and T in °C). Simulated sulfate shown is non-sea-salt-sulfate. All measurement and model output are binned at 500 m resolution and campaign-median values plotted at the mid-point of each bin starting at 250 m above the surface. Lines show linear interpolation between these values.

Section S2: Mean fractional errors

MFEs for figure panels	BASE	noABLNUC	noMSOA	noDMS	noSHIP	noSS
2015						
MBL size dist. Fig 2	0.20	0.95	0.76	0.44	0.31	0.31
Number Fig 3	0.31	0.39	0.40	0.26	0.25	0.30
Surface area Fig 3	0.43	0.68	0.73	0.43	0.44	0.43
Volume Fig 3	1.22	1.04	0.96	1.12	1.21	1.22
N3 Fig 4	0.51	0.75	1.02	0.43	0.44	0.53
N10 Fig 4	0.24	0.43	0.23	0.20	0.24	0.25
N3-N10 Fig 4	0.88	1.04	1.34	0.90	0.92	0.87
Sulfate Fig 5	0.39	0.26	0.25	0.27	0.34	0.39
Organic mass Fig 5	0.52	0.51	0.73	0.52	0.52	0.53
Black carbon Fig 5	0.44	0.45	0.45	0.44	0.44	0.44
DMS Fig 6	0.12	0.12	0.12	0.67	0.40	0.12
Average of 2015	0.42	0.68	0.67	0.50	0.46	0.45
2016						
MBL size dist. Fig 2	0.33	0.51	0.31	0.27	0.13	0.24
Number Fig 3	0.37	0.60	0.38	0.43	0.34	0.37
Surface area Fig 3	1.04	1.10	1.16	1.09	1.06	1.04
Volume Fig 3	0.50	0.46	0.39	0.44	0.49	0.50
N3 Fig 4	0.35	0.74	0.43	0.62	0.36	0.37
N10 Fig 4	0.31	0.61	0.31	0.47	0.34	0.30
N3-N10 Fig 4	1.08	1.48	1.10	1.40	1.11	1.10
Sulfate Fig 5	0.52	0.52	0.52	0.16	0.56	0.52
Organic mass Fig 5	0.60	0.61	0.84	0.59	0.60	0.60
Black carbon Fig 5	0.78	0.78	0.78	0.78	0.78	0.78
DMS Fig 6	0.26	0.26	0.26	0.67	0.31	0.26
Average of 2016	0.50	0.66	0.53	0.55	0.46	0.49
2017						
MBL size dist. Fig 2	0.04	0.89	0.84	0.43	0.23	0.12
Number Fig 3	0.60	0.91	0.50	0.73	0.60	0.61
Surface area Fig 3	0.88	1.12	1.18	1.02	0.91	0.87
Volume Fig 3	0.78	0.61	0.56	0.67	0.77	0.79
N3 Fig 4	0.43	0.86	0.49	0.69	0.47	0.45
N10 Fig 4	0.58	0.97	0.49	0.81	0.59	0.56
N3-N10 Fig 4	1.09	1.47	1.01	1.40	1.11	1.04
Sulfate Fig 5	0.17	0.18	0.17	0.27	0.19	0.17
Organic mass Fig 5	0.65	0.65	1.03	0.63	0.66	0.66
Black carbon Fig 5	0.47	0.48	0.48	0.47	0.47	0.47
DMS Fig 6	0.18	0.18	0.20	0.67	0.20	0.18
Average of 2017	0.43	0.78	0.68	0.65	0.49	0.45
Average all years	0.45	0.71	0.63	0.57	0.47	0.46

Table S2: Mean fractional error (MFE) between the six simulations described in Table 1 and the measurements for the panels of Figs. 2 through 6. Results for Fig. 2 are weighted to include MFEs for first four moments of the MBL aerosol size distributions. All MFEs are calculated for altitude below 6 km, except below 2 km for DMS due to the decrease over orders of magnitude above 2 km. The MFEs are calculated following Eq. 1 with a summation over the altitude bins that are defined in Sect.2.

Section S3: Role of new particle formation

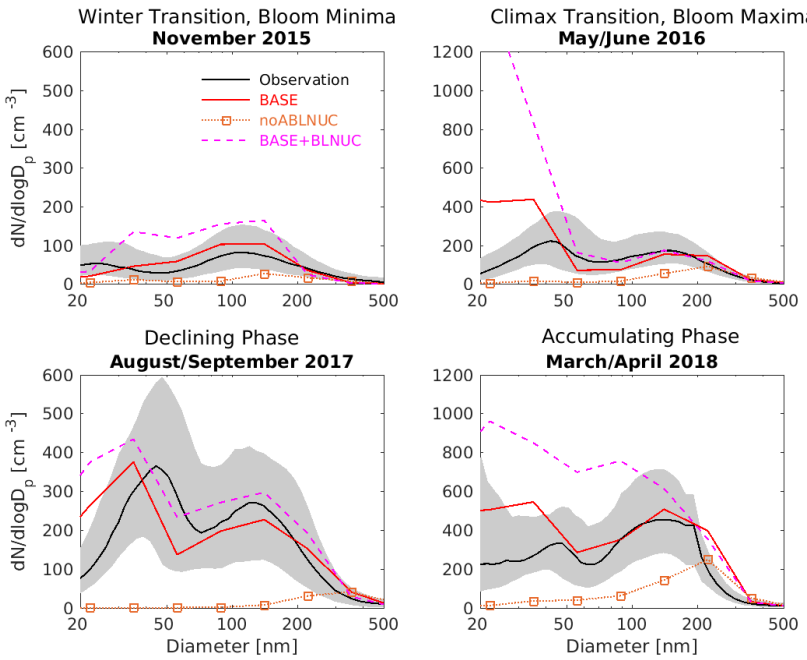

Figure S5: NAAMES cruise-track campaign-median marine boundary layer aerosol size distributions from marine-influenced SEMS observations (black, with 25th to 75th percentiles in grey) and for three GEOS-Chem-TOMAS simulations with different assumptions for surrogate above boundary layer nucleation. noABLNUC: surrogate activation nucleation scheme above the boundary removed; BASE+BLNUC: surrogate activation nucleation scheme extended from 2 km to the surface layer; BASE as described in Table 1 and Section 2, including surrogate activation nucleation scheme from above the boundary layer to 2 km.

	Nov 2015 Bloom Minima	May/June 2016 Bloom Maxima	Aug/Sept 2017 Declining Phase	Mar/Apr 2018 Accumulating	Annual Mean
BASE	0.20	0.33	0.04	0.28	0.21
noABLNUC	0.95	0.54	0.89	0.50	0.72
BASE+BLNUC	0.36	0.56	0.20	0.48	0.40

Table S3: Mean fractional error between observations and three GEOS-Chem-TOMAS simulations for the ship-track campaign-median aerosol size distributions shown in Supplementary Fig. S5.

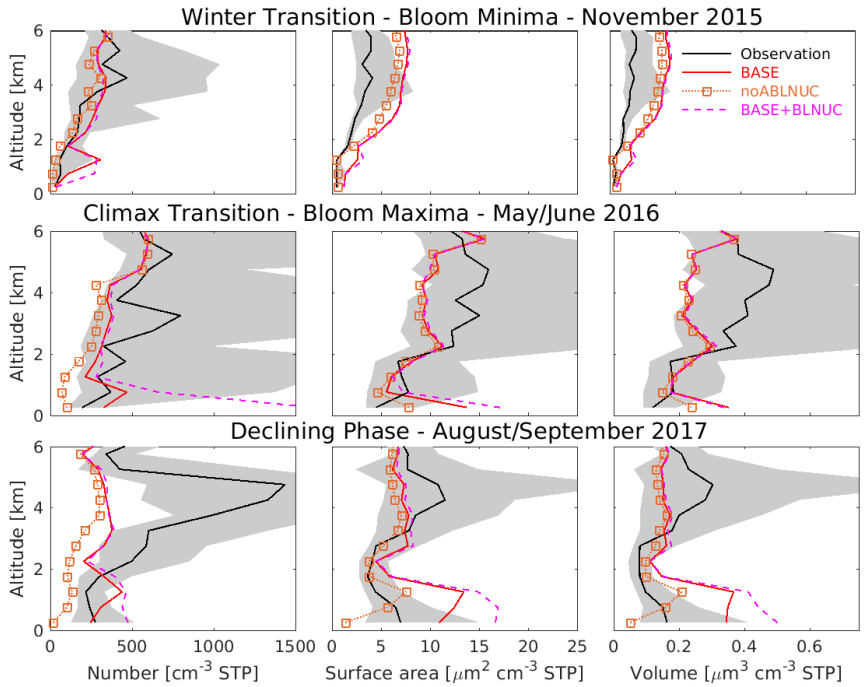

Figure S6: Vertical profiles of NAAMES campaign-median integrated SMPS observations at standard temperature and pressure (STP) for particles with diameters of 10 to 282 nm (black, with 25th-75th percentiles in grey) and at STP for three GEOS-Chem-TOMAS simulations with different assumptions for above boundary layer nucleation. noABLNUC: surrogate activation nucleation scheme above the boundary removed; BASE+BLNUC: surrogate activation nucleation scheme extended from 2 km to the surface layer; BASE as described in Table 1 and Section 2, including surrogate activation nucleation scheme from above the boundary layer to 2 km. All measurement and model output are binned at 500 m resolution and campaign-median values plotted at the mid-point of each bin starting at 250 m above the surface. Lines show linear interpolation between these values.

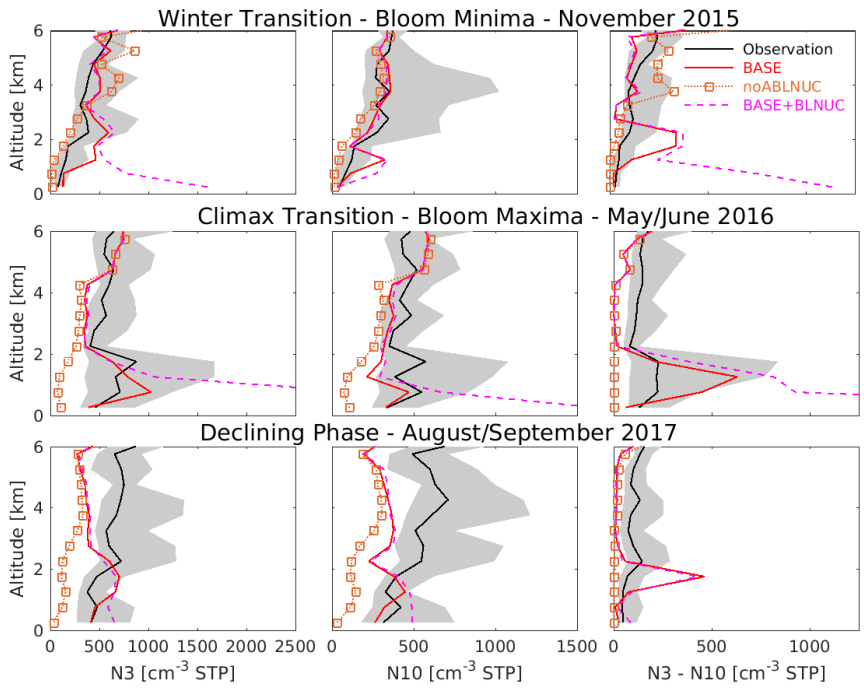

Figure S7: Vertical profiles of NAAMES campaign-median total number concentrations for particles with diameters larger than 3 nm (N3), 10 nm (N10) and between 3 to 10 nm (N3-N10) from CPC observations at standard temperature and pressure (STP) (black, with 25th-75th percentiles in grey) and at STP for three GEOS-Chem-TOMAS simulations with different assumptions for above boundary layer nucleation. noABLNUC: surrogate activation nucleation scheme above the boundary removed; BASE+BLNUC: surrogate activation nucleation scheme extended from 2 km to the surface layer; BASE as described in Table 1 and Section 2, including surrogate activation nucleation scheme from above the boundary layer to 2 km. All measurement and model output are binned at 500 m resolution and campaign-median values plotted at the mid-point of each bin starting at 250 m above the surface. Lines show linear interpolation between these values.

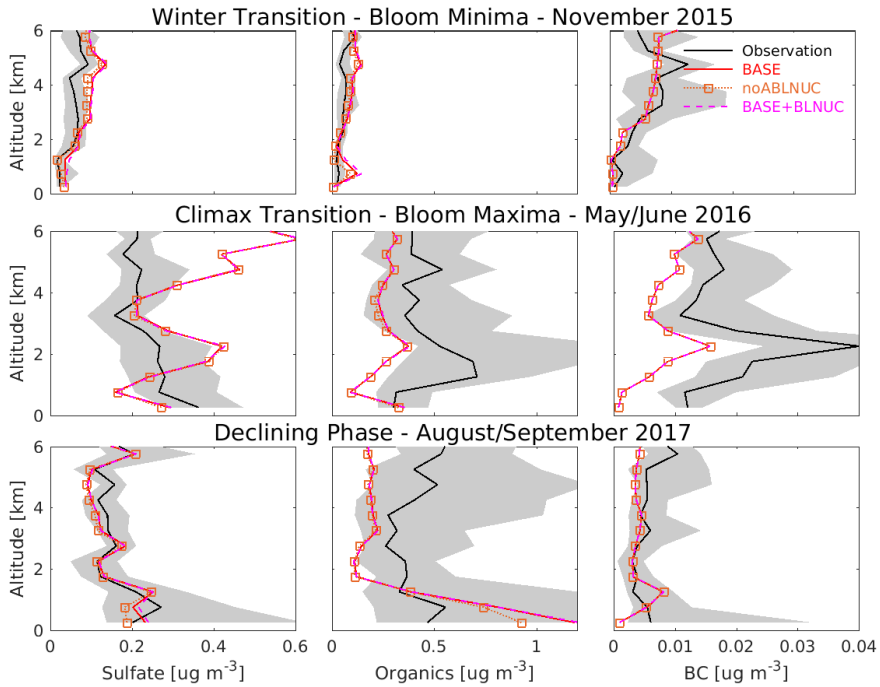

Figure S8: Vertical profiles of NAAMES campaign-median aerosol non-refractory sulfate and organic mass concentrations from Aerosol Mass Spectrometer and refractory black carbon from SP2 observations at standard temperature and pressure (STP) (black, with 25th-75th percentiles in grey) and at STP for three GEOS-Chem-TOMAS simulations with different assumptions for above boundary layer nucleation. noABLNUC: surrogate activation nucleation scheme above the boundary removed; BASE+BLNUC: surrogate activation nucleation scheme extended from 2 km to the surface layer; BASE as described in Table 1 and Section 2, including surrogate activation nucleation scheme from above the boundary layer to 2 km. All measurement and model output are binned at 500 m resolution and campaign-median values plotted at the mid-point of each bin starting at 250 m above the surface. Lines show linear interpolation between these values.

Section S4: Role of ship emissions

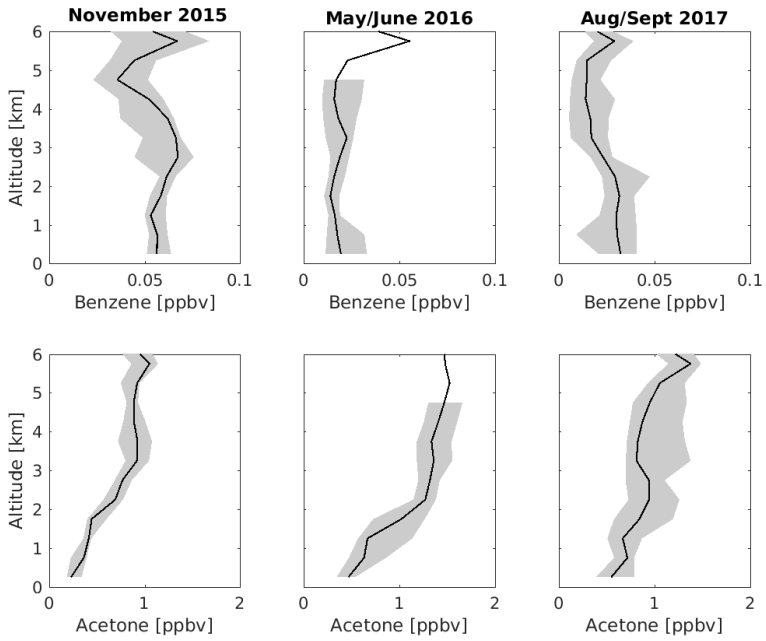

Figure S9: Vertical profiles of NAAMES campaign-median benzene (top row) and acetone (bottom row) mixing ratios obtained from a Proton-Transfer-Reaction Time-of-Flight Mass Spectrometer (PTR-ToF-MS) aboard the NASA C130 aircraft (black, with 25th-75th percentiles in grey). All measurements are binned at 500 m resolution and campaign-median values plotted at the mid-point of each bin starting at 250 m above the surface. Lines show linear interpolation between these values.

.

Section S5: Role of sea spray

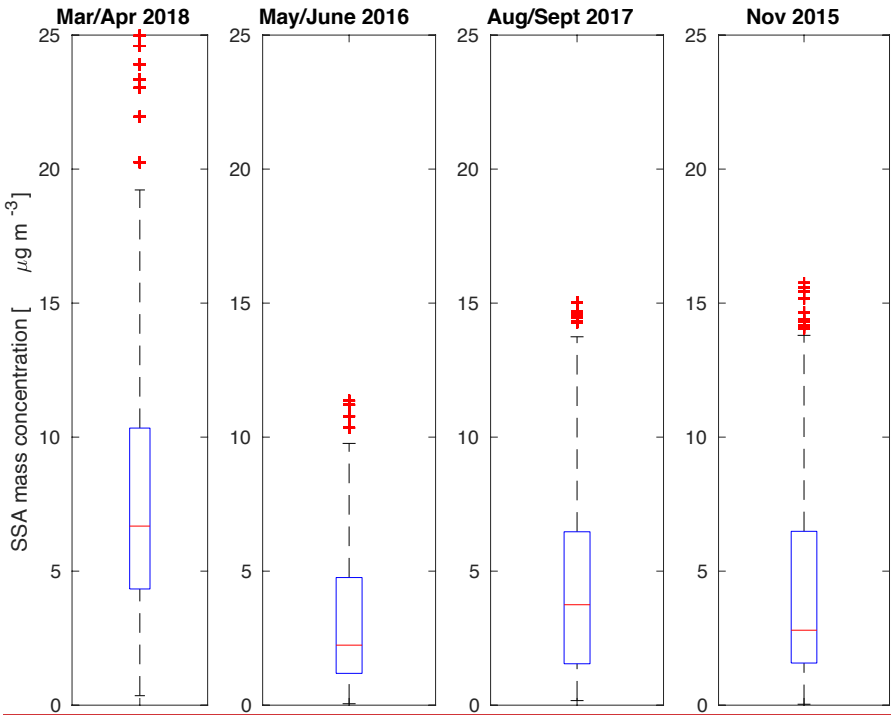

Figure S10: Box plots of simulated ship-track campaign-median sea spray aerosol mass concentrations for the four years of the NAAMES campaigns for simulation BASE. Red line shows median and box limits are 25th and 75th percentiles. Outliers are shown with red plus symbol.

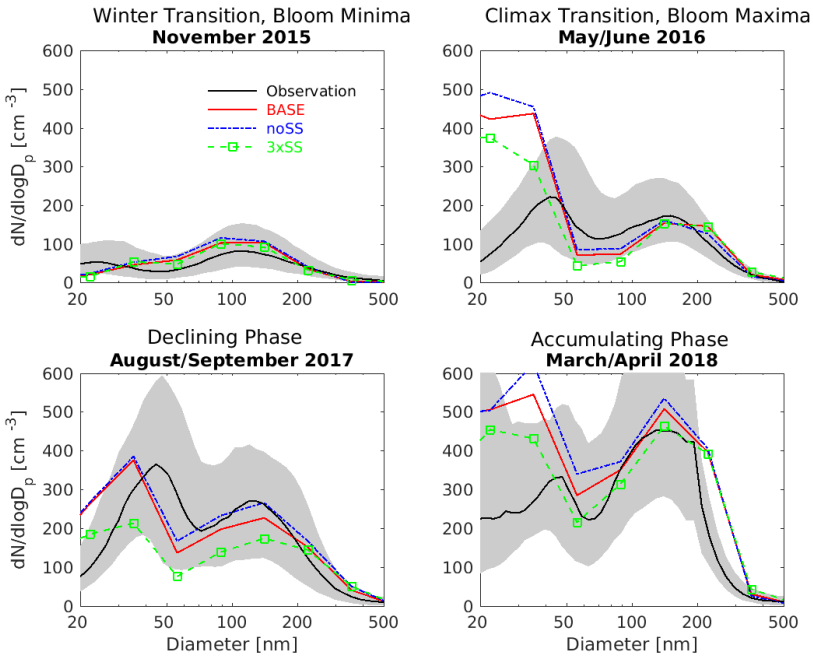

Figure S11: NAAMES cruise-track campaign-median marine boundary layer aerosol size distributions from marine-influenced SEMS observations (black, with 25th to 75th percentiles in grey) and for three GEOS-Chem-TOMAS simulations with different assumptions for the sea spray emissions. noSS: no sea spray emissions; 3xSS: sea spray emissions scaled up by 3; BASE as described in Table 1 and Section 2.

	Nov 2015 Bloom Minima	May/June 2016 Bloom Maxima	Aug/Sept 2017 Declining Phase	Mar/Apr 2018 Accumulating	Annual Mean
BASE	0.20	0.33	0.04	0.28	0.21
noSS	0.31	0.24	0.12	0.28	0.24
3xSS	0.05	0.38	0.14	0.28	0.21

Table S4: Mean fractional error between observations and three GEOS-Chem-TOMAS simulations for the ship-track campaign-median aerosol size distributions shown in Supplementary Fig. S11.

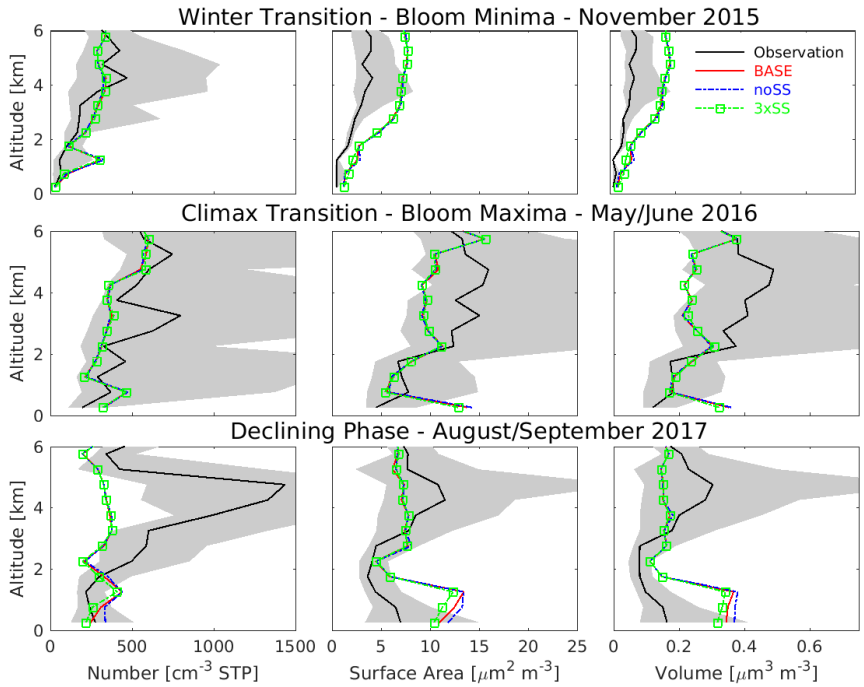

Figure S12: Vertical profiles of NAAMES campaign-median integrated SMPS observations aboard aircraft at standard temperature and pressure (STP) for particles with diameters of 10 to 282 nm (black, with 25th-75th percentiles in grey) and at STP for three GEOS-Chem-TOMAS simulations with different assumptions for the sea spray emissions. noSS: no sea spray emissions; 3xSS: sea spray emissions scaled up by 3; BASE as described in Table 1 and Section 2. All measurement and model output are binned at 500 m resolution and campaign-median values plotted at the mid-point of each bin starting at 250 m above the surface. Lines show linear interpolation between these values.

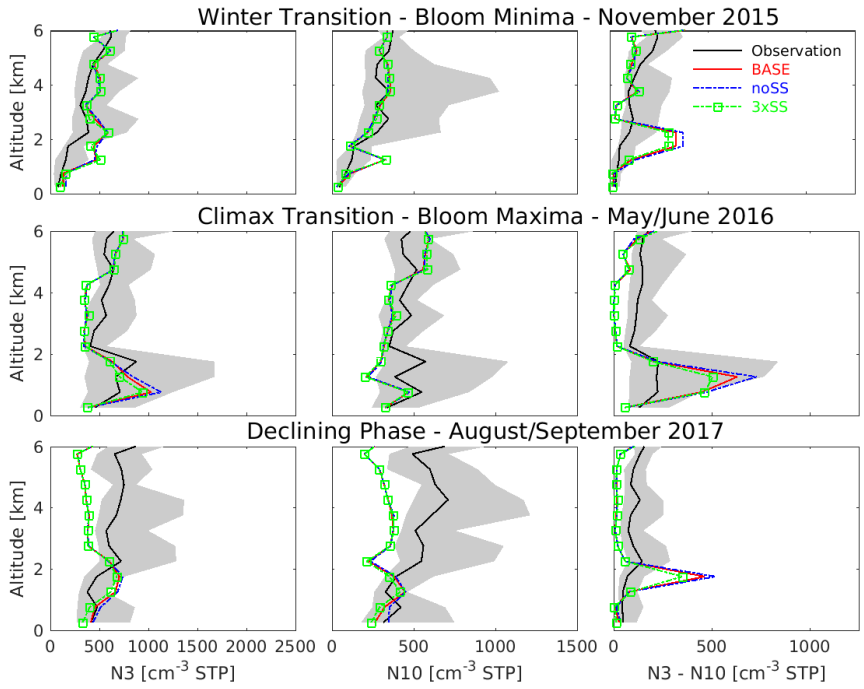

Figure S13: Vertical profiles of NAAMES campaign-median total number concentrations for particles with diameters larger than 3 nm (N3), 10 nm (N10) and between 3 to 10 nm (N3-N10) from CPC observations board aircraft at standard temperature and pressure (STP) (black, with 25th-75th percentiles in grey) and at STP for three GEOS-Chem-TOMAS simulations with different assumptions for the sea spray emissions. noSS: no sea spray emissions; 3xSS: sea spray emissions scaled up by 3; BASE as described in Table 1 and Section 2. All measurement and model output are binned at 500 m resolution and campaign-median values plotted at the mid-point of each bin starting at 250 m above the surface. Lines show linear interpolation between these values.

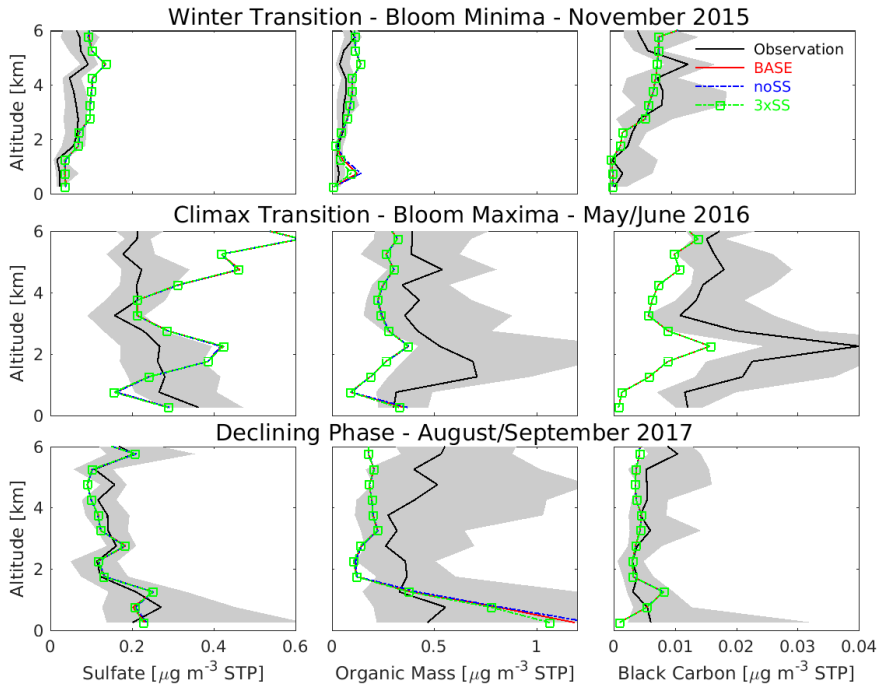

Figure S14: Vertical profiles of NAAMES campaign-median aerosol non-refractory sulfate and organic mass concentrations from Aerosol Mass Spectrometer and refractory black carbon from SP2 observations aboard aircraft at standard temperature and pressure (STP) (black, with 25th-75th percentiles in grey) and at STP for three GEOS-Chem-TOMAS simulations with different assumptions for the sea spray emissions. noSS: no sea spray emissions; 3xSS: sea spray emissions scaled up by 3; BASE as described in Table 1 and Section 2. All measurement and model output are binned at 500 m resolution and campaign-median values plotted at the mid-point of each bin starting at 250 m above the surface. Lines show linear interpolation between these values.

Deleted: ¶